DURBAN UNIVERSITY OF TECHNOLOGY
INYUVESI YASETHEKWINI YEZOBUCHWEPHESHE

# VOLTAGE RISE MITIGATION AT THE POINT OF COMMON COUPLING OF LARGE RENEWABLE DISTRIBUTED GENERATION AND DISTRIBUTION NETWORK

**by**


**AKINYEMI AYODEJI STEPHEN**

***M.Sc. Electrical Engineering***


**Thesis submitted in the fulfilment of the requirements of the degree of**

**Doctor of Engineering in Electrical Engineering**

**in the Faculty of Engineering and the Built Environment**

**at the Durban University of Technology**

**Supervisor: Dr. M. Kabeya**

**Co-Supervisor: Prof. I. E. Davidson**

**February 2022**

As the candidate's supervisor I agree to the submission of this thesis

Dr M. Kabeya

NAME OF SUPERVISOR SIGNATURE

Prof I.E. Davidson _ _____

NAME OF CO-SUPERVISOR SIGNATURE

# DECLARATION

I hereby declare that this thesis is my work, and each text has been correctly referenced or cited. Moreover, this work has not been previously published in portion or whole for another degree at any other University.

This research was duly supervised by Dr Kabeya Musasa and Prof Innocent E. Davidson at the Durban University of Technology.

Submitted by:

24/02/2022

……. ……..……..

Akinyemi Ayodeji Stephen Date

Student Number: 21960204

# DEDICATION

*To*

*My Mum & Dad,*

*Chief Alfred Ali Akinyemi*

*Chief (Mrs) Lydia Ibitayo Akinyemi*

*and to*

*my supervisors, families, mentors, friends, colleagues, teachers, and students who contributed in one way or the other to the success of this great achievement.*

# ACKNOWLEDGEMENTS

I give glory, honour and adoration to God almighty for his infinite mercy and unmerited favour he bestowed on me before, during and after the completion of this higher degree programme, may his name be praised for evermore.

Special thanks to my supervisors, Dr. M. Kabeya and Prof. I. E. Davidson for their love, encouragement and supervisory role, their guidance, advice and support throughout the course of this research work. To all academic and non-academic staff of the Department of Electrical, Power Engineering, Durban University of Technology, Durban, South Africa, you are highly appreciated.

Finally, special thanks to a virtuous and intelligent woman Dr (Mrs) Oluwatoyin Akinyemi for her support, my pastor, families, friends, colleagues, and the people that contributed to the success of this great achievement, you are honoured and thank you all.

# ABSTRACT

A lot of changes are taking place in the power system as a result of the introduction of Renewable Distributed Generation (RDG) (e.g., wind and PV systems). Gradually, electricity generated by fossil fuel is being replaced by electricity generated from Renewable Energy Sources (RESs). The deregulation of generation, transmission, and distribution systems due to the introduction of RDGs has brought competition to the electricity market. The electricity generation assets are no longer owned by one or a few owners, as investors have been attracted to the electricity market. Individuals can now generate their own electricity from renewable energy sources such as solar, wind, hydro, wave, tide, and geothermal etc. RDGs are predicted to play a crucial role in the power system transformation in the near future; they are the key to a sustainable energy supply infrastructure because of their inexhaustible and non-polluting nature. However, the integration of RDGs into the power system would have an impact on power system planning, voltage profiles and power quality requirements within the Distribution Network (DN). The voltage rise (or over-voltages) at the busbars within the conventional power system with centralized large power generating units are actually of less concern due to advances in control and protection technologies, but the issue of excessive voltage drop at the far end of transmission lines cannot be overemphasized. The introduction of RDGs into the power system has eliminated the occurrences of the severe under voltage at the far end of transmission lines, but the voltage rise effects and the bidirectional power flow issues at the point of common couplings (PCCs) between RDGs and DN are now of major concern. Indeed, the integration of RDGs can make the power system become bidirectional as electricity can flow from RDGs as well as from DN with a centralised generator. This causes various problems with regards to the power quality, power flow control, frequency control, system voltage profile, etc. Furthermore, the voltage rise effects at PCC with connected-RDG has been a noticeable issue in recent years and requires remedial action. The standard grid code requires that output parameters of RDGs (i.e., voltage profile, current, voltage-current harmonic distortions, power factor, frequency, etc.) at PCC shall be regulated to avoid damage to sensitive equipment connected to the DN, meet up with the power quality criteria, and shall continue providing power support to the DN. Hence, this study focuses on the following two main problems:

– firstly, the voltage rise effect, and secondly, the bidirectional power flow constraint at the PCC between RDGs and DN.

The analysis and simulations in this thesis are conducted on an IEEE 13-bus sample model and DUT Steve Biko network with penetration of a large RDG. The capacity of the RDG integrated to DN is 1 MW (solar PV). In order to investigate the effect of voltage rise and bidirectional power flow in a DN, a mathematical model of a power distribution network connected with RDG is developed. Intensive simulations are carried out using MATLAB/Simulink software. Furthermore, a control strategy is recommended at PCC for mitigating or minimizing the impacts of voltage rise and reverse power flow when operating at a worst critical scenario, such as minimum load and maximum generation. The control structure consists of the installation of a static compensator (STATCOM) with Pulse Width Modulation (PWM), and the block/deblock and in-loop filtering circuit control scheme to control the active and reactive power. The proposed control strategy also mitigates the voltage-current harmonic distortions, improves the power factor and voltage stability at PCC, and also protects the converter-PWM scheme from grid disturbances and fault currents, as the control of active and reactive power is independent of the grid. This thesis also provides a review of various types of renewable energy resources (RERs) prospects in Africa, looking at how they can be deployed faster within the continent. The thesis also analyses power quality and compensators.

# LIST OF PUBLICATIONS

[1] **A.S. Akinyemi**, M. Kabeya, and I.E. Davidson, “Analysis of voltage rise phenomena in electrical power network with high concentration of renewable distributed generations”, *Scientific Report*, 12, pp 1-22, 2022.

[2] **A.S. Akinyemi,** M. Kabeya, and I. E. Davidson “Modelling of Solar PV Under Varying Condition with an Improved Incremental Conductance and Integral Regulator”, *Energies,* pp 1-24, 2022.

[3] **A.S. Akinyemi**, M. Kabeya, and I. E. Davidson, “Enhancement of Large Renewable Distributed Generation Penetration Levels at the Point of Common Coupling”, *Energy Engineering: Journal of the Association of Energy Engineers,* pp 1-30, 2022.

[4] **A.S. Akinyemi**, M. Kabeya, and I. E. Davidson, “Enhancement of Solar PV Output Error Under Variable Irradiation and Temperature Using an Improved Regulation Strategy”, submitted to *PowerAfrica*, Kigali-Rwanda, August 2022.

[5] **A.S. Akinyemi**, M. Kabeya and I.E. Davidson., “Voltage Rise Regulation with a Grid Connected Solar Photo Voltaic System”, *Energies,* 14(22), pp 1-31, 2021.

[6] **A.S. Akinyemi**, M. Kabeya, and I.E. Davidson, “Voltage Rise with Increase in Penetration Level of a Grid Connected Renewable Distribution Generation”, *International Conference & Exhibition on Clean Energy (ICCE),* Ottawa Canada, August 2021.

[7] **A.S. Akinyemi** and I.E. Davidson, “Impact of Renewable Energy Generation on Voltage Flicker with Dynamic Load Connected to Distribution Network”, *International Journal of Applied Engineering Research*, 14(14), pp 3137-3145, 2019

[8] **A.S. Akinyemi** and O.O. Osaloni, "Voltage Profile Improvement and Loss Reduction in LV Distribution Network Using Generic Algorithm", *International Journal of Scientific & Engineering Research* Vol. 10, Issue 7, pp. 1857-1863, 2019

[9] **A. S. Akinyemi**, "Optimum Impacts of Renewable Energy Generation on Voltage Dip and Voltage Profile in a Distribution Network", *International Journal of Scientific & Engineering Research* Vol. 10, Issue 8, pp. 280-291, 2019

[10] **A.S. Akinyemi** and K. Awodele, "Voltage Profiles Improvement with Wind Energy Converter Connected to a Distribution Network", *Southern African Universities Power Engineering Conference (SAUPEC),* Johannesburg, pp 1-6, February 2015

**PAPER UNDER REVIEW**

[11] **A.S. Akinyemi**, M. Kabeya, and I. E. Davidson, "A Review on Renewable Energy Resources Prospects in Africa continent", submitted to the ***International Journal of Renewable Energy Development.***

[12] **A.S. Akinyemi**, M. Kabeya, and I. E. Davidson, "Dynamic Performance Analysis of STATCOM Response for Network Stability", submitted to the Journal of ***Electric Power Components and system***

# TABLE OF CONTENTS

# LIST OF FIGURES

# LIST OF TABLES

# LIST OF ABBREVIATIONS

| | |
|---|---|
| AC | alternating current |
| ADB | African Development Bank |
| AEC | African Energy Commission |
| AHP | Analytic Hierarchy Process |
| ARAEO | Annual Report of African Economic Outlook |
| AVR | automatic voltage regulator |
| CPU | Central Processing Unit |
| CSI | Current Source Inverter |
| CSIR | Council for Scientific and Industrial Research |
| CSP | Concentrating solar power |
| CTF | Clean Technology Fund |
| DC | Direct Current |
| DC-DC | Direct Current to Direct Current |
| DG | Distributed Generation |
| DN | Distribution Network |
| DUT | Durban University of Technology |
| EMS | energy management system |
| ETCCDI | Climate Change Detection and Indices |
| FACTS | Flexible alternating current transmission system |
| FEWSNET | Famine Early Warning Systems Network |
| FF | Fill Factor |
| FIT | Feed-in Tariff |
| GA | Government Agencies |
| GDP | Gross Domestic Product |

| | |
|---|---|
| GNP | Gross National Product |
| GW | Giga Watt |
| IC | Incremental Conductance |
| IEA | International Energy Agency |
| IESO | Independent Electricity System Operator |
| IGBT | Insulated-Gate Bipolar Transistor |
| IRENA | International Renewable Energy Agency |
| IR | Integra Regulator |
| kW | kilowatt |
| KVA | kilo volt ampere |
| LVUR | Line Voltage Unbalance Rate |
| MATLAB | matrix laboratory |
| MVA | mega volt ampere |
| MV | Medium voltage |
| MW | Megawatt |
| NEMA | National Equipment Manufacturer's Association |
| NERC | National Energy Regulatory Commission |
| PCC | point of common coupling |
| PLL | Phase Lock Loop |
| PPP | Peak Power Point |
| PPPT | Peak Power Point Tracking |
| PV | Photo-Voltaic |
| PU | per unit |
| PVUR | Phase Voltage Unbalance Rate |
| P & OA | Perturb and Observe Algorithm |
| PR | Parasitic Resistances |

| | |
|---|---|
| RDG | Renewable Distributed Generation |
| RE | Renewable Energy |
| RES | Energy Resources |
| RPP | Renewable power plant |
| RES | Renewable Energy Resources |
| SCR | Short circuit ratio |
| STATCOM | Static Compensator |
| SVC | Static Var Compensator |
| SR | Set-Reset |
| SSSC | Static Synchronous Series Compensator |
| T&D | Transmission and distribution |
| TCR | Thyristor-Controlled Reactor |
| TCSC | Thyristor-Controlled Series Capacitor |
| THD | Total Harmonics Distortion |
| TRIAC | Triode for Alternating Current |
| TW | Terawatt |
| UN | United Nations |
| UPS | Uninterrupted Power Supply |
| UPR | Unity Power Factor |
| V | Volt |
| VR | Voltage Régulation |
| VSC | Voltage Source Converter |
| VSI | Voltage Source Inverter |
| W | Watt |
| DSTATCOM | Distribution static compensator |

# TABLE A1: NOMENCLATURE SYMBOL

| | | |
|---|---|---|
| 1 | $P_{load}(t)$ | Load power of time *(t)* |
| 2 | $\Delta t$ | Change in time *(t)* |
| 3 | P(t) | Actual power generated |
| 4 | $PV_{power}(t)$ | Power generated by the PV |
| 5 | $D_{energy}$ | Discharging energy |
| 6 | $\mathcal{E}_{converter}$ | Converter efficiency |
| 7 | $P_{generating\ set}$ | Power of the generator |
| 8 | $P_{dummy\ load}(t)$ | Power of the dummy load |
| 9 | $P_{load}(t)$ | Load power of time *(t)* |
| 10 | $\mathcal{E}_{charging}$ | Charging efficiency of the battery storage |
| 11 | $PV_{power}(t)$ | Power generated by the PV |
| 12 | *P(t)* | Actual power generated |
| 13 | $P_{load}(t)$ | Load power of time (*t*) |
| 14 | $\mathcal{E}_{converter}$ | Converter efficiency |
| 15 | $\Delta t$ | Change in time (*t*) |
| 16 | $\mathcal{E}_{discharging}$ | Discharging efficiency of the battery storage |
| 17 | $C_{energy}$ | Charging energy |
| 18 | $D_{energy}$ | Charging energy |
| 19 | $V_{pv}$ | Solar system output voltage |

| | | |
|---|---|---|
| 20 | $V_{c1}$ | Capacitor voltage |
| 21 | $I_{l1}$ | Inductor current |
| 22 | $C_1$ | The capacitor |
| 23 | $d_1$ | Converter duty cycle |
| 24 | $V_{bat}$ | Battery voltage |
| 25 | $I_{l2}$ | Inductor current of the battery |
| 26 | $V_{c2}$ | Capacitor voltage of the battery |
| 27 | $d_2$ | Converter duty cycle of the battery |
| 28 | $I_d$ | Direct axis current such as active power injected into the system |
| 29 | $I_q$ | Quadrature current such as reactive power injected to the system with respect to the reference $(\mathrm{dq})$ |
| 30 | $V_{dc}$ | Direct current coupling voltage |
| 31 | $m_d \; and \; m_q$ | Converter modulation indices |
| 32 | $\omega$ | Fundamental frequency |
| 33 | $V_d \; and \; V_q$ | Synchronous AC voltage. |
| 34 | $(I_{Gr}^*)$ | Grid reference current |
| 35 | $(I_{LA}, I_{LB})$ | Load current |
| 36 | $(V_{pccAB}, V_{pccBC})$ | PCC line voltage |
| 37 | $(V_{dc})$ | DC link voltage |
| 38 | $(V_{pccA}, V_{pccB}, V_{pccC})$ | PCC phase voltage |

| | | |
|---|---|---|
| 39 | $I_{Gd}^{*}$ | d-axis grid current |
| 40 | $I_{Ld}^{*}$ | d-axis load current |
| 41 | $I_{loss}$ | VSC losses |
| 42 | $I_{PVpcc}$ | Solar power output at PCC |
| 43 | $I_{VRq}$ | Approximated current component that controls PCC voltage |
| 44 | $I_{Lq}^{*}$ | q-axis load current |
| 45 | $V_{\emptyset A}$ | Amplitude of the phase voltage |
| 46 | $e_{VR}$ | Error |

# CHAPTER 1

# INTRODUCTION

## 1.1 Background and motivation

Generation and consumption of electrical energy play a crucial role in the nation's advancement, and per capita consumption of this energy takes the lead among the yardsticks to measure the development and progress of a country. The constant supply of power and easy accessibility can shape the daily lives, ways of life, and fate of any nation's people. Conversely, inadequacy of consistent power quality, can harm a nation's economic and industrial growth [1], [2]. The increase in an advanced society's economic growth is directly proportional to the increase in power consumption demand, with power supply sources primarily derived from fossil fuels. Continuously accessing and processing fossil fuel can cause the climate to change, which has an adverse effect on all living things and which exacerbates global warming. Hence, using alternative energy that is clean and renewable on a human time scale is vital. Consequently, Renewable Energy Resources (RERs) that are deployable in the form of Renewable Distributed Generation (RDG) have gained prestigious attention in the recent years [3], Furthermore, market operations are shifting away from unilateral and centralized decision making and toward more distributed and transactive frameworks in which actors at various levels of the grid hierarchy (ranging from individual energy prosumers to utility companies and system operators) actively participate in energy transactions via interactor value exchanges [4]. Modern electricity systems or smart grids prioritize distributed (dispersed, decentralized) generation (DG) over centralized generation (DG) due to the numerous benefits it has on distribution system (DS) planning and operation [5]. In 2020, renewable energy sources (RES) generated 29 % of global electricity according to studies, this percentage is expected to reach 33 % by 2025 [6]. RDG benefits distribution networks in a variety of ways, including increased reliability, voltage regulation support, and reduced energy losses [7]. The European Council has set a 27 % RER mix target for 2030, to prevent the global change in temperature rising above 2 $^{0}$C. Over 30 countries signed the Paris climate change agreement in 2015 which takes effect from 2020 [8]. In 2019, the worldwide level of installed renewable energy capacity was over 33 %. The International Renewable Energy

Agency (IRENA) report forecasts that renewable energy will grow to 85 % of the total energy capacity in 2050 [9]. Therefore, energy generated from renewable sources can give hope in term of climate sustainability and electricity price consideration as compared to that generated from fossil fuels [10]. The integration of RDGs into the power system is being embraced worldwide due to its energy conservation and greenhouse emission benefits. This has resulted in power system restructuring and deregulation, whereas traditional power systems were intrinsically radial, i.e., power flows in only one direction: from the power plant to the transmission network, to the distribution network, and to the loads.

These flows are traditionally managed through the dispatch of generation and network equipment such as tap-change transformers that can adjust network voltages, i.e., the voltage settings at the last controllable transformer before the loads are often set at 5 – 10 % higher than the nominal end-use voltage to accommodate line losses and voltage drops along the line. These losses and associated voltage drop depend, of course on the actual current flows that are being demanded by the loads. However, the introduction of RDG affects the dynamic of the network because power flows may change significantly and potentially in both directions. In other words, the network becomes an active system with power flows and voltages determined by the mix of centralised power, RDG and as well as the load. Thus, with significant increase in penetration levels of a large RDG, over voltage will occur at PCC. The voltage at the load end would be greater than the feeder supply voltage; this is called voltage rise and can also cause power/current to flow back to the feeder supply side known as reverse power flow. The reverse power flows and voltage rise are worsened when customer demand is at its lowest and RDG supply is at its highest. Such an issue would be critical especially on the long feeders as found in rural areas. The greater the voltage level, the greater the proportion of the investment in the insulation component of the power equipment in the total investment in the equipment. If an insulation accident occurs, it will not only damage valuable equipment and cause massive economic losses, but it will also endanger the personal safety of power workers [11], active power curtailment is suggested in [12], a flexible RDG deployment is presented [13] to reduce overvoltage, optimized algorithm of voltage regulation is employed in [14], RDG locational incremental contribution (LIC) is used to assess a wider range of RDG penetration, concentration, and system reliability in [15]. It is established

in [16] that traditional approaches like switched capacitors cannot provide reactive power that is continuously adjustable at short time scales to regulate the voltage profile to meet the relevant standards. [17] employed automatic overvoltage control strategy to supressed voltage rise while the repeated switching of RDG systems on and off or complete disconnection of RDG from the grid and other methods suggested in [18], [19] in response to voltage rise and the reverse power flow issues could only provide a temporary solution. Consequently, the resultant effects can impose consequent cycling of network voltage control equipment with associated asset life and maintenance impacts, can cause partial/total outages or excessive under voltages at the far end of the DN, damaging online power component, end-use equipment and causing voltage instability [20], [12], [13]. Hence, a permanent solution is required.

This thesis focuses on the following two main problems: − the voltage rise effects and the reverse power flow constraint at the PCC of DN with a large RDG penetration level. The analysis and simulations in the thesis are conducted on an IEEE 13-bus sample model and DUT Steve Biko network with penetration levels of a large RDG (solar farm of 1 MW). The simulations are carried out using MATLAB/Simulink software, while a mathematical model of a distribution grid integrating RDGs is developed for studying the effects of voltage rise and bidirectional flow of power. Furthermore, a control strategy is proposed to be installed at PCCs of the DN to control/mitigate the voltage rise effects and to limit the reverse power flow when operating at a worst critical scenario, such as minimum load and maximum generation from RDGs. The control structure consists of installations of static compensators (STATCOM), which incorporate the Pulse Width Modulation (PWM), the block/deblock and in-loop filtering circuit control scheme at PCC for the control of active and reactive power. The proposed control strategy also mitigates the voltage-current harmonic signals, improves the power factor and voltage stability at PCC, and also protects the converter-PWM scheme from grid disturbances and fault current as the control of active and reactive power is independent of the grid. The increasing share of RDG in the energy mix is expected to operate in its maximum active power capacity in a predetermined duration at a power factor of unity as soon as the PCC's voltage rise and reverse power flow issues are resolved. The proposed solution can be easily implemented by the utility and the independent own power producers at the planning stage of RDG integration and on the existing grid infrastructure.

## 1.2 Problem statement

The operating condition of DN would be vital when considering a large RDG with increasing penetration levels due to the potential voltage rise and reverse power flow threat at PCC. The PCC voltage rises at the critical scenario of low load and peak RDG generation, such that the depth of voltage rise depends on the injection of active and reactive power from the RDG. The bidirectional flow of energy from the RDG as well as the main utility grid causes several difficulties regarding the DN voltage profile, power quality, security, power flow control, energy management, frequency control and protection. Network protection and security when a large RDG is connected to DN has been a significant concern in recent years and needs urgent attention. RDG injects active and reactive power into the grid at the PCC. Thus, the PCC point is more active than other nodes in the system. There is a tendency that the PCC's voltage would be higher than other busbar voltages within the network. The more the PCC becomes an active point due to the increase in the RDG penetration levels, the more of a voltage rise and reverse power flow threat at the PCC there is. The voltage rise beyond the required limit set by the utility will occur at the critical scenario. At this crucial stage, either the RDG is disconnected from the network to avoid damage to other facilities within the system or the voltage rise and the reverse power flow occurrence are regulated to an acceptable range. The unprecedented behaviour of the feeder due to impact of large RDG systems has drawn keen interest from researchers worldwide and has resulted in the development of analytical tools for investigating these impacts so as to develop mitigation measures to curb some of the issues and challenges on distribution feeders.

The various grid codes hitherto prescribe the disconnection of these RDGs to prevent damage to the load, the power system component and the equipment. However, with increased installed RDG capacity and a substantial injection of power to the host grid, the disconnection of high capacity RDG during voltage rise is avoided to forestall potential grid network outages and grid instabilities. As a consequence of the emerging RDGs penetration levels, voltage regulation should be provided at PCC to avoid disconnection as specified in IEEE 1547 and South African grid code requirement. The occurrence of voltage rise, reverse power flow, voltage instability, voltage dips, power factor problem, harmonics and voltage unbalance with a large RDG integration are among the issues

limiting the fully exploitation of RDG integration potentials. These issues are comprehensively investigated in this thesis and remedies are provided. Thus, it is crucial to present an understanding of these issues in a simple form, and to propose a control measure that will be easy, cost-effective, and affordable to mitigate such challenges. The proposed method presented in this thesis will mitigate these issues and remove limitations to the high penetration levels of a large RDG into the power system.

## 1.3 Objectives of the research

The objectives of this thesis are:

- To carry out a state-of-the-art review on the current status of RER prospects, power quality issues and power system compensators.
- To model a distribution network of 13-bus with an integration of a large RDG for the investigation of the effects of voltage rise and reverse power flows at PCC and to develop an appropriate time domain model of DC-AC converter based DN and analysis for the investigation of the impacts of a large RDG integration under critical situation of low demand and peak generation.
- To design an appropriate time domain model of DC-AC converter based with automatic restoration scheme incorporating block/de-block control and filtering circuitry that can switch the converter on/off in the advent of grid fault and reject PCC disturbances.
- To propose a control scheme that can be connected to the developed discrete-time domain model DC-AC based DN and RDG integration for mitigating the effects of voltage rise, reverse power flow, harmonic, power factor correction and fluctuation.
- To develop a control strategy that can reduce tracking time and error signal generated to zero between instantaneous and the incremental conductance during PPP tracking. To minimize output oscillations, ripples and improve the accuracy of both the system's large and small step sizes when the operating level is far from the PPP and for the adaptation of the solar system to the ever-changing climatic

condition.

## 1.4 Research questions

- What are the impacts of renewable distributed generation in rural communities where there is no access to the national grid?
- What are the adverse effects of voltage rise and reverse power flow at the point of common coupling of RDG and DN?
- What approach can be utilized at the point of common of coupling to mitigate voltage rise and river power flow with a high RDG penetration level without disconnecting from the grid?
- What method can be used to minimize tracking error signal generated between the instantaneous and the incremental conductance when accessing the peak power point of solar photovoltaic?
- What strategy can be employed to regulate PVA output oscillations and ripples by the continuous peak power point tracking system of the time domain DC-AC converter with variation in the irradiance, temperature and loads?

## 1.5 Methodology

A cutting-edge literature review was conducted on the current state of RER prospects, power quality issues, voltage rise, reverse power flow and power system compensators. The investigation of the voltage rise mitigation at PCC of a large RDG integration into a distribution network is carried out by modelling a standard test system. A modified IEEE 13-bus test feeder and DUT Steve Biko network were modelled. Both networks are designed in MATLAB/SIMULINK environment by considering the following:

- To develop time domain converter-based distribution system with IEEE 13 bus system and integration of RDG to investigate the effect of voltage rise and reverse power flow impact on the PCC.
- To develop time domain converter-based distribution system with IEEE 13 bus system and integration of RDG to mitigate voltage rise and reverse power flow at the PCC.

- To develop an algorithm that can reduce tracking error while accessing peak power point of solar photovoltaic.
- To develop time domain converter-based distribution system with DUT network and track peak power point of solar photovoltaic system under varying load, sun's irradiation fluctuation and changing temperature condition thereby maintaining constant output voltage/power and reduce oscillation.
- To design an automatic block and de-blocking restoration control scheme for controlling the grid converter switching mechanism thereby preventing the grid component from fault current/grid fault and voltage rise

## 1.6 Scope of the Research

System modelling and analysis are crucial to investigating how the designed DC-AC system, a large RDG and DN respond to voltage rise at PCC, among other issues. This is significant for analysis, design, and authentication. Thus, the time-domain models of grid regulation systems are developed from the typical grid supporting systems. This is achieved by measuring the active and the reactive power injected into the grid by the voltage source converter STATCOM to determine the output voltage amplitude and frequency according to the measured values. Counter-wise, the grid-supporting current source converter measures the voltage amplitude and frequency, in order to inject a desired amount of active and the reactive power accordingly.

The reactive power injection is vital for the grid voltage rise attenuation, and the droop controllers make the frequency of the converter deviate from the nominal value in case there is a mismatch between the measured electrical output power and its nominal value. The converter is self-regulating, which can synchronize the grid frequency. Furthermore, the power injection of the source is shared according to the droop coefficients, which is proportional to the assigned nominal power values.

This research work concentrates on implementing a regulation scheme with PCC's voltage rise, a simple and quick method of control for eliminating the challenge of a large RDG integration with high penetration levels, management, power quality of DN and the load. The compensator device is capable of injecting electrical power dynamically while

following the frequency of the grid, and the voltage source converter of the STATCOM with PWM control scheme injects active and reactive currents according to the rotating frame of the grid voltage at the PCC. The converter interface running in the grid supporting mode can thus achieve voltage rise attenuation at PCC while contributing to the main grid voltage and frequency regulation. Furthermore, in the advent of grid fault, block/de-block control strategy is proposed for the converter to automatically block any grid fault current that can affect the device and the power equipment connected to PCC.

Furthermore, the purpose of the voltage regulation scheme developed in this work is to prevent the grid supporting RDGs from further inducing a reverse power flow in the occurrence voltage rise, ultimately leading to power generation damage. However, there is an insignificant voltage rise contribution from a small RDG based system. Thus, the extensive RDG integration, for instance, negatively impacts overall grid reverse power flow during voltage rise. Consequently, a large number of RDGs are controlled with the utmost flexibility to forestall shut down and subsequent disconnection due to over voltage protection activation.

This research work focused on the PCC voltage regulation with a large RDG integration into the DN. RDGs are primarily power-electronic dependent for energy conversion as compared to a typical conventional power generator. Therefore, there is non-existence of significant inertia in the converter-based systems, especially in solar systems. The power electronic conversion systems possess the advantage of fast control response capability; voltage rise is sensed at the PCC, and the capability to supress such occurrence is utilized in this work. Thus, unwanted reverse power flow to the substation is adequately controlled with the proposed PCC regulation scheme. Similarly, the block/de-block control strategy proposed for the converter based RDG in this work is carried out with the assumption of automatically blocking the fault current from the grid to the converter and power equipment connected to the PCC.

### 1.7 Research Contribution to knowledge

The contributions of the research work carried out in this thesis can be summarised as follows:

- Provision of mathematical model and the analysis approach of PCC's voltage rise with RDG integration to the DN is developed. The aim is to have the foreknowledge of the extent of the effects of voltage rise and the reverse power flow cause by the high penetration levels of RDG integration on the power systems to provide a deterministic approach for DSO and IPPs in carrying out a preventive measure during planning and integration of RDG into the DN.
- A voltage regulation approach has been proposed for the PCC with a large RDG connection. This control approach can be adapted to PCC of DN systems since it can handle the voltage rise, reverse power flow and any uncertainties that can occur with a large RDG integration. The aim is to achieve active, and the reactive power injected to the PCC by the voltage source converter (STATCOM) and determine the output voltage amplitude and frequency according to the measured values. Counter-wise, a grid-supporting voltage source converter measures voltage amplitude and frequency to inject a desired amount of active and the reactive power accordingly. The reactive power injection is vital for the PCC voltage rise attenuation, the droop controllers cause the frequency of the converter to deviate from the nominal value in case there is a mismatch between the measured electrical output power and its nominal value. The converter is self-regulating which can synchronize the grid frequency.
- Based on the voltage rise regulation approach at the PCC, a block/de-block control scheme has been proposed for the PCC converter. The aim is to protect the converter from the grid fault current. The block/de-block module comprises 4 input and 2 output, where the first input is the state of opening the grid circuit breaker when the state is low or zero, the second input is the event to de-block the converter after the closing of the circuit breaker by the AND gate. The third input is the event to block the converter when it receives an unwanted signal such as over-voltage or a fault current which will reset the set-reset trigger, and the Q input will go to zero or low state thereby opening the circuit breaker. The reset input resets the device to its original state with an output Q which will be either at high level 1 or low level 0 depending on the set/reset condition.
- An improved incremental conductance with integral regulator strategy is proposed. The aim is to obtain a perfect efficiency and time reduction in tracking PPP of

PVAs. The error signal generated at PPP during instantaneous conductance and the incremental conductance is reduced to zero by the application of proportional integral strategy which is used to derive the error signal (*e*) to zero. When the proportional integral regulator is added to the incremental conductance, there will be a reduction in the output oscillation resulting in a better digital resolution of the output, perfect control and adaptation of the solar system to the ever-changing climatic condition, thus, the system efficiency is improved. A proportional integral controller improves the precision of both the system's large step sizes when the operational level is far from the PPP and when the small step sizes of PPP is reached to extract the maximum possible level of power. The application of addition control strategy (integral controller) to the PPP of the solar system minimizes the error $\left(\frac{dI}{dV}+\frac{I}{V}\right)$ between the instantaneous conductance and the incremental conductance, reduces ripple and improves the accuracy of both the system's large and small step sizes when the operating level is far from the PPP or when reached to harness the uppermost possible level of power. Thereby, the regulator output will be equal to duty cycle correction. When error $\left(\frac{dI}{dV}+\frac{I}{V}\right)$ is minimized, the regulator output = Duty cycle correction.

- Designed in-loop filtering algorithm is provided to detect any unwanted harmonics signal at the PCC. The aim is to filter any form of unwanted disturbance/distortion or unbalance signals from the load current and phase voltage at the PCC where their components are approximated before the approximation of the reference grid current. The filtering stages of the control is of an in-loop type which has a super harmonic rejection capability. The current that flows across the loads and the phase voltage at the PCC are transformed to stationary reference frame control known as αβ-control. It regulates control signals in stationary two-phase frame $(I_{L\alpha})$, $(I_{L\beta})$ and $(V_{pcc\alpha})$, $(V_{pcc\beta})$. Any unwanted signals generated from the PCC are suppressed by the filtering circuit while the approximated quadrature components and undistorted in-phase signal are$(I^*_{L\alpha p})$, $(I^*_{L\beta p})$, $(V^*_{pcc\alpha p})$ and $(V^*_{pcc\beta p})$ of $(I_{L\alpha})$, $(I_{L\beta})$ and $(V^*_{pcc\alpha})$, $(V^*_{pcc\beta})$. In the same way, $(I^*_{L\alpha q})$, $(I^*_{L\beta q})$ and $(V^*_{pcc\alpha q})$, $(V^*_{pcc\beta q})$ are undistorted quadrature of $(I_{L\alpha})$, $(I_{L\beta})$ and $(V_{pcc\alpha})$, $(V_{pcc\beta})$.

- The boost DC-DC, DC-AC converters and the grid voltage are regulated during loads fluctuation and solar irradiance variations while constant supply is maintained to the grid. Grid voltage stability is achieved with PPPT system during variable load, solar irradiance variation, and the changing temperature.

## 1.8 Outline of the Thesis

The thesis is organised as follows:

***Chapter one*** gives the background, objectives, methodology, contributions to knowledge, scope, and the outline of the thesis.

***Chapter two*** assesses the major renewable energy sources. How these renewable energy resources can cheaply be deployed, the reasons for agitation of renewable energy integration into Africa energy mix and the challenges of the cost of renewable energy in Africa are also enumerated. A comprehensive state-of-the-art- power system compensator, power quality, the importance of power quality, classification, types, causes of power quality, parameters of power quality, how voltage, current and power quality are related, possible solutions to power quality issues, power quality issues on the utility, the grid, and the load side, electrical load classifications, types, and how the power quality can be sustained in power system are detailed.

***Chapter three*** discusses RDG technology, the relationship between RDG and smart grids, RDG deployment, microgrid system, classification and types, off-grid microgrids, grid tie microgrids, microgrid backbone, microgrid controls, microgrid energy management, converter building blocks, types, advantages and disadvantages of RDG.

***Chapter four*** presents power system design and RDG distribution network modelling with mathematical analysis of voltage rise, test system description, test system simulation without/with RDG integration, voltage rise concept, impacts of RDG on distribution network, RDG integration and voltage rise at PCC, and the voltage rise compensation with RDG integration.

***Chapter five*** investigates the compensation strategy, voltage rise regulation at PCC, compensator mathematical analysis with RDG integration, compensator connection

model, dynamic response and modelling of static compensator, regulatory capability of static compensator, voltage rise mitigation at PCC with static compensator, response of static compensator during fault conditions, and simulation comparison between static compensator and static volt-ampere reactive compensator.

***Chapter six*** investigates the voltage rise regulation with a grid connected Solar Photo-voltaic systems, solar systems, solar and battery modelling, factors affecting solar array performance, energy management and solar power tracking are adequately discussed. Design and simulation of a proposed microgrid for DUT, control strategy, load variation under PV system, effect of PV variation on a system, and grid behaviours during static compensator's UPF and VR mode are analysed.

***Chapter seven*** investigates grid voltage regulation under varying solar irradiation. It explores the solar tracking algorithms, perturb and observe strategy, incremental conductance, improved incremental conductance with integral regulator to track peak power point of solar system, modelling of a boost converter, proposed converter restoration scheme, and converter block/de-block scheme.

***Chapter eight*** provides conclusions and recommendations for future work.

# CHAPTER 2

# LITERATURE REVIEW

## 2.1 Introduction

Chapter 2 presents renewable energy resources, advantages, disadvantages, the reasons why there is worldwide agitation for a renewable energy resource and the benefits of renewable energy generation. A review of similar works of literature on the state of the art of power system compensators, design, analysis, types, and applications are detailed. The chapter explores the power quality concept, classification of power quality, causes of poor power quality, the grid occurrences, voltage rise and reverse power flow, the relationship between the utility, the grid and the loads. In addition, the power quality versus voltage, the classification of various electrical loads, the theoretical framework of power quality in relation to the voltage, current and the loads are also enumerated. In summary, the work presents a review of similar works of literature. The contributions of this review are manifold:

- It proposes future research goals on the development of renewable energy resources to reduce greenhouse emissions, to improve access to power in rural communities across the continent, and to provide methods enabling continents to link their goal with renewable energy trade options in the energy markets to boost the continent's power system reliability and stability.
- It reveals the trend of power system compensators and application.
- It provides the details required for an understanding of power quality concept, as well as the relationship between power quality, voltage quality and current quality in a distribution network.

## 2.2 Renewable Energy Resource

Generation and consumption of electrical energy play a crucial role in a nation's advancement, and per capita consumption of this energy takes the lead among the yardsticks to measure the development and progress of a country. The constant supply

of power and ease of access can shape the daily living, way of life and fate of the people of any nation. Conversely, inadequacy of constant power quality can be a detriment to the economic and industrial growth of a nation [1], [2]. The increase in the economic growth of an advanced society is directly proportional to power consumption demand and the power supply sources being largely from fossil fuels. Continuously accessing and processing fossil fuel can cause the climate to change and the adverse effect on plants and living things can be disastrous. It also exacerbates global warming. Hence, alternative energy that is clean and renewable on a human time scale is vital. Consequently, Renewable Energy Resources (RES) and Renewable Distributed Generation (RDG) have gained prestigious attention in the recent years [3], [21], [22], [23], [24], [8]. An energy mix of 27% is targeted by the European Council in 2030, to prevent global temperature from increasing more than $2^0$C. More than 30 countries subscribed to the Paris climate change agreement in 2015 that takes effect from 2020. More than 33% of the world's installed energy was renewable in 2019. Based on the forecast of International Renewable Energy Agency (IRENA) report, renewable energy will grow to 85% of the total energy in 2050. Therefore, energy generated from renewable sources can give hope in terms of climate sustainability and electricity price consideration as compared to fossil fuels [9], [10], [20]. Since the RES is being embraced worldwide due to its energy conservation and greenhouse emission benefits. Hence, it is anticipated that the RES will play a crucial role in the future power supply. For example, the cumulative global capacity of renewable electricity increased from 2,181 GW to 2,355 GW between 2017 and 2018. In 2018, renewable electricity accounted for 20.5 percent of total electricity capacity and 17.6 percent of total annual generation in the United States. Annual renewable capacity additions increased by 45 percent to nearly 280 GW in 2020, the largest year-on-year increase since 1999. Solar PV capacity additions are expected to reach 162 GW by 2022, indicating a nearly 50% increase over the pre-pandemic level of 2019 [25].

Because of advancements in renewable technologies and lower-cost costs, the green revolution to construct an energy system, the transition to net-zero greenhouse gas emissions is happening faster than expected. Renewable Energy Resources can be described as any form of energy from solar, geophysical, or biological sources that are replenished by natural processes at a rate that equals or exceeds its rate of use [26]. It is

obtained from the persistent flows of energy occurring in the natural environment such as Wave, Tidal, Geothermal, Biomass, Hydro, Wind, and Solar energy [27]. Therefore, various renewable energy sources are described below.

### 2.2.1 Wave energy

Wave energy is one of the types of renewable energy sources that is produced from capturing wind waves or air gusting across the sea surface. It occurs in the form of wind circulation on the surface of the sea, which creates a divergent strain and exerts force on the sea surface resulting in a moving wave. This moving wave is used to drive a turbine or generator to produce electrical power [28]. Wind wave is shown in Figure 2.1, which can be trapped and used as a prime mover to drive an alternator where mechanical energy is converted to electrical power.

***Advantages****:* It is a renewable source of energy that produces no harmful effect in the atmosphere and environment such as poisonous gas, waste or pollution that can cause heat and global warming. The source is replenished which means it can never dry up as waves will always be booming and crashing around the seashore or coastal area. It is clean.

***Disadvantages:*** Wave energy is not so common everywhere, it is stochastic in nature since a wave is associated with wind streams, therefore, it is not stable. A site is needed where the wave is prominent and strong to harness. The wave is usually propagated to the seashore, and so its stability in energy generation may be more complex due to the hydrodynamic nature of the airstream. The technology development faces challenges from the fact that ocean environment (especially in offshore) is uncertain [29], [30]. The maintenance and operation are hectic and challenging due to the violence of sea wave which can destroy the wave equipment.

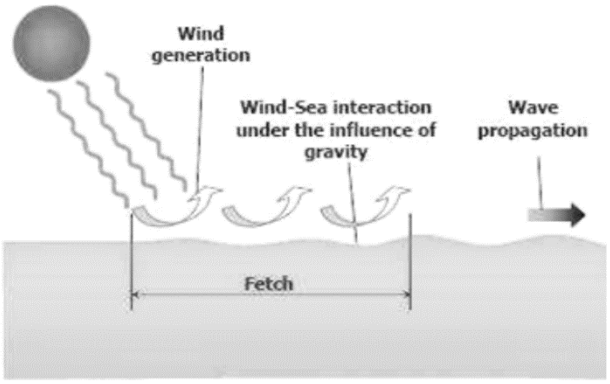


**Figure 2.1:** Wave Energy [31].

### 2.2.2 Tidal energy

Tidal energy can be described as the form of a renewable energy source that is produced from the rising and falling of the sea level, which occurs due to the collective effect of gravitational force from the sun, moon, and the revolution of the earth. The Moon is the main tide-generating body. Due to its greater distance, the Sun's effect is only 46% of the Moon's [32]. Renewable energy from the tide is obtained by the surge of the ocean rising and falling. The kinetic energy of the change in the flow of the tide is used to drive a turbine connected to an alternator and the energy from the moving fluid is extracted to produce electrical power. The change in the sun and the moon's position with respect to the Earth, the rotation of the Earth, its effect, the geography of the sea's coastline and floor all determine the magnitude of the tide at a location. Electricity is generated from the tidal zone when tides come in and go out. The turbine is driven by the power of the sea in both directions as shown in Figure 2.2.

**Figure 2.2:** Tidal Energy [33].

Electrical power can be generated directly from the tidal energy source in two ways. Firstly, through the water level difference between the low and high tide, and secondly

through the tidal currents obtained by the energy of water flows. Both ways make use of tidal range and stream devices. The tidal stream method is more popular than the tidal range method because the cost of installation is cheap, it is more efficient at larger scales and there is a reduction in ecological and environmental effects. Therefore, it receives more research attention from industry, government and institutions [34], [35], [36]. The tide source is inexhaustible thereby is regarded as a renewable energy.

***Advantages:*** It is less vulnerable to climate change unlike conventional sources that are all vulnerable to the random changes in climate. Tides are predictable but not active 24 hours, and do not require any fuel. Tidal power plants last longer, say 100 years and there is no production of gas and pollution involved [36] .

***Disadvantages:*** The initial capital construction cost is high, it is available in a small number of regions, and it can displace wildlife habitats. It can alter ecosystems. Tides are not active 24 hours

### 2.2.3 Geothermal energy

Geothermal energy is the energy generated from the heat inside the Earth's crust. Geo means Earth while thermal is something related to heat. Geothermal energy is the energy obtained mainly from the Earth's internal heat as shown in Figure 2.3. Although, the sun heats the Earth's surface, the heat inside the Earth's crust is not as a result of the heat from the sun. The heat inside the Earth's crust is because of natural decay of radioactive isotopes of Potassium, Uranium and Thorium inside the crust. The rock present inside the Earth is extremely hot. The heat formation of the rock is a result of the fission of these radioactive materials, thereby stored inside the Earth and flowing constantly. The heat can be accessed by using water to absorb the heat. The heated water forms steam, the transformation of water to a steam at higher pressure produces hot springs and transports it to the surface of the Earth to provide geothermal power. The hot steam is produced in such a way that two holes are dug deep into the earth's crust and cold water is pumped through the first one while steam comes out from the second through a very long pipe which can be used to generate electrical power.

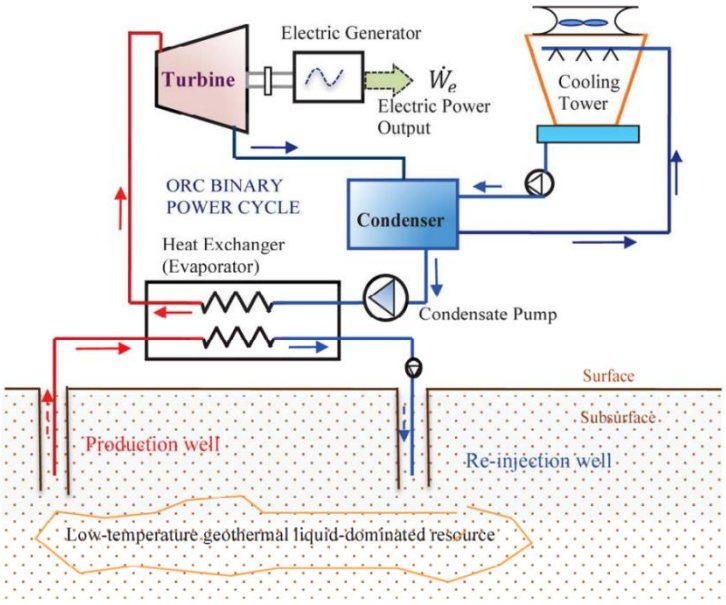


**Figure 2.3:** Geothermal Energy [37].

The stored and generated heat in the Earth's crust is unlimited and it is independent of weather conditions. Geothermal power uses the Earth's internal heat which comes from a combination of residual heat from planetary accretion (about 20%) and heat produced through radioactive decay (80%) [38], however, power deployment of this technology may face challenges [39].

***Advantages:*** It has a low maintenance cost, and the generator does not occupy a lot of space. It does not depend on weather conditions; and the energy produced from geothermal energy can be used directly to heat houses and cooking. It is environmentally friendly, clean and there is no wastage or generation of by-products.

***Disadvantages:*** A higher installation cost, the danger of volcanic eruptions, few sites have the potential of Geothermal Energy and easy rusting of steam water pipes.

### 2.2.4 Biomass

Biomass is a type of renewable energy source that is produced by living plants and animals. This includes waste such as wood, agricultural products, solid waste, scraps, logs, chips, bark, manure, garbage and sawdust as depicted in Figure 2.4. So far as trees, crops and wastes exist, biomass will always be a renewable energy source. This is

demonstrated in Figure 2.4, where plants take in water through their roots, carbon dioxide through their leaves and radiant energy from the sun by the process known as photosynthesis to produce glucose and oxygen (6H20 + 6CO2 + Radiant energy = C6H12O6 + 6O2).

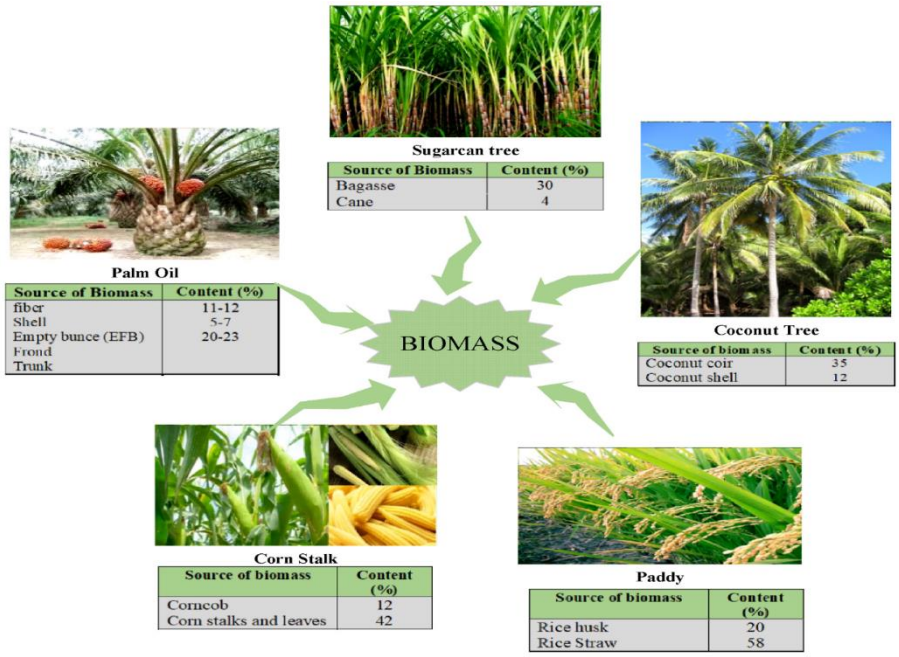


**Figure 2.4:** Biomass Energy [40].

When these materials are burnt through the process known as Torrefaction, chemical energy in biomass is released as heat. The carbon dioxide and water contained in plants and animals are released back into the atmosphere when they are burned (re-absorb carbon) so it is regarded as a renewable energy source. Fossil fuel cannot re-absorb carbon. Biomass contains energy first derived from the sun. Plants absorb the sun's energy through photosynthesis and convert carbon dioxide and water into nutrients (carbohydrates). Biomass is the only renewable energy source that can be converted into liquid biofuels such as ethanol and biodiesel. Examples of biofuel crops are switchgrass, wheat, sunflower, cottonseed oil, soy, jatropha, palm oil, sugar cane, canola, corn. Ethanol is made by fermenting biomass that is high in carbohydrates, such as sugar cane, wheat, or corn. Biodiesel is made from combining ethanol with animal fat, recycled cooking fat, or vegetable oil.

***Advantages:*** Biomass feedstocks, such as switchgrass, can be harvested on marginal lands or pastures, where they do not compete with food crops. Biomass is a clean, renewable energy source. Its initial energy comes from the sun, and plants or algae. Biomass can regrow in a relatively short amount of time, and it can also be used to power vehicles.

***Disadvantages:*** Most biomass requires arable land to develop. This means that land used for biofuel crops such as corn and soybeans is unavailable to grow food or provide natural habitats. Most biomass plants require fossil fuels to be economically efficient. Biomass has a lower “energy density” than fossil fuels. As much as 50% of biomass is water, which is lost in the energy conversion process. Burning biomass releases carbon monoxide, carbon dioxide, nitrogen oxides, and other pollutants and particulates. If these pollutants are not captured and recycled, burning biomass can create smog and even exceed the number of pollutants released by fossil fuels.

### 2.2.5 Hydroelectric power

Hydroelectric power is the renewable energy source that makes use of waterpower in motion as shown in Figure 2.5. The process of converting the kinetic energy of a moving body of water to drive a turbine couple to an alternator and generate electricity is known as hydroelectric power.

***Advantages:*** It has the lowest operating costs and longer plant life; water is renewable and is not subject to fluctuations in the market. It does not pollute the air. Impoundment of hydropower creates reservoirs that offer a variety of recreational opportunities. Hydroelectric power systems have good ramping capabilities and energy storage possibility in the form of hydro reservoirs, The advantage of hydroelectric power is its low generating cost and short initiating time [41], [42].

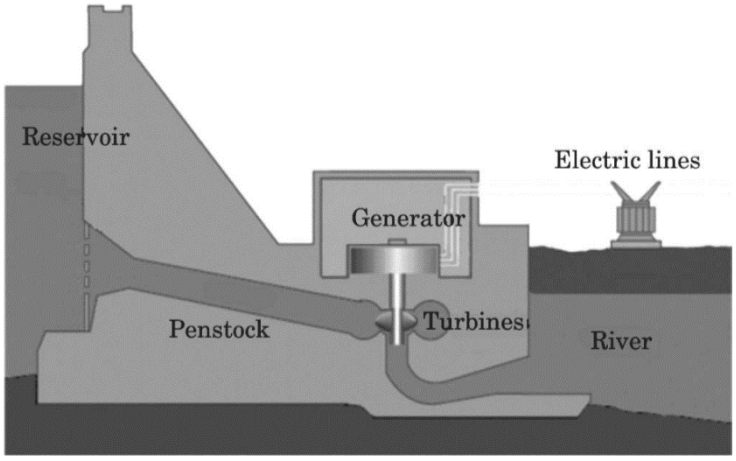


**Figure 2.5:** Hydroelectric Energy [43].

***Disadvantages:*** Fish populations can be impacted regardless of location, large-scale hydro generation is affected by increasing concerns about its environmental effects, capital costs, and long development times [44]. Fish cannot migrate upstream past impoundment dams to spawning grounds or they cannot migrate downstream to the ocean. Hydropower can impact water quality and flow.

### 2.2.6 Wind Energy

Wind energy is one of the types of renewable energy sources that makes use of wind flow to drive a turbine connected to an alternator to generate electricity. The kinetic energy in the wind is such that it translates the aerodynamic force of wind rotations or turns two or three propeller blades around a rotor as depicted in Figure 2.6. The rotor is connected to the main shaft, which rotates a generator to produce electrical power. Wind is produced by uneven heating of the earth's surface by the sun. The hot air rises and cool air flows in to take its place and the air moves to a low-pressure area from high pressure areas.

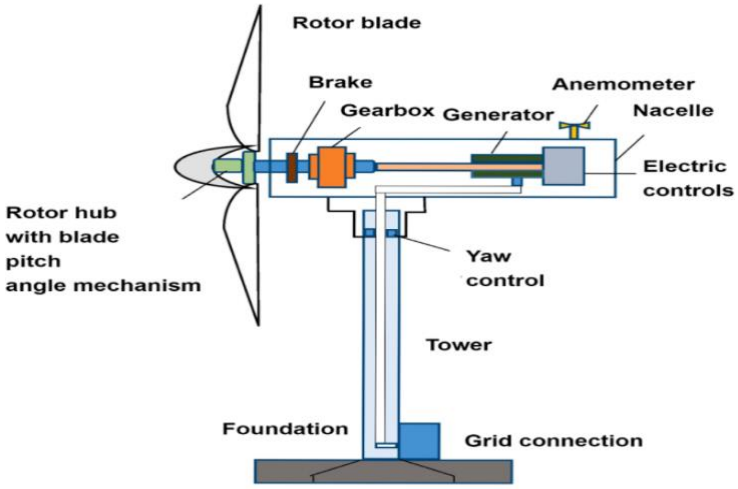


**Figure 2.6:** Wind Energy [45].

***Advantages:*** Wind energy does not create air pollution, it is a clean source of energy, having no atmospheric emissions. It can be built on existing farmland. It does not contaminate water or generate waste. It is inexhaustible. It has a lower operating cost once a turbine is erected. Wind energy is not only a favourable electricity generation technology that reduces emissions (of other pollutants as well as CO2, SO2 and NOx), it also avoids the high external costs associated with conventional fossil fuel-based electricity generation [46].

***Disadvantages:*** Wind fluctuates, which can affect the power output of the generator that generates the electricity. Initial capital and installation to set up wind farm is expensive. Wind turbines pose a threat to birds and can cause noise pollution. Wind power variations are hard to predict with high accuracy [47].

### 2.2.7 Solar Energy

Solar energy is one of the renewable energies that is derived from the radiation of the sun. Solar energy can be harnessed in two forms, that is photovoltaic and solar thermal [48]. A photovoltaic process occurs when photons produced from the radiation of the sun are collected by an array of cells called photovoltaic cells to generate electricity as shown in Figure 2.7.

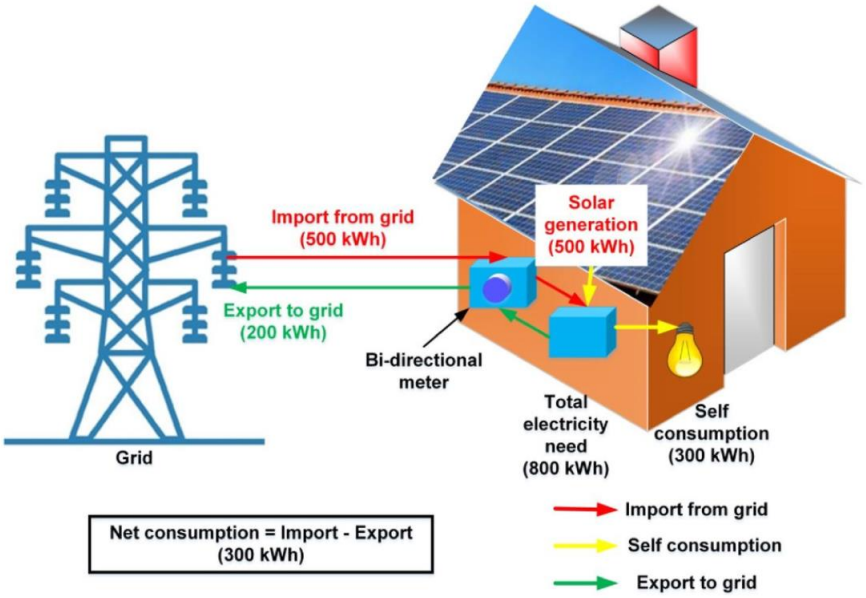


**Figure 2.7:** Solar Energy [49].

This process is known as the photovoltaic effect. It occurs when sunlight hits a semiconductor material (usually silicon) and knocks electrons loose from atoms, setting them in motion to generate an electric current. Solar thermal captures heat from the sun. A solar cell may be Monocrystalline which means it is cut from silicon, or polycrystalline which it is cut from many smaller crystals. There is also solar power made by amorphous or thin-film solar cells.

***Advantages:*** Solar energy is a renewable source that makes use of sunlight as fuel in generating electricity. It has low maintenance costs, it is abundant, cheap and clean. No air pollution, water pollution, or greenhouse gases are associated with the production of solar energy.

***Disadvantages:*** The sun does not shine 24 hours a day. At night and in shade solar panels can stop generating electricity, therefore it is weather dependent.

### 2.3. Why a worldwide need for Renewable Energy?

Generally, fossil fuels are used for multipurpose in everyday living such as heating and powering our homes, fuelling our vehicles etc., because of their abundant availability. Nevertheless, these fossil fuels are being consumed more rapidly than they are being created. Eventually, they will not be sufficient to meet the world's need, or they will run

out one day because there is an increase in the energy demanded by the world population on a daily basis. Hence, it is a necessity to provide a method that can meet up with this energy growth to avoid crises. According to world energy forecasted in [50], world energy consumption will keep on increasing more than it is being produced now. Convectional method of electricity generation is mostly from fossil fuel, petrol, diesel, nuclear, gas, and coal fired plants. The risk of the fossil lies not in the use, but the unpalatable effects they create after usage. Fossil fuels are not sustainable, as their method and processes are non-renewable energy sources. Apart from the fact that these sources are depleted, they will also run dry one day. They can also generate CO2, NOx, and Sox emissions which are harmful to the environment and can contribute to global warming, and temperature increase resulting in the melting of ice in the Arctic and Antarctica causing an abnormal rise in sea level, which in turn leads to floods affecting life and property across the world [51], [52]. Since this conventional method has a tendency to produce a more harmful effect in their cycles and processes while generating electricity, there is a need to look for an alternative source of generating electricity that will be a renewable source on a human timescale and that can produce little or no harmful effect on the environment from their cycles and processes. At least if electricity generation by the conventional methods is not totally neglected, the energy mix should be encouraged to minimize the harmful effect and a source of energy that cannot be depleted. Modern economies need long-term energy security that will be available, sufficient, and uninterrupted at an avoidable price for domestic power, industrial power and transport. Most vehicles are running on petrol, diesel and oil, which are all extracted from fossil fuel. The source will become depleted one day, and the vehicle industry must find new source of energy such as hybrid systems, or a total renewable system to continue the functioning of the business. There is a need for all the countries of the world to diversify their energy production to reduce dependence on fossil fuel.

### 2.4. Benefits of Renewable Energy Generation

***Environmental benefits***: The conventional power system makes use of fossil fuels and oil; they are thereby environmentally unsustainable because they are based on exhausting resources. Such resource extraction, exhaustion and transportation can result in greenhouse gas emissions, leading to global warming. The RDGs are environmentally sustainable since they make use of renewable energy sources, thereby resulting in a reduced and improved environmental influence as compared to the extraction, conversion and delivery of conventional methods that use fossil fuels. Renewable energy resources are considered clean energy resources and are critically important due to their environmentally friendly nature. With the increase in awareness of a clean environment, it is believed that traditional dependence on fossil fuels has led to carbon dioxide (CO2) emissions, greenhouse gas problems and environmental pollution [53], [54], [55], [30], [56].

***Economic benefits***: RDG systems could simply survive with individual failures, because each consumer connected to an electrical node may be serviced by multiple RDG units as compared to the conventional method of power generation, where a fault in the system can affect the electrical power in the whole system. A sole proprietor can manage a RDG unit for power generation, such that electrical power can be generated by him and be

consumed by the same person otherwise known as prosumer i.e., producer and consumer. Moreover, a RDG can be connected to a micro and main grid. With the fast expansion of RDG in the power system, more rural communities will have access to electrical power in the near future.

## 2.5 Compensators

A compensator is a component or device that can be used to regulate another system, usually to correct or offset some disturbing action in a system or network. Most of the time, it is done by conditioning the input or the output to that system. The common compensators in the power system are referred to as Passive shunt and series compensators [57]. They have been used to improve the power quality of the power system by enhancing the efficiency and utilization of equipment in transmission and distribution networks. They comprise lossless reactive elements such as capacitors and inductors with and without switching devices. The passive compensators are used for improving the transient, steady state, and dynamic, voltage and angle stabilities. Moreover, these also help in reducing losses, enhancing the loadability, improving transmission capacity, damping power system oscillations, and mitigating sub synchronous resonance (SSR) and other contingency problems in transmission systems [58]. The passive shunt and series compensators are also extensively used in distribution systems for improving the voltage profile at the point of common coupling (PCC), reducing losses, power factor correction (PFC), load balancing, neutral current compensation and for better utilization of distribution equipment [59]. Ideally, the passive compensators can supply or absorb variable or fixed reactive power locally to mitigate the power quality problems. This section focuses on the review of the concepts and methodologies of passive shunt and series compensators in distribution systems.

### 2.5.1 Passive Shunt and Series Compensators

Passive compensation has become an established technology to provide reactive power compensation for power factor correction and/or voltage regulation, load balancing, and reduction of neutral current in AC networks. It has evolved during the past century with development in varying configurations and requirements. Passive compensators are used for regulating the terminal voltage, suppressing voltage flicker, improving voltage balance, power factor correction, load balancing and neutral current mitigation in three-

phase distribution systems [60], [61]. These aims are accomplished either individually or in combination, depending upon the necessities and configurations that need to be selected appropriately. The reactive power compensation employing lossless passive components in a distribution system has been used in practice for a long time for improving the voltage profile at the load end by the utilities and enhancing the power factor in the industries for avoiding the penalty by the utilities [62]. In the early twentieth century, Steinmetz discovered that an unbalanced single-phase resistive load may be realized as a balanced load using lossless passive elements in a three-phase supply system [63]. This concept was later extended in many directions such as balancing three-phase unbalanced loads, power factor correction at the supply system, compensation of of negative-sequence and zero-sequence currents, and voltage regulation. It has become quite important because in practice there are many single-phase and unbalanced loads such as traction, metros, furnaces, residential, and commercial loads. There are many methods to implement these compensators in practice for improving power quality, especially voltage quality, for the consumers nearby the fluctuating loads, such as arc furnaces. Since these compensators are simple, cost effective, and easily realizable in practice, they are still used in large power rating.

### 2.5.2 Passive Shunt and Series Compensators Classification

Passive compensators can be classified based on the topology and the number of phases. The topology can be shunt, series, or a combination of both. The other classification is based on the number of phases, such as two-wire (single-phase) and three or four-wire (three-phase) systems [64].

***Topology Based Classification:*** The passive compensators can be classified based on the topology, for example, series, shunt, or hybrid compensators. Figure 2.18 shows the examples of basic series, shunt, and hybrid compensators.

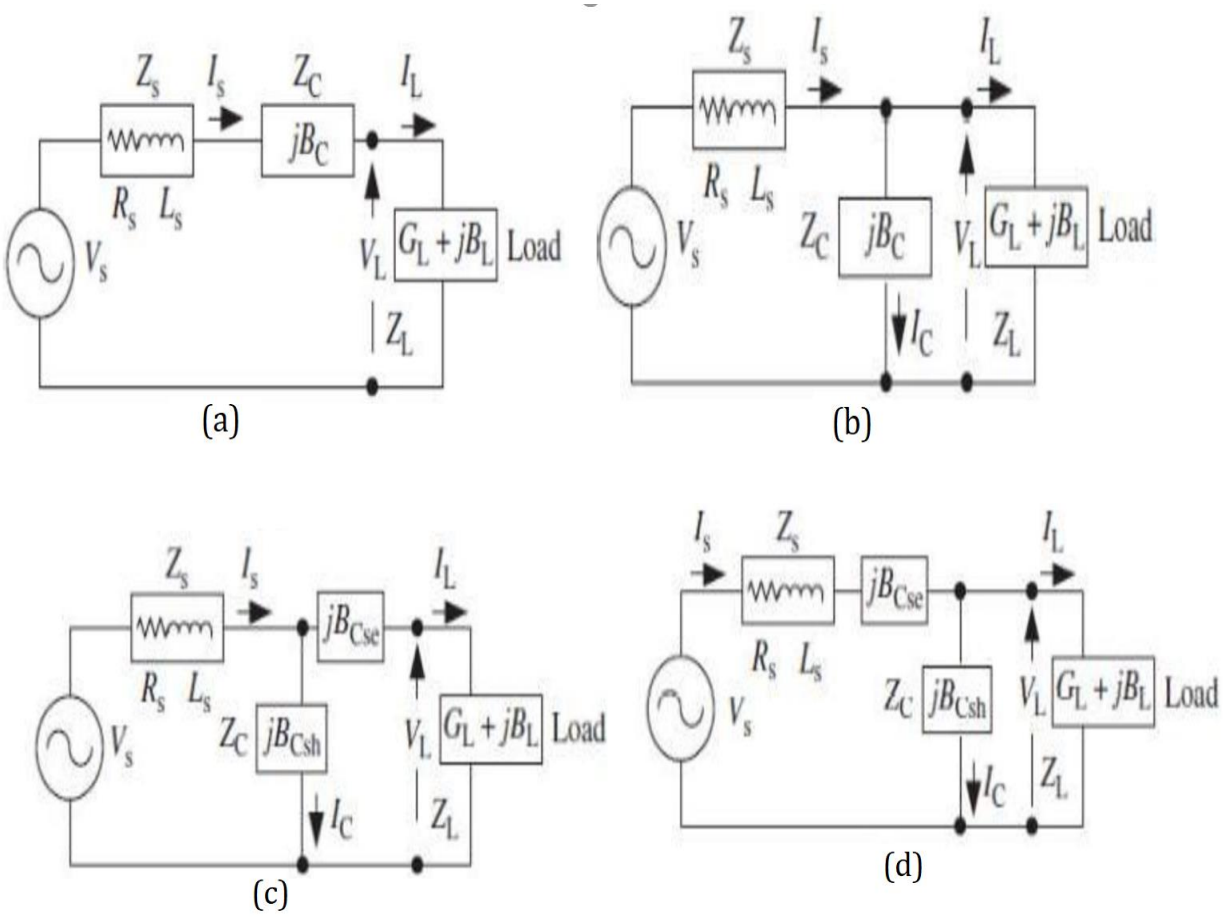


**Figure 2.18:** Load compensation using (a) a series compensator (b) a shunt compensator(c) a short-shunt hybrid compensator (d) a long-shunt hybrid compensator.

Passive series compensators have limited applications in the distribution systems as they affect the performance of the loads to a great extent and have resonance problems. The passive series compensators are used in transmission systems to improve power transfer capability, of course with restricted capacity to avoid series resonance. The passive series compensators are also used in stand-alone self-excited induction generators for improving the voltage profile and enhancing stability. In the majority of cases, mainly shunt compensators are used in practice as they are connected in parallel to the loads and do not disturb their operation [65]. These are mainly used at the load end. So, current-based compensation is used at the load end. These inject equal compensating currents, opposite in phase, to cancel reactive power components of the load current for power factor correction at the point of connection. The passive shunt compensators are also used for voltage regulation and load balancing at the load end. These are also used as

static VAR generators in the power system network for stabilizing and improving the voltage profile [66]. The passive hybrid compensators shown in Figure 2.18 (c-d) as combinations of passive series and shunt elements in both short-shunt and long-shunt configurations are used in stand-alone self-excited induction generators for improving the voltage profile and enhancing the stability.

***Supply System-Based Classification:*** Mainly passive shunt compensators are used in the distribution system for reactive power compensation and load balancing, so these are studied in detail here. This classification of passive compensators is based on the supply and/or the load systems having single-phase (two-wire) and three-phase (three-wire and four-wire) systems. There are many varying loads such as domestic appliances connected to single-phase supply systems. Some three-phase unbalanced loads are without neutral terminal, such as AC motors, traction, metros, and furnaces fed from three-phase three-wire supply systems. There are many other single-phase loads distributed on three-phase four-wire supply systems, such as heating and lighting systems, among others. Hence, passive compensators may also be classified as single-phase two-wire, three-phase three-wire, and three-phase four-wire passive shunt compensators.

***Two-Wire Passive Compensators:*** Single-phase two-wire passive compensators are used in all three modes, that is, series, shunt and a combination of both. Figure 2.18 a–d shows four possible configurations of passive series, passive shunt and a combination of both as short-shunt and long-shunt configurations. Passive series compensators are normally used for reducing voltage sags, swell, fluctuations, and so on, while shunt compensators are used for voltage regulation or power factor correction using reactive power compensation. Therefore, shunt compensators are commonly used in the distribution systems. Figure 2.19 a–d shows a typical configuration of a passive shunt compensator along with its phasor diagrams for power factor correction and zero voltage regulation (ZVR) at the load end.

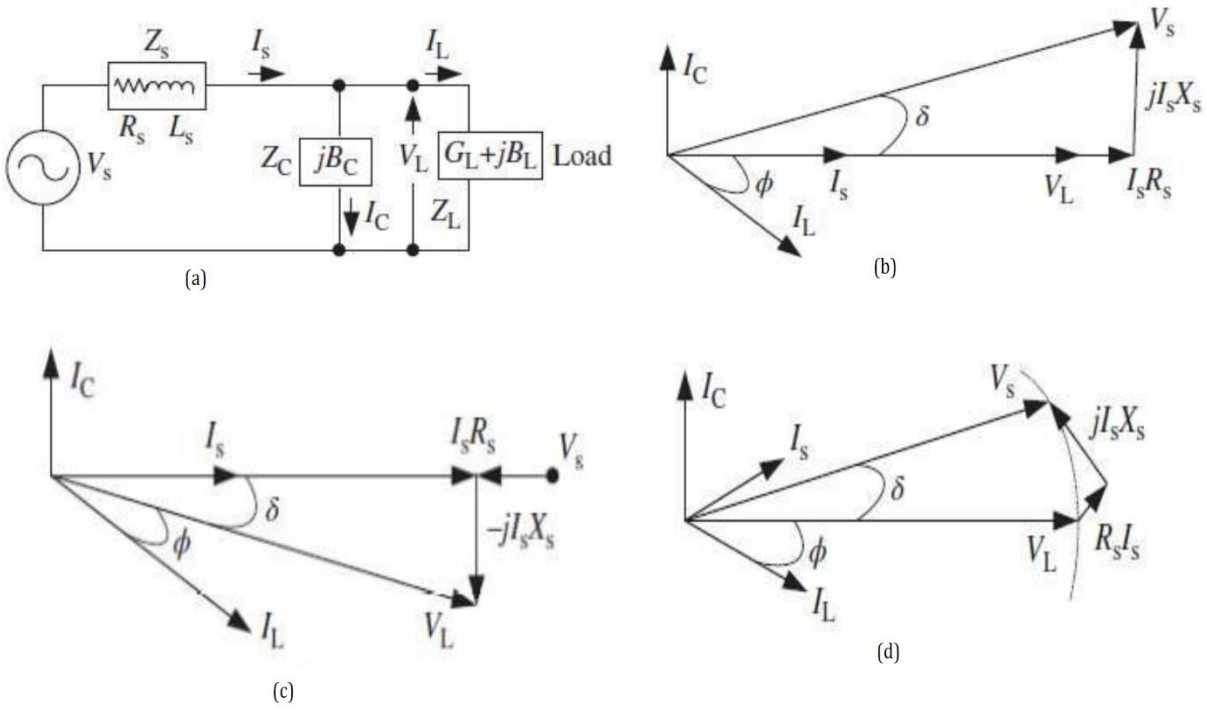


**Figure 2.19:** (a) A shunt compensator (b) phasor diagrams for PFC at load terminals (c) phasor diagrams for PFC at substation (d) phasor diagrams for ZVR at load terminals.

***Three-Wire Passive Compensators:*** Three-phase three-wire loads such as AC motors are one of the major applications. In addition, there are many unbalanced loads on a three-wire supply system such as traction, metros, and furnaces, which are fed from a three-wire supply system. Passive shunt compensators are also designed sometimes with isolation transformers for proper voltage matching, independent phase control, and reliable compensation in unbalanced systems. Figure 2.20 a–f shows typical configurations of a passive shunt compensator for power factor correction and zero voltage regulation at the load end.

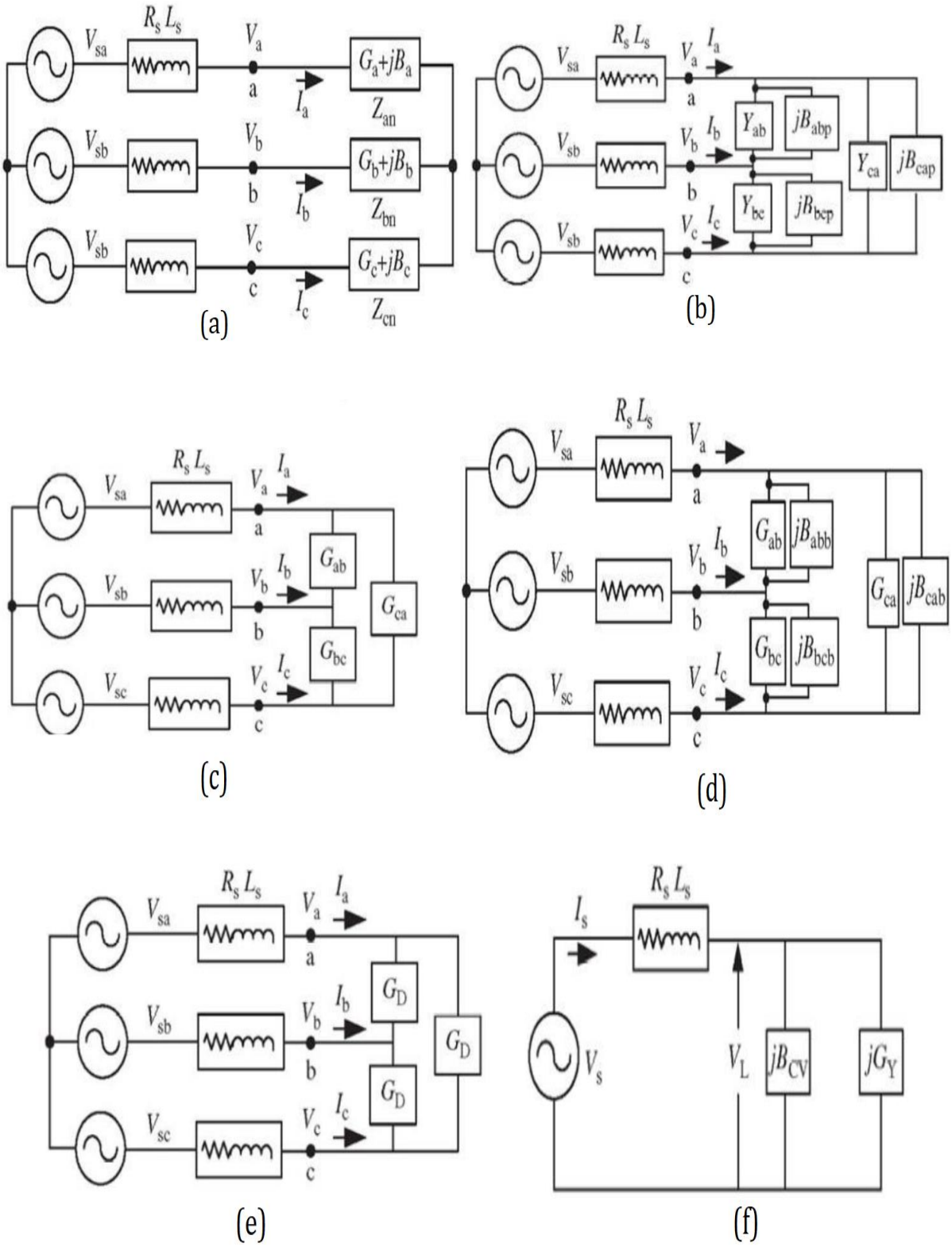
$R_s$ $L_s$
$V_{sa}$
$V_{sb}$
$V_{sb}$
$V_a$
$V_b$
$V_c$
a
b
c
$I_a$
$I_b$
$I_c$
$G_a+jB_a$
$G_b+jB_b$
$G_c+jB_c$
$Z_{an}$
$Z_{bn}$
$Z_{cn}$
(a)
$Y_{ab}$
$jB_{abp}$
$Y_{bc}$
$jB_{bcp}$
$Y_{ca}$
$jB_{cap}$
(b)
$G_{ab}$
$G_{bc}$
$G_{ca}$
(c)
$jB_{abb}$
$jB_{bcb}$
$jB_{cab}$
(d)
$G_D$
(e)
$I_s$
$V_s$
$V_L$
$jB_{CV}$
$jG_Y$
(f)

**Figure 2.20:** (a) A Three Phase three-wire star connected load with isolated neutral terminal(b) Compensation for PFC of a three phase three-wire delta connected load as an equivalent of (a) (c) An unbalanced delta connected unity power load after PFC at each phase load as an equivalent of (b) (d) Load balancing of a delta connected unbalanced unity power load of (c) (e) A balanced delta connected unity power load after compensation of load of(d) (f) Compensation for ZVR of a per phase basis balanced star connected unity power load as an equivalent of (e).

***Four-Wire Passive Shunt Compensators:*** A large number of single-phase loads may be supplied from a three-phase AC distribution system with the neutral conductor. They cause neutral current and reactive power burden and unbalanced currents. To reduce these problems, four-wire passive compensators have been used in practice. Figure 2.21 a and b shows typical configurations of a passive shunt compensator with delta (D) and star (Y) connections of lossless passive elements for power factor correction and zero voltage regulation with neutral current mitigation at the load end.

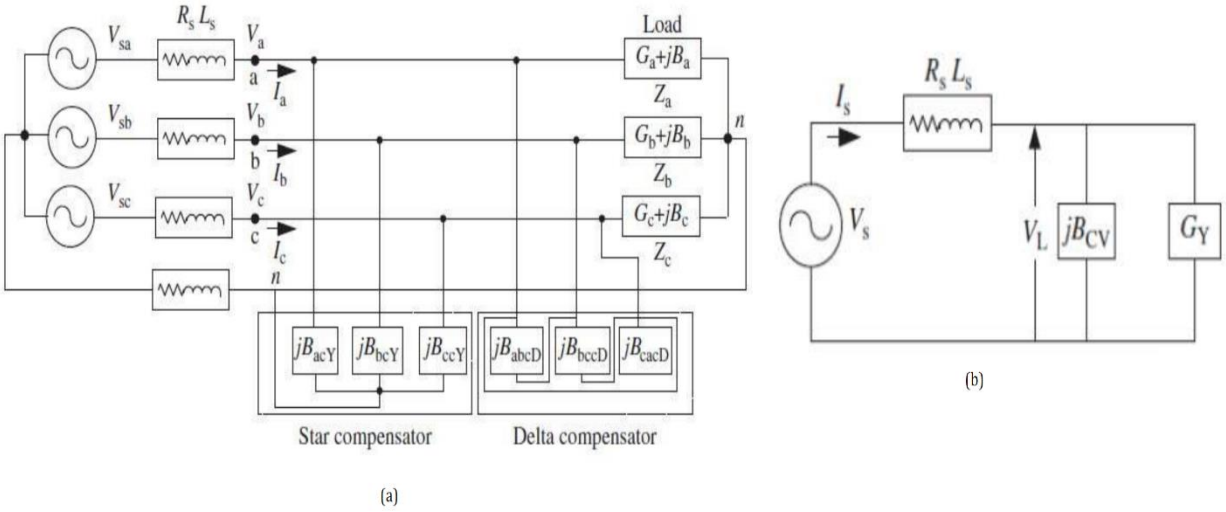


**Figure 2.21:** (a) Compensation for PFC, load balancing, and neutral current of a three-phase four-wire unbalanced load(b) Compensation for ZVR of a per-phase basis balanced star connected load as an equivalent of (a).

### 2.5.3 Principle of Operation of Passive Shunt and Series Compensators

The core objectives of passive shunt compensators are to provide reactive power compensation for linear AC loads for improving the voltage profile (even for zero voltage

regulation or power factor correction) at the AC mains in single-phase and three-phase circuits using lossless passive elements such as capacitors and inductors. In three-phase three-wire circuits, the passive shunt compensators using lossless passive elements also provide load balancing at the AC mains in addition to ZVR or PFC. Moreover, in three phase four-wire circuits, the passive shunt compensators using lossless passive elements also provide neutral current mitigation at the AC mains in addition to load balancing, ZVR, or PFC. This aspect of passive shunt compensators has been perceived for many years and is an established practice, even before the introduction of solid-state control [67], [68]. However, with the introduction of solid-state control, their performance was further improved in terms of response, flexibility, reliability, and so on. It is mainly known as classical load compensation and used in many applications such as furnaces, traction, metros, industries and distribution systems. Nowadays, the passive shunt compensators are also used in distributed, stand-alone, and renewable power generating systems. The passive compensators are also used in a series configuration and a combination of shunt and series configurations depending upon application and their effectiveness. The passive series compensators are used for voltage regulation and enhancing power flow control in transmission systems. The passive series compensators are more effective in large power transmission systems. However, they have much severe resonance problems than passive shunt compensators; therefore, they are used cautiously and up to a certain part of compensation to avoid such divesting resonance problems. In a hybrid configuration, the series elements are used with shunt elements in some applications such as stand-alone self-excited induction generators [69]. However, the series compensators are connected in series with the loads and affect the voltage across the loads; thus, they are not very popular in distribution systems.

### 2.6 Analysis and Design of Passive Shunt Compensators

In recent years, there has been an increased demand for the compensators to compensate large rating loads such as arc furnaces, traction, metros, commercial lighting and air conditioning. If these loads are not compensated, then these create system unbalance and lead to fluctuations in the supply voltages [70]. Therefore, such a supply system cannot be used to feed sensitive loads such as computers and electronic equipment. However, the importance of balanced load on the supply system has long

been acknowledged. The unbalanced loads cause neutral current and reactive power burden, which in turn result in low system efficiency, poor power factor and disturbance to other consumers. The passive shunt and series compensators are used for reactive power compensation for power factor correction or voltage regulation in single-phase systems. In addition, these are used for load balancing in three-phase three-wire systems [71]. In three-phase four-wire systems, the passive compensators are also used for neutral current compensation along with load balancing and reactive power compensation for power factor correction or voltage regulation.

### 2.6.1 Analysis and Design of Single-Phase Passive Shunt Compensators

Single-phase passive shunt compensators are used for power factor correction or zero voltage regulation across the loads. Figure 2.19 a–d shows the circuit of a shunt compensator along with its phasor diagrams for these two cases. The rating of the compensator may be estimated using the system data and given load data, for which compensation is to be made.

***Shunt Compensators for Power Factor Correction*:** Normally for the power factor correction of the load at the AC mains, a passive shunt compensator is used as it is connected directly across the load to be compensated. This shunt compensator does not affect the voltage across the loads to a great extent. Passive series compensators can also improve/correct the power factor, but they may affect the voltage across the load depending upon the load power factor and its current magnitude; therefore, they are not much preferred in the distribution system.

***Shunt Compensators for Zero Voltage Regulation:*** In many situations, it is considered relevant to maintain the load terminal voltage equal to the AC mains voltage (for zero voltage regulation) by using a compensator connected at the load end. It means to recover the voltage drop in the distribution feeder [72]. It has the following advantages,

- Avoids the voltage swells caused by capacitor switching.
- Reduces the voltage sags due to common feeder faults.
- Controls the voltage fluctuations caused by customer load variations.
- Reduces the frequency of mechanical switching operations in load tap changing

(LTC) transformers and mechanically switched capacitors for drastic reduction in their maintenance.

- Enhances the load ability of the system, especially for improving the stability of the load such as an induction motor under major disturbances.

### 2.6.2 Analysis and Design of Three-Phase Three-Wire Passive Shunt Compensators

Three-phase passive compensators may be used for power factor correction or zero voltage regulation along with load balancing by connecting lossless passive elements across the unbalanced three-phase three-wire loads. The rating of the lossless passive elements of the comparator may be estimated using the system data and given load data, for which compensation is to be made as given in the following section.

***Compensators for Power Factor Correction:*** Any three-phase unbalanced ungrounded star connected load, which is shown in Figure 2.20 (a), may be transformed to a three-phase unbalanced delta connected load as shown in Figure 2.20 (b) by star–delta transformation as follows:

$$Y_{ab} = \frac{1}{Z_{ab}} = \frac{Z_{cn}}{Z_{an}Z_{bn}+Z_{bn}Z_{cn}+Z_{cn}Z_{an}} \quad 2.1$$

$$Y_{ba} = \frac{1}{Z_{ba}} = \frac{Z_{an}}{Z_{an}Z_{bn}+Z_{bn}Z_{cn}+Z_{cn}Z_{an}} \quad 2.2$$

$$Y_{ca} = \frac{1}{Z_{ca}} = \frac{Z_{bn}}{Z_{an}Z_{bn}+Z_{bn}Z_{cn}+Z_{cn}Z_{an}} \quad 2.3$$

where $Z_{an}$, $Z_{bn}$, and $Z_{cn}$, are three-phase load impedances of any three-phase unbalanced ungrounded star connected load. Therefore, any three-phase unbalanced ungrounded star connected load, shown in Figure 2.20 a, may be converted to an equivalent three-phase delta connected unbalanced reactive load shown in Figure 2.20 b.

### 2.6.3 Analysis and Design of Three-Phase Four-Wire Passive Shunt Compensators

Three-phase four-wire passive shunt compensators may be used for power factor correction or zero voltage regulation along with load balancing by connecting lossless passive elements across the unbalanced three-phase four-wire loads. The rating of the

lossless passive elements of the compensator may be estimated using the system data and given load data.

### 2.7 Performance of Passive Shunt and Series Compensators

Compensator's modelling is carried out to demonstrate their performance for their effectiveness and basic understanding of load compensation through voltage and current waveforms. After design of the passive compensators, these are connected in the system configuration and waveform analysis through simulation to study their effect on the system and to observe their interactions with the system and occurrence of any phenomena such as sub synchronous resonance and parallel resonance. All the practical conditions, which are not considered in the design of the passive compensators, are taken into account. Earlier, the simulation study of these compensators with the system has been quite cumbersome. However, with various available simulation packages such as MATLAB, PSCAD, EMTP, PSPICE, SABER, PSIM, ETEPP and Desilent, the simulation of the performance of these compensators has become quite simple and straightforward. Nowadays, for a particular application, after the design of these compensators, their performance is studied in simulation before these are implemented in practice.

### 2.8 Active Shunt Compensator

Present-day AC distribution systems are facing a number of power quality problems, especially due to the use of sensitive equipment in most of the industrial, residential, commercial, and traction applications. These power quality problems are classified as voltage and current quality problems in distribution systems. The compensator devices namely, static compensators (STATCOMs), dynamic voltage restorers (DVRs) and unified power quality conditioners (UPQCs) are used to mitigate some of the problems depending upon the requirements [73], [74]. Out of these CPDs, STATCOMs are extensively used for mitigating the current-based power quality problems. There are a number of current-based power quality problems such as poor power factor, or poor voltage regulation, unbalanced currents and increased neutral current. Therefore, depending upon the problems, the configuration of the STATCOM is selected in the practice. With the objective of mitigating the current-based power quality problems especially in distribution systems, this section focuses on the configurations, design,

control algorithms, modelling and illustrative examples of STATCOMs. These problems further aggravate in the presence of harmonics either in the voltage or in the currents. The shunt active compensators are also reported with some modifications as cost-effective shunt active power filters to eliminate harmonic currents in nonlinear loads. Of course, the main objective of shunt active power filters has been to eliminate harmonic currents at the PCC voltage normally created by nonlinear loads.

### 2.9 State of the Art STATCOM technology

The STATCOM technology is a mature technology for providing reactive power compensation, load balancing and/or neutral current and harmonic current compensation (if required) in AC distribution networks. It has evolved in the past quarter century with development in terms of varying configurations, control strategies and solid-state devices [75], [76]. These compensating devices are also used to regulate the terminal voltage, suppress voltage flicker, and improve voltage balance in three-phase systems. These objectives are achieved either individually or in combination depending upon the requirements and the control strategy and configuration that need to be selected appropriately. STATCOM belongs to the family of Flexible Alternating Current Transmission Systems called FACTS device. In AC distribution systems, current-based power quality problems have been faced for a long time in terms of poor power factor, poor voltage regulation, load unbalancing, and enhanced neutral current. Classical technology of using power capacitors and static VAR compensators using thyristor-controlled reactors (TCRs) and thyristor switched capacitors (TSCs) has been used to mitigate some of these power quality problems. However, STATCOM technology is considered the best technology to mitigate all the current-based power quality problems [77], this is because STATCOM exhibits constant current characteristics when the voltage is low/high or under/over the limit, which allows STATCOM to deliver constant reactive power at the limits compared to other FACTS devices [78]. STATCOMs are basically categorized into three types, namely, single-phase two-wire, three-phase three-wire, and three-phase four-wire configurations to meet the requirements of three types of consumer loads on supply systems. Single-phase loads such as domestic lights and ovens, TVs, computer power supplies, air conditioners, laser printers, and Xerox machines cause power quality problems. Single-phase two-wire STATCOMs have been investigated in

varying configurations and control strategies to meet the needs of single-phase systems. Starting from 1984, many configurations have been developed and commercialized for many applications. Both current source converters (CSCs) with inductive energy storage and voltage source converters (VSCs) with capacitive energy storage are used to develop single phase STATCOMs.

### 2.9.1 Classification of STATCOMs

STATCOMs can be classified based on the type of converter used, topology, and the number of phases. The converter used in the STATCOM can either be a current source converter or a voltage source converter. Different topologies of STATCOMs can be realized by using transformers and various circuits of VSCs. The third classification is based on the number of phases, namely, single-phase two wire, three-phase three-wire, and three-phase four-wire systems [79].

***Converter-Based Classification:*** Two types of converters are used to develop STATCOMs. Figure 2.22 shows a STATCOM using a CSC bridge. A diode is used in series with the self-commutating device (IGBT) for reverse voltage blocking. However, GTO-based STATCOM configurations do not need the series diode, but they have restricted frequency of switching. They are considered sufficiently reliable but have high losses and require high values of parallel AC power capacitors. Moreover, they cannot be used in multilevel or multistep modes to improve the performance of STATCOMs in higher power ratings

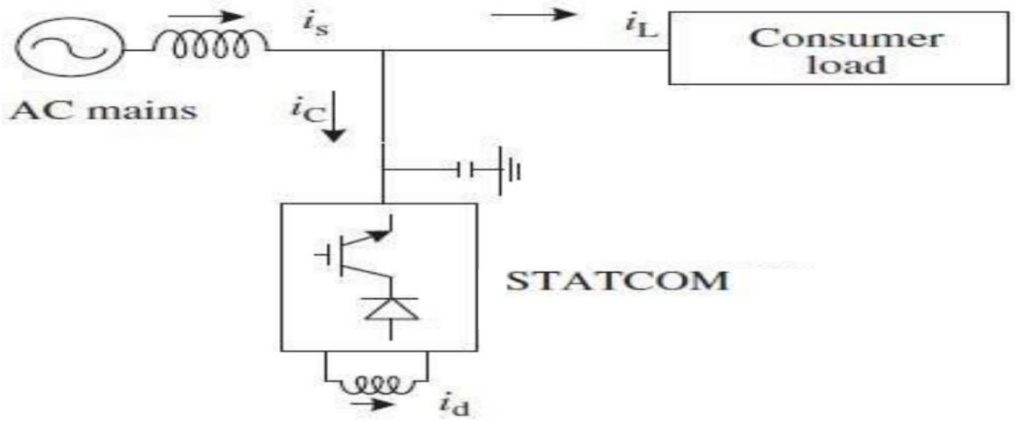


**Figure 2.22:** A CSC-based STATCOM.

The other converter used in a STATCOM is a voltage source converter shown in Figure 2.23. It has a self-supporting DC voltage bus with a large DC capacitor. It is more widely used because it is light, cheap and expandable to multilevel and multistep versions, to enhance performance with lower switching frequencies [80], [81].

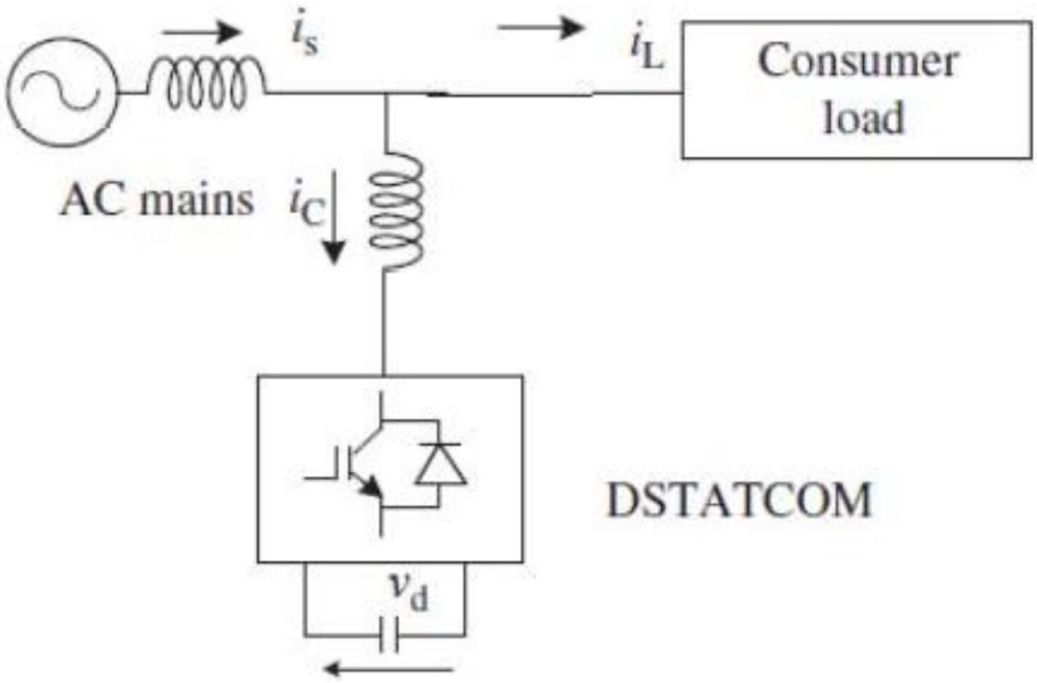


**Figure 2.24:** A VSC-based STATCOM.

***Topology-Based Classification:*** STATCOMs can also be classified based on topology, for example, VSCs without transformers, VSCs with non-isolated transformers, and VSCs with isolated transformers. STATCOMs are also used as enhanced static VAr generator (ASVG) in the power system network for stabilizing and improving the voltage profile [82]. Therefore, a large number of STATCOMs circuits with and without transformers have evolved for meeting the specific requirements of the applications.

***Supply System-Based Classification:*** This classification of STATCOMs is based on the supply and/or the load system, for example, single phase two-wire, three-phase three-wire, and three-phase four-wire systems. There are many varying loads, such as domestic appliances connected to single-phase supply systems. Some three-phase loads are without neutral terminals, such as traction, furnaces, and adjustable speed drives (ASDs) fed from three wire supply systems [83], [84]. There are many single-phase loads

distributed on three-phase four-wire supply systems, such as computers and commercial lighting. Hence, STATCOMs may also be classified accordingly as two-wire, three-wire, and four-wire STATCOMs.

***Two-Wire STATCOMs:*** Two-wire (single-phase) STATCOMs are used in both converter configurations, a CSC bridge with inductive energy storage elements and a VSC bridge with capacitive DC bus energy storage elements, to form two-wire STATCOM circuits. Figure 2.25 (a) shows a configuration of a STATCOM with a CSC bridge using inductive energy storage elements. A similar configuration based on a VSC bridge with capacitive energy storage at its DC bus is obtained by considering only two wires (phase and neutral terminals) as shown in Figure 2.25 (b).

***Three-Wire STATCOMs:*** There are various configurations of capacitor supported STATCOMs based on the type of VSC used and auxiliary circuits. The classification of three-phase three-wire STATCOMs is shown in Figure 2.26 (a), consisting of isolated and non-isolated VSC-based topologies of STATCOMs. The non-isolated configurations include three-leg VSC-based STATCOMs and two-leg VSC-based STATCOMs. These circuit configurations are shown in Figures 2.26 (b) and (c), respectively.

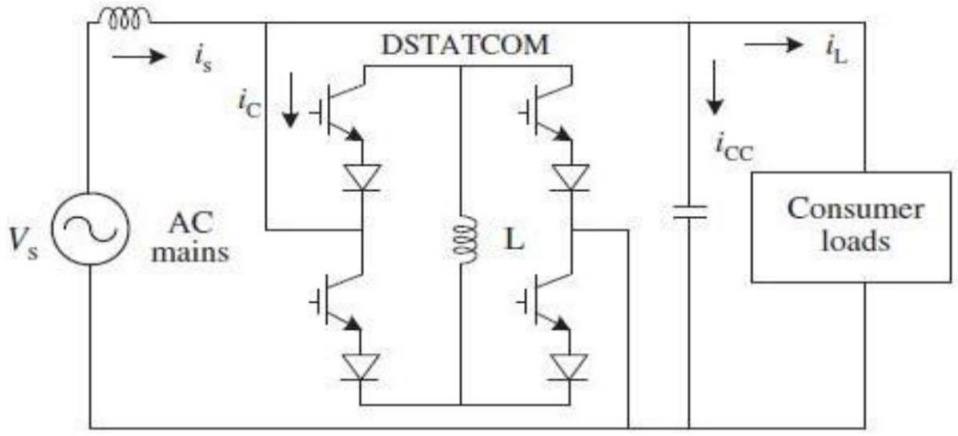


(a)

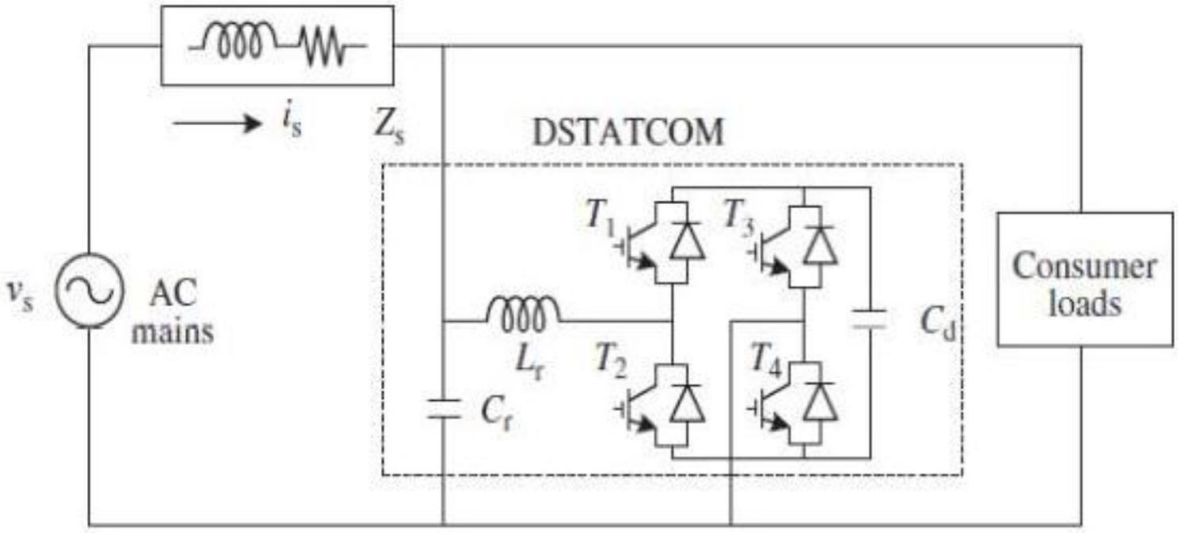


**Figure 2.25:** (a) A two-wire STATCOM with a CSC, (b) A two-wire STATCOM with a VSC.

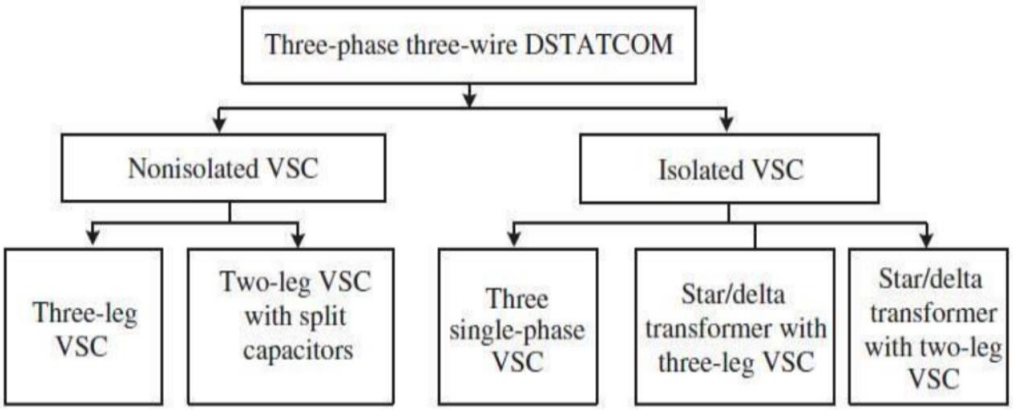


(a)

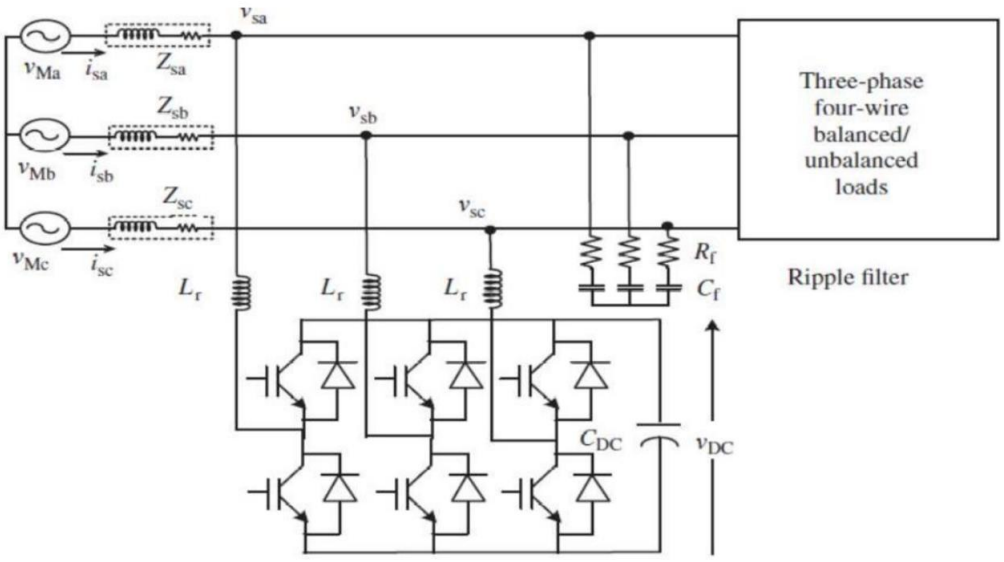


(b)

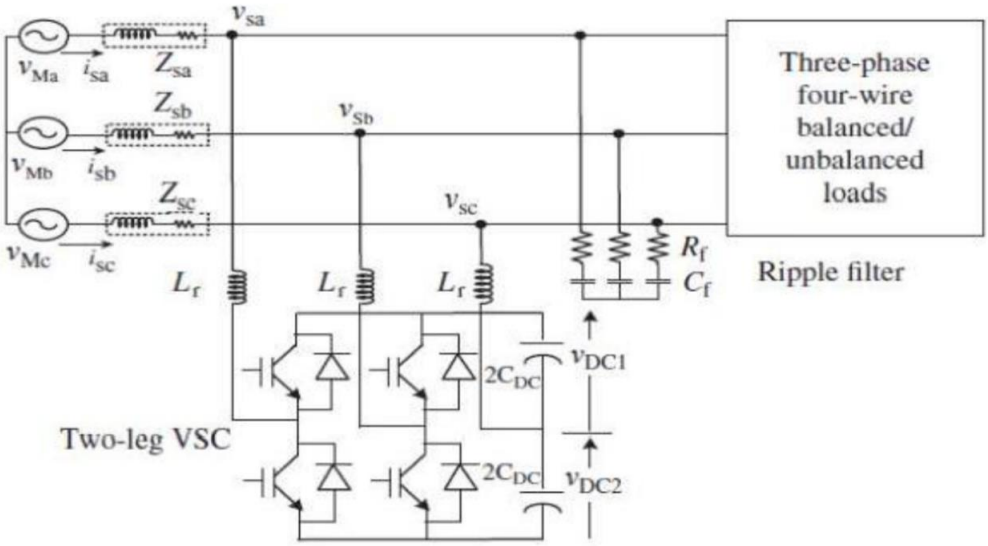


(c)

**Figure 2.26:** (a) Topology classification of three-phase three-wire STATCOMs, (b) A three-leg VSC-based three-phase three-wire STATCOM, (c) An H-bridge VSC and midpoint capacitor-based three-phase three-wire STATCOM.

The two-leg VSC-based STATCOM has the advantage that it requires only four switching devices, but there are two capacitors connected in series and the total DC capacitor voltage is twice the DC bus voltage of the three-leg VSC topology. The isolated

configurations include three single-phase VSC-based STATCOMs, three-leg VSC-based STATCOMs, and two-leg VSC-based STATCOMs [85]; these configurations are shown in Figures 2.27a-c, respectively. The advantage of the isolated VSC-based STATCOM topology is that the voltage rating of the VSC can be optimally designed as there is an interfacing transformer. Three single-phase VSC-based STATCOMs require 12 semiconductor switches, whereas in three-leg VSC based STATCOMs there are only 6 switches. However, two-leg VSC-based STATCOMs require only four switches.

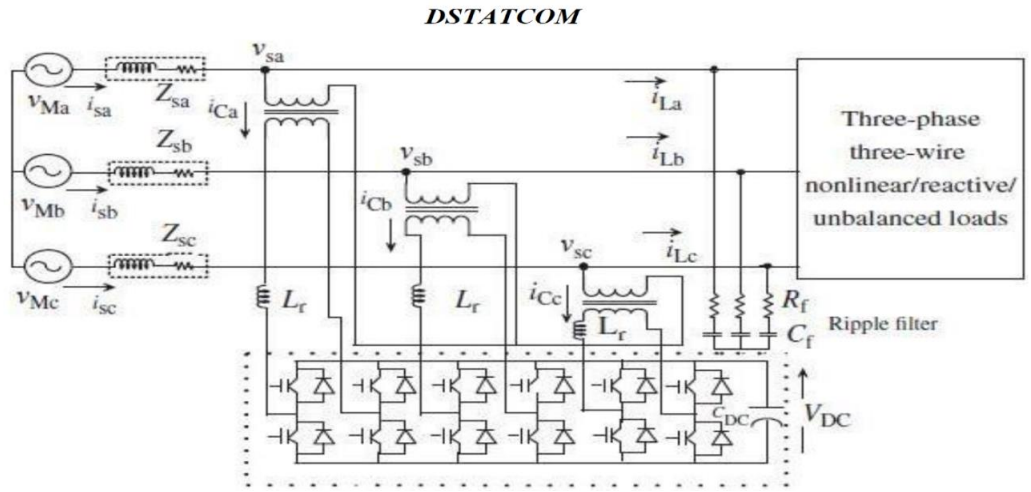


(a)

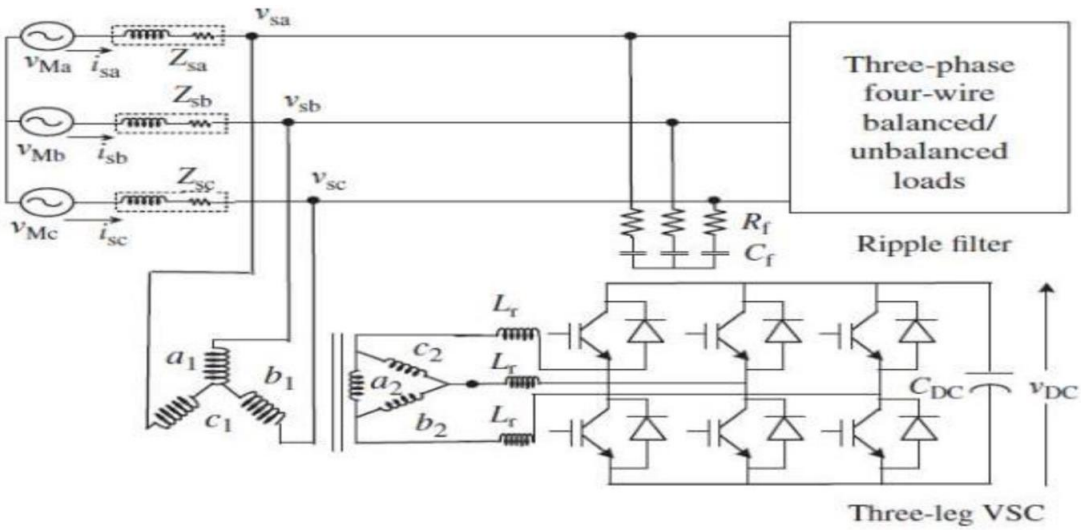


(b)

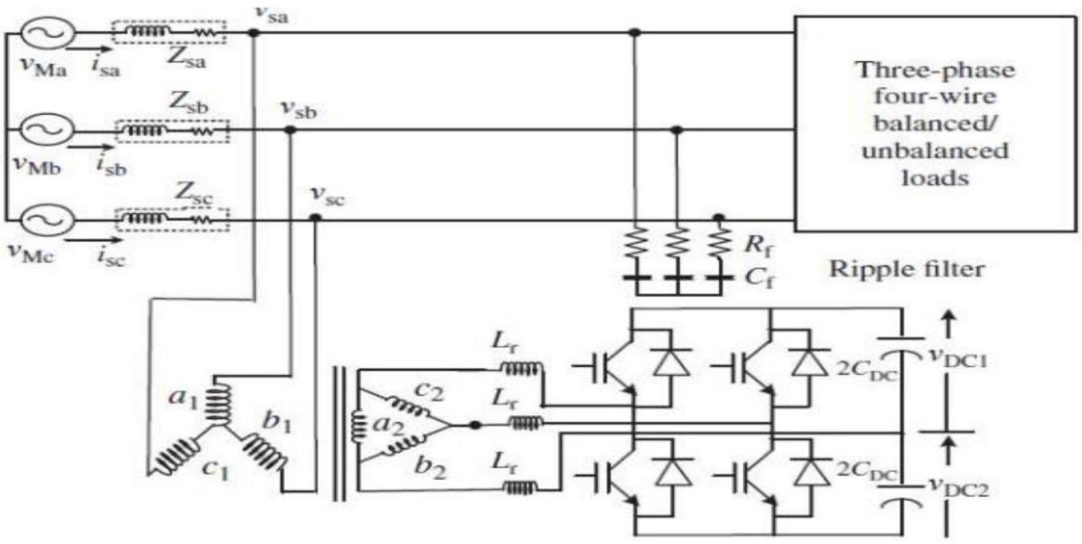


**Figure 2.27:** (a) A three single-phase VSC-based three-phase three-wire STATCOM, (b) An isolated three-leg VSC-based three-phase three-wire STATCOM, (c) An isolated H-bridge VSC and midpoint capacitor-based STATCOM.

***Four-Wire STATCOMs:*** In a three-phase four-wire distribution system, there are three-phase loads and single-phase loads depending upon the consumers' demands. This results in a severe burden of unbalanced currents along with the neutral current on the distribution feeder. To prevent the unbalanced currents from being drawn from the distribution bus, a shunt compensator, also called STATCOM, can be used. It ensures that the currents drawn from the distribution bus are balanced and sinusoidal and, moreover, that the neutral current is compensated. A STATCOM is a fast-response, solid-state power controller that provides power quality improvements at the point of connection to the utility distribution feeder [86]. It is the most important controller for distribution networks. It has been widely used to regulate the system voltage precisely and/or for load compensation. It can exchange both active and reactive powers with the distribution system by varying the amplitude and phase angle of the voltage of the VSC with respect to the PCC voltage, if an energy storage system (ESS) is included in the DC bus. However, a capacitor supported STATCOM is preferred for power quality improvement in the currents, such as reactive power compensation for unity power factor or voltage regulation at PCC, load balancing, and neutral current compensation. The classification of three-phase four-wire STATCOM topologies is shown in Figure 2.28 (a), based on the type of VSC used. They are mainly classified as non-isolated and isolated VSC-based

STATCOMs. The non-isolated VSC-based STATCOMs consist of the following configurations: four-leg VSC, three leg VSC with split capacitors, three-leg VSC with three DC capacitors, three-leg VSC with transformers and two-leg VSC with transformers [87]. The transformers used are a zigzag transformer, a star/delta transformer, a Scott transformer, a T-connected transformer, a star/hexagon transformer, and a star/polygon transformer. The isolated VSC-based STATCOMs consist of the following configurations: three single-phase VSCs, three-leg VSC with transformers, and two-leg VSC with transformers. Various transformers used for isolation are a zigzag transformer, a star/delta transformer, a T-connected transformer, a Scott transformer, a star/hexagon transformer, and a star/polygon transformer. The schematic diagram of a four-leg VSC-based three-phase four-wire STATCOM connected to a three-phase four-wire distribution system appears in Figure 2.28 (b-c), showing the schematic diagram of a three single-phase VSC-based three-phase four-wire STATCOM connected to a three phase four-wire distribution system. Figure 2.28 (d) shows the schematic diagram of a three-leg VSC with split capacitor-based three-phase four-wire STATCOM connected to a three-phase four-wire distribution system. Three-phase four-wire STATCOM configurations based on non-isolated three-leg VSCs with a zigzag transformer, a star/delta transformer, a T-connected transformer, a star/hexagon transformer, a star/polygon transformer, and a Scott transformer are shown in Figures 2.28 (e-j) respectively. Similarly, three-phase four-wire STATCOM configurations based on non-isolated two-leg VSCs with a zigzag transformer, a star/delta transformer, a T-connected transformer, a star/hexagon transformer, a star/polygon transformer and a Scott transformer may be realized for load compensation. Three-phase four-wire STATCOM configurations based on isolated three-leg VSCs with a zigzag transformer, a star/delta transformer, a T-connected transformer, a star/hexagon transformer, a star/polygon transformer, and a Scott transformer may be realized in a similar manner to the three-wire STATCOM configurations. Three-phase four-wire STATCOM configurations based on isolated two leg VSCs with a zigzag transformer, a star/delta transformer, a T-connected transformer, a star/hexagon transformer, a star/polygon transformer, and a Scott transformer may also be realized in a similar manner to non-isolated three-wire STATCOMs using the neutral terminal of the transformers of the supply side.

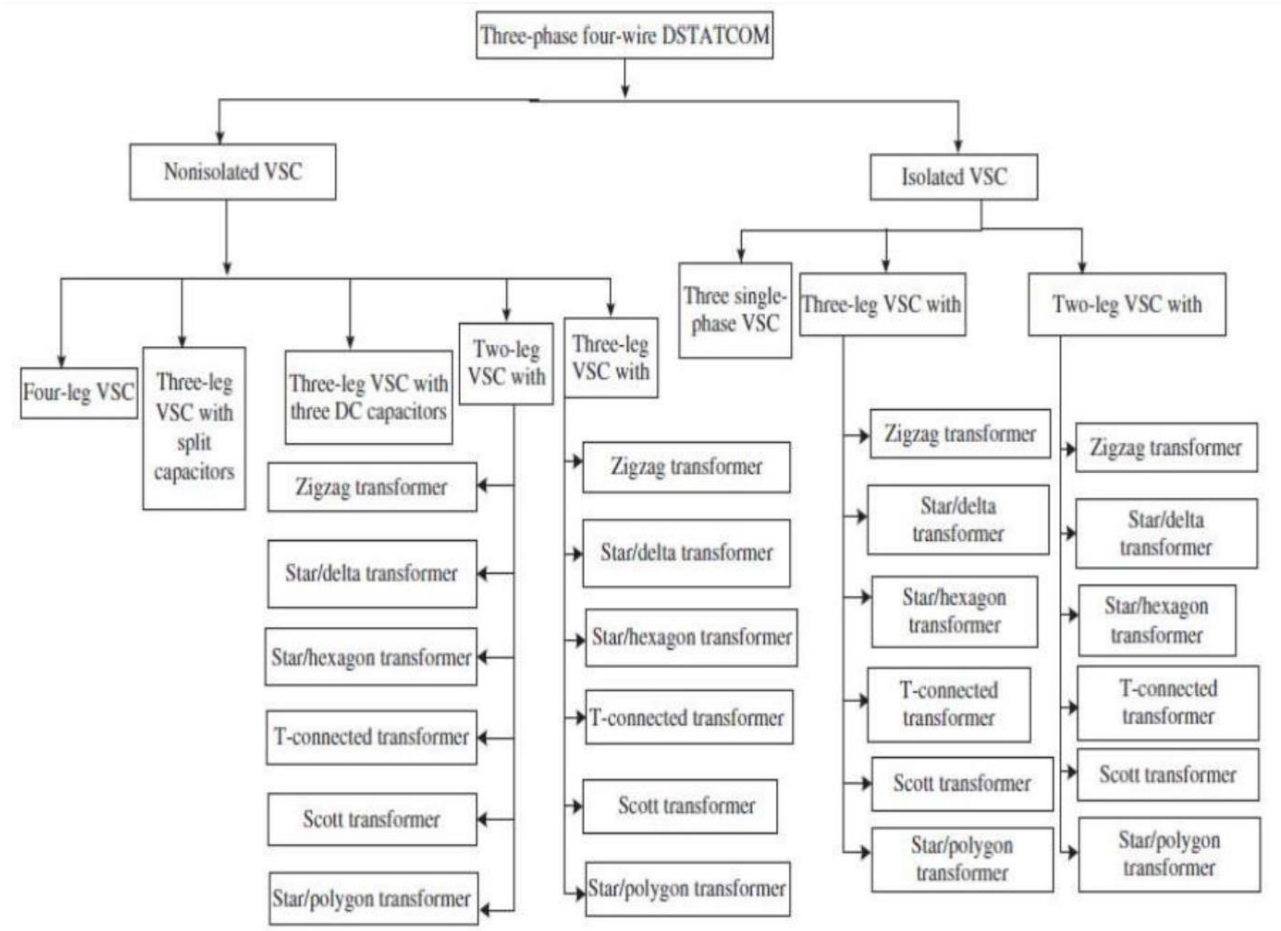
Three-phase four-wire DSTATCOM
Nonisolated VSC
Isolated VSC
Four-leg VSC
Three-leg VSC with split capacitors
Three-leg VSC with three DC capacitors
Two-leg VSC with
Three-leg VSC with
Three single-phase VSC
Three-leg VSC with
Two-leg VSC with
Zigzag transformer
Star/delta transformer
Star/hexagon transformer
T-connected transformer
Scott transformer
Star/polygon transformer
Zigzag transformer
Star/delta transformer
Star/hexagon transformer
T-connected transformer
Scott transformer
Star/polygon transformer
Zigzag transformer
Star/delta transformer
Star/hexagon transformer
T-connected transformer
Scott transformer
Star/polygon transformer
Zigzag transformer
Star/delta transformer
Star/hexagon transformer
T-connected transformer
Scott transformer
Star/polygon transformer

(a)

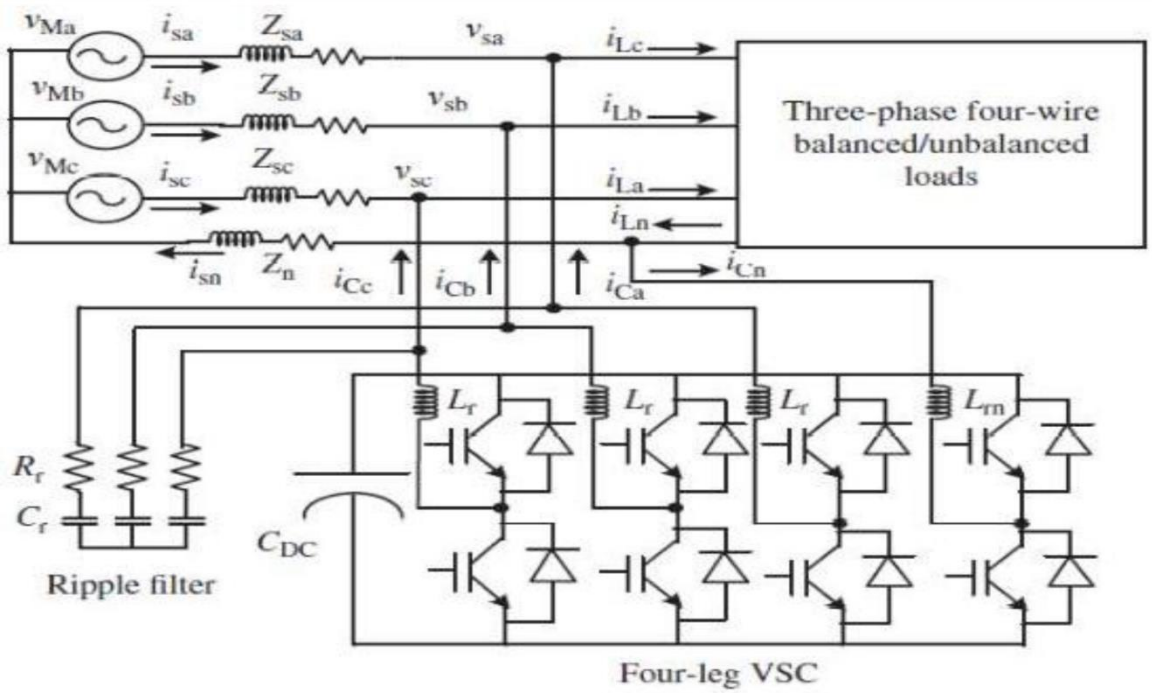
$v_{Ma}$
$i_{sa}$
$Z_{sa}$
$v_{sa}$
$i_{Lc}$
$v_{Mb}$
$i_{sb}$
$Z_{sb}$
$v_{sb}$
$i_{Lb}$
$v_{Mc}$
$i_{sc}$
$Z_{sc}$
$v_{sc}$
$i_{La}$
$i_{Ln}$
$i_{sn}$
$Z_n$
$i_{Cc}$
$i_{Cb}$
$i_{Ca}$
$i_{Cn}$
Three-phase four-wire balanced/unbalanced loads
$L_f$
$L_f$
$L_f$
$L_{fn}$
$R_f$
$C_f$
$C_{DC}$
Ripple filter
Four-leg VSC

(b)

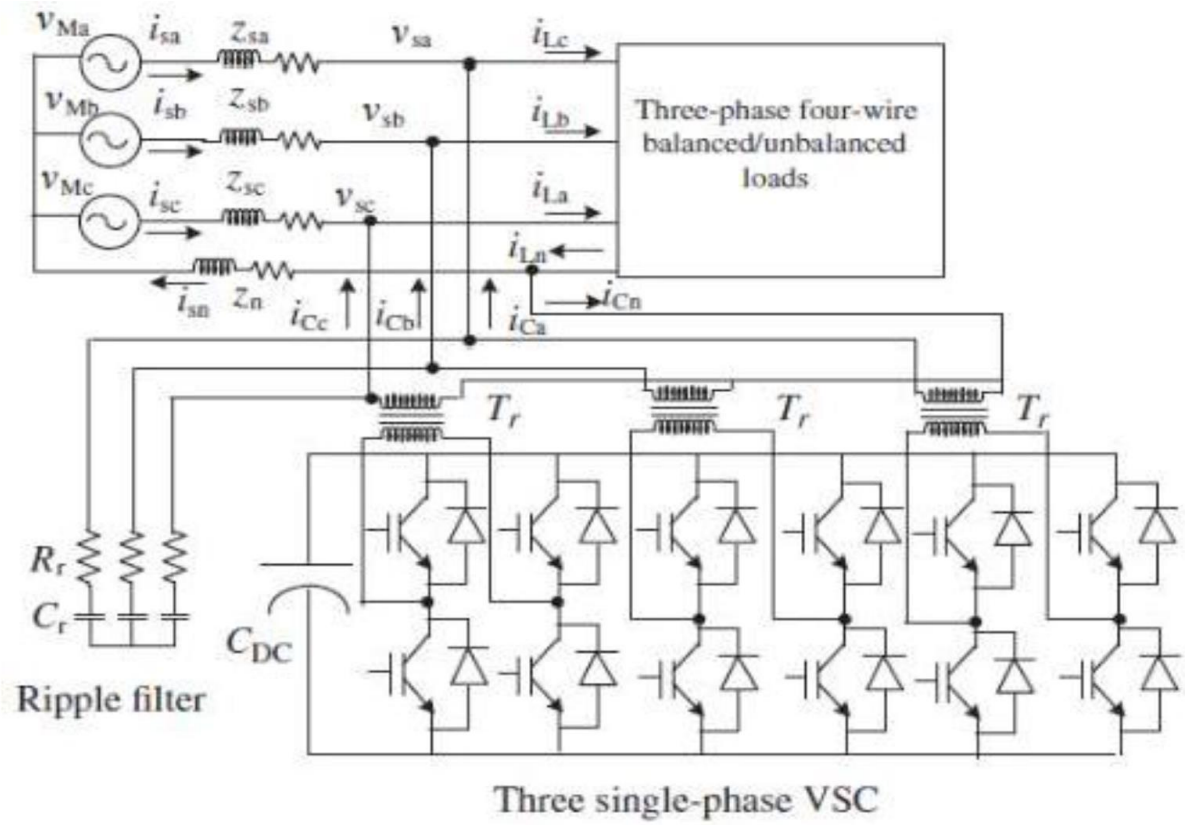
Three-phase four-wire balanced/unbalanced loads
Ripple filter
Three single-phase VSC

(c)

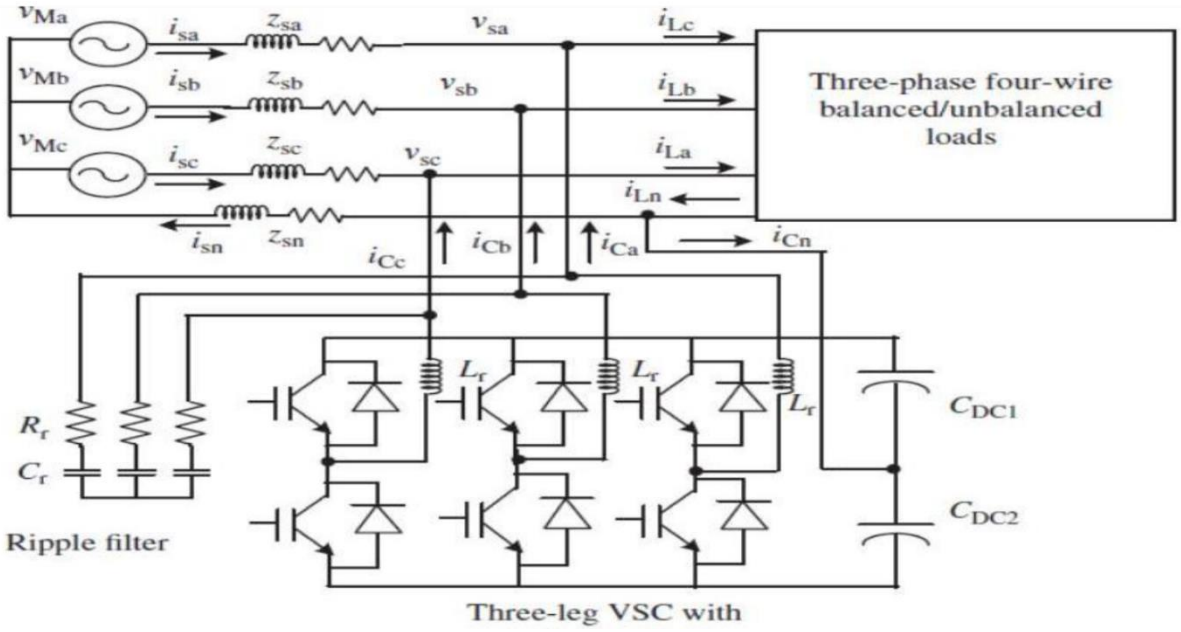
Three-phase four-wire balanced/unbalanced loads
Ripple filter
Three-leg VSC with

(d)

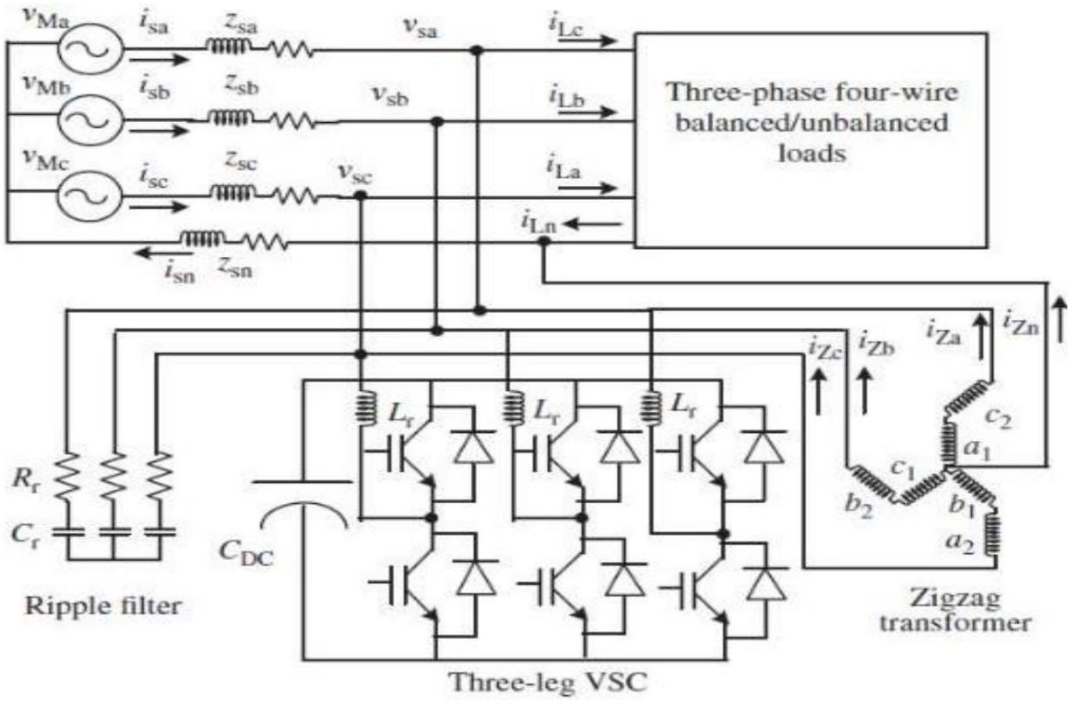
Three-phase four-wire balanced/unbalanced loads
Ripple filter
Three-leg VSC
Zigzag transformer

(e)

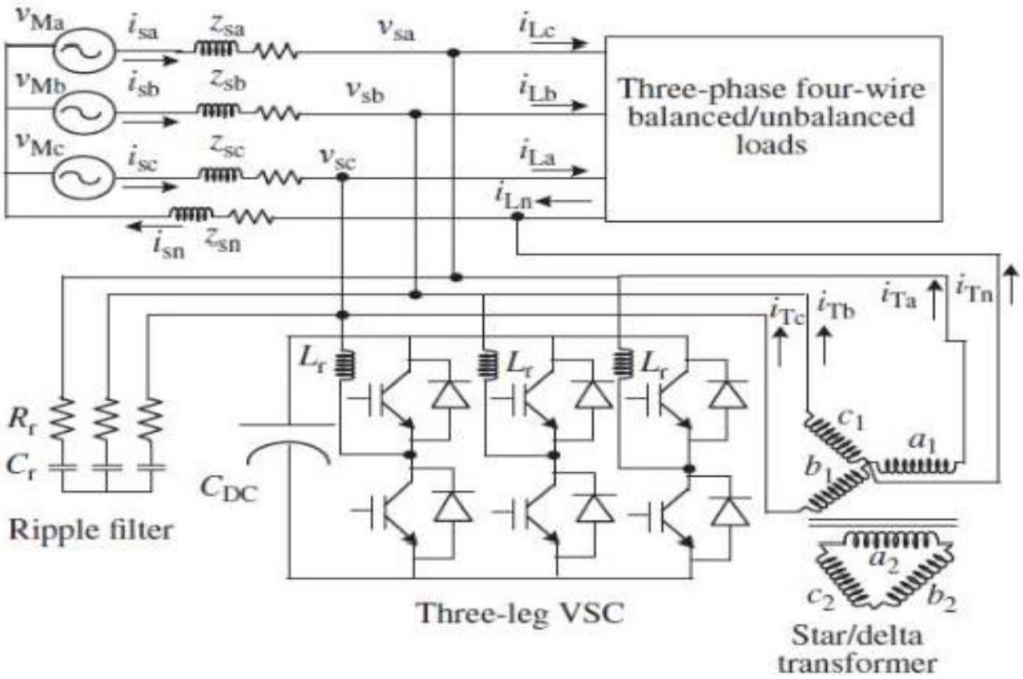
Three-phase four-wire balanced/unbalanced loads
Ripple filter
Three-leg VSC
Star/delta transformer

(f)

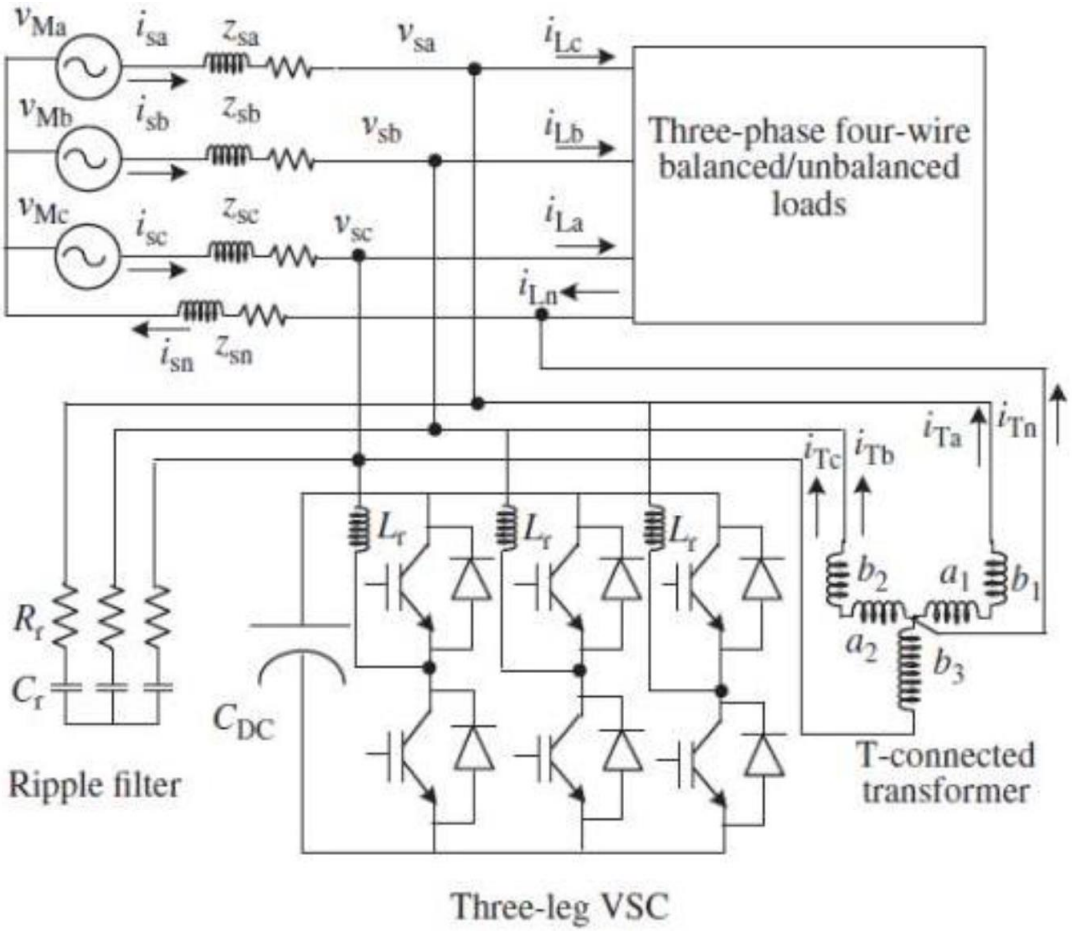
Three-phase four-wire balanced/unbalanced loads
Ripple filter
T-connected transformer
Three-leg VSC

(g)

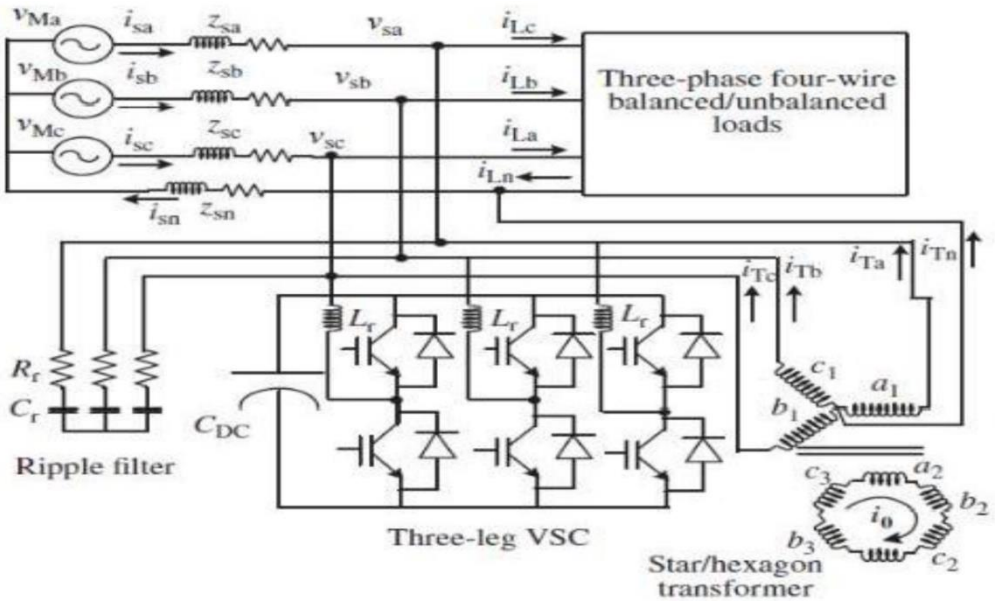
Three-phase four-wire balanced/unbalanced loads
Ripple filter
Three-leg VSC
Star/hexagon transformer

(h)

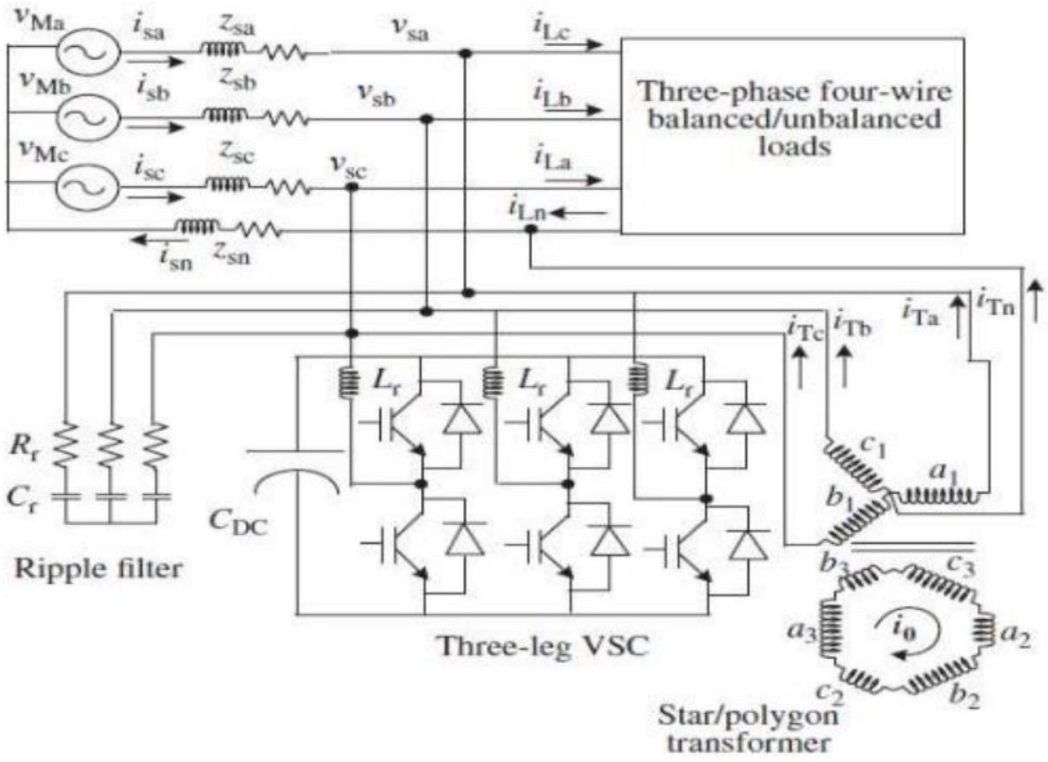


(i)

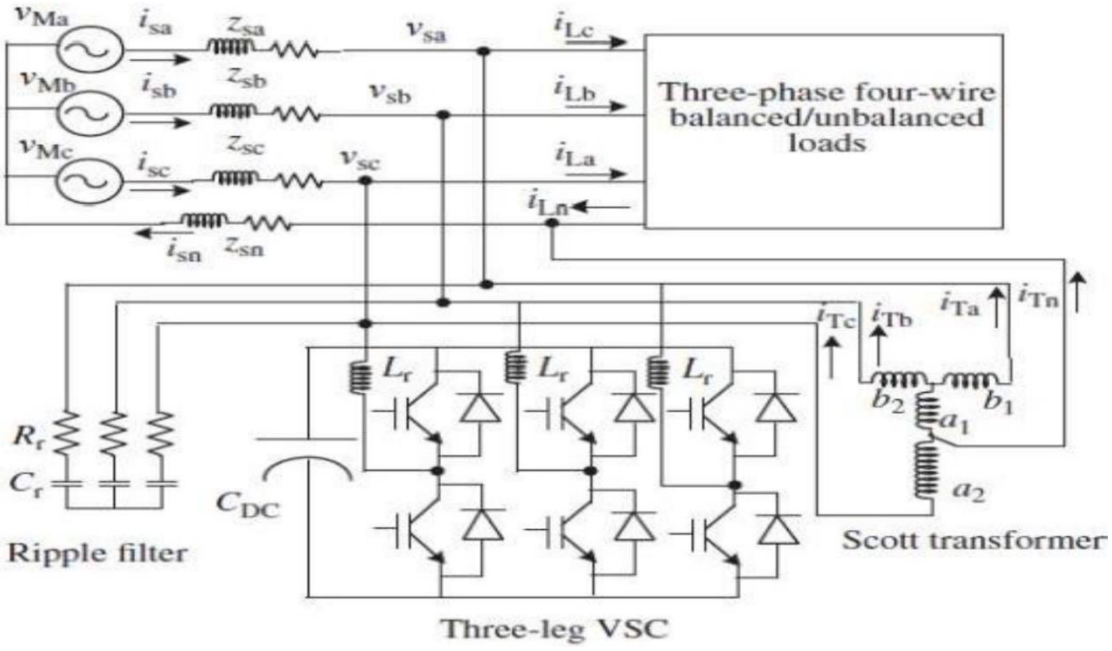


**Figure 2.28:** (a) Topology classification of three-phase four-wire STATCOMs, (b) A four-leg VSC-based three-phase four-wire STATCOM connected to a three-phase four-wire system, (c) A three single-phase VSC-based three-phase four-wire STATCOM connected

to a three-phase four-wire system, (d) A three-leg VSC and split capacitor-based three-phase four-wire STATCOM connected to a three-phase four-wire system, (e) A three-leg VSC and zigzag transformer-based three-phase four-wire STATCOM connected to a three-phase four-wire system, (f) A three-leg VSC and star/delta transformer-based three-phase four-wire STATCOM connected to a three-phase four-wire system, (g) A three-leg VSC and T-connected transformer-based three-phase four-wire STATCOM connected to a three-phase four-wire system, (i) A three-leg VSC and star/polygon transformer-based three-phase four-wire STATCOM connected to a three-phase four-wire system, (j) A three-leg VSC and Scott transformer-based three-phase four-wire STATCOM connected to a three-phase four-wire system.

### 2.9.2 Operation and Control of STATCOMs

The basic function of STATCOMs is to mitigate most of the current-based power quality problems such as reactive power, unbalanced currents, neutral current, harmonics and to provide sinusoidal balanced currents in the supply with the self-supporting DC bus of the VSC used as a STATCOM. A fundamental circuit of the STATCOM for a three-phase three-wire AC system with balanced/unbalanced loads is shown in Figure 2.26 (a). An IGBT-based current-controlled voltage source converter (CC-VSC) with a DC bus capacitor is used as the STATCOM. Using a control algorithm, the reference STATCOM currents are directly controlled by estimating the reference STATCOM currents. However, in place of STATCOM currents, the reference supply currents may be estimated for an indirect current control of the VSC [88]. The gating pulses to the STATCOM are generated by employing hysteresis (carrier less PWM pulse-width modulation) or PWM (fixed frequency) current control over reference and sensed supply currents resulting in an indirect current control. Using the STATCOM, the reactive power compensation and unbalanced current compensation are achieved in all the control algorithms.

***Operation of STATCOMs:*** The main objective of STATCOMs is to mitigate the current-based power quality problems in a distribution system. A STATCOM mitigates most of the current quality problems, such as reactive power, unbalance, neutral current, harmonics (if any) and fluctuations present in the consumer loads or otherwise in the system and provides sinusoidal balanced currents in the supply with its DC bus voltage

regulation. In general, a STATCOM has a VSC connected to a DC bus and its AC sides are connected in shunt normally across the consumer loads or across the PCC as shown in Figures 2.26 (b-d). The VSC uses PWM control; therefore, it requires small ripple filters to mitigate switching ripples. It requires hall effect voltage and current sensors for feedback signals and normally a DSP is used to implement the required control algorithm to generate gating signals for the solid-state devices of the VSC of the STATCOM. The VSC is normally controlled in PWM current control mode to inject appropriate currents in the system [89]. The STATCOM also needs many passive elements such as a DC bus capacitor, AC interacting inductors, injection and isolation transformers and small passive filters.

***Control of STATCOMs:*** The main objective of a control algorithm of STATCOMs is to estimate the reference currents using feedback signals. These reference currents along with corresponding sensed currents are used in PWM current controllers to derive PWM gating signals for switching devices (IGBTs) of the VSC used as a STATCOM. Reference currents for the control of STATCOMs have to be derived accordingly and these signals may be estimated using a number of control algorithms [90], [91]. There are many control algorithms reported in the literature for the control of STATCOMs, which are classified as time-domain and frequency-domain control algorithms. There are more than a dozen time-domain control algorithms that are used for the control of STATCOMs. A few of these control algorithms are as follows:

- Unit template technique or PI controller-based theory.
- Power balance theory (BPT).
- I cos Φ control algorithm.
- Current synchronous detection (CSD) method.
- Instantaneous reactive power theory (IRPT) also known as PQ theory or α–β theory.
- Synchronous reference frame (SRF) theory also known as d–q theory.
- Instantaneous symmetrical component theory (ISCT).
- Singe-phase PQ theory.

- Singe-phase Q theory.
- Neural network theory (WIDROW"S LMS based ADALINE algorithm).
- Enhanced phase locked loop (EPLL) based control algorithm.
- Conductance-based control algorithm.
- Adaptive detecting control algorithm, also known as adaptive interference canceling theory.

These control algorithms are time-domain control algorithms. Most of them have been used for the control of STATCOMs and other compensating devices. Similarly, there are around the same number of frequency-domain control algorithms. Some of them are as follows:

- Fourier series theory.
- Discrete Fourier transform theory.
- Fast Fourier transform theory.
- Recursive discrete Fourier transform theory.
- Kalman filter-based control algorithm.
- Wavelet transformation theory.
- Stock well transformation (S-transform) theory.
- Empirical decomposition (EMD) transformation theory.
- Hilbert–Huang transformation theory.

These control algorithms are frequency-domain control algorithms. Most of them are used for power quality monitoring for a number of purposes in the power analysers, PQ instruments, and so on. Some of these algorithms have been used for the control of STATCOMs. However, these algorithms are sluggish and slow, requiring a heavy computational burden; therefore, these control methods are not preferred for real-time control of STATCOMs compared with time-domain control algorithms.

### 2.9.3 Analysis and Design of STATCOMs

The analysis and design of STATCOMs include a detailed analysis for deriving the design equations for calculating the values of different components used in their circuit configurations. There are a large number of STATCOMs topologies. Therefore, it is not practically possible to include here the design of all circuit configurations due to space constraints.

***Design of a Three Phase Three-Wire STATCOM:*** The design of a STATCOM involves the estimation and selection of various components of the VSC of the STATCOM such as DC capacitor value, DC bus voltage, interfacing AC inductor and a ripple filter. A ripple filter is used to filter the switching ripples from the voltage at PCC. The design of the interfacing inductors and a ripple filter is carried out to limit the ripple in the currents and voltages. The design of a DC bus capacitor depends on the energy storage capacity needed during transient conditions. The rating of the STATCOM depends on the required reactive power compensation and degree of unbalance in the load. Hence, the current rating of the STATCOM is affected by the load power rating and its voltage rating depends on the DC bus voltage.

### 2.9.4 Applications of STATCOM

Improvement in the power system stability with the use of FACTS devices cannot be overemphasized as they produce significant benefits:

- Improve power factor.
- Assist voltage after grid faults/voltage stability.
- Voltage rise attenuation.
- Stabilization of weak system voltage.
- Reduce transmission losses.
- Enhance transmission capacity.
- Flicker mitigation.
- Power oscillation damping.

- Reduce harmonics from grid disturbances and fault current as the control of active and reactive power is independent of the grid.

## 2.10 Power Quality Concept

Power quality is seen as important because of its economic value. Economically, it affects utilities, their customers, and suppliers of load equipment. This power quality can be quantified by the smooth functioning of customer equipment. Power quality not only affects the utility, but also the customers. The adverse effect of poor power quality can result in a huge cost, particularly for sensitive essential services, commercial and industrial loads. For example, the cost of poor power quality such as disturbance, interruptions, voltage dips, harmonics, lightning, over-voltages, etc., is substantial if they cause sensitive industrial equipment to malfunction. It may take a very long time to resolve such issues, which can result in severe financial losses. In an advanced society, **essential public services** such as hospitals, banks, data processing centres, telecommunications traffic controllers, etc., the usage of automated systems, monitoring devices, programmable processing control machines, adjustable speed drives in industry, manufacture of semi-conductors, cement production, water treatment, materials handling, printing, steelworks, petrochemicals industry, or services like laboratories, microprocessor drives, automatic primers, information processing equipment, fluo-compact lighting in the commercial and domestic areas are all interconnected. These categories of equipment are all vulnerable to voltage variation and generate disturbance themselves. Their multiple use within individual processes requires a power supply which can provide ever increasing performance in terms of continuity and quality. The temporary shutdown of just one element in the chain may interrupt the whole process and cause a serious mis-operation resulting in damage to valuable materials and products. Residential customers may not suffer directly from the financial loss or the ability to earn income as a result of power quality issues, but they can be regarded as a potent force in realizing that the utility is delivering poor service. The usage of computers has increased significantly in the past years and more transactions are carried out on the Internet. Hence, customers become more sensitive to interruptions when they are dependent on such technology. The power quality explanation may be ambiguous to define and quantify. However, it can be explained by the quality of the output voltage and current

waveform generated. Voltage quality is not only the responsibility of the network operator, but in certain respects, depends on the producers and customers. Power quality can be described as the rate at which energy is being delivered and is proportional to the product of the voltage and current. Hence, power quality involves both voltage and current quality which entails the interaction between the network, power equipment and the load connected to the system. The consumer's goal is the availability, reliability, continuity, and quality of power supply. There is a cordial relationship between them as depicted in Figure 2.29. The power quality issues often involve interactions between the supply system, the customer facility and equipment. Power reliability is the existence of appropriate voltage on the customer meter side while power quality is the value of the voltage and other electrical parameters as a percent of the nominal value at the consumer meter. The utility can regulate the quality of the voltage supply, but there is usually a limitation over the control of current that loads can draw.

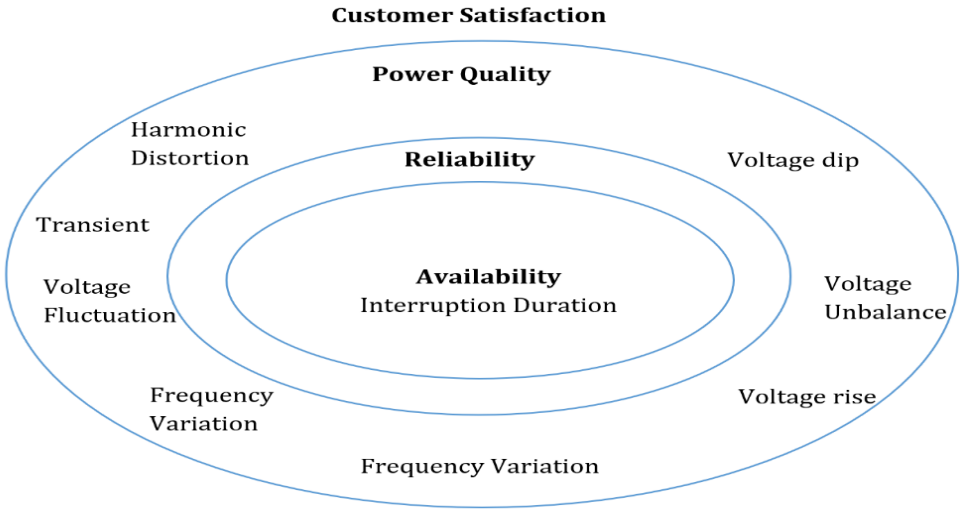


**Figure 2.29:** Power quality, Power reliability and Availability Relationship *(created by Author)*.

## 2.11 Power Quality classification

Power quality issues in the power system can be classified based on supply from the utility, the grid occurrences such as transient state, steady state, and the customer side (loads) as shown in Figure 2.30.

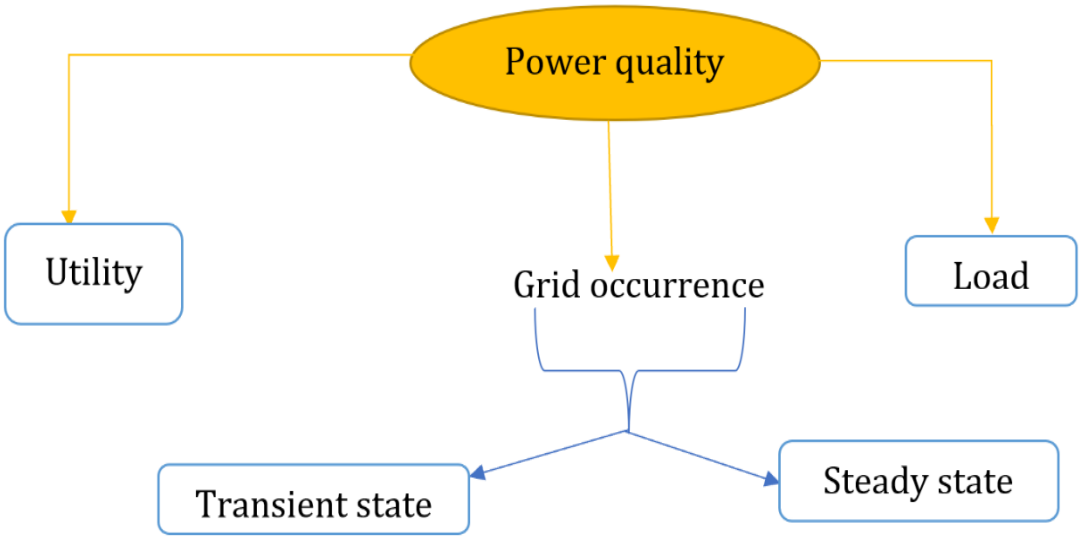


**Figure 2.30:** Power Quality Classification *(created by Author).*

### 2.11.1 Supply from the Utility

When the power issue occurs with a piece of equipment, and users complain to the utility about the causes, utility records may not show any unusual occurrences on the customer feeder. It is worthwhile to note that there are several events resulting in end-user challenges that never show up in the utility statistics. For an example, when the capacitor is switched on by the utility, which is usual and normal, it can initiate transient over-voltages that disrupt manufacturing machinery, or temporary faults elsewhere in the system, resulting in voltage sag or rise for a short period of time at the location of the customer in question. This might cause an adjustable-speed drive or a distributed generator to trip, but the utility will have no indication of such occurrence on the feeder unless it has a power quality monitor installed.

To understand the vital importance of power quality in the power system, a basic knowledge of power generation, transmission, distribution to various houses and facilities is required. Electrical energy can be generated from the generating station usually from coal, nuclear, oil, gas, water motion, etc. This electrical energy generated is usually less than 25 kV and is stepped up by transformers to a high voltage and transmitted over a long distance to distribution substations. The distribution station steps the high voltage down to an appropriate voltage level, and also supply to the load/house as shown in Figure 2.31.

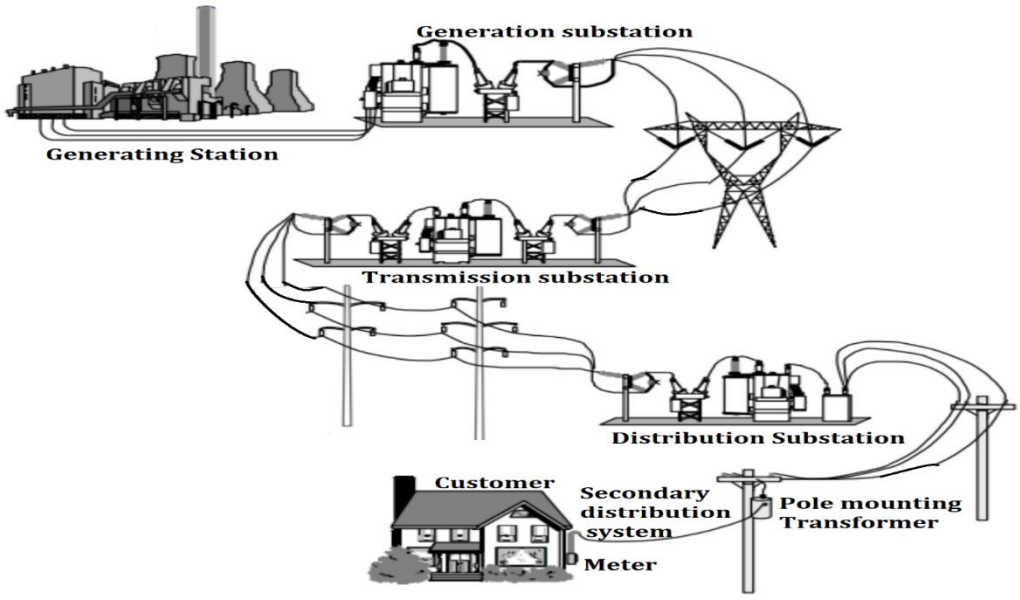


**Figure 2.31:** Electrical power Generation/Transmission/Distribution [92].

The utility that supplies power to the customer is either single phase with voltage level 120 V/230 V, 240 V to houses, offices, and shops for appliances and lighting or three phases with voltage level 120 V/208 V, 277 V/400 V, 480 V, 347 V/600 V to industries, and factories for heavy equipment usage. The supply and connection are depicted in Figure 2.32. Different connections produce a difference voltage level, for examples phase to phase or phase to neutral connections. Most power supply issues can be related to utility reliability such as low voltage supply, burnt or broken transmission or distribution cables, failed power equipment like transformers, relays, poor power generation, poor earthing system, etc., which can have direct effects on the grid and the loads connected to the system e.g., causing an outage and total blackout. Some of the outage may occur due to natural events such as weather-related issues like lightning strikes, wind, rain etc. Although these occurrences may not be totally prevented from happening, adequate measures should put in place to prevent such occurrences from affecting a constant supply of power to the customer. An example of a preventive measure is a lightning arrester.

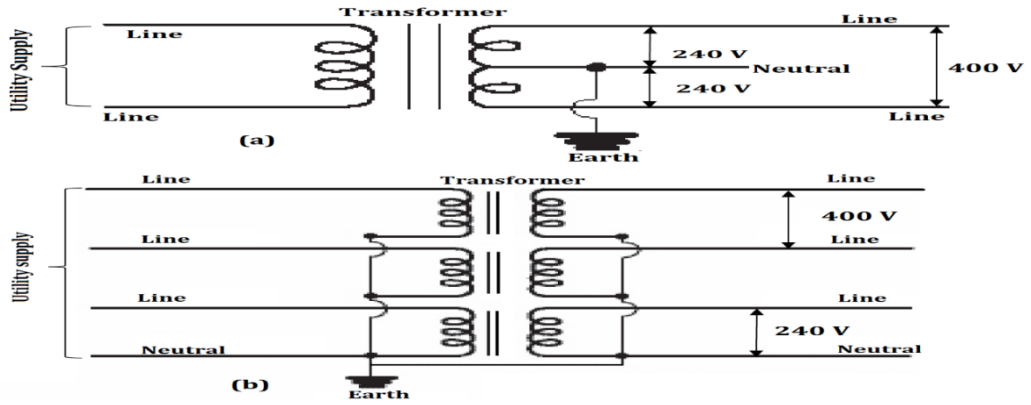


**Figure 2.32:** Single and Three phase supply [92].

### 2.11.2 Grid Occurrence

The power quality here is due to events that occur on the grid. Sometimes, it may be the reflection of what has happened at the distribution station. It can be grouped into transient and steady state occurrence. **Transient state** grid occurrences are switching of capacitors, impulsive or oscillatory events such as voltage dip, voltage rise, short-duration voltage variations, power frequency variations, voltage fluctuations, and grid faults. The **steady-state** types of power quality problems include long-duration voltage variations, waveform distortions, unbalanced voltages, notches, DC offsets, flicker, poor power factor, unbalanced load currents, load harmonic currents, and excessive neutral current. The second classification can be made on the basis of quantities such as voltage, current, and frequency. For the voltage, these include voltage distortions, flicker, notches, noise, sag, swell, unbalance, under voltage, and overvoltage; similarly, in terms of current, these include a reactive power component of current, harmonic currents, unbalanced currents, and excessive neutral current.

### 2.11.3 Electrical Load

An electrical load can be described as any external circuit that is connected to the electrical circuit output as depicted in Figure 2.33. It can also be defined as a component part of an electrical circuit that converts electrical power to another form of energy such as light, heat, mechanical, motion etc. Electrical load can be grouped into two parts namely: linear and non-linear loads. Electrical loads that exist are Resistive electrical loads, inductive electrical loads, capacitive electrical loads and combination electrical

loads.

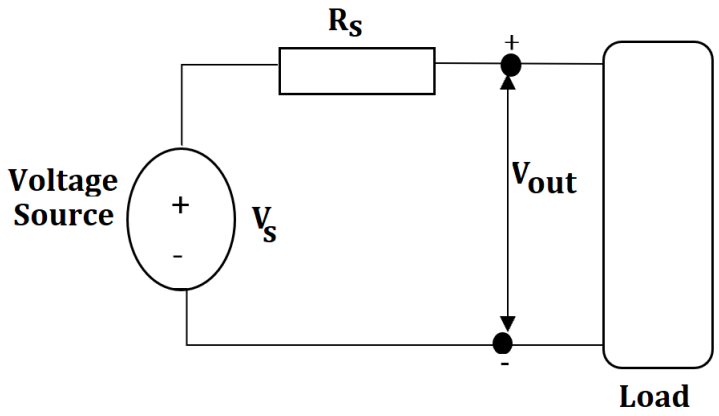


**Figure 2.33:** Electrical load *(created by Author).*

***Linear Electrical load:*** Linear electrical load can be described as a load connected to an electrical circuit where the generated sinusoidal output waveform of the steady state current follows the applied sinusoidal voltage waveform as shown in Figure 2.34 [92]. The load connected to the circuit does not change the shape of the output waveform of the current but, the timing (phase) between the voltage and the current may change. Hence, the current drawn by the load is proportional to the applied voltage. The impedance of the linear load remains constant with changing the voltage applied such that the current drawn by the load is sinusoidal similar to that of the voltage. The connected load does not change the applied frequency nor produce any new frequency otherwise known as harmonics. Examples of linear loads include power factor improvement capacitors, Incandescent Lamps, Heaters, transformers, motors etc.

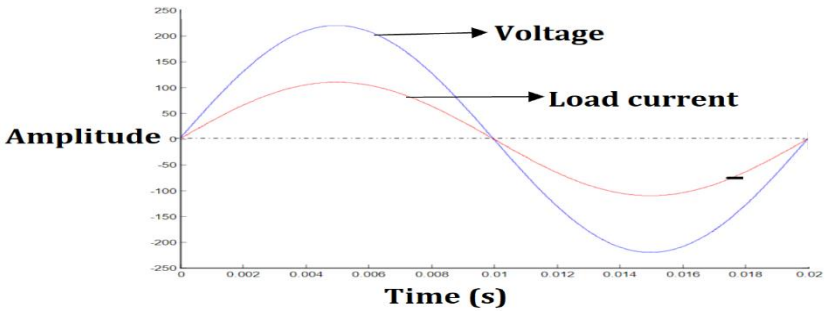


**Figure 2.34:** Linear Load Waveform [92].

***Non-linear Load:*** Non-linear electrical load can be described as a load connected to

electrical circuit where the generated sinusoidal output waveform of the steady state current does not follow the applied sinusoidal voltage waveform as shown in Figure 3.7 [92]. The load connected to the circuit changes the shape of the output waveform of the current. The currents drawn by the load are in the form of abrupt short pulses. These pulses distort the current waveforms, which in turn generates harmonics. Hence, the current drawn by the load is not proportional to the applied voltage. AC current causing distortion of the current waveform leads to distortion of the voltage waveform. The impedance of the non-linear load has not remained constant with changing the voltage applied such that the current drawn by the load is not sinusoidal even if it is connected to a sinusoidal input voltage and not similar to that of the voltage. The connected load changes the applied frequency and produces a new frequency otherwise known as harmonics. These non-sinusoidal currents comprise harmonic currents that interact with the impedance of the power distribution system to create voltage distortion that can affect both the distribution system equipment and the loads connected to it. An example of non-loads includes computers, fax machines, printers, refrigerators, TVs and electronic lighting ballasts etc.

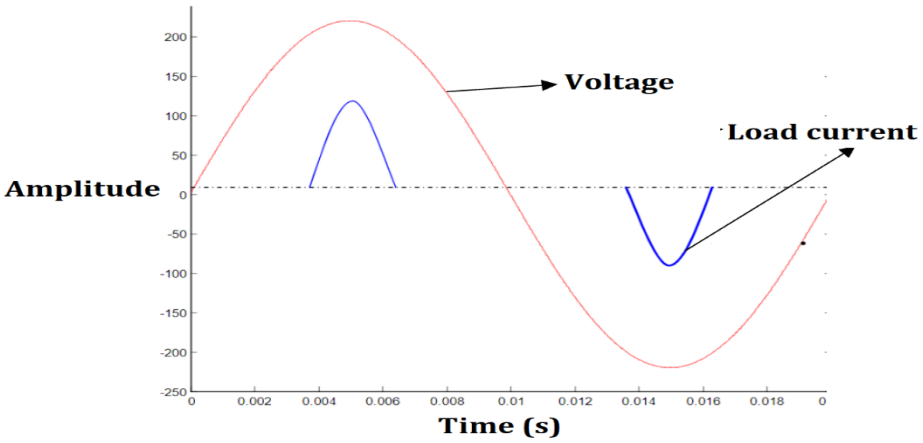


**Figure 2.35:** Non-linear Load Waveform [92].

***Types of Loads*:** Electrical load type can be divided into two: the nature of the load and the power system loads as shown in Figure 2.36.

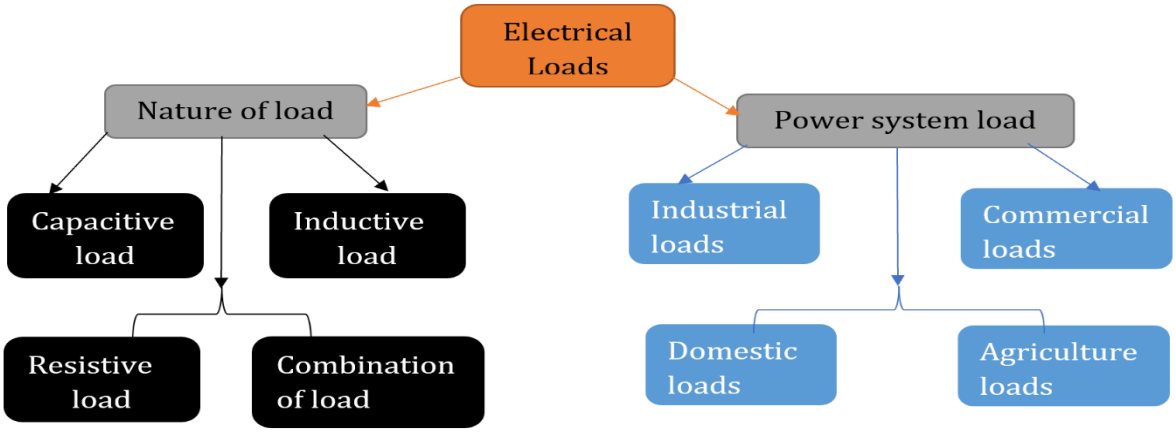


**Figure 2.36:** Electrical loads Classifications *(created by Author).*

**Power system loads**

***Industrial loads****:* Industrial loads can be described as loads from a small-scale industry, medium scale industries, large scale industries, heavy industries, and cottage industries. The induction motor forms a high proportion of the composite load. The industrial loads are the composite load. The composite load is a function of frequency and voltage and it forms a major part of the system load.

***Commercial loads:*** Loads, consisting mainly of lightning of shops, offices, etc. such as fans, heating, air conditioning and many other electrical appliances used in establishments such as market restaurants, etc. are considered as a commercial load.

***Domestic loads:*** The domestic load can be described as the total energy consumed by electrical appliances in a household. It depends on everyday living standards, the weather, and types of residence. Examples are lights, fans, refrigerators, air conditioners, mixers, grinders, heaters, ovens, small pumps, motors, etc. Domestic loads consume very little power and are independent of frequency.

***Agriculture loads:*** This type of load is mainly motor pump-sets for irrigation purposes. The load factor of this load is very small.

**There are four categories of electrical loads:**

- Resistive electrical load.

- Capacitive electrical load.
- Inductive electrical load.
- Combination of electrical loads.

***Resistive Electrical Load:*** Resistive Electrical Loads can be described as a type of electrical load that resists the flow of electricity across it. It converts some of the electrical energy into heat (thermal energy) resulting in drops in the amount of electrical energy transferred across it. The voltage and current flow across the resistive load are in phase as shown in Figure 2.37. Hence, the power factor is usually unity. Examples are lighting lamps, irons, heaters etc.

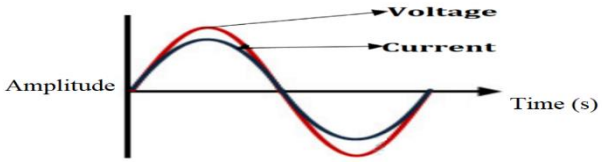


**Figure 2.37:** Resistive Load Waveform [92] .

***Capacitive Electrical Load:*** Capacitive electrical load can be described as a type of electrical load that stores energy in the form of electrical energy. The voltage and the current are out of phase as shown in Figure 2.38, but the current waveform leads the voltage waveform. Hence, the power factor in capacitive load is always leading. The voltage across the terminals starts out at zero volts while the current is at its maximum, as the charge builds on the capacitor plate, the voltage rises and the current falls; as the capacitor discharges, the current rises as the voltage falls. Examples are electric motors, radio circuits, and power supplies.

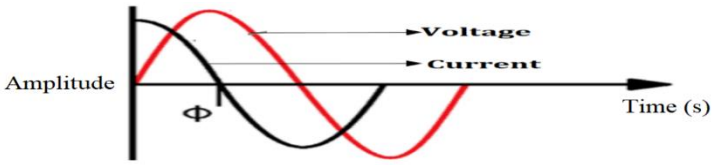


**Figure 2.38:** Capacitive Load Waveform [92].

***Inductive Electrical Load:*** Inductive electrical load can be described as a type of electrical load that uses a magnetic field for operation and opposes the change in current.

When changing current passes through an inductor, it induces a magnetic field around itself. The current waveform lags the voltage waveform. Hence, the current and the voltage are out of phase as shown in Figure 2.39. Inductive load pulls a large amount of current (an inrush current) when first energized. After a few cycles or seconds the current settles down to the full load running current. The power is the addition of real and reactive power. Examples are electrical motors, electrical power generators, and transformers.

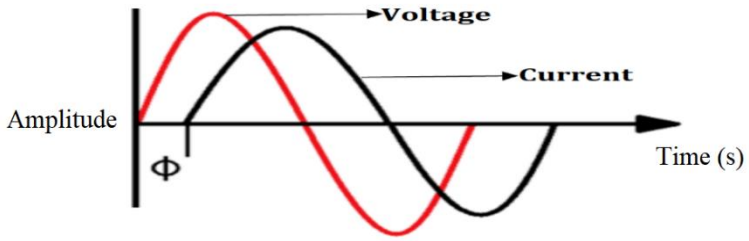


**Figure 2.39:** Inductive Load Waveform [92].

***Combination of Electrical Loads:*** Combination of electrical loads can be described as a connection of two or more types of electrical loads together such as resistive, inductive, and capacitive loads in a single circuit. An example is the connection of a motor with a starting capacitor. The power factor of the loads will either cause unity, leading, or lagging. Examples are cable and conductors, radio tuning circuits, and a cathode ray tube.

**External Safety on Electrical Loads to Enhanced Power Quality**

*A* ***Grounding system*** that steadily connects the electrical system and loads to the ground is mandatory as shown in Figure 2.40. It protects the electrical network, life, property and the equipment from superimposed voltages from lightning and contact with higher voltage systems. Limiting over voltage with respect to the ground during system faults and upsets provides for a more predictable and safer electrical system. The ground also helps prevent the build-up of potentially dangerous static charge in a facility. Grounding resistances can minimize the voltage rise during system upsets and improves protection for the equipment and life. The neutral wire and the ground are also connected together at the secondary transformers in the distribution system. Connection of the neutral and ground wires at any other points in the system is not safe for it can result in

a power quality problem.

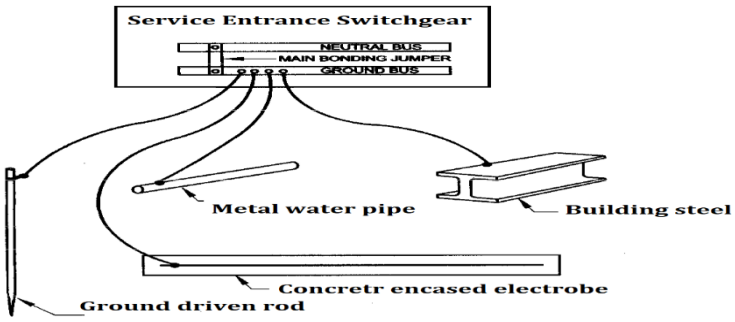


**Figure 2.40:** Grounding Method.

***Equipment Bonding*** effectively interconnects all non-current carrying conductive surfaces such as equipment enclosures, raceways and conduits to the system ground as shown in Figure 2.41. The purpose of equipment bonding is to minimize voltages in electrical equipment, thus protecting personnel from shock and electrocution. Personnel may contact the equipment to provide a low impedance path of ample current-carrying capability to ensure the rapid operation of over-current devices under fault conditions.

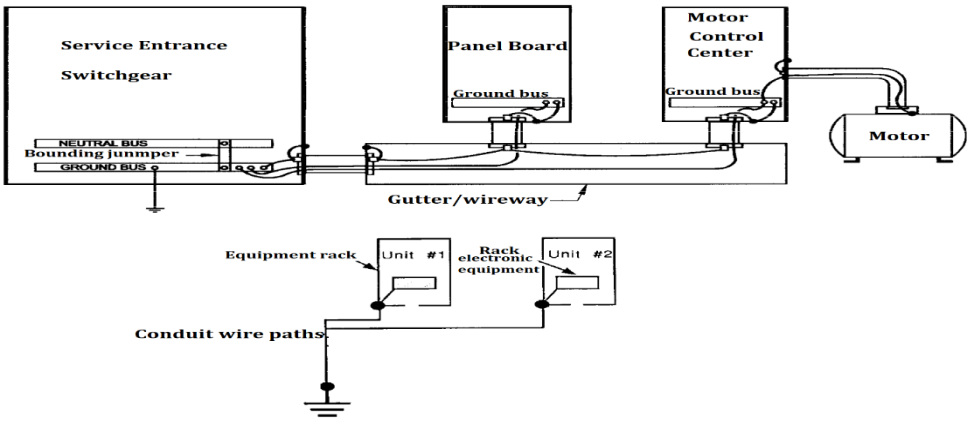


**Figure 2.41:** Bounding of Equipment.

## 2.12 Voltage Quality Versus Power Quality in Power System

As previously discussed, power quality involves both voltage and current quality. Since there is a limit to what currents draw by, the loads can be controlled on the grid side by the utility. However, voltage generated, and supply can be regulated. Hence, voltage quantity offers more parameters to measure power quality, either from the utility, or grid

occurrences and connected loads in any network. Based on this, by analogous thinking voltage quality is equal to the power quality.

### 2.13 Power Quality Parameters

- Current Quality.
- Waveform Distortion.
- Voltage Unbalance.
- Transients.
- Power Frequency Variations.
- Long-Duration Voltage Variations.
- Short-Duration Voltage Variations.
- Voltage Fluctuation.

#### 2.13.1 Current Quality

The current quality issue is the deviation of the current output waveform from the ideal sinusoidal current of constant magnitude and frequency. Alternating Voltage/Current (AC) in the electrical circuit changes direction (oscillate below and above zero) between positive and negative value. The quality of voltage generated, and the supply of customers can be regulated by the utility, but the current drawn by a certain load may not be easily controlled by the utility. Hence, the power quality could be attributed to the keeping of supply voltage to the certain required range. The functioning of power system to the load can also be regarded as voltage quality while the behaviours of loads to the power system can be described as the current quality. From a practical point of view, a utility may supply ideal sinusoidal voltage output waveform but:

- The current passing through the impedance of the system can generate distortions to the voltage.
- The short circuit current can cause voltage dip or outage.

- Lightning strokes current passing through the power system cause high-impulse voltages that frequently flash over insulation resulting in short circuits.
- Distorted currents from non-linear loads also distort the voltage as they pass through the system impedance. Hence, a distorted voltage is generated for other end users.

### 2.13.2 Waveform Distortion

Waveform distortion can be described as unexpected deviation in the flow of voltage/current output waveform especially at steady state [93]. Waveform distortion can be grouped into four fundamental output waveform distortions such as:

- Noise.
- Harmonics and inter-harmonics.
- Notching.
- DC offsets.

***Noise:*** Noise can be described as undesirable electrical signals or interference that is superimposed on the conductor carrying current/voltage and signal line. It is the unexpected signal that is missing with the required signal which has an effect on the output performance of electrical circuits. It is usually less than 200 kHz, which can cause a spontaneous change in the flow of voltage/current. When electricity is transmitted sometimes it causes a change in the impedance of the power line because of the randomness of the power line medium, noise is therefore mixed with the data transmitted on low voltage power line because of a multipath effect. Hence, the reliability of communication is greatly reduced [94].

***Causes:*** The source of noise in power system could large load, arcing appliances/equipment, devices with power electronics, fluorescent lighting tubes, and control circuits. Internal electrical resistance is a source of resistive noise, solid-state rectifying loads, switching circuits etc., [95], [96].

***Mitigation:*** Noise in electrical circuits can be attenuated by employing filters, large loop bandwidth, isolation transformers, and line conditioners [97].

***Harmonics:*** Power systems are constructed to function at a fundamental frequency of 50 or 60Hz, but some loads can generate sinusoidal voltage/current that deviates from this fundamental frequency, which means that the frequency is the integer multiples of 50 or 60 Hz. The generation of these higher frequencies causes signal pollution called harmonics. Harmonics change the shape of the current waveform from a sine wave to some other form. Harmonic currents are created in addition to the original (fundamental frequency) AC current causing distortion of the current waveform leads, and distortion of the voltage waveform. Under these conditions, the voltage waveform is no longer proportional to the current as shown in Figure 2.42. Harmonics cause the current drawn not to be sinusoidal even when it is connected to a sinusoidal voltage. The harmonics interact with the impedance of the power distribution system to create voltage distortion that can affect both the distribution system equipment and the loads connected to it. The measure of the effective value of harmonic distortion is a circuit is known as total harmonics (THD). IEEE Standard 519-1992 described the ratio of the root mean square of the harmonic content to the root mean square value of the fundamental quantity, expressed as a percent of the fundamental current expressed as a percentage [98], [99], [100], [101], [102]. Harmonics are stated in terms of its order such as the second 120 Hz, third 180 Hz, and fourth order 240 Hz. As it increases in order and frequency, so it decreases in magnitude. Inter-harmonics occurs when the frequency is not the integer multiples of the 50 or 60 Hz. It may be generated in the form of discrete frequencies or as a wideband spectrum.

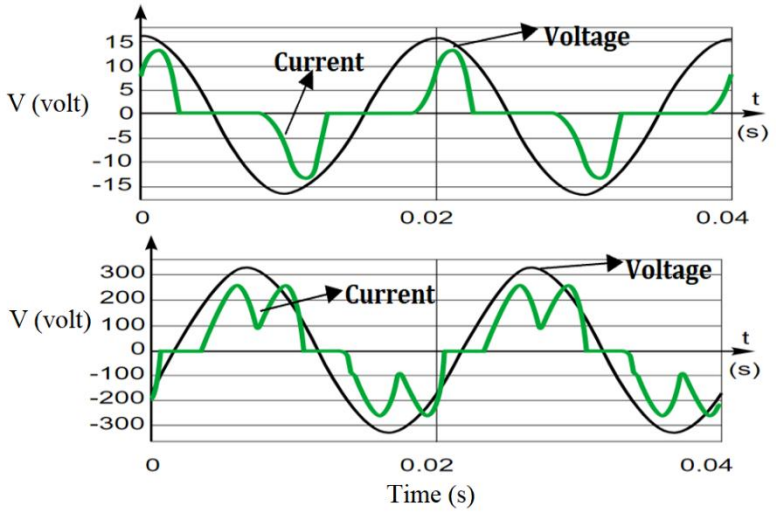


**Figure 2.42:** Harmonics Voltage/Current Distortion Waveform [99].

The equation 2.4 describes the harmonic expansion of a periodic function x (t) while equation 2.5 expresses total harmonic distortion. The voltage or current harmonic is therefore defined in equation 2.6, by the application of the root mean square value of current in equation 2.7 to obtain equation 2.9.

$$x(t) = X_0 + \sum_{h=1}^{h=\infty} X_h \sqrt{2} \sin(hwt - \varphi_h) \tag{2.4}$$

$$THD = \sqrt{\sum_{h=2}^{h=H} \left[\frac{X_h}{X_1}\right]^2} = \frac{\sqrt{X_2^2 + X_3^2 + \cdots + X_H^2}}{X_1} \tag{2.5}$$

$$THD_i \; or \; THD_v = \sqrt{\sum_{h=2}^{h=H} \left[\frac{I_h}{I_1}\right]^2} \quad or \quad \sqrt{\sum_{h=2}^{h=H} \left[\frac{V_h}{V_1}\right]^2} \tag{2.6}$$

$$I_{rms} = \sqrt{\sum_{h=1}^{h=H} I_h^2} \tag{2.7}$$

$$THD_i = \sqrt{\left[\frac{I_{rms}}{I_1}\right]^2 - 1} \quad (2.8)$$

$$I_{rms} = I_1\sqrt{1 + THD_i^2} \quad (2.9)$$

Where $(X_0)$ is the value of the DC component, generally zero, $(X_h)$ is the root mean square value of the harmonic of order h, (ω) is the angular frequency of the fundamental frequency, $(\varphi_h)$ is the displacement of the harmonic component at t = 0.

***Causes:*** It usually originates from industrial, commercial, and residential non-linear loads [103]. The loads draw non-sinusoidal current from a sinusoidal voltage source. It causes nonlinear characteristics in devices. For instance, adjustable-speed drives exhibit high THD values for the input current when operating at very light loads. Examples of non-linear loads that produce harmonics are AC or DC motor drives, electric arc furnaces, static VAR compensators, inverters, and switch-mode power supplies, such as those found in computers, lighting ballasts, and industrial electronic gear, large UPS systems, lighting systems, electronic office equipment, silicon-controlled rectifiers, Thyristors etc. Inter-harmonics may be caused by static frequency converters, cycloconverters, induction furnaces, and arcing devices.

***Harmonic Effects:*** The resultant effect of harmonics generation in power systems could result in overheating of neutral conductors, power equipment, transformer losses, a reduced life span in motors, increased copper and iron losses, insulation stress, noise and component failure, tripping of overcurrent protection resulting in equipment shut down, capacitor impedance reductions with increasing frequency resulting in capacitor overheating due to increased dielectric losses, short circuits, fuse failure, capacitor failure, incorrect readings on meters, mis-operation of protective relays, and interference. The adverse effects of harmonics may not be noticed immediately, but result in an increase demand for power, system loss, and shorter equipment lifetimes.

***Mitigation Technique:*** Harmonics can be mitigated in a power system by considering the following methods:

- Usage of filtering circuitry such as active and passive filters. These consist of a

capacitor bank and an induction coil. The filter is designed or tuned to the predetermined non-linear load and to filter a predetermined harmonic frequency.

- Circuit Detuning.
- Computer Simulations. It is advisable to simulate the effect of a large distorting load before it is connected to the network because the solutions can be planned and evaluated “on paper” and perhaps implemented when the load is installed.
- Employing low distorting Loads.
- Phase cancellation strategy: Harmonic cancellation is performed with harmonic canceling transformers called phase-shifting transformers. A harmonic canceling transformer has built-in electromagnetic technology designed to remove high neutral current and the most harmful harmonics from the 3rd through 21st. The strategy used in the transformers is known as low zero phase sequencing and phase shifting.

A reviewed edition of IEEE Standard 519 [99], [104] recommends limits for harmonic current at the PCC between the customer and the power system as shown in Table 2.5. The overall power system suggests the power quality that a customer can anticipate. Where (h), $(I_{sc})\ and\ (I_L)$ are the individual harmonic order, there is maximum short-circuit current at PCC and maximum demand load-current (fundamental frequency component) at PCC.

**Figure 2.5:** 1EEE 519 Harmonics Limit.

| $I_{sc}/I_L$ | <11 | 11≤h<17 | 17≤h<23 | 23≤h<35 | 35≤ | TDD |
|---|---|---|---|---|---|---|
| <20 | 4.0 | 2.0 | 1.5 | 0.6 | 0.3 | 5.0 |
| 20-50 | 7.0 | 3.5 | 2.5 | 1.0 | 0.5 | 8.0 |
| 50-100 | 10.0 | 4.5 | 4.0 | 1.5 | 0.7 | 12.0 |
| 100-1000 | 12.0 | 5.5 | 5.0 | 2.0 | 1.0 | 15.0 |
| >1000 | 15.0 | 7.0 | 6.0 | 2.5 | 1.4 | 20.0 |

***Notching:*** Voltage notching can be described as the periodic voltage waveform alteration generated by the usual operation of power electronic devices when current commutates from one phase to another [105]. Converters with 3-phase usually produce voltage notching as depicted in Figure 2.43. The gravity of the notch is established by the source inductance between the converter and the monitoring point. It always occurs continuously within an electronic circuit. Voltage notching has disastrous effects on commercial and industrial loads. It can cause CPUs to shut down, laser printers to fail, synchronization problems, UPS output voltage oscillation, and some digital clocks to run fast causing the electronic components to perform irregularly. The outcome would be component stress and equipment failure leading to downtime and higher repair cost.

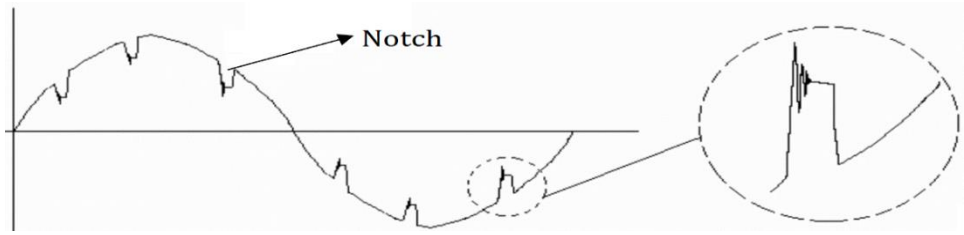


**Figure 2.43:** Voltage Notching [105].

***Mitigation:*** The secret to getting rid of line voltage notching is inserting inductive reactance (reactor in series with the input terminals) in the line. Inductive reactance tends to oppose the change in current which is directly related to the voltage.

***DC offset:*** DC offset can be described as the induction of Direct Current/Voltage into an AC power system. This occurs because of component mismatch or electronic converter/rectifier failure in the electric circuit which may be as a result of geomagnetic disturbance and asymmetry of electronic power converters [106]. For example, when a transformer is saturated and overheats, DC offsets can circulate around the transformer coil since it is unable to deliver its full rated power to the load resulting in the distorted output waveform. The impact will be on the electronic load equipment connected to the system [107], [108].

DC offset can best be explained when there is a sudden occurrence of a fault in an electrical circuit, and the flow of voltage/current unexpectedly becomes asymmetrical (the positive and negative peaks are not equidistant from zero), and then returns to normal (symmetrical) after a few cycles as shown in Figure 2.44.

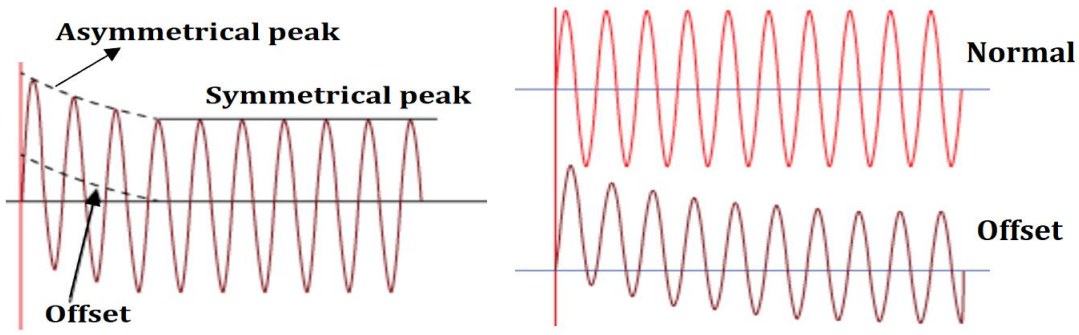


**Figure 2.44:** DC offsets [109].

This natural asymmetrical response of voltage/current to the fault is called DC Offset and it is a naturally occurring phenomenon of the electrical system [109], [110], [111], [112], [113] . The extent and period of DC Offset depends on:

- The reactance/resistance ratio (X/R) of the circuit at the occurrence of the fault such as the generator coils, and the load connected to the system. The X/R ratio at the generator is usually very high due to the generator being a pure inductor.

Hence, there would be a larger value of DC Offset if the fault location is closer to the generator. If the system is not linked to a pure inductor, the resistance in the X/R ratio rises as the distance between the fault and the generator widens, therefore the time constant would be higher. Also, the offset would be minimized as a result of an increase in source impedance.

- The magnitude of the voltage lies at the fault location. A fault at zero degrees of the Phase one voltage means that there is zero voltage when the fault is applied to the system. When the voltage is zero in an inductive circuit, the current must be maximized. Hence a DC offset happens when there is zero voltage. The remaining phases may not be zero when Phase 1 voltage is zero, different phases will respond to the same fault differently.

- The generator capability to respond to the fault and the time required to regain the steady state.

### 2.13.3 Voltage Unbalance

Voltage unbalances can be described as the inequality in the voltage/current supplied by the 3-phase power system such that there is a variation in the value of the root mean square voltage i.e., when the phase angles between the 3-phases supply are not equal [114]. It can also occur when the loads connected to a system are not balanced because of the unequal distribution of single-phase loads over three-phase power systems such that the supplied voltages are not equal. This voltage unbalance is not a waveform distortion issue, it arises in 3-phase power distribution systems where a phase is supplying power to single phase equipment, and also delivering power to 3-phase loads [115]. In a 3-phase system, voltage unbalance takes place when the magnitudes of phase or line voltages are different and the phase angles differ from the balanced conditions, or both. A 3-phase supply system comprises 3-phase angles displaced by 120° from each other in a balanced system, as shown in Figure 2.45 (a) where $(V_{oa})$, $(V_{ob})$ and $(V_{oc})$ phase-to-neutral voltages, $(V_{ab}), (V_{oa})$ and $(V_{ca})$ are line-to-line voltages such that $(V_{Line})$ is equal to $\sqrt{3} \times V_{phase}$ when the phase angle shifts from the balanced 120° phase displacement, a voltage unbalance has occurred, and the triangular three-phase voltage profile will become unbalanced as shown in Figure 2.45 (b) [116], [117], [118].

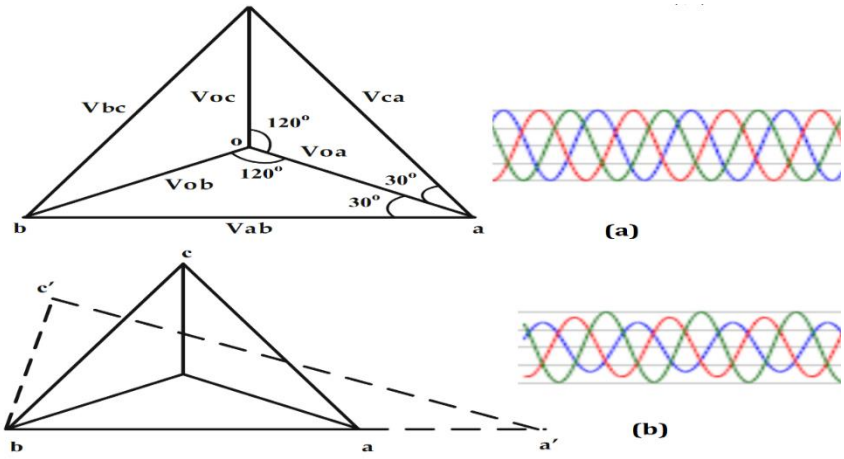


**Figure 2.45:** (a) Phase displacement of a balanced three-phase supply (b) Balanced versus unbalanced three-phase voltage [116].

It is defined by the National Equipment Manufacturer's Association (NEMA) in Equation 2.10 where LVUR is Line Voltage Unbalance Rate. It is believed that the average voltage is always equal to the rated value while IEEE states LVUR as Phase Voltage Unbalance Rate (PVUR) which is defined in equation 2.11. Both descriptions are the same. The difference is that the IEEE uses phase-to-phase voltages while NEMA uses line-to-line voltages. Hence, voltage unbalance can be described as the ratio of the negative sequence voltage components to the positive sequence voltage components in Equation 3.9 where %UVF is the percentage voltage unbalance [119], [120]. The positive and negative sequence voltage components are obtained by resolving three-phase unbalanced line or phase voltages $(V_{ab})$, $(V_{bc})$ and $(V_{ca})$ into two symmetrical components $(V_p)$and $(V_n)$ of the line or phase voltages in equations 2.13 and 2.14 where (a) and $(a^2)$ are 1∠120° and 1∠240°. Equation 2.15 can provide an approximate answer solution for an unbalanced situation where the induction motor has both positive and negative sequence voltages because of its magnitude and angles (complex algebra) where $(V_{abe})$ is the difference between line voltage and $(V_{ab})$ and the average line voltage [121], [122], [123]. The main source of voltage imbalance less than 2% is unbalanced single phase loads on a three-phase circuit, blown fuse on one phase of a three-phase bank and severe voltage unbalance greater than 5% that can result from single-phasing conditions.

$$\%LVUR = \frac{max\ voltage\ deviation\ from\ the\ average\ line\ voltage}{Average\ Line\ Voltage} \times 100 \qquad (2.10)$$

$$\%PVUR = \frac{max\ voltage\ deviation\ from\ the\ average\ phase\ voltage}{Average\ phase\ Voltage} \times 100 \qquad (2.11)$$

$$\%UVF = \frac{negative\ sequence\ voltage\ component}{positive\ sequence\ voltage\ component} \times 100 \qquad (2.12)$$

$$V_p = \frac{V_{ab} + a.V_{bc} + a^2.V_{ca}}{3} \qquad (2.13)$$

$$V_n = \frac{V_{ab} + a^2.V_{bc} + a.V_{ca}}{3} \qquad (2.14)$$

$$\%\ Voltage\ Unbalanced = \frac{82.\sqrt{V_{abe}^2 + V_{bce}^2 + V_{cae}^2}}{average\ line\ voltage} \qquad (2.15)$$

### 2.13.4 Transients

A transient voltage can be described as a sudden and temporary unwanted voltage that occurs in an electrical circuit. It usually passes through the path of least resistance to the ground, resulting in the circuit components and semiconductor devices heating up, causing malfunction and failure. It ranges between a few volts to several thousand volts (microseconds or milliseconds). It is caused by the sudden release of stored energy that drives a large amount of current/voltage in electrical circuit resulting in the system moving from a stable to a momentarily disturbed state and back to a stable state [124]. The stable condition after the transient has died down is known as the steady-state condition. Electrical transient voltages can begin from the load's internal source, utility or from external sources which can circulate through several levels of electrical and data systems. The sources of transient voltages can be from lightning stroke, contact bounce, current interruption motors, power electronics operation, Line/cable switching, wiring error, transformer switching, capacitor switching, electrostatic discharges, nuclear electromagnetic pulses, faulty contactors, contact and relay closure load start-up or disconnect, arcing (electrical flash over) etc., [125]. Over voltage transient can cause a dielectric insulation breakdown if the insulation rating is exceeded, resulting in the

breakdown and failure of equipment breakdown. Transient voltage can be grouped into impulsive and oscillatory transient, according to IEEE 1159-2019 standard [126].

***Impulsive Transient:*** An impulsive transient can be described as a sudden, non-power frequency change from the nominal condition of voltage and current which can be unidirectional in polarity, either positive or negative. It can be considered by its peak range/value, rise and decay, duration times and spectral content. For example, considering an impulsive transient voltage of 1.2/50 waveshape, 1.2 means a degree of the rise time such that 10 % to 90 % of peak in microseconds and 50 means a measure of the duration from beginning to 50 % peak in microseconds [127]. Sources of impulsive transients are lightning stroke, electrostatic discharge etc. Figure 2.46 shows that a lightning stroke transient current discharge carries a large amount of current which can cause damage to the electrical power system.

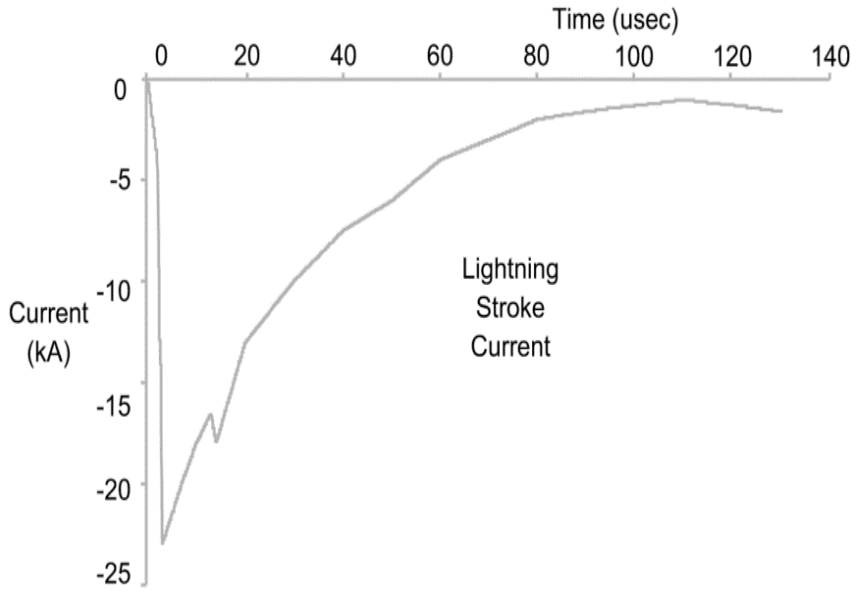


**Figure 2.46:** Lightning Stroke Transient [127].

***Oscillatory Transient:*** An oscillatory transient can be described as a sudden, non-power frequency change in the steady-state condition of voltage and current such as a positive and negative polarity value [128]. The generated voltage/current changes polarity fast several times and usually decays within a fundamental-frequency cycle. An oscillatory transient can be measured with/without fundamental frequency components with its magnitude indicated. It ranges can be defined by the magnitude, duration, spectral

content and rising time that it produces. Table 2.6 shows the ranges of the oscillatory transient as described by the IEEE regulation [126].

**Table 2.6:** Oscillatory Transient Range.

| S/N | Categories | Spectral Content | Duration | Voltage Magnitude |
|---|---|---|---|---|
| 1. | Nano-second | 5 ns rise | <50 ns | |
| 2. | Micro-second | 1 µs rise | 50 ns to 1 ms | |
| 3. | Milli-second | 0.1 ms rise | >1 ms | |
| 4. | Low frequency | <5 kHz | 0.3 to 5o ms | 0 to 4 pu |
| 5. | Medium frequency | 5 to 500 kHz | 20 µs | 0 to 8 pu |
| 6. | High frequency | 0.5 to 5 MHz | 5 µs | 0 to 4 pu |

Oscillatory transients' occurrence is high when the frequency component is above 500 kHz and measured in microseconds. It is usually caused by switching events, and commutation and resistance/inductance/capacitance (RLC) snubber circuits. Transient occurrence between 5 and 500 kHz in microseconds can be regarded as medium-frequency transients. A back-to-back capacitor initiation causes higher oscillatory transient currents to flow when the energising capacitor is in close electrical proximity to a bank of capacitors already installed, as depicted in Figure 2.47. When a capacitor bank is switched on, a large inrush current passes through to charge the capacitors resulting in an initial notch voltage waveform [129]. The system voltage, recovers quickly and overshoots its original point, constantly oscillates or rings. The ringing of the system voltage is due to the addition of capacitance to a system that is inductive by nature, and

typically ends within one-half to one full cycle. Various loads such as variable speed drives are vulnerable to this ringing, and it will trip off. The energized capacitor bank detects the de-energized bank as a low impedance path but can be minimized by the small inductance of the connected bus banks [130], [131].

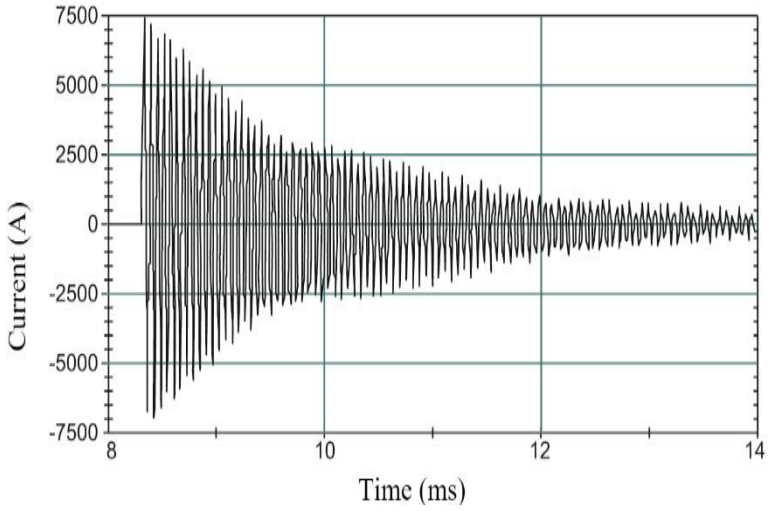


(a)

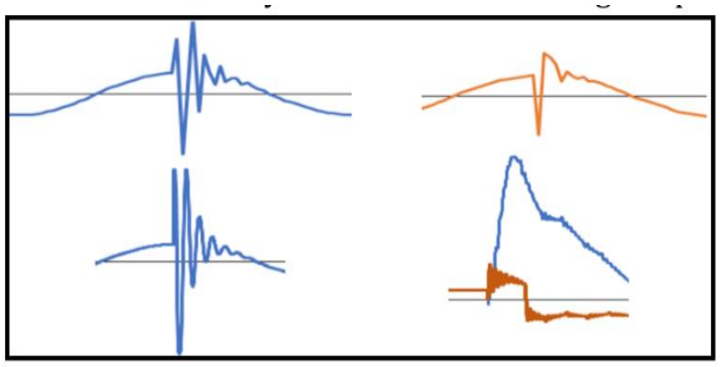

(b)

**Figure 2.47:** (a) Oscillatory Current Flows Through Capacitor (b) Transient Voltage at Millisecond [130], [131].

**The Effects of Transients Voltage/Current**

- Intermittent interruption resulting in erratic behavior leading to the tripping of equipment causing loss of data, loss of revenue and diminished quality of the end-product.

- Power components' degradation.
- Power system components and equipment failure. Solid-state products such as microprocessor-based devices and programmable logic controllers are susceptible to damage from voltage transients such as waveform voltage shown in Figure 3.20. Equipment components are becoming smaller and their susceptibility to damage from voltage transient has increased.
- Frequent transient voltages can cause fire, burn switch contact and make equipment inoperable.

**Mitigation of Transient Voltage/Current**

- ***Earthing screen*** which is made of copper conductors placed around equipment like a shield or a cage and connected to ground at some points which conduct the lightning away from the equipment to the ground, thus protecting the equipment.
- Overhead ground wires.
- Lightning arresters, or surge diverters.

### 2.13.5 Power Frequency Variations

The AC that oscillates between positive and negative for 50 or 60 times in a second is known as **frequency** of 50 or 60 hertz. The power supply is usually supplied at 50 hertz with a very narrow tolerance. Any deviation in the frequency from the allowable range can result in a power quality issue. To avoid power quality issues due to frequency, supply generators are usually connected and synchronized (locked) together at high voltage with other generators, allowing spinning at 50 or 60 hertz to form a single stable supply. Grid frequency can be influenced by the amount of change in electricity demand and supply. Decrease in frequency may arise when there is more electricity demand than supply, or an increase when the supply of electricity is high. Frequency is usually monitored to avoid a larger error in merging [132].

### 2.13.6 Long-Duration Voltage Variations

Long-duration voltage variations can be described as the deviation in the voltage root mean square from the nominal voltage or complete loss of voltage on one or more phase conductors for a time greater than 1 min. It is usually typified by the frequency of the variation and the magnitude. Long-duration voltage variations can be divided into two groups namely: over-voltage/voltage rise and under-voltage. The over-voltage and under-voltage in this context are usually not as a result of a fault from the system but occur because of load fluctuation within the system and the switching control of the network. This type of fluctuation can be verified by plotting the root mean square value of the voltage at the time taken.

***Long Duration Overvoltage/Voltage Rise:*** An overvoltage occurs when the root mean square voltage of a system is more than or equal to 110 % and the time of occurrence is longer than 1 minutes at the power frequency.

***Causes:*** Initialization/starting of capacitor banks, switching on/off a large load, incorrect tap settings on transformers.

***Long Duration Under-voltage:*** Undervoltage occurs when the root mean square voltage is less than or equal to 90 % (0.1 and 0.9 p.u. with a duration between 0.5 cycles to 1 min) of the nominal voltage and the time of occurrence is longer than 1 minutes at the power frequency [133]. When there is a supply of voltage longer than 1 minute, it can be regarded as a sustained interruption which needs the attention of power technicians/engineers to check the cause for adequate restoration. Based on the IEEE Std 1453-2015 a change in voltage because of occurrences such as a motor starting, switching a capacitor bank on and voltage regulation all can be regarded as Rapid Voltage Changes (RVC). Here the change in voltage is prolonged over a repeated cycle and also, 5% and 3% voltage change are approved for medium voltage and low voltage at PCC by IEEE 1547-2018 per second averaged over one second as the acceptable rapid voltage [134], [135], [136]. The sensitivity of the RVC may differ subject to:

- The duration of a steady-state condition between two voltage changes.
- The rate of change of the voltage (dv/dt).

- The magnitude of the voltage change.

***Causes:*** Switching on/off a large load, starting of the capacitor bank.

### 2.13.7 Short-Duration Voltage Variations

Short duration voltage variation can be described as the type of voltage fluctuation which can result in voltage dip and brief interruption in the power system. It usually depends on the time of occurrence such as instantaneous, momentary and temporary. Table 3.3 shows the different categories. Sources of short-duration voltage variations are large loads with high starting currents, partial loose connections in the circuit wiring resulting in an irregular drop in voltage, overvoltage, or loss of supply [137]. Short duration voltage variations can also occur due to a fault event on the network and can be categorized as voltage dip, voltage rise and interruption.

***Short Duration Voltage dip:*** Short duration voltage dip in the context of short duration voltage variation occurs when the grid voltage is in the range of 0.1 and 0.9 pu (root mean square value of the voltage decreases to between 10% and 90% of the nominal value) in root mean square voltage or current at the power frequency for the time range of 0.5 cycle to 1 minute which can be divided into instantaneous voltage dip, momentary voltage dip, and temporary voltage dip as shown in Table 3.3.

***Causes:*** Starting of large loads, starting of large motors.

***Short Duration Voltage Rise:*** Short duration voltage rise or overvoltage in the context of short duration voltage variation can be described as the voltage increase/rise between 1.1 and 1.8 pu (root mean square value of the voltage increases to between 110 and 180 % of the nominal value) in rms voltage or current at the power frequency for the time of 0.5 cycle to 1 minutes which can occur as a result of fault or over generation of RDG to the grid. Short duration voltage rise can be instantaneous voltage rise, momentary voltage rise, and temporary voltage rise as shown in Table 3.3.

***Causes:*** The voltage rises on the un-faulted phases during a single line to ground fault and switching off a large load, over generation or RDG and switching to a large capacitor bank.

***Interruption:*** Interruption takes place when the voltage supply or load current declines to less than 0.1 pu for a duration not beyond 1 minute. The interruption can be an instantaneous voltage interruption, momentary voltage interruption, and temporary voltage interruption as shown in Table 2.7.

**Table 2.7:** Short Time Voltage Variation.

| **Short Duration Voltage dip** | | | |
|---|---|---|---|
| S/N | Interruption | Magnitude | Duration |
| 1. | Instantaneous | 0.1 to 0.9 pu | 0.5 to 30 cycles |
| 2. | Momentary | 0.1 to 0.9 pu | 30 cycles to 3 sec |
| 3. | Temporary | 0.1 to 0.9 pu | 3 sec to 1 min |
| **Short Duration Voltage Rise** | | | |
| S/N | Interruption | Magnitude | Duration |
| 1. | Instantaneous | 1.1 to 1.8 pu | 0.5 to 30 cycles |
| 2. | Momentary | 1.1 to 1.4 pu | 30 cycles to 3 sec |
| 3. | Temporary | 1.1 to 1.2 pu | 3 sec to 1 min |

| **Interruption** | | | |
|---|---|---|---|
| S/N | Interruption | Magnitude | Duration |
| 1. | Instantaneous | < 0.1 pu | 0.5 to 30 cycles |
| 2. | Momentary | < 0.1 pu | 30 cycles to 3 sec |
| 3. | Temporary | < 0.1 pu | 3 sec to 1 min |

### 2.13.8 Voltage Fluctuation

Voltage fluctuations can be described as systematic variations of the voltage envelope or random amplitude changes where the root mean square value of the voltage is between 90 and 110 % (0.9 to1.1 pu) of the nominal voltage. Voltage variations occur when loads connected to a network demonstrate constant and quick variations in the magnitude of the load current, resulting in the fluctuation of voltage. These can be referred to as voltage flicker.

***Voltage flicker*** originates from the voltage fluctuation that causes the lamps to blink and can be perceived by the human eye. Flicker can be described as a visual impression of unsteadiness induced by a light stimulus of which the luminance or spectral distribution fluctuates with time. When the lighting fixture is driven by AC-mains directly, the emitted brightness changes along with the line voltage transition periodically in double the line frequency resulting in flicker. Flicker is caused by the fluctuations of the grid voltage. The voltage fluctuations are caused by changes in the power flow in the power grid [138]. It influences the cycle of sight and the human mind's response, resulting in weariness, distress and a decrease in concentration [139]. The low frequency flicker (3 Hz –70 Hz)

is known to have negative impacts on the human body, it can also cause epileptic seizures [140]. Both voltage fluctuation and flicker are related as shown in equations 2.16 and 2.17 respectively. Hence, by controlling the reactive force in the equation, flicker can be controlled. Flicker can be compensated for by using shunt and series compensation strategy. The reaction force intertwined by the trim is kept constant at a suitable value in shunt while in the series type compensation, the voltage drop can be reduced, and the reaction force remains stable despite load variations by controlling the reactance of the line. The impact of voltage fluctuation on the lamps that cause flicker can be measured and grouped into short time and long-time voltage flicker [141].

$$\frac{\Delta V}{V_n} = \frac{R\Delta P + X\Delta Q}{V_n^2} \tag{2.16}$$

Where $\Delta P$ = Active power change.

$\Delta Q$ = Reactive power change.

$V_n$ = Nominal line voltage.

$R$ = Short circuit resistance.

$X$ =Short circuit reactance. (in practice R << X).

Flicker can also be measured in terms of its severity as shown in Figure 2.48 which can be grouped into short and long-time flicker or minimum and maximum. Short term Flicker perceptibility (Pst) is the measure over a short period (a few minutes) of flicker occurrence while the long-term flicker perceptibility (Plt) is a further measure for cumulative irritation caused by very irregular gross flicker events, which may be too infrequent. The maximum, minimum severity and the flicker index can therefore be calculated as percentage [142].

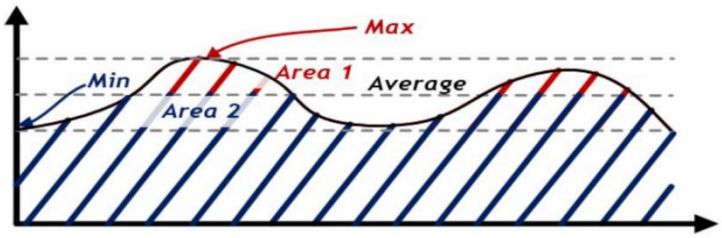


**Figure 2.48:** Flicker Illustration [142].

$$\%\ Flicker = \frac{L_{max} - L_{mini}}{L_{max} - L_{mini}} \times 100 \qquad (2.17)$$

$$Flicker\ Index = \frac{Area\ 1}{(Area\ 1 + Area\ 2)} \qquad (2.18)$$

Where $(L_{max})$ =Maximal luminance.

$(L_{mini})$ =Minimal luminance over a repetitive light cycle and the flicker. Area 1 =Integrated luminous intensity above average.

Area 2 =Integrated luminous intensity below average.

## 2.14 Proposed Compensator for a Voltage Rise Control at PCC

Literature reviewed in, [143], [144], [145], [146], and [147] confirms that the STATCOM is extensively used to: maintain distribution system stability, transient response control [148], capacitor voltage balancing [149], [150], [151], [152] and [153], harmonic current control [154], disturbance and error rejection control [155], voltage regulation during symmetrical fault, asymmetrical faults, and minimisation of surge currents [156], wind farm stability [157], [158] and [159]. It can also improve grid voltage [160], oscillation regulation [161], and flicker control [162], [163]. However, voltage rise and reverse power flow mitigation using STATCOM compensator scheme at PCC with large RDGs penetration levels are not covered in the literature review. STATCOM's response time and the rate of delivering capacitive power capability are not comprehensively presented in the literature review. This thesis proposes a control strategy to be installed at PCCs of the DN to control/or mitigate the voltage rise effect and to limit the reverse power flow when operating at a worst critical scenario, such as minimum load and maximum

generation from RDGs. The control structure consists of installations of static compensators (STATCOM), which incorporates the Pulse Width Modulation (PWM), and the block/deblock and in-loop filtering circuit control scheme at PCC, for the control of active and reactive power. The proposed control strategy would be used to mitigate the voltage-current harmonic signals, improve the power factor, voltage stability at PCC, and also protect the converter-PWM scheme.

### 2.15. Summary

A better decentralization of policy making in terms of renewable energy (generation, transmission, distribution) from national to provincial or local government levels, diversification of energy mix, energy conservation, efficiency and energy pricing that can better reflect market realities will liberate the development of renewable energy across the world. This thesis has presented an insightful survey on recently published research on STATCOM power quality enhancement in distribution networks. Voltage profile improvement, power loss mitigation, minimizing total harmonic distortion, average voltage deviation, investment cost reduction, and system reliability improvement are observed to have been the main focus of STATCOM compensators. This chapter also discussed the following aspects of power quality in detail: power quality concept, importance of power quality, the classification, types, causes of power quality, parameters of power quality, how voltage, current and power quality are related, possible solutions to power quality issues, power quality issues on the utility side, power quality on the grid and on the load side, electrical load classifications, types, and power quality can be sustained in power systems. The overall deduction is that a larger percentage of power quality challenges may be ascribed to the end user. The voltage supply by the utility can be controlled but it has no control over the current drawn by the load. Most of the power quality issues emanate from end users and grid occurrences. For power quality to be sustained in a system, the power supply from utilities and grid events and load should be adequately controlled.

# CHAPTER 3

# POWER SYSTEM AND RENEWABLE DISTRIBUTED GENERATION

## 3.1 Introduction

For many years, power production systems were primarily bulk power systems comprising generation, transmission, and distribution systems. The greatest substantial changes in power systems globally are the swift growth of RDGs and the transformation from bigger traditional synchronous machine resources to smaller-sized and renewable distributed generation resources. Nations across the world are better informed of the environmental consequence of using fossil fuel for electrical power generation and thus they are employing the Renewable Distributed Generation (RDG) into their energy mix. RDGs' integration into the power system is seen as a vital development in the advancement of the electrical utility grid. Conventional generators make use of rotating machines and drives while RDG based technologies are mostly converter/inverter interface. Based on Independent Electricity System Operator (IESO) and International Renewable Energy Agency (IRENA) policies, the RDGs are limited to small, medium, and large scale usually driven by renewable source(s) located near the load centre [164], [165]. Due to the policy pertaining to the regulation of energy because of global warming, increasing environmental concerns about the adverse effect of fossil fuel usage, regular outages and blackouts, inadequate access to the utility grid for rural communities and the high price of electricity billing, RDGs deployment could be the best option for rural electrification. This chapter discusses renewable distributed generation technology; the relationship between RDG and smart grids; RDG deployment; microgrid systems, classification and types; off-grid microgrid; grid tie microgrid; microgrid backbone; microgrid controls; microgrid energy management; converter building blocks, types, advantages and disadvantages of RDG.

## 3.2 Renewable Distributed Generation Technology

RDG can be described as an electric power supply that is driven by renewable source(s) and connected directly to the distribution network or on the customer site of the meter or to the load. The technology involves solar photovoltaic power, wind power, small hydro,

geothermal power, and biomass as shown in Figure 3.1. The point at which it is connected to the Distribution Network (DN) is referred to as Point of Common Coupling (PCC). The capacity can vary from 1 kW – 5 kW, 5 kW– 5 MW, 5 kW– 50 MW and 50 kW to < 1 GW which can be regarded as micro, small, medium, and large scale [166], [167]. RDG can be owned by the independent power producer, individually or by the utility. It can also be designed to perform certain functions as depicted in Table 3.1. The environmental impact of RDG, its technical and economic intention may be altered by the designation of the RDG size, the type and the allocation. Hence, an appropriate RDG size should be installed in the right location [22], [23]. If RDGs are properly installed in a strategic location, benefits depicted in Figure 3.2 can be obtained.

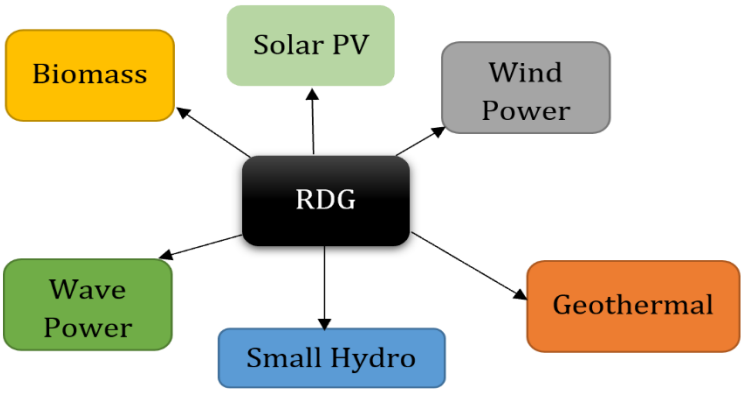


**Figure 3.1:** RDG Sources *(created by Author).*

**Table 3.1:** RDG type classification [168]

| DG Type | | Function |
|---|---|---|
| Type 1 | P-type | Type1: This type DG is capable of delivering only active power such as photovoltaic, micro turbines, fuel cells, which are integrated to the main grid with the help of converters/inverters. However, according to current situation and grid codes the photovoltaic can and in sometimes are required to provide reactive power as well. |
| Type 2 | Q-type | DG capable of delivering both active and reactive power. DG units based on synchronous machines (cogeneration, gas turbine, etc.) come under this type |
| Type 3 | $PQ^{+}$ type | DG capable of delivering only reactive power. Synchronous compensators such as gas turbines are the example of this type and operate at zero power factors |
| Type 4 | $PQ^{-}$ type | DG capable of delivering active power but consuming reactive power. Mainly induction generators, which are used in wind farms, come under this category. However, doubly fed induction generator (DFIG) systems may consume or produce reactive power i.e. operates similar to synchronous generator |

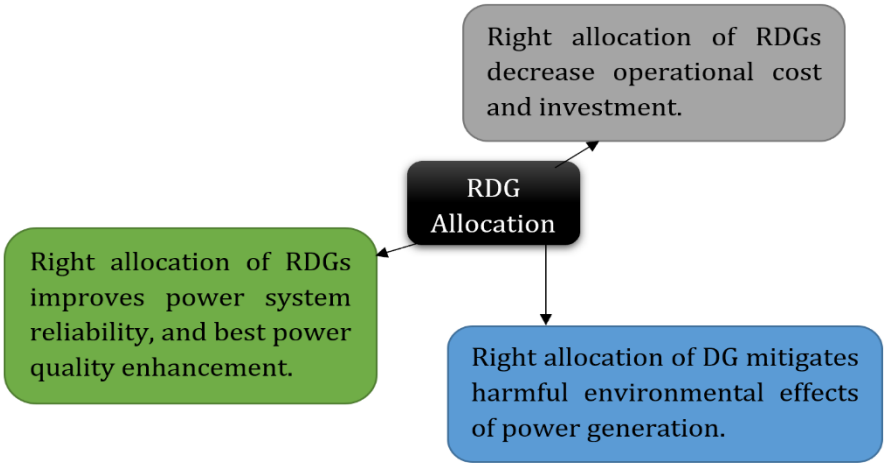


**Figure 3.2:** RDG Allocation Benefits *(created by Author).*

### 3.3 RDG Versus Smart Grid

The point at which RDG is connected to a distribution network will form an active point because it injects active power and a voltage higher than the voltage at that point. The active zone is the node in the network with the ability to monitor and control the network conditions remotely while the weak zone is the node with the highest voltage fluctuations in the feeder. The integration of RDGs will make the weak zone become active, while a further increase in the number of RDGs will result in fewer weak zones. As a result, by incorporating an automation system, communication, and information technology systems capable of monitoring power flows from points of generation to points of consumption, active zones become smart. The increase in the number of RDGs and the capacity will eventually result in a sufficiently smart point to control the whole local network. Consequently, a local network becomes a local smart zone. With a further increase in the number of local smart zones, the whole network will be covered with smart zones, resulting in smart grid and smart distribution systems as shown in Figure 3.3.

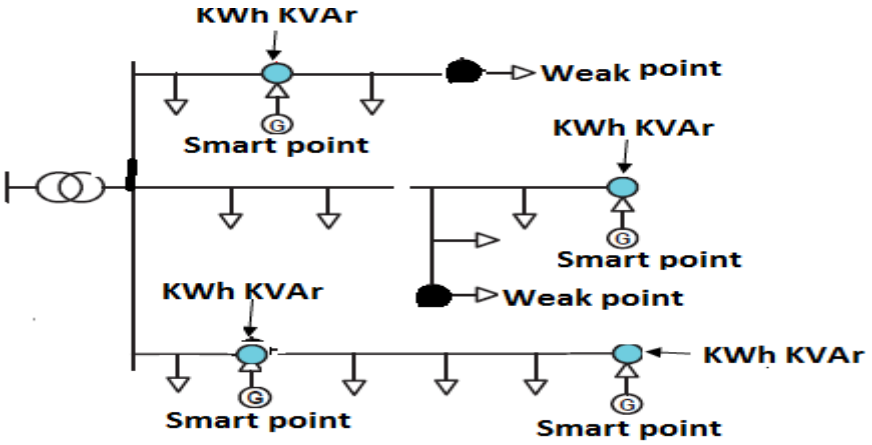


**Figure 3.3:** Line with Smart Points and Weak Points *(created by Author).*

### 3.4 Deployment of Renewable Distributed Generation to the Power System

The effective methods by which RDGs can be deployed to the power system are by pico-grid, nano-grid, mini-grid, and microgrid systems, which if interconnected can result in a smart grid system. For many years, the world depended on conventional centralized utility power grid for heat and electricity demand. However, many communities, districts or region were still unable to connect to the central electricity grid. The extension of electrical power did not even reach some areas, while some can view the grid from far off but do not have access to the connection due to high price of billing. Also, with the daily increase in the world population, there would be an increase in electricity demanded for basic living. If the existing grid does not expand, the rate of congestion on the grid will be very high resulting in many unusual occurrences on the grid, which affects consumer loads. If another means of electricity generation is not thought of, communities that are very far to the grid connection will not have access to electricity. Several methods of local energy generation have tried to address this challenge. Former centralized energy generation was decentralized with the aid of RDG units that can be deployed to the power system in the form of **pico-grid, nano-grid, mini-grid and microgrid systems.** RDGs generate electricity near the load centre. They can serve a single structure such as a home, business, or tie into the larger electricity delivery system, such as a major industrial facility, or college campus. They can reduce electricity losses along transmission and distribution lines. RDG is inherently robust against grid related failures. It can be built bottom up by individuals who decide to invest [169], [170], [7]. RDGs are mostly used in

isolated areas where there is no access to the utility grid and in the city to minimize the peak demand.

An electricity grid system is defined not by the size or name given to it, but by the function through which they operate. Macrogrid or megagrid system can be referred to as conventional grid, which involves centralized method of power generation while microgrid is a single grid system and fragment of macrogrid. It is usually distributed generation with smart management. Similarly, nanogrid is a single grid system and a fragment of microgrid, and, it is building level circuit.

The pico, nano, mini and microgrid systems can be grid tie and off grid system.

- Grid tie
- Off-grid/Stand-alone.

### 3.4.1 Grid-tie RDG

A grid-connected system can be described as the means of powering a load such as home appliances, or small business with renewable energy generation (solar system, wind etc.), while any excess electricity generated is fed back into the grid. In a grid-tie system, a grid-tie inverter delivers power to the grid. The device converts the DC voltage produced by the RDG to sinusoidal AC voltage output to synchronise with the grid as depicted in Figure 3.4. The grid-tie inverter monitors the grid supply characteristics, which are voltage and frequency, and adjusts the output accordingly to match the grid [171], [172]. In a grid-tie system, a storage unit is not compulsory, the system can easily be installed, and the maintenance is reduced due to the fact that there is no storage unit [173].

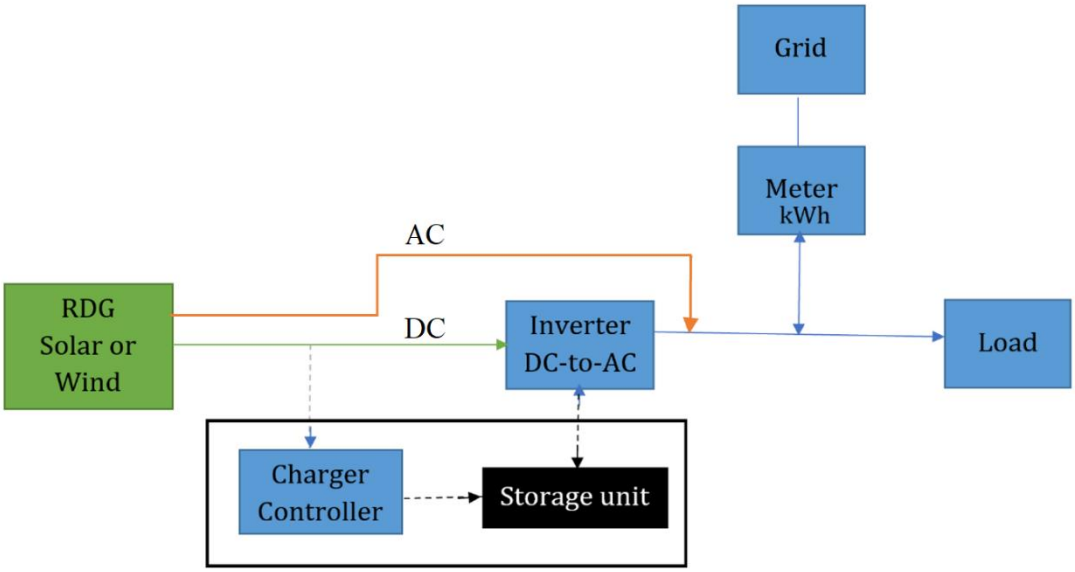


**Figure 3.4:** Block Diagram of Grid-tie System *(created by Author).*

**Features of Grid-tie RDG**

- It improves voltage profile when connected to a distribution network.
- Reduction in power loss and increased overall energy efficiency.
- Reduction in security risk.
- Relieved transmission and distribution (T&D) congestion.
- Better customer control over their energy.
- Helps in peak load shaving and load management programmes.
- Improved competitiveness and market opportunities.

### 3.4.2 Off-grid

Supplying electricity to the load using a small renewable energy system that is not connected to the national electricity grid is known as standalone or off-grid system. It relies exclusively on generating power on site while remaining close to the load centre. Usually, this kind of system involves electricity storage such as lead-acid batteries, lithium batteries, other battery technologies, supercapacitors and hydrogen, power source(s) such as RDGs (solar panels, wind turbines, micro-hydro or combination of two or more) and inverters as shown in Figure 3.5. For developed countries, off-grid systems consist of mini-grids for rural communities, institutional buildings and commercial/industrial plants and buildings and solar PV power generation in residential households. The latter

category is relatively small, and most residents still rely on the grid for part of their load. Standalone (off-grid) renewable energy systems are used all around the world, not only in developing countries, as they are the most competitive way to supply electricity in locations where the distance to the transmission and distribution electrical grid is relatively high, for example in remote rural communities, farms, telecom stations, etc. Even in some cases, grid-connected systems can become off-grid systems to avoid dependence on the national grid system. However, disconnecting from the grid usually implies a higher cost of electricity [174].

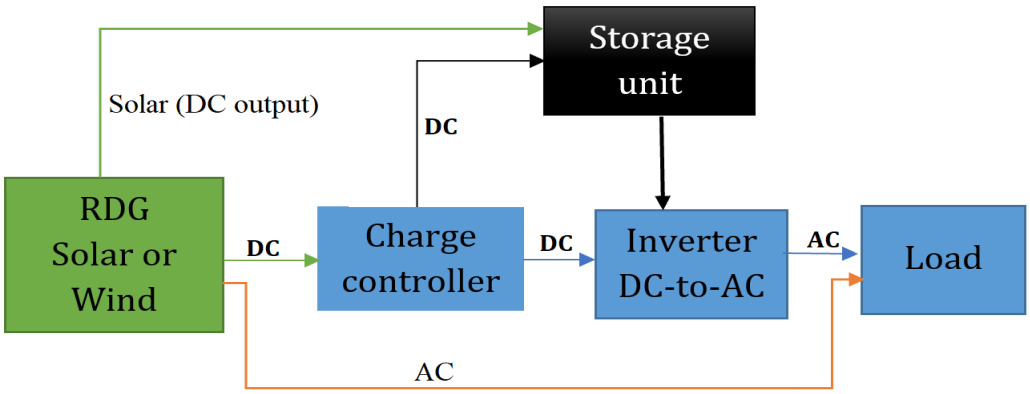


**Figure 3.5:** Block Diagram of Off-grid System *(created by Author).*

**Features of Off-grid RDG**

- It provides electricity more cheaply than grid extension, especially in rural areas where there is no access to grid connected electricity.
- It is an efficient and reliable means of power generation.
- Allows better use of local natural resources.
- It is modular and relatively easily assembled from standardized packages.
- Low-cost sources serve demand during peak price period.

### 3.5 Pico-grid System

The pico-grid system is the method of power generated locally from renewable sources to power a very small load such as a phone set charging, or telemetry. It is a self-sufficient, adequately smaller power supply system capable of providing electricity to a small load [1]. It is a simple technology, easier to implement and affordable. It enables daily

household routine tasks to run without connection to the nano-grid or microgrid system. The capacity can be less 20 W.

### 3.6 Nano-grid System

Nano-grids can be described as locally generated renewable energy typically less than minigrid. It can be a standalone wind or solar source which supplies power to limited capacity or each home is powered by an independent wind or photovoltaic system such small building, shop. It can also be referred to as a building level circuit. It exists where there is no existence of a microgrid or minigrid system and connection fees cannot be afforded by villagers. It helps to keep day to day home activities such as dishwasher, drier and vacuum cleaner running. The capacity can be between 10 W and 500 W.

### 3.7 Mini-grid System

RDGs can supply power to a small geographical location that can be independently operated or/and exchange power with the main grid otherwise known as a **Mini-grid system**. The capacity can be between 5 kW and 200 kW, which can be prominent where access to the national grid does not exist. Mini-grid can provide electricity to shops, houses, community health houses, streetlights and boreholes.

### 3.8 Microgrid System

Due to the development of smart devices, smart cities and smart living, the need for clean renewable alternative energy cannot be over emphasised. To tackle the depletion of conventional energy resources around the globe, researchers have focused on developing renewable energy resources and microgrids [175]. A microgrid is a network of electrical energy distribution systems that depends on distributed means of electricity generation which can independently function and/or synchronize with a nationwide grid within a definite region. A microgrid is advantageous in terms of reliability and revenue. It enables a community, organization, industry or data farm to enjoy reliable energy supply where outages may be exceedingly costly. It also enables them to make profits, sustain economic activities, reduce environmental pollution produced by the conventional energy method of power generation and to enjoy unlimited energy generation from renewable energy sources. Microgrid comprises a power generation source, interface (power

electronic), and energy storage systems to power a load. The capacity can be between 200kW and 900kW. Microgrids, Mini-grids, Nano-grids and Pico-grids are interrelated but microgrid is the most popular and widely used. Microgrid can supply power to industries, college campuses, communities, or district facilities due to its reliability and competitiveness as compared to the centralized power method of generation.

### 3.8.1 Microgrid structure

The microgrid system is usually structured to combine renewable sources, storage systems and conventional means of energy generation to supply power to the consumers. The renewable aspect may be wind, solar, geothermal, tidal, biomass, small hydro, while the storage system may be connection of batteries in series/parallel or a conventional method such as a generator powered by fuel or diesel. Microgrid can be integrated into the national grid at a low voltage level or medium voltage level (grid tied) with the aid of converter/inverter system and it can be operated in isolated mode (off grid). An Energy Management Scheme (EMS) can be incorporated into the modern microgrid for best performance, fast response, self-healing from grid disturbance and optimization. The types of power structure and the loads with which they adapt and derive their electrical energy form govern the microgrid [176], [177].

## 3.9 Type of Microgrid

The primary form of microgrid can be Alternating Current (AC) type, Direct Current (DC) type and Hybrid type as shown in Figure 3.6.

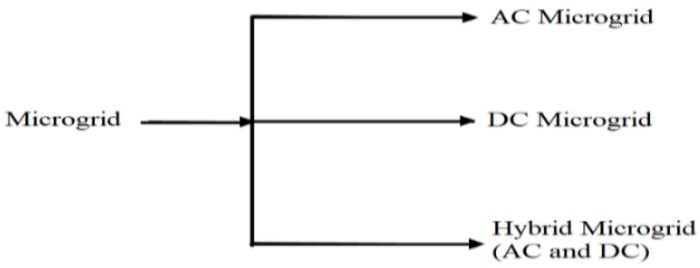


**Figure 3.6:** Microgrid Configuration *(created by Author).*

### 3.9.1 AC type microgrid

AC type microgrid connects the load either directly to the AC bus bar or by means of a converter depending on the types of electrical energy they produce or consume as shown in Figure 3.7. The operating voltage, the frequency, and the phase/phases either single, double or 3-phase are considered in AC type microgrid.

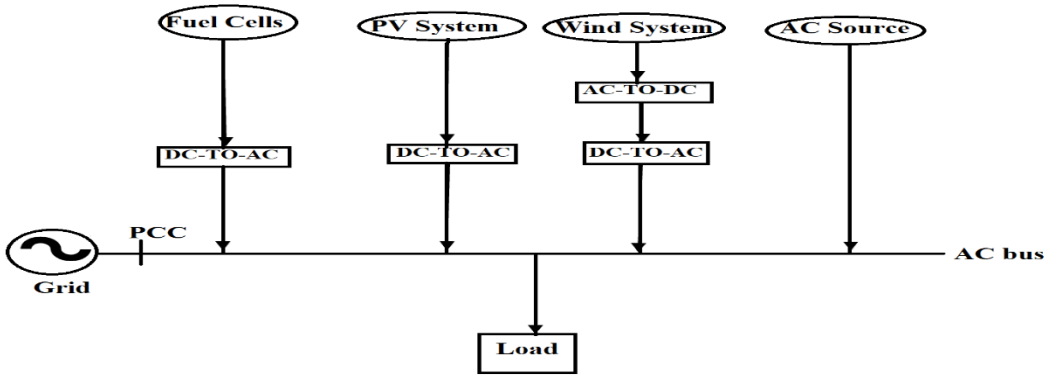


**Figure 3.7:** AC Type Microgrid *(created by Author).*

### 3.9.2 DC type microgrid

DC type microgrid connects load directly to the DC bus bar or by means of a converter (DC-DC converter). Since there are different levels of DC voltage output in renewable energy sources and battery storage systems, power electronic converters are needed to integrate all the renewable energy source depending on the types of electrical energy they produce or consume as depicted in Figure 3.8. DC microgrid possesses the advantage of unidirectional power flow with a converter connected to the system, thus, power flow control is easier. The direction of voltage, current and power are closely interrelated and there is a higher possibility of network reliability and fewer losses generated in the system. The DC type microgrid system can be made up of renewable energy source (PV, wind, fuel cell), load and battery storage system.

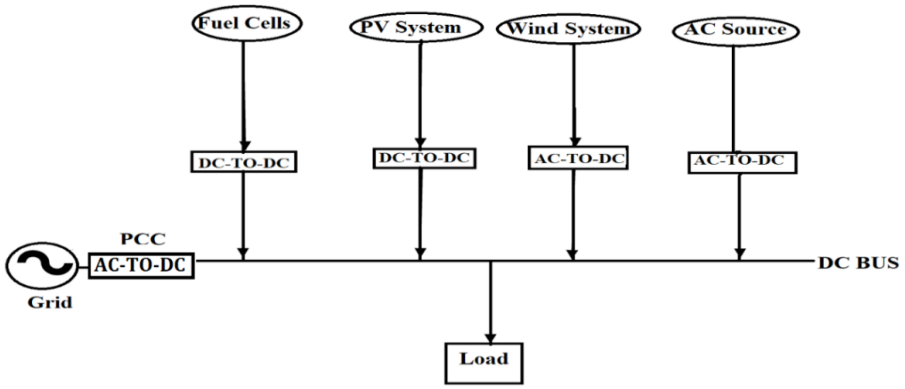


**Figure 3.8:** DC Type Microgrid *(created by Author).*

### 3.9.3 Hybrid microgrid/Advance microgrid

Hybrid microgrid exhibits the features of both AC and DC microgrid. Conversion to electrical energy is easier due to the presence of power electronic converters in the AC and DC buses of the system as depicted in Figure 3.9. Hybrid microgrids consist of different kind of loads and the battery storage depends on the type of energy they draw or generate. The composition of Microgrids can be grouped into Renewable Energy Sources (such as wind, solar, small hydro, etc.), Energy Storage System (such as lead acid battery or lithium battery), Fuel Generating Set (such gasoline or diesel generator), loads (such residential or industrial load) and the Power Grid (such as off grid or on the grid). It is expected that microgrid should be safe, reliable and the energy generated should be affordable.

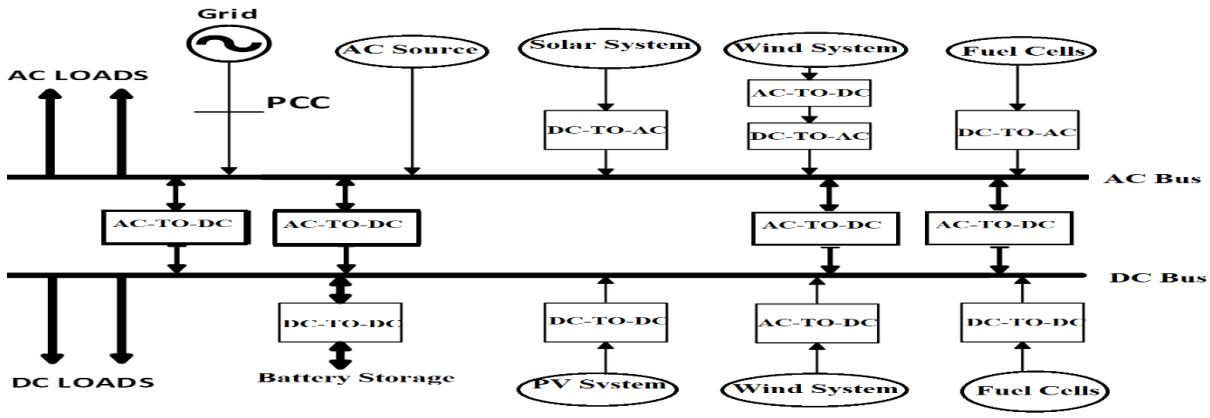


**Figure 3.9:** Hybrid/Advance Microgrid structure *(created Author).*

### 3.10 Microgrid Energy Management Scheme (EMS)

The energy management scheme in the microgrid system provides the rate at which the system is smart and reliable. For a system to be smart, the measurement capability should be present, communication strategy should be in place, rate of load-energy consumption prioritization should be assured and flow of power across loads buses should be easily monitored. EMS will play a critical role in the modern micro-smart grid system. The energy management scheme is very critical especially when microgrid is not connected to the main grid system due to the fact that there will be more than a source of energy generation with a different power capacity integrated together and the system may not have a dominant infinite bus. Also, some microgrid systems may not possess power electronic converters for extremely fast response for voltage and power angle stability. Therefore, the energy management scheme is of great importance in the microgrid system. As shown in Figure 3.10, the energy management scheme accesses the latest and forecasted data from the generating source, the consumers and the market information to manage the consumption level of the national grid system, distributed source and the consumers.

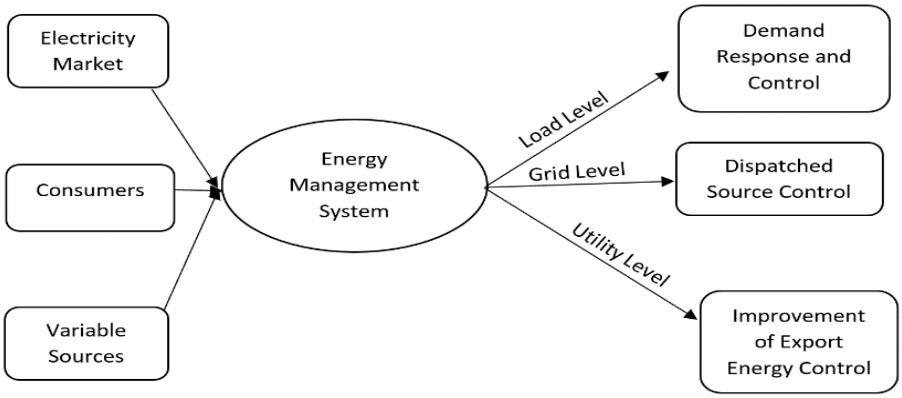


**Figure 3.10:** Microgrid Energy Management System *(created by Author).*

EMS provides a real and active power allocation strategy between renewable and non-renewable energy sources, manages microgrid disturbances, discovers energy set point of the distributed sources and allows the microgrid to be synchronized to the national grid system if need be. The national grid is supposed to adapt variation in active and reactive power supply and consumers from the microgrid by controlling power generated from real

distributed sources, active power buses, real power and voltage buses. But when the microgrid is not integrated into the national grid, the overall energy generated should meet the consumer loads demanded, or else, shedding of consumer loads demanded to match energy production will be inevitable. To reduce the effect of dynamic behaviours of the microgrid such as harmonic and transient oscillation, simple but active control strategies may be essential. Microgrid power management solutions (PMS) should be capable of controlling the load profile of its consumers, synchronized to the national grid, operate within an acceptable power quality requirement and maintain stability during grid disturbance.

### 3.11 Microgrid Control Schemes

The control scheme of the microgrid can be selected according to its characteristics and the interface between the distributed resources as shown in Figure 3.11. Microgrid active and reactive power, frequency and voltage are the main considerations in designing a control strategy. A Microgrid control scheme may be interacting with a national grid or may be non-interactive with the national grid. When the voltage and frequency at the point of common coupling are indirectly involved, a grid following approach can be used. But if the power generated or load of a particular distributed generation can be independently controlled of the other distributed generation or load, the non-interactive approach can be considered. Power set points may be considered on the power dispatch arrangement or by the compensation of consumer load [178]. However, the real and the reactive power set point requirement as an input control is dependent on the interactive scheme.

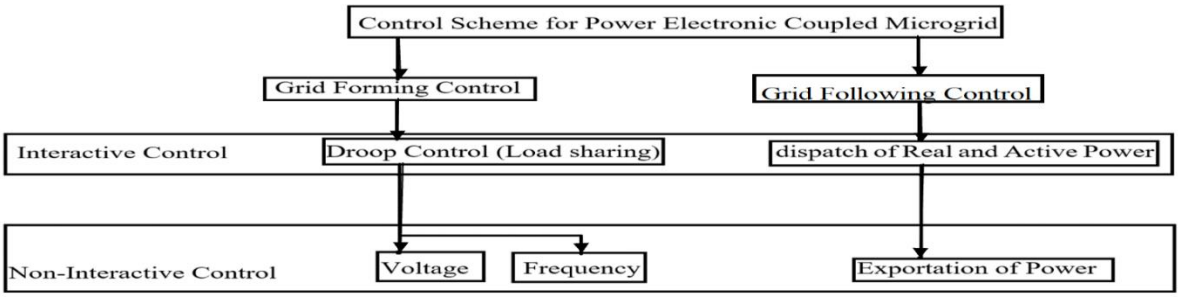


**Figure 3.11:** Control Scheme for Power Electronic Coupled Microgrid *(created by Author)*.

### 3.11.1 Grid Forming Arrangement

When a microgrid is not integrated into the national grid, it exhibits the characteristics of the swing source. Microgrid frequency and the voltage at the point of common coupling can be controlled by the grid forming component. The real and the active power components can be allocated by the voltage and frequency droop scheme if more than one distributed resource is involved grid control and stability. In such a situation, the rated value of the microgrid's voltage and frequency may deviate depending on the features of the droop and system loading. A simple block diagram of droop control scheme is shown in Figure 3.12 (a). The differences in the measurement of the voltage and frequency from the distributed generation of the microgrid feeds the controller. The differences in the amount of energy produced by the individual distributed generation in the microgrid can be controlled by selecting the slope of the individual droop that is proportionate to the rated value of the equivalent distributed generation to limit overloading in the system. The voltage and the frequency droop are depicted in Figure 3.12 (b) and (c) as indicated by the slope of the graph $(K_{KP})$ and $(K_{VQ})$ and the rated voltage and frequency of the base point signify by $(V_0), (Q_0)$ and $(F_0), (P_0)$. When distributed generation allocation of power level alters to reset the voltage and the frequency to a new value, the dynamic restoration of the adjustment of the distributed generation operating point can control the droop coefficient and the base point. This process may be slow, but it can be achieved during microgrid synchronization.

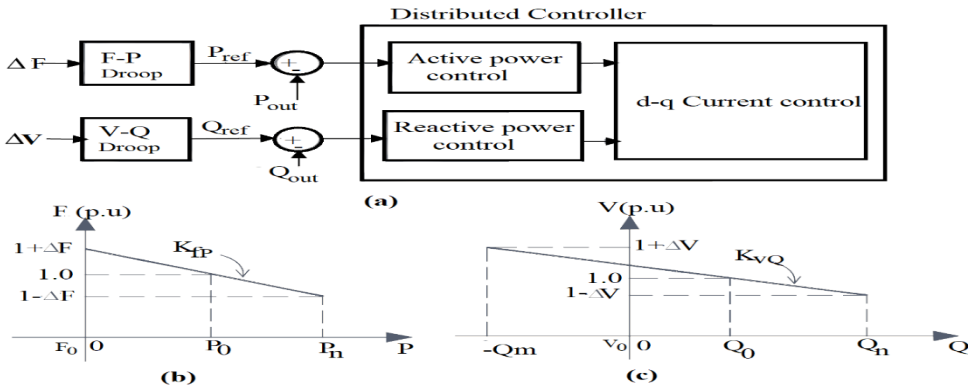


**Figure 3.12:** Frequency and Voltage droop.

### 3.11.2 Grid Following Arrangement

The output voltage, frequency and power of the distributed sources can be controlled by the arrangement of the grid following scheme where a converter such as a voltage source converter is used at the point of common coupling. The waveform of the reference voltage can be achieved by a current controlled scheme for the pulse width modulation (PWM) of the voltage source converter. The point of common coupling voltage can be tracked to synchronize reference signal to the frequency of the microgrid. The axis known as direct and quadrature axis (d-axis and q-axis) of the output currents of the power electronic converter related to the real and reactive power components can be executed by the control scheme $(\mathrm{dq0})$. The $(\mathrm{dq0})$ control scheme and the extraction of the voltage source converter's current components (d-axis and q-axis) from $(\mathrm{abc})\ \mathrm{to}\ (\mathrm{dq0})$ controller scheme compares the reference signal of the voltage control loop or external power. To obtain $(\mathrm{V_d})\ \mathrm{and}\ (\mathrm{V_q})$ of the d-axis and q-axis reference signal voltage component, error signals are supplied to current control $(\mathrm{dq})$. The reference signal for pulse width modulation can be generated by the extraction of $(\mathrm{abc})\ \mathrm{from}\ (\mathrm{dq0})$ as depicted in Figure 3.13 (a). External and internal control are subject to a change depend on the control mode and the source. In the unbalanced system, the same method can be employed. When $(\mathrm{dq})$ control scheme is substituted for the reactive power and the DC-link voltage, the DC-link receives its input from distributed sources to improve its voltage. The voltage swell/rise can thus be controlled when the converter current $(\mathrm{d}-\mathrm{axis})$ value is selected to compensate for the input and output power of the DC-link. The converter current $(\mathrm{q}-\mathrm{axs})$ reference value is chosen by the reactive power controller in Figure 3.13 (b), if the power factor that is closer to unity is required, the $(\mathrm{Q_{ref}})$ can be set to zero. The block diagram also consists of PIs for controlling current of the d-axis and q-axis, voltage and feed-forward system. The comparison of the d and q axis current out together with the reference signal provides input to the PWM. The main benefit of this system is that it limits the microgrid converter output current during disturbance, thereby protecting the converter from overcurrent and limiting the fault current within the microgrid system.

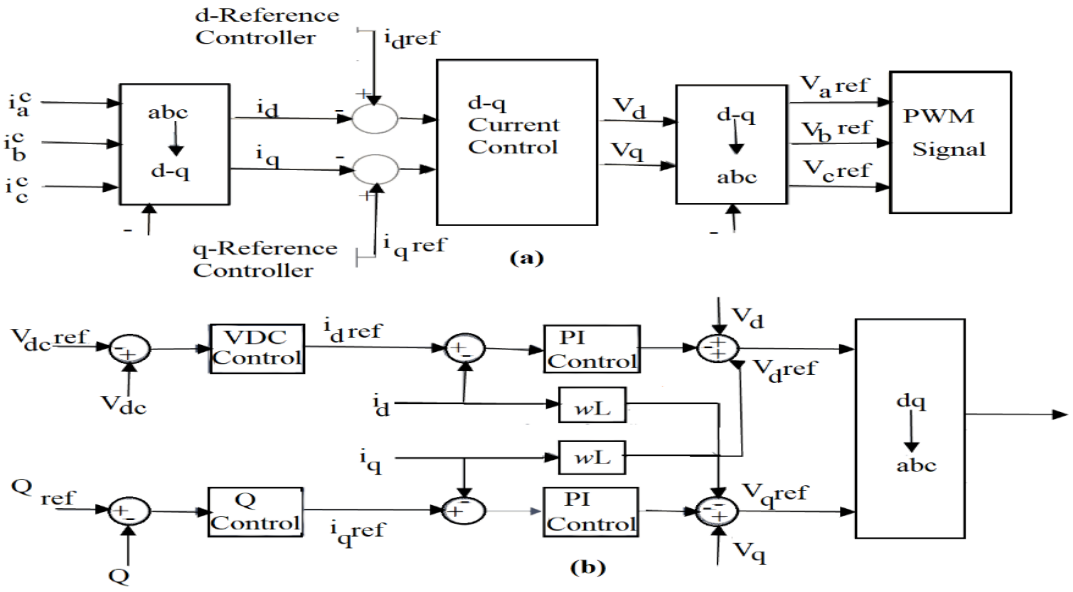


**Figure 3.13:** Voltage Source Converter dq Control Scheme at PCC.

### 3.11.3 Active and Reactive Power Control Scheme

The active and reactive power of the distributed sources integrated with the microgrid need to have an appropriate control strategy to monitor the power flow along the load buses within the system. The real and the reactive power compensation is necessary by making use of prespecified value. As depicted in Figure 3.14, $(P_{ref})$ and $(Q_{ref})$ establish the active and the reactive power of the reference point while $(P_{out})$ is the output of the real power and $(Q_{out})$ is the output of the reactive power obtained from the measured voltage and the current of the system output. The reference to active and the reactive power can be set by forecast and calculation with respect to the microgrid power profiles and load fluctuation. The effectiveness of the reactive power control in a microgrid system is also dependent on the voltage regulation at the point of common coupling and the power factor requirement.

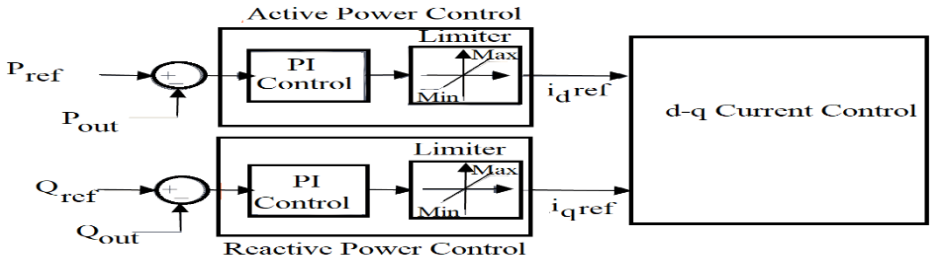


**Figure 3.14:** Active and Reactive Control.

### 3.12 Microgrid Hierarchical Arrangement

For the optimum performance of the microgrid system, the control scheme hierarchy is of great importance, as depicted in Figure 3.15. This microgrid control hierarchy is divided into segments of the local control scheme, which may be in milli-seconds; the primary control scheme which could be seconds; the secondary control scheme which could be in minutes and lastly the tertiary control scheme which could also be in hours or days [179], [180]. The first microgrid hierarchical control ensures network stability and dynamic response of voltage and current in milli-seconds. It provides the reference for the primary level control strategy, and it can make use of the pulse width modulation control converter. The next microgrid hierarchical control is the primary control scheme which maintains the operating point of the microgrid provided by the local control level. It maintains the control strategic level in seconds. The microgrid power flow adjustment is maintained by the secondary hierarchical control strategy. This is achieved by calculating the energy consumed by the load with respect to the storage system and distributed resources. The microgrid operational limit, energy equilibrium, network power quality capability and power reference are maintained by the microgrid secondary hierarchical control scheme. The negotiation of price, market and services between the independent own power supply and the consumers is maintained at the tertiary level [181].

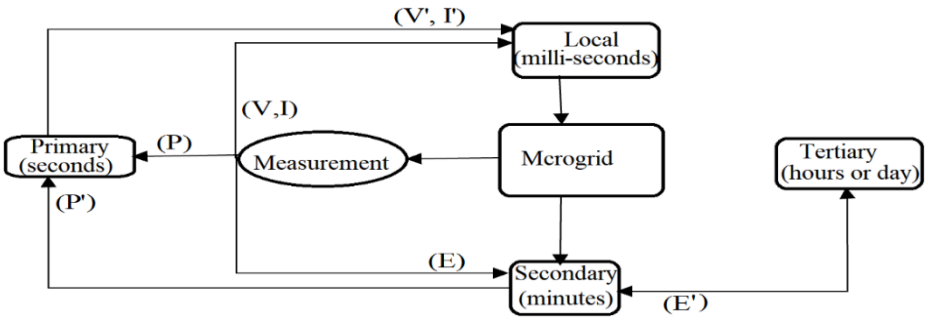


**Figure 3.15:** Microgrid Hierarchical Control *(created by Author).*

### 3.13 Microgrid Backbone

The advent of Microgrid and possibility of utility companies accessing RDG integration to a distribution network was facilitated by the development in power electronic devices otherwise known as power semiconductor devices. The main backbone of any microgrid is the power electronic converter as depicted in Table 3.2. Power electronic converters play a crucial role in converting power from one form to another to meet the need of the consumers. The processing and control of electrical energy to provide voltage and current in a suitable manner to the load is also part of the converters' function. A typical converter is made of electronic components such as diode, transistor, resistor, Silicon-Controlled Rectifier (SCR), Triode for Alternating Current (TRIAC), Insulated-Gate Bipolar Transistor (IGBT). The basic block diagram of a typical converter is depicted in Figure 3.16. It is pertinent to know that the advancement of power electronic circuits and control strategy have improved the capability of microgrid in the power system operation. The purpose of the converter in a microgrid is to provide conditioning power as demanded by the loads. A microgrid converter system involves AC-to-DC, DC-to-DC, DC-to-AC and AC-to-AC converters for AC buses, DC buses and loads in the system. This is because consumers need a reliable, constant voltage and power quality supply which can be achieved by using controllable converters. Depending on the control strategy, the harmonics generated by the converters to the network can be minimized. The application of power electronics converters is of great importance for advanced technology due to its higher power handling capacity. It is an integral part of the microgrid system and other functions such as heat and light controls, electric motor control and power supplies, vehicle propulsion system and high voltage direct current systems.

**Table 3.2:** Power flow control and conversion configuration for DGs.

| S/N | DG | Source | Converter | Control scheme |
|---|---|---|---|---|
| 1 | Non-renewable DG | Diesel engine, small hydro | Synchronous generator | Governor/AVR control (+P, ±Q) |
| | | Fixed-speed wind turbine | Induction Generator | Pitch control (+P, -Q) |
| 2 | Renewable DG | Variable speed wind turbine | AC-DC-AC | DC link voltage and speed control (+P, ±Q) |
| | | Solar system, Fuel cell | DC-DC-AC | DC link and voltage control (+P, ±Q) |
| 3 | Long-term storage | Battery system | DC-DC-AC | Charge/frequency/ voltage control (±P, ±Q) |
| 4 | Short-term storage | Super capacitor, flywheel | AC-DC-AC | Speed control (+P, ±Q) |

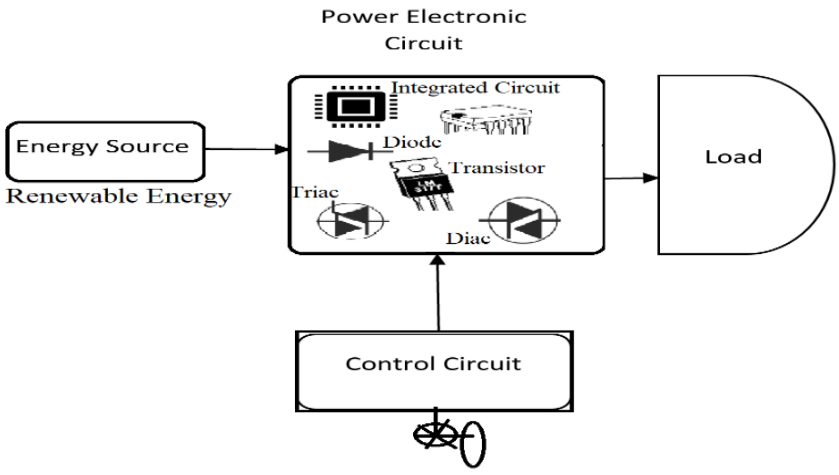


**Figure 3.16:** Electronic Converter Block Diagram *(created by Author).*

### 3.14 Converter Building Block

A microgrid converter consists of power and the control segment. The power segment section, which is made of transformers, fuses, diodes, transistors, capacitors, Triacs, chokes, resistors, SCRs, Diac, etc., transfers energy to the consumers from the source, while the control segment section, which may be analogue or digital type regulates the element behaviours in the power segment section. Based on a specific function of a converter in a microgrid system, it can be grouped into AC-to-AC, AC-to-DC, DC-to-DC and DC-to-AC converters.

#### 3.14.1 AC-to -AC Converter

This is the type of energy converter that transforms AC voltage from one stage to the other by shifting the magnitude and the frequency of the source voltage. The amount of power delivered to the consumers is controlled by connecting AC supply to the AC load. This is done at a constant frequency by regulating the Root Mean Square (RMS) of the voltage output. The example of the AC-to-AC converter is depicted in Figure 3.17 where the control strategy of the shunt Thyristors 1 and 2 is controlled to regulate voltage delivers to the load. Power flows to the load when $(T_1)$ is triggered and forward biased by the source voltage during the first positive half cycle while it is in off state during negative half cycle. $(T_2)$ is forward biased when it receives a trigger from the source voltage. By strategically regulating the triggering action of both $(T_1)$ and $(T_2)$ in their half cycle, the

voltage across the load is controlled. Triac $(\mathrm{Trc}_1)$ and Diac $(\mathrm{Drc}_2)$ can be combined to control the load voltage. In such cases, both positive and negative are triggered by the Diac to the Triac where the average output controls the load voltage.

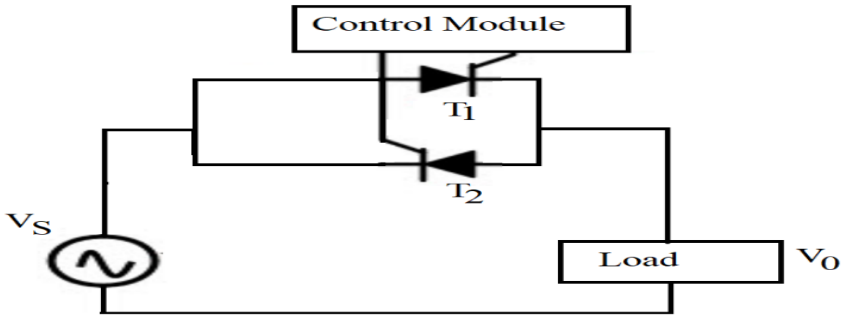


**Figure 3.17:** AC-to-AC converter *(created by Author).*

### 3.14.2 AC-to-AC Frequency converter

This type of converter varies the frequency of the supply voltage and current to the load's frequency requirement. This is done for the purpose of speed adjustment. Such application can be useful in industry where machine drives and induction heating are required. An AC-to-AC frequency converter can be a matrix or cyclo-converter. A cyclo-converter is useful in converting the frequency of specific ranges while a matrix converter has unlimited frequency capability.

### 3.14.3 DC-to-AC Converter

A DC-to-AC Converter can be described as a device which converts a DC source to an AC voltage that is variable. This type of DC supply has a fixed input. Such a converter can also be referred to as an inverter. The fixed input can be from a battery storage or from any DC link or source, while the produced output voltage of the inverter can be a fixed AC voltage or variable AC voltage with fixed or variable frequency as depicted in Figure 3.18. Inverters are usually connected between the DC source of a fixed input and variable AC consumers.

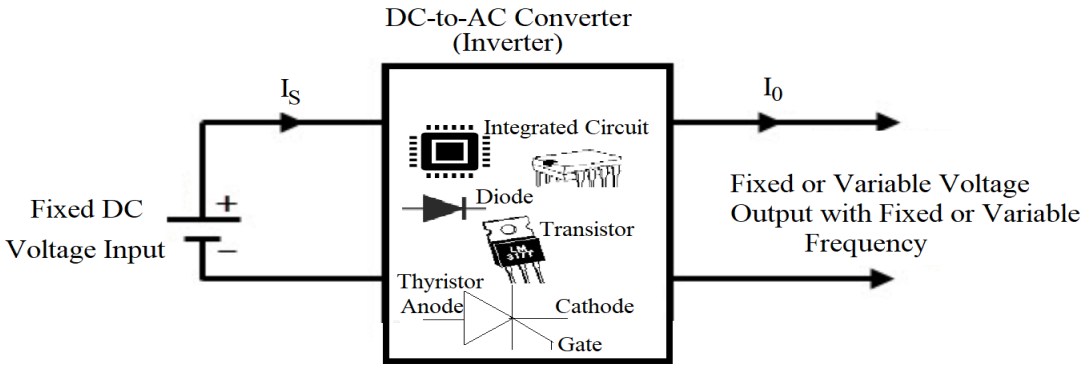


**Figure 3.18:** DC-to-AC Converter (Inverter) *(created by Author).*

The variable output voltage of a DC-to-AC converter or inverter can be obtained by strategically controlling the firing angle of the electronic component, such as thyristor. The DC-to-AC inverter can be single or three phase depending on the input source. The inverter can also be grouped into Voltage Source Inverter (VSI) or Current Source Inverter (CSI), both of which make use of pulse width modulation or multilevel.

### 3.14.4 DC-to-DC Converter

Diverse types of loads need different kinds of DC voltage level drawn from a fixed DC source for them to operate and function smoothly. To meet this demand, DC-to-DC converters come in to play. The process of obtaining variable DC output voltage or fixed voltage output of a magnitude higher or lower than the source value from a fixed DC input source is known as DC-to-DC converter or chopper. It is used between the DC source and the DC loads. The output of the chopper can be unidirectional or bidirectional based on the load requirements such electric vehicles, DC drives etc. DC-to-DC converters or choppers can be grouped into boost converters, bulk converters and boost/bulk converters. A **Boost Converter** otherwise known as a **step-up chopper** is a type of converter in which the voltage output generated is higher than the voltage input. A **Bulk converter** also known as a **step-down chopper** produces a DC output voltage that is less than the DC supply voltage, while a Boost/Bulk converter is a converter in which the output can be varied and used as a boost (step up) or bulk (step down) converter by varying the power electronic component use. If the voltage output is lower than the input voltage, it will act as bulk converter and if the output voltage is higher than the input voltage, it is otherwise used as boost converter.

### 3.14.5 AC-to-DC Converter

An AC-to-DC converter is a type of converter that converts AC voltage to DC voltage. The converter is known as a rectifier, as shown in Figure 3.19. A complete rectifier consists of transformer units that step the high voltage to low voltage. The rectifier circuit such as diodes or Thyristors converts the low voltage to DC voltage (a control unit may be incorporated if the Thyristors are used for the rectification). A filtering unit smooths the output of the rectifier circuit such capacitors. An AC-to-DC converter can be divided into two groups, controlled and uncontrolled rectifiers.

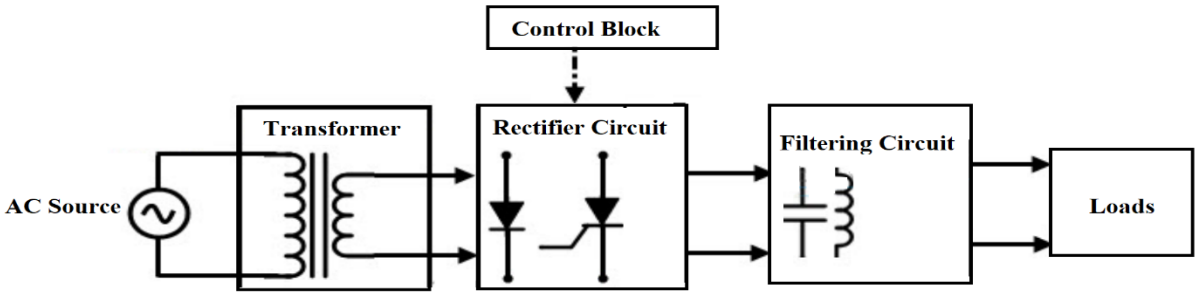


**Figure 3.19:** AC-to-DC Block Diagram *(created by Author).*

### 3.14.6 Controlled AC-to-DC Converter

This controlled AC-to-DC converter makes use of electronic components that can be controlled as a rectifying circuit, such as thyristors which can be controlled using a microprocessor or microcontroller to regulate and control the firing angle of the component. It is also known as a phase-controlled AC-to-DC converter. An AC-to-DC converter is further divided into a single-phase half wave converter, a single-phase full wave mid-point converter, a single wave full wave bridge converter, a three-phase half wave converter, and a three phase full wave converter.

### 3.14.7 Uncontrolled AC-to-DC Converter

An uncontrollable AC-to-DC converter rectifies the AC voltage to DC using diodes. The diode is an uncontrollable electronic component; no triggering is needed. Any type of converter that is made of diodes as rectification can only be regarded as an uncontrollable converter, it may be single or three phases. It can be divided into a single-phase half

wave rectifier, a single-phase centre tapped full wave rectifier, a single-phase full wave bridge rectifier, a three phase half wave diode rectifier and a three phase full wave diode bridge rectifier or six pulse rectifiers.

### 3.15 Advantages of RDG Integration

The potential advantages of RDGs integration into the power system can be summarised in Table 3.3

**Table 3.3:** Potential benefits of RDG

| | **Advantages of RDG** |
|---|---|
| 1. | Voltage profile improvement. |
| 2. | Losses reduced if adequately installed in the proper location and with an appropriate size. |
| 3. | Reduction in power transmission stress by providing power near load centres, while the need to transmit bulk power for longer distance is eliminated. |
| 4. | It provides environmentally friendly technology with no greenhouse emissions. |
| 5. | It is a good option for rural electrification where there is no access to the national grid. |
| 6. | It can serve as a relief for feeders' overload when installed in the proper location and size. |
| 7. | It defers the upgrade of T&D systems [182]. |
| 8. | Quick and easy installation of Modular RDG by utility or customers. |
| 9. | Improvement of power quality and reliability. |
| 10. | Low cost as compared to conventional power systems. |

| | |
|---|---|
| 11. | It creates power source diversity in power systems. |
| 12. | It creates competition in the electricity market, thereby bringing low cost electricity bills. |
| 13. | It provides low investment risk and a short lead time. |
| 14. | It provides for close tracking of load variation. |
| 15. | It occupies less space as compared to conventional power methods. |
| 16. | It can be efficient in peak shaving. |
| **Disadvantages of RDG** | |
| 1. | It causes bi-directional power flows in the grid, which alter power system operator planning and protection strategies as compared to the conventional power system with unidirectional power flows. |
| 2. | Voltage rise/over at PCC can cause harm to sensitive equipment and maintenance crew. |
| 3. | The control process for an independently owned RDG may be challenging. |
| 4. | The intermittent nature of the RDG can cause fluctuation in power out. However, solar depends on irradiation from the sun while wind depends on the breeze speed. Hence, they are non-dispatchable units. |
| 5. | RDG can inject harmonics into the electric grid due to power electronic interface. |
| 6. | Short-circuit current flow may increase due to the bi-directional power flows of the RDG. |

## 3.16 Summary

This chapter has presented in detail the renewable distributed generation technology, relationship between RDG and smart grid, RDGs deployment, microgrid system, classification and types, off-grid microgrid, grid tie microgrid, microgrid backbone, microgrid controls, microgrid energy management system, converter building blocks, types, advantages and disadvantages of RDG. The overall deduction from this chapter is that a microgrid system with RDGs integration would be the fastest and best option for rural electrification.

# CHAPTER 4

# MATHEMATICAL CONCEPT OF VOLTAGE RISE AT THE POINT OF COMMON COUPLING

## 4.1 Introduction

The strategic issues relating to Renewable Distributed Generation (RDG) which are high on the schedule of any utility company are: how abundant RDG will appear in the distribution grids, what consequence will the RDG have on the technical performance of the grid; what effect will the RDG have on the financial performance of the utility; and what deviations in technical design or commercial practice will be operational within a distribution utility with RDG integration. The Power flows and Voltage profiles of a traditional distribution system will differ when substantial amounts of renewable energy-based distributed generation are integrated. Typical RDGs inject active power into the grid, resulting in an over-voltage/voltage rise at the Point of Common Coupling (PCC). The evolution of RDGs' integration into the electrical grid is increasing and at the same time raising the attention of power system operators due to the fact that over-generation of electrical energy from this facility and its penetration levels may cause serious damage to the system components/equipment and therefore the consumers. This chapter investigates power system design and renewable distributed generation, mathematical analysis of voltage rise, test system description, test system simulation without/with RDG integration, voltage rise concept, impacts of RDG on distribution network, RDG integration and voltage rise at PCC, and the voltage rise compensation methods that can be employed in power systems with RDG integration. This chapter aims to:

- Provide the mathematical knowledge of RDG integration and voltage rise concept at PCC and the control.
- Explore the improvement of distribution network voltage profiles with RDG integration.
- Provide methods that can regulate the potential voltage rise threat.

- Provide worst case scenarios with RDG integration and possible solutions.

The following are the research questions that guide this chapter:

- Can RDG integration improves voltage profile of a distribution system?
- What is the impact of RDG integration on a distribution system?

### 4.2 Power System Design and Renewable Distributed Generation

Based on the initial design of a conventional distribution network, power flows from the substation to the loads in a unidirectional manner as shown in Figure 4.1. Integration of RDGs into the power system changes the features of the power system as power flows change from unidirectional to bidirectional. The summary is depicted in Table 4.1. Active and reactive power usually flow from higher voltage potential to a lower voltage level. The ratio of reactance to the resistance of the distribution network is less than or equal to $\left(\frac{1}{2}\right)$, while that of the transmission network is greater than or equal to 10 [183]. Consequently, the value of the resistances in the transmission network is lower as compared to the distribution network. This high resistance in the distribution network is responsible for the voltage drop along the feeders from the sending end to the receiving loads.

**Table 4.1:** Power System Design and RDG.

| **Comparison Between Conventional Power System and RDG Design** | | |
|---|---|---|
| S/N | Conventional | RDG |
| 1. | Unidirectional power flow. | Bidirectional power flow. |
| 2. | Centralized generation. | Distributed generation. |
| 3. | Manual monitoring. | Self-monitoring. |

| | | |
|---|---|---|
| 4. | Manual restoration. | Automatic restoration. |
| 5. | One-way communications. | Two-way communications. |
| 6. | Electromechanical. | Digital. |
| 7. | Few sensors. | More sensors. |
| 8. | Limited control. | Full control. |
| 9. | Failures and blackouts. | Adaptive and resilient. |
| 10. | Managed by the Utility company/Govt. | Managed by a few people/individuals. |

### 4.3 Mathematical Analysis of Voltage Rise

Considering a distribution network of the two-bus system in Figure 4.1, an analysis of the drop in the voltage along the line can be obtained. Equation (4.1) defines the sending end voltage while equation (4.2) defines the power supply from the distribution network, while the current flowing through the line is defined by equation (4.3).

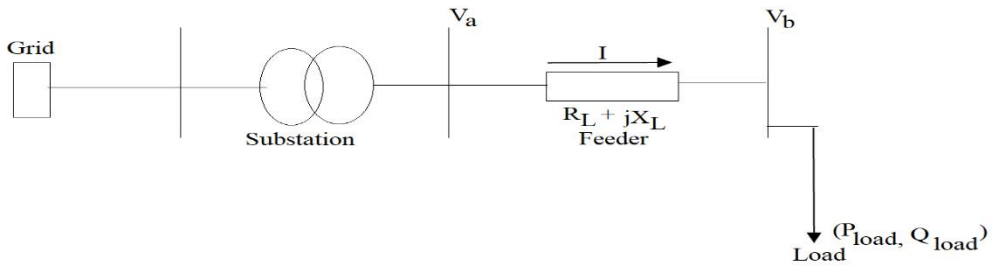


**Figure 4.1:** Equivalent circuit of Distribution system *(created by Author).*

$$\hat{V}_a = \hat{V}_b + \hat{I}(R + jX) \quad (4.1)$$

$I = |\hat{I}|$

$$P + jQ = \hat{V}_a \hat{I}^* \quad (4.2)$$

$$\hat{I} = \frac{P - jQ}{\hat{V}_a} \quad (4.3)$$

Where $\hat{V}_a$ = Sending end Voltage.

$\hat{V}_b$ = Receiving end Voltage.

R = Resistance of the line.

X = Reactance of the line.

$\hat{I}$ = Current flowing through the line.

P = Real Power flowing through the network to the load.

Q = Reactive Power flowing through the network to the load.

$P_{Load}$ = Real Power of the load.

$Q_{Load}$ = Reactive Power of the load.

By substituting equation (4.3) into equation (4.1), the sending end voltage can be further expressed in equation (4.4),

$$\hat{V}_a = \hat{V}_b + \frac{P + jQ}{\hat{V}_a}(R + jX)$$

$$\hat{V}_a = \hat{V}_b + \frac{RP + XQ}{\hat{V}_a} + j\frac{XP + RQ}{\hat{V}_a} \quad (4.4)$$

Hence, the voltage drop between the sending end and the receiving end can be expressed in equation (4.5).

$$\Delta\hat{V} = \hat{V}_a - \hat{V}_b = \frac{RP + XQ}{\hat{V}_a} + j\frac{XP + RQ}{\hat{V}_a} \quad (4.5)$$

The angle that exists between the sending end voltage and the receiving end voltage is very small or negligible, the voltage drop would be equal to the real part of equation (4.5) and if the reference bus is considered to be the sending end bus, the voltage angle at that point would be zero (0) such that $\hat{V}_a = |V_a| = V_a$, the equation (4.5) can therefore be re-expressed in equation (4.6).

$$\Delta V \approx \frac{RP+XQ}{V_a} \quad (4.6)$$

The sending end voltage $(V_a)$ in equation (4.6) can be regarded as a unity. If the sending end voltage of the system in Figure (5.1) is regarded as base voltage, then the equation (4.6) can be re-expressed in equation (4.7).

$$\Delta V \approx RP + XQ \quad (4.7)$$

The amount of voltage at the PCC of consumers is vital for power quality. As specified by IEEE 1547 std., which allows ±6 variation in PCC voltages due to penetration of RDG into AC grid while South Africa allows -15 % to +10 % (0.85 to 1.1 voltages per unit) for low voltage and ± 10 % for medium and high voltage around nominal voltage. The voltage level at the point of load connection can be described by the standard IEEE 13 Node feeder test system in Figure 4.2.

### 4.3.1 Test System Description

A modified IEEE 13-bus test system is used in this research study to investigate the impacts of RDC integration at the PCC of the distribution network. The IEEE 13-bus test system is a standard test system that has a challenging voltage management feature, as it demonstrates extreme voltage concerns. It comprises both medium and low voltage distribution networks (4.16 kV to 480 V ) and is one of four standard distribution models developed by the IEEE Power Engineering Society's Power System Analysis Computing and Economics Committee [184], [185]. The test feeder is short and relatively highly loaded. It is very indicative of the types of distribution systems in use for research. The test system is modified and modelled as balanced three phase in a MATLAB/SIMULINK environment. All the underground lines are modelled as overhead lines because there is no underground cable in the simpower systems library of Simulink. The network loading is modified to be 1.5 MVA while the capacity of the distribution station is 510 kVA with 4.16 kV voltage level. The total length of the network is 25km. The detail parameters of the system are depicted in Appendix A.

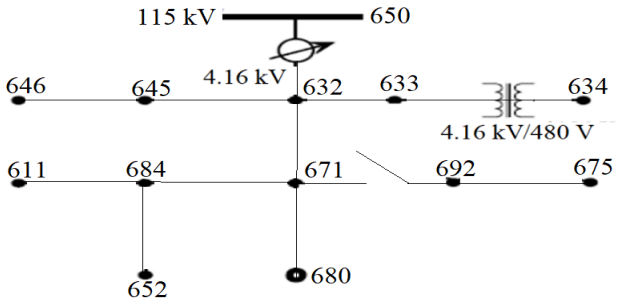


**Figure 4.2:** IEEE 13 Node feeder test system [184], [185].

### 4.3.2 Test System Simulation

The test system is simulated, and the graphical representation of the measured voltage parameters obtained from the system are shown in Figure 4.3. The network allowable voltage variation is guided by the IEEE 1547 which allows for ±6 variation in PCC voltages and the South Africa grid code that allows -15 % to +10 % (0.85 to 1.1 voltages per unit) for low voltage and ± 10 % for medium and high voltage around nominal voltage [186], [187]. It is observed that the system voltage profile variations are within the specified limit of both ±6 and -15 % to +10 %. Whereas, if the distance of the distribution line is longer than 25 km and the loads connected to the system are greater, by analogue thinking, the farthest nodes of the network will fall outside the specified voltage limit. Hence, utility companies usually run their networks to be within the allowable voltage ranges and regulate the network voltage with the aid of an automatic voltage regulator and on tap changing transformers.

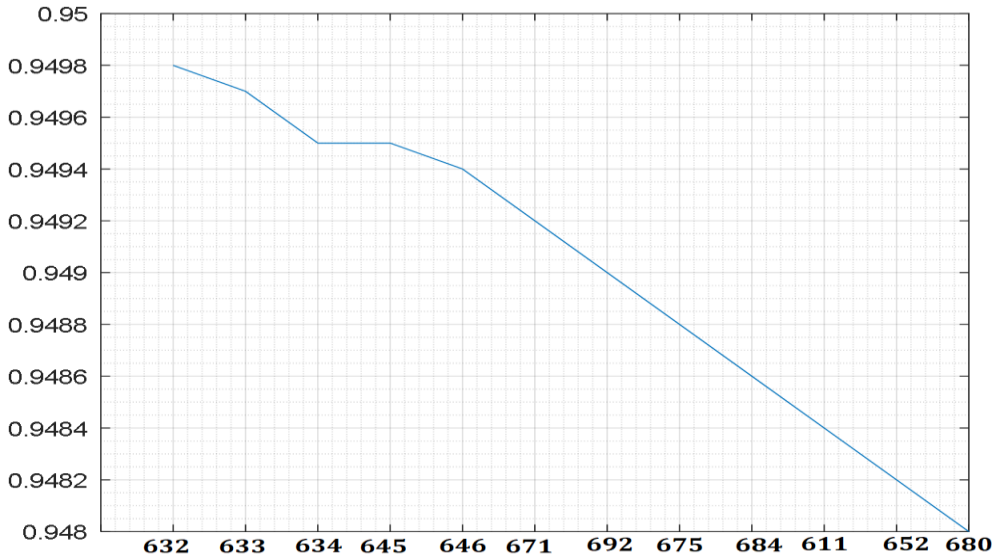


**Figure 4.3:** Test System Voltage Profile.

### 4.3.3 Voltage Rise Concept

The conventional distribution networks are usually designed to have a stable voltage profile initially. Voltage rise may not be a concern but when RDGs are integrated into the network, the power flow is not unidirectional anymore. Power flows not only from the substation to the farthest node of the system anymore, but it can also now flow back from the farthest node towards the substation due to the RDG integration. The system voltage profile would definitely be affected by the RGDs integration because the network is not passive but has become an active network. The voltage generated by the RDGs must be higher as compared to the voltage of the other nodes around the PCC for the power to be exported to another part of the network. This can be best described by equation 4.7. Therefore, the receiving end voltage $(V_b)$ can be expressed in equation 4.8.

$$V_b \approx V_a + RP + XQ \tag{4.8}$$

The change in the power flow direction results in the RDGs voltage being generated to rise above the sending end voltage such that the node at which RDG is connected to a distribution network will form an active point. The weak node will become an active node, while further increase in the number of RDGs and the penetration levels will make the nodes near the PCC more active resulting in fewer weak zones in the system. Hence, active zones become smart zones, while further increase in RDGs penetration levels will

eventually result in a smart point which can control the whole local network. The more the PCC becomes an active point, there is a potential voltage rise threat at that point if the voltage at that point is not regulated which can be explained in Figure 4.4.

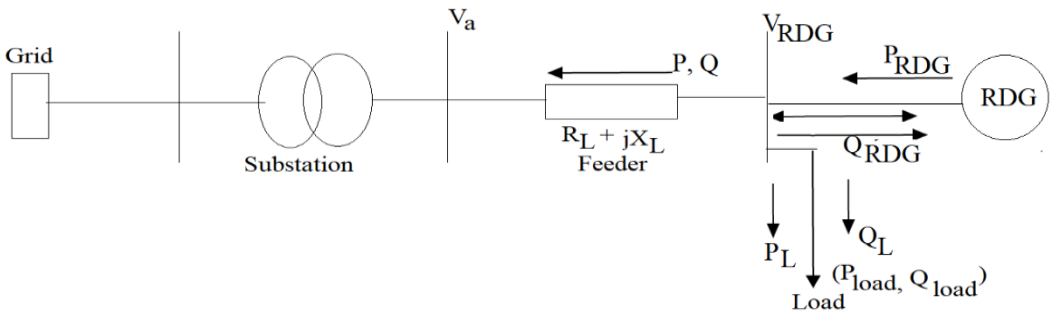


**Figure 4.4:** RDG Integration to Distribution Network *(created by Author).*

RDG is integrated into a distribution network via the distribution line with impedance as shown in Figure 4.4, where:

$P_{RDG}$ = RDG Active Power.

$Q_{RDG}$ = RDG Reactive Power.

$P_L$ = Active Power of the Load.

$Q_L$ = Reactive Power of the Load.

$R + jX$ = Impedance of the Line.

The rise in voltage at PCC due to the RDG integration can be expressed in equation (4.9).

$$\Delta V = V_{RDG} - V_{Gen} \approx \frac{RP+XQ}{V_{RDG}} \quad (4.9)$$

Where $P = (P_{RDG} - P_L)$ and $Q = (-Q_L \pm Q_{RDG})$

From equation 4.9, $V_{GEN}$ can be expressed in term of per unit in equation 4.10.

$$\Delta V = V_{RDG} - V_{Gen} \approx R(P_{RDG} - P_L) + X(-Q_L \pm Q_{RDG}) \quad (4.10)$$

Most of the time, RDG exports active power $(+P_{RDG})$ to the grid and the reactive power $(\pm Q_{RDG})$ can be exported or imported from or to the grid while the active load and the reactive power $(P_L and\ Q_L)$ are consumed by the loads. Depending on the type of RDG that is integrated into the distribution network, some export real power to the grid when the loads connected reduce below the generator output. Reactive power could be exported or absorbed depending on the settings of the RDG's excitation scheme. For example, a synchronous generator can be used for a wind energy converter while an induction generator consumes reactive power to operate. Solar Photovoltaic exports real power to the grid at a predetermined power factor. The flow of power could occur in both directions based on the real and the reactive power loading of the system as compared to the output of the generator and the system losses.

### 4.4 Impact of RDG on Distribution Network

This section investigates the impact of RDG on Distribution Network (DN). A RDG (solar farm of 100 kW to 1 MW) is integrated into the network of Figure 4.2 at bus 684 (the network designed in Simulink can be found in Appendix A, Figure A1-A6) as shown in Figure 4.5 to meet a certain customer load demand while the distribution substation voltage is controlled at 100 %. Penetration level is the ratio of the installed RDG capacity to the total load demanded, i.e., In a network with total loading of 1.2 MVA, RDG rated power of 120 kVA will be equal to the 10 % penetration level in the network. Figures 4.6 and 4.7 depict the graphical representation analysis of the simulation results. It is observed that the network voltage profiles improved considerably with increased RDG integration penetration levels and is within an acceptable voltage range. It is also observed that the voltage of node 684 at which the RDG is connected (PCC) is higher than any other voltages of the network as previously said, as shown in Figures 4.6 and 4.7. This is because of the injection of active power by the RDG which makes that particular bus voltage (PCC) more active than any other node. The impacts are noticeable at the PCC and the closest node in both directions around the PCC. The voltage profiles are within an acceptable range as specified by IEEE 1547 and the South Africa grid code act of RDG connection at PCC. The investigation of the impacts of RDG integration into the power system based on the research investigation and the simulation carried out with the results obtained in this section implies that impact of RDG integration

will improve the distribution network voltage profiles and make the weak node/bus/network active. Hence, a weak node can become an active node with RDG integration while a weak network can become an active network.

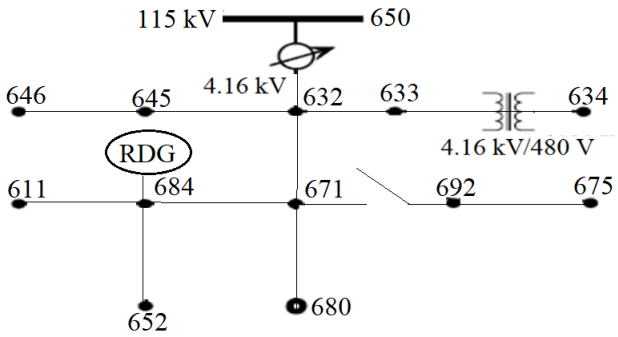


**Figure 4.5:** RDG Connection to DN.

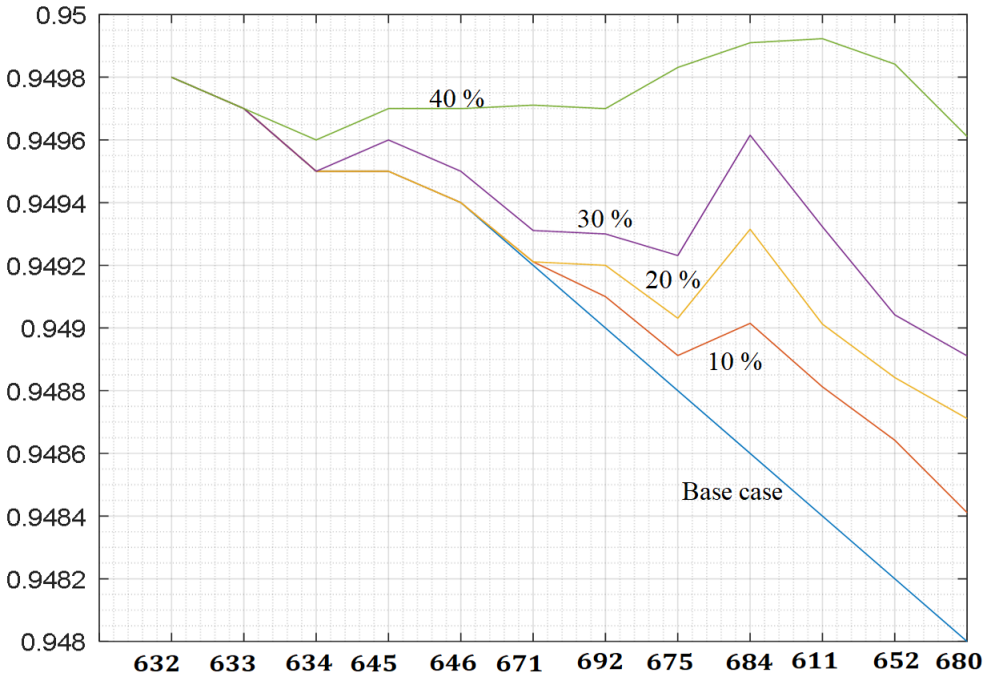


**Figure 4.6:** Improved DN Voltage Profiles at (10 %- 40 %).

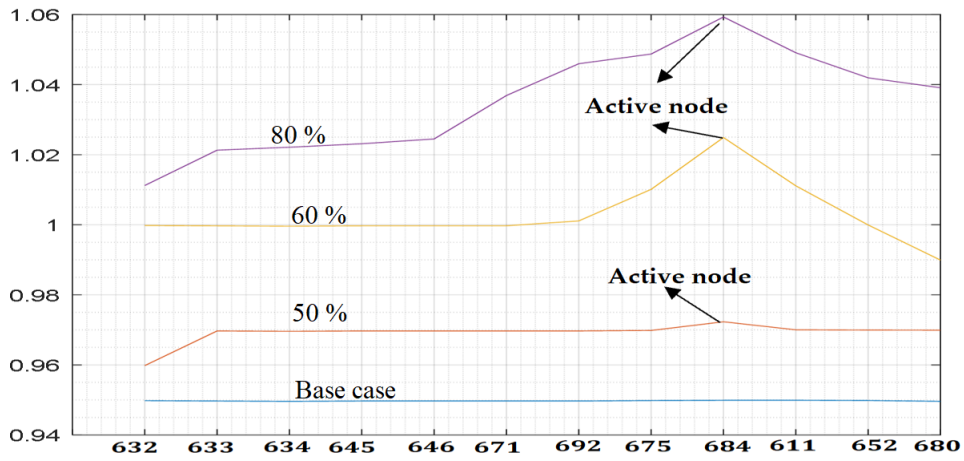


**Figure 4.7:** Improved DN Voltage Profiles at (50% - 80%).

## 4.5 RDG Integration and Voltage Rise at PCC

The network loading remains the same while penetration levels of RDG into the network increases from 60%, 70%, 80%, 90% and 100% at bus 684. The graphical analysis of the simulation are shown in Figure 4.8. The increase in the RDG penetration levels causes reverse power flow towards the distribution substation as depicted in Figure 4.8 around the nodes 675 and 692. The voltage at bus 684 (PCC) rises above the allowable voltage range of maximum 1.1 pu due to the integration of large RDG. The over voltage occurs in both directions such that the power flows towards the distribution substation and also to the farthest bus of the network. By analogous thinking, similar occurrences may take place during low load and high generation of RDG integration. It is therefore worthy to note that before considering RDG integration to the power system, the power system operator should consider the possibility of power being exported back to the substation in case there is an over generation of power from RDG as this will give them the ideal of choice of transformer to be installed that can tolerate the operation of reverse power flow.

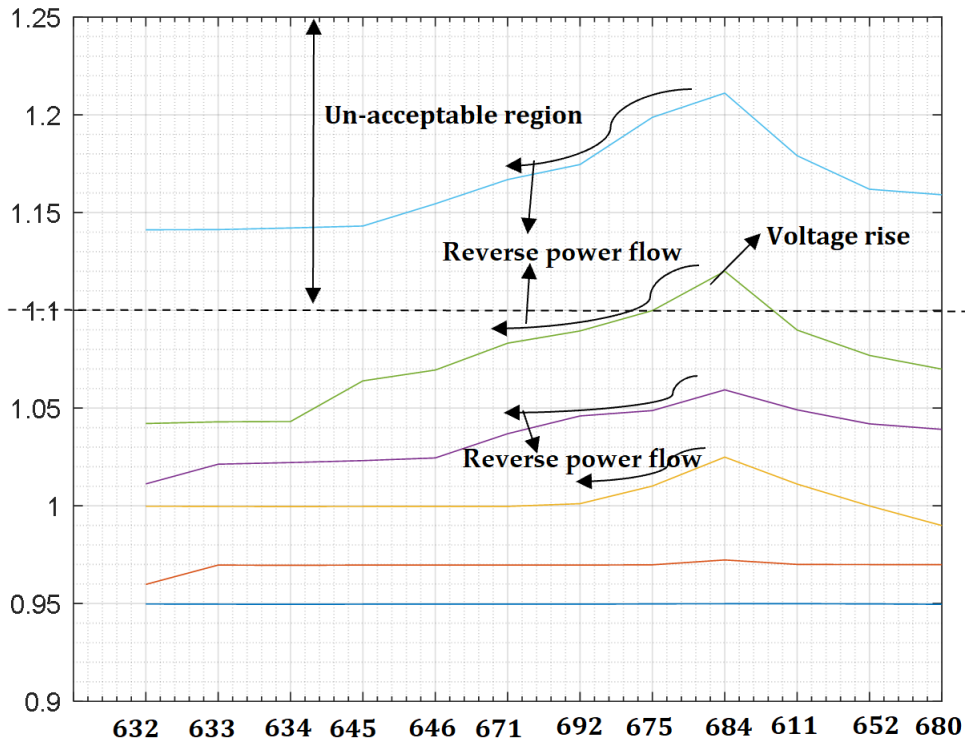


**Figure 4.8:** Improved DN Voltage Profiles at (60 - 100%).

The simulation in Figure 4.8 satisfies the equation 4.10 such that RDG exports active power $(+P_{RDG})$ to the grid. Hence, with RDG integration, the threat that under voltage potential will occur at the far end cannot exist. Power system deregulation, reliable power supply, power quality, meeting customers' load demands, economic value and the environmental regulation of greenhouse emissions are some of the primary aims of integrating RGDs into the power system. Therefore, equation 4.10 can be further expressed in equation 4.11.

$$P_G \approx \frac{P_{RDG} - V_a + RP_L - X(-Q_L \pm Q_{RDG})}{R} \qquad (4.11)$$

Thus, from equation 4.11, the level of RDG that can be integrated into a distribution network can be deduced. It depends on the following:

- The voltage at the distribution substation.
- The voltage level at the farthest bus.
- The distance of the network and the conductor size.

- Load demand within the network.

There are critical situations that can be investigated, and the outcome put into consideration when RDGs are to be integrated into a distribution network in order to regulate the activities of RDGs at the PCC, especially the impacts on the voltage rise such as:

- Peak load and Peak RDG generation.
- Peak load and low RGD generation.
- Low load and Peak RDG generation.
- No load and Peak RDG generation.

If the most critical situation is to be considered such that there is a reduction in the load demanded with a peak RGD generation, the analysis of such situation can be expressed by employing equation 4.10 and re-stated in equation 4.12. Meanwhile, if the network is operating at unity power factor, then equation 4.13 is valid. Based on this assumption, equation 4.10 can be re-expressed in equation 4.14.

$$P_L = 0, Q_L = 0, and\ P_{RDG} = P_{RDG\ Max} \tag{4.12}$$

$$\pm Q_{RDG} = 0 \tag{4.13}$$

$$\Delta V_{Critical} = V_{RDG\ Max} - V_a \approx RP_{RDG\ Max} \tag{4.14}$$

From equation 4.14, it can be observed that the PCC voltage rise depends on the resistance (R) of the distribution lines and the penetration power of the RDG. Hence, if the resistance of the distribution line remains unchanged, the equation 4.14 can be re-expressed in equation 4.15. From equation 4.15, it can be deduced that the amount of voltage in a distribution network with RDGs integration is directly proportional to the active power injected into the network by the RDGs.

$$\Delta V_{Critical}\ \alpha\ P_{RDG\ Max} \tag{4.15}$$

A linear relationship exists between the active power generated by the RDGs and the occurrence of voltage rise at PCC. The voltage rise would be burdensome and raise a concern when there is no load demand in the network due to the fact that the power injected by the RDG would be exported back into the distribution substation. If such a thing happens, damage to power system equipment and components is inevitable. Furthermore, the occurrence of voltage rise at PCC because of impacts of RDGs penetration levels can limit the amount and the extent at which RDG can be integrated into the power system. The above statement can be proved from equation 4.13, which can be re-expressed in equation 4.16.

$$P_{RDG\ Max} = \frac{V_{RDG\ Max} - V_a}{R} \tag{4.16}$$

The amount of RDG that can be integrated into the existing network would be limited by the peak/maximum voltage produced by the RDG connected to PCC which is expressed in equation 4.17.

$$P_{RDG\ Max} \leq \frac{V_{RDG\ Max} - V_a}{R} \tag{4.17}$$

Hence, from the critical situation, it can be observed that the resistance of the distribution line and the voltage rise at the network nodes is vital to the amount of RDGs penetration to the distribution network.

### 4.6 Voltage Rise Compensation Methods

With RDG integration into the distribution network, the voltage level of the system will be altered, and power flows will now be bidirectional. With the integration of RDGs into the power system, the voltage sag may not be the foremost concern anymore since active power injected by the RDG will cause the system voltage to increase. Hence, RDG integration introduces a new challenge, the voltage at the Point of Common Coupling (PCC) of RDG is higher as compared to the other buses of the network. Hence, active power increases with an increased penetration. This results in a voltage increase at the PCC, thereby causing a voltage rise. Voltage rise challenges were reported as the foremost concern against the connection of RDG to medium and low-voltage distribution networks [188], [189], [111]. A large RDGs integration into a distribution network can

cause an extreme voltage rise at PCC if not regulated or controlled appropriately. Conventionally, most of the distribution substations are fortified with an automatic over-voltage protection strategy to safeguard the power system equipment, components and loads from excessive voltage rise. Nevertheless, sometimes the protection scheme arrangement can disconnect RDG permanently from the network or can also disconnect distribution supply from the main grid which can have a critical effect on the customer loads connected to the system, therefore causing independent power producers to lose revenue. The voltage rises at the PCC with RDG integration can be mitigated through the following:

- Reduction in the distribution resistance.
- Distribution substation Voltage control method.
- RDG penetration curtailment.
- Reactive power compensation strategy.

### 4.6.1 Distribution Line Resistance Reduction

The voltage rise at the PCC poses a great limitation of a large RDG integration into a distribution network. This is because voltage is directly proportional to the current flowing through a resistance (Ohm's law), which means voltage increases as current or resistance increases. For alternating current networks, the impedance comprises inductance, resistance and capacitance. By adjustment of these components, voltage increases or decreases. Thus, the voltage drops as a result of the impedance of the feeder. The flow of the current, the load, the transformer and the source voltage define the voltage at the end of the feeder. If the amount of RDG integration into the Distribution network remains unchanged, equation 4.18 can be deduced from equation 4.16.

$$\Delta V_{Critical} \; \alpha \; R \qquad (4.18)$$

The equation 4.18 shows the critical situation whereby the voltage rise from RGD peak penetration is directly proportional to the distribution line resistance. Hence, by reducing the line resistance the voltage rise would be reduced considerably. This process can be logically carried out by increasing the size of the conductors of the distribution network.

This method may be slightly difficult to implement on the existing distribution system, but it can be proposed and implemented for the new distribution network. It is therefore recommended that the utility company consider reducing the distribution line resistance by increasing the conductor size while constructing a new distribution system as this will enable large RDGs integration into the system.

### 4.6.2 Distribution Substation Voltage Control Method

In a conventional distribution system, it is usually a standard to sustain distribution substation voltage above nominal voltage value. This process is carried out to keep the network voltage within an acceptable range as specified by the IEEE 1547 and South Africa Connection Act ( $\pm 6$ or 0.85 to 1.1 pu). However, this situation is not valid when RGDs are integrated into the system as investigated and confirmed in the simulation result in Figure 4.8. From equation 4.19, if the voltage supply from the distribution substation can be controlled, then the voltage drop can be regulated.

$$\Delta V_{Critical} = V_{RDG\ Max} - V_a \tag{4.19}$$

This method of controlling the voltage supply from the distribution substation can easily be carried out using Online Tap Changing Transformer (OLTCT). The voltage regulation is possible in this regard in a short distribution network however, such practice may be cumbersome in a long-distance distribution network because more transformers exist in a long distribution system, carrying out such a practice may not be practicable. Nevertheless, by optimising the supply voltage value and online tap changing transformer tap position, the system voltage can be regulated to the minimum.

### 4.6.3 RDG Penetration Level Curtailment

The occurrence of voltage rises at the PCC because of the integration of large RGDs into a distribution can be regulated through curtailing the RDGs integration penetration level. The consequence of RDGs curtailment can be expressed in equation 4.20. This equation can be re-expressed in equation 4.21.

$$P_{RDG\ Max} \approx P_{RDG\ Curtailment} + \frac{V_{RDG\ Max - V_a}}{R} \tag{4.20}$$

$$RP_{RDG\ Max} \approx RP_{RDG\ Curtailment} + V_{RDG\ Max-V_a}$$

$$V_{RDG\ Max} - V_a = RP_{RDG\ Max} - RP_{RDG\ Curtailment}$$

from eq. 4.9, $\Delta V_{Critical} = V_{RDG\ Max} - V_a$

$$V_a = V_{RDG\ Max} - \Delta V_{Critical}$$

$$V_{RDG\ Max} - V_{RDG\ Max} + \Delta V_{Critical} = RP_{RDG\ Max} - RP_{RDG\ Curtailment}$$

$$\Delta V_{Critical} \approx RP_{RDG\ Max} - RP_{RDG\ Curtailment}$$

$$\Delta V_{Critical} \approx RP_{RDG\ Max} - RP_{RDG\ Curtailment} \quad (4.21)$$

From equation (4.21), it can be observed that by curtailing RDG integration penetration levels, voltage rise can be therefore regulated at PCC. The critical situation does not always occur such that the minimum load is positioned versus peak RDG generation. Therefore, it is desirable to tolerate large RDG integration at PCC and curtail it whenever there is voltage rise occurrence to certain set voltage range. The total amount of RDG curtailment annually can be determined by how often minimum load versus peak RDG generation occurs. The only disadvantage of RDG curtailment is the reduction in revenue which can affect the utility and the independent power producers because the electricity price is normally influenced by the amount of load demanded. Logically, the loss of revenue would not be so much as the RDG curtailment will normally occur during the low load and RGD peak generation situation. Hence, the amount of curtail may be moderately low.

### 4.6.4 Reactive Power Compensation Strategy

Reactive power control is critical in the electrical grid to avoid voltage breakdown, voltage instability, and voltage rise when there is an unusual occurrence or eventualities at PCC. Voltage rise and instability occur in a system wherever there is insufficient reactive power during RDG over generation, heavy loading and disturbances such as grid faults [190]. Installing Flexible Alternating Current Transmission System (FACTS) devices such as STATCOM and SVC connected to the PCC of a large renewable farm, allows dynamic compensation of reactive power and voltage rise control capability to be realized since

the lesser the voltage at PCC, the more reactive power is needed [191]. It is also very valuable in power system interruptions. Reactive power may be supplied by mechanisms embedded in the network itself and by additional elements inserted into the network to balance the reactive power of this system [192]. The FACT compensation method should be a requirement for a system with non-linear loads and RDGs integration to provide voltage support, and attenuate voltage rise at PCC and stability in the event of network disturbance. If the voltage rise at PCC with Large RDGs integration is to be regulated, a FACTS device will be installed at PCC which can be expressed from equation 4.10 to produce equation 4.22. The equation 4.22 can be re-expressed in equation (4.23).

$$\Delta V = V_{RDG} - V_a \approx R(P_{RDG} - P_L) + X(\pm Q_c - Q_L \pm Q_{RDG}) \quad (4.22)$$

Where $\pm Q_c$ = Compensator reactive power (it can generate or absorb). The voltage rise can be easily controlled with a reactive compensator. When the device is strategically installed at the PCC to generate or absorb reactive power, the voltage rise at that point would be considerately minimized. This could also allow more RDG penetration levels without the fear of PCC over voltage or voltage rise.

$$\Delta V = V_{RDG} - V_a \approx R(P_{RDG} - P_L) + XQ_{Import} \quad (4.23)$$

Where $Q_{Import} = \pm Q_c - Q_L \pm Q_{RDG}$

If a critical situation is to be considered and the network operates at unity power factor, equation 4.23 can be re-expressed in equation 4.24.

$$\Delta V_{Critical} \approx RP_{RDG\ Max} + XQ_{Import} \quad (4.24)$$

RDGs always export active power $(+P_{RDG})$. Thus, a RDG may also export or import reactive power $(\pm Q_{RDG})$ depending on the RDG parameters e.g., a synchronous generator can import power at a 0.95 power factor, whereas a wind turbine with uncompensated induction generator can import power at about a 0.9 power factor. Whereas the load consumes both active $(P_L)$ and reactive $(Q_L)$ power and the compensators may export or absorb only, reactive power $(\pm Q_c)$ depends on the voltage rise occurrence at PCC. From the equation 4.24 it can be deduced that the increase in the amount of reactive power imported would bring the regulation of voltage rise at PCC.

The higher the negative value of $(XQ_{Import})$, the lower the reduction in the voltage rise at PCC.

### 4.7 Summary

Chapter four has presented power system design and renewable distributed generation, a mathematical analysis of voltage rise, test system description, test system simulation without/with RDG integration, voltage rise concept, impacts of RDG on distribution network, RDG integration and voltage rise at PCC, and the voltage rise compensation methods that can be employed in a power system with RDG integration. The overall deduction from this chapter is that for every RDG integration into a distribution network, voltage profile would be improved. When a large RDG is considered for integration, there would be a potential voltage rise threat at the PCC which the utility or independent power producers should include in their plan for installing a compensator at PCC for voltage rise regulation. This should be done before such RDG integration is allowed, to protect power equipment and the loads connected to the system.

# CHAPTER 5

# VOLTAGE RISE REGULATION WITH RDG INTEGRATION AT PCC

## 5.1 Introduction

In recent times, the growth in peak load requirement and the integration of RDGs into a distribution network raised worries regarding the grid voltage security, power fluctuations, instability, and voltage collapse. Primarily, loss of voltage support in a system can make voltage unable to recover which can lead to a voltage failure. As the voltage reduces, voltage sag protection relay trips, thereby decreasing the capacity of the grid to cope with the failing voltage. These challenges are considered accountable for numerous important disturbances in a transmission and distribution network and substantial research attempts are ongoing to limit the occurrence. Power system equipment is designed to operate at a certain voltage range. However, in the event of under voltage or if voltage goes out of the equipment limits due to overloading, or grid disturbance, then such equipment can malfunction and be damaged. But with large renewable energy integration into the grid, there would be an improved voltage profile as investigated and confirmed in Chapter 5. RDGs integration is getting attention across the globe and the rate of development is quite rapid. This is because of its positive impacts in that it is a clean energy, it is pollution free, it is naturally replenished on a human time scale and it is able to improve grid voltage profiles [193]. However, large-scale RDG farms' integration into electrical grids could also bring negative impacts such as, voltage rise, voltage fluctuation, grid instability when there is a disturbance, and over generation due to the fact that most mechanical switches are failing to keep pace with the dynamic swings of the power system. Hence, static electronic devices called Flexible Alternating Current Transmission Systems (FACTS) come into play to enhance line power transmission/distribution capability, maintain grid reliability and balance and reduce power flow on overloaded lines. FACTS also improve steady and transient stability, provide network security and make for a more energy efficient transmission system. There are various kinds of compensator devices such as, Thyristor-Controlled Reactors (TCR), Static Synchronous Series Compensators (SSSC), Thyristor-Controlled Series Capacitors (TCSC), Static Var Compensators (SVC), STATCOM [194] etc., that are used for power system applications. But STATCOM and

SVC are more efficient when it comes to reactive power control, voltage dip mitigation and grid stability, as they compensate for load imbalance, voltage/angle control and damp oscillations [195]. Literature reviewed in, [143], [144], [145], [146], and [147] confirmed that STATCOM and SVC are used extensively to maintain distribution system stability. STATCOM demonstrates more transient response stability than SVC in [148]. The STATCOM compensator device is used to balance capacitor voltage in [149], [150], [151], [152] and [153], while [154] employs the same compensator to control harmonic current. Disturbance and error rejection control is proposed in [155], voltage mitigation during symmetrical and asymmetrical faults, and minimisation of surge currents is carried out with STATCOM compensator in [156]. Wind farm stability is tested in [157], [158] and [159], to improve voltage and transient stability in [160], mitigate oscillation in [161], and mitigate flicker in [162], [163]. However, the compensator device has not been used to mitigate voltage rise with RDG at PCC. Its response time and the rate of delivering capacitive power capability are not covered in the literature review. Although there are different application of STATCOM, this research thesis is limited to the investigation of the dynamic response of STATCOM to regulate the voltage rise at PCC which has not been done before. STATCOM controlled capability is compared with other FACTS devices such as SVC in terms of capacitive reactive power output. To control the voltage rise with renewable energy integration at PCC, it is expected that the grid codes continually require the capacity of dynamic voltage control by constant adjustment of reactive power delivered to the grid. Therefore, the rate at which the reactive energy is delivered/absorbed during the voltage rise at PCC should be an important precondition for most RDGs, such as wind solar farms. Hence, how to accomplish this objective in the most economical way, STATCOM becomes a vital research area in voltage rise mitigation. The installation of STATCOM at the PCC is an essential way for a large RDG penetration to accomplish dynamic reactive power compensation and voltage stability [157], [158], [159], [160], [145]. If transience occurs like unexpected loading, or voltage rise at PCC due to large RDG integration and network catastrophes, the grid component/equipment and loads could be exposed to greater strain [161], [162], [163]. Hence, by the installation of STATCOM with PWM control scheme into the network, grid instability can be minimized to a required limit and PCC voltage rise subdued. This chapter investigates STATCOM's compensation strategy and its mathematical analysis

in mitigating voltage rise at PCC. The chapter also presents STATCOM's dynamic response, modelling, regulatory capability, simulation of the voltage rise mitigation at PCC, and its response during fault conditions. A simulation comparison between STATCOM and SVC is also presented. The following are the contribution of this chapter:

- Voltage rise at PCC is compensated through reactive power control of STATCOM.
- Continuous operation of a large RDG integration is achieved without violation of voltage rise limit in relation to grid code at PCC.
- Dynamic grid voltage control during network disturbance.

Research questions that guide this chapter are:

- How can voltage rise be regulated at PCC with a large RDG penetration level?
- Can a large RDG integration continue operation or be disconnected at PCC due to voltage rise?

## 5.2 Compensation Strategy and Mathematical Analysis of STATCOM

Reactive power control is critical in the electrical grid to avoid voltage breakdown, voltage instability, and voltage rise when there is an unusual occurrence or eventualities at PCC. Voltage rise and instability occur in a system wherever there is insufficient reactive power during a large RDG integration, heavy loading and disturbances such as grid faults [190]. When installing STATCOM and SVC connected to the PCC of large renewable farms, dynamic compensation of reactive power and voltage rise control capability can be realized, since the lower the voltage at point of common coupling, the higher the reactive power desired in any network [191], [192]. The compensation method should be a requirement for a system with a large RDGs integration to provide voltage support, attenuate voltage rise at PCC and offer stability in the event of network disturbance. If the voltage rise at PCC with a large RDGs integration is to be regulated, a compensator device will be installed at PCC which can be expressed from equation 4.10 to produce equation 5.1. The equation 5.1 can be re-expressed in equation 5.2

$$\Delta V = V_{RDG} - V_a \approx R(P_{RDG} - P_L) + X(\pm Q_c - Q_L \pm Q_{RDG}) \quad (5.1)$$

Where $\pm Q_c$ = Compensator reactive power (it can generate or absorb), to control the

voltage rise at PCC with continuous operation of RDG integration, a reactive compensator has a great role to play. When the device is strategically installed at the PCC to generate or absorb reactive power, the voltage rise at that point would be considerately minimized. This could also allow more RDG penetration levels. If the compensator voltage is lower than PCC voltage, Qc becomes positive, as the compensator absorbs reactive power. When the voltage of the compensator surpasses the PCC voltage, and Qc is negative, the compensator produces a reactive power. When the voltage of the compensator is equal to the PCC voltage, the compensator will remain unactive.

$$\Delta V = R(P_{RDG} - P_{RDG}) + RQ_{export} \approx R(P_{RDG} - P_L) + XQ_{Import} \quad (5.2)$$

Where $Q_{Import} = \pm Q_c - Q_L \pm Q_{RDG}$

If a critical situation is to be considered and the network operates at unity power factor, equation 5.2 can be re-expressed in equation 5.3.

$$\Delta V_{Critical} \approx RP_{RDG\,Max} + XQ_{Import} \quad (5.3)$$

RDGs always export active power $(+P_{RDG})$. Thus, it may also export or import reactive power $(\pm Q_{RDG})$ depending on the RDG parameters e.g., a synchronous generator can import power at a 0.95 power factor, whereas a wind turbine with an uncompensated induction generator can import power at about a 0.9 power factor. Whereas the load consumes both active $(P_L)$ and reactive $(Q_L)$ power and the compensators may export or absorb only reactive power $(\pm Q_c)$, depending on the voltage rise occurrence at PCC. From equation 5.3, it can be deduced that the increase in the amount of reactive power imported would bring the regulation of voltage rise at PCC. The higher the negative value of $(XQ_{Import})$, the lower the reduction in the voltage rise at PCC. The compensator device employed in this research investigation to mitigate voltage rise at PCC is a static compensator (STATCOM), which incorporate the Pulse Width Modulation (PWM) control scheme.

### 5.3 Compensator Device Connection Model to PCC

This section presents the details of the structural representation of STATCOM to mitigate the voltage rise at PCC and the corresponding basic circuit equivalent. The STATCOM is a shunt device using power electronics to control power flow and improve transient stability of the power grids. STATCOM structure in MATLAB/SIMULINK has three terminals. ABC as depicted in Figure 5.1, $(V_{ref})$ is the input of external voltage while trip represents logical input signal (0 or 1). When this input is high, the STATCOM is disconnected, and its control system is disabled. It is also used to implement a simplified version of the protection system. STATCOM parameters are grouped in two categories: Power and Control tab. Converter rating, current, nominal voltage, DC link voltage, impedance, and capacitance rating are specified in power tab while control tab consists of modes of operation (var and voltage control) and droop that control the slope (the regulator gains Kp and Ki).

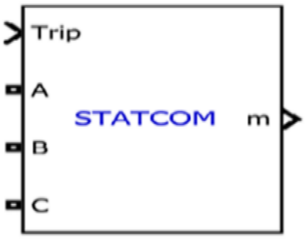


**Figure 5.1:** STATCOM Structure in Simulink.

STATCOM is a circuit-fed reactive power compensation device which is able to produce and/or absorb reactive power, such that the precise data of the grid is controlled to modify the output voltage [196]. STATCOM is a Voltage Source Inverter (VSC) that rectifies the direct current input (DC) voltage in an AC output voltage to complement the active and reactive power required by the system [197], [198], [199]. The STATCOM schematic representation and connection model to PCC is depicted in Figure 5.2. 3-Ø voltage source $(V_{ga}, V_{gb}, and\ V_{gc})$ represents an AC system which in series connection with a transmission line, $(L_g)$ represents inductance of the line while the resistance and transformer are assumed to be negligible. By controlling the real power of the system,

($V_{dc}$) can be regulated. The ($V_{dc}$) is supported by a Direct Current (DC) source which can be a DC energy source such as battery banks. ($P_s$) compensates for the VSC power loss.

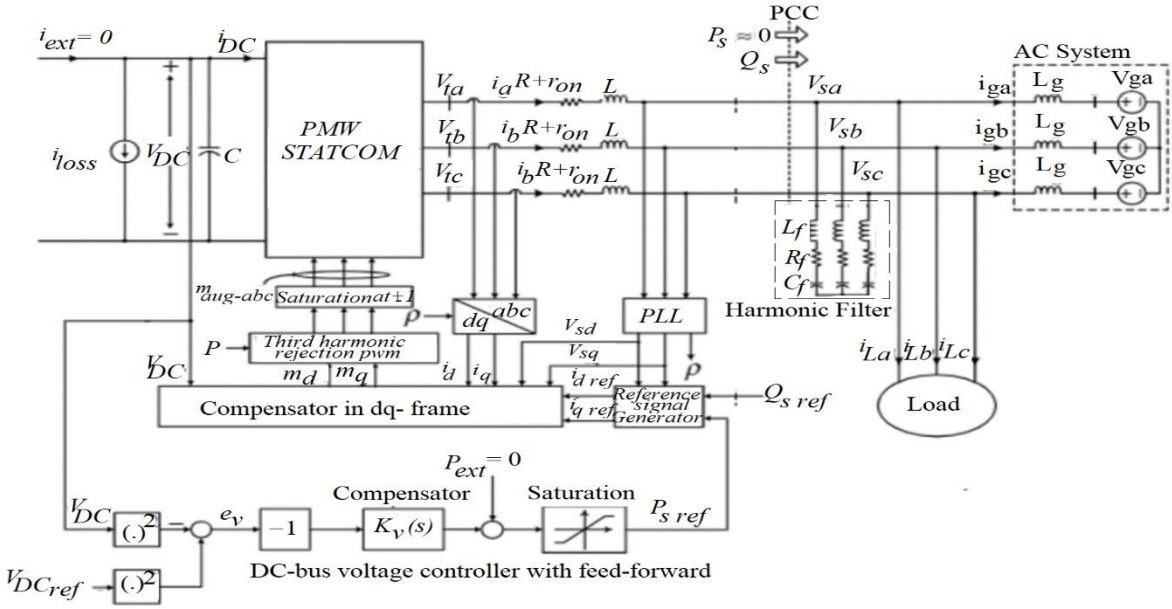


**Figure 5.2:** Compensator (STATCOM) Connection to PCC [199] .

The electrical nodes on STATCOM connection to 3-Ø AC constitute PCC. The voltages at that point are ($V_{sa}, V_{sb}$ $and$ $V_{sc}$). The phase lock loop PLL input is taken from PCC, and 3-Ø loads are also supplied from the PCC. 3-Ø RLC filters are connected in shunt with the STATCOM at PCC to filter unwanted current harmonics, amplitude and frequency signals of the load voltage from flowing into the grid. The STATCOM has constant current characteristics when there is under-voltage/over-voltage, below/above the boundary, which permits STATCOM to provide constant reactive power. The relationship between the Alternating Current of the network voltage and the voltage at the STATCOM Alternating Current side terminals offers the influence of reactive power flow. When the terminal voltage of the STATCOM contact is above the network voltage, STATCOM would inject reactive power to the grid and STATCOM acts like a capacitor. As soon as the STATCOM voltage is below the AC voltage, STATCOM functions as an inductor and the reactive power flow is reversed. When the network voltage is equal to the STATCOM voltage, there is no energy exchange [200], [201].

## 5.4 Dynamic Response and Modelling of STATCOM

The modelling of STATCOM's dynamic voltage regulation at PCC involves linearizing the non-linear circuit elements at the operating point of STATCOM, as well as when the behaviour becomes non-linear at the PCC. The modelling is divided into two signals; the first signal modelling is the STATCOM's dynamic voltage response which is obtained by applying a small (AC) signal on top of the DC operating points called large signal while the second modelling is to obtain a DC operating point of STATCOM at PCC called small signal.

### 5.4.1 STATCOM Dynamic Voltage (Large Signal)

The voltages at the PCC $(V_{sa}, V_{sb}\ and\ V_{sc})$ are being regulated by STATCOM with $(i_{La}, i_{Lb}\ and\ i_{Lc})$ while $(i_a, i_b\ and\ i_c)$ are controlled. The relationship is presented in equation 5.4 to 5.9, where $(V_{null})$ is the voltage of the AC system neutral point with respect to the midpoint of the VSC DC bus. When the space phasor of balanced 3-Ø is considered, the sinusoidal function is produced in equation 5.10, where $(\hat{f})$, ($\theta_0$) and ($w$) are amplitude, phase angle and angular frequency. The sinusoidal function of the space phasor is given in equation 5.13. Equations 5.4 and 5.5 multiply both sides of equation 5.11 and add to equation 5.12. Space phasor does not contain $(V_{null})$, therefore, equations 5.4 to 5.6 are added to produce equation 5.13.

$$V_{sa} = L_g \frac{di_{ga}}{dt} + V_{ga} + V_{null} \tag{5.4}$$

$$V_{sb} = L_g \frac{di_{gb}}{dt} + V_{gb} + V_{null} \tag{5.5}$$

$$V_{sc} = L_g \frac{di_{gc}}{dt} + V_{gc} + V_{null} \tag{5.6}$$

$$i_{ga} = i_a - i_{La} \tag{5.7}$$

$$i_{gb} = i_b - i_{Lb} \tag{5.8}$$

$$i_{gc} = i_c - i_{Lc} \tag{5.9}$$

$$f_{a^{(t)}} = \hat{f}\cos(wt + \theta_0), f_{b^{(t)}} = \hat{f}\cos\left(wt + \theta_0 - \frac{2\pi}{3}\right),$$

$$f_{c^{(t)}} = \hat{f}\cos\left(wt + \theta_0 - \frac{4\pi}{3}\right) \quad (5.10)$$

$$\vec{f}(t) = \frac{2}{3}\left(e^{j0}f_{a^{(t)}} + e^{j\frac{2\pi}{3}}f_{b^{(t)}} + e^{j\frac{4\pi}{3}}f_{c^{(t)}}\right) \quad (5.11)$$

$$\overrightarrow{V_s} = L_g\frac{\overrightarrow{di_g}}{dt} + \overrightarrow{V_g} \quad (5.12)$$

$$e^{j0} + e^{j\frac{2\pi}{3}} + e^{j\frac{4\pi}{3}} \equiv 0$$

$$\overrightarrow{i_g} = \vec{i} - \overrightarrow{i_L} \quad (5.13)$$

Consider the AC voltage $(V_{ga}, V_{gb}, and\ V_{gc})$:

$$V_{ga} = \hat{V}_g\cos(w_{0^t} + \theta_0), V_{gb} = \hat{V}_g\cos\left(w_{0^t} + \theta_0 - \frac{2\pi}{3}\right)$$

$$V_{gc} = \hat{V}_g\cos\left(w_{0^t} + \theta_0 - \frac{4\pi}{3}\right) \quad (5.14)$$

Where $(\hat{f})$ = Amplitude of the line to neutral.

$w_0$ = AC frequency.

$\theta_0$ = Phase angle.

$(V_{null})$ = Voltage of the AC system neutral point.

When equation 5.14 is multiplied by equation 5.11, equation 5.15 is obtained. From Figure 5.5, if $(dq)$ frame with angle $(p)$ is used to control STATCOM, equation 5.11 can be substituted to give equation 5.16. Similarly, equation 5.11 is substituted to give 5.14. Following the similar substitution in equation 5.13, equations 5.18 and 5.19 are produced. By comparison, the real and imaginary component can be obtained through derivative of equation 5.15 multiplied by $e^{jp}$ to obtained equations 5.20 and 5.21. $\left(w = \frac{dp}{dt}\right)$ and (w) is controlled by a phase lock loop (PLL) based on equation 5.22. The $[w(t)]$ in equation 5.22 represents a nonzero steady state value when $(V_{sd})$ settles at zero. A dynamic

system is represented by equations 5.18 to 5.22, where $(V_{sq})$ is the output, $(I_d)$ and $(I_q)$ are control input $(I_{Id})$ and $(I_{Iq})$ are disturbance inputs. Hence, the dynamic variable $(w)$ depends on the operating point, but to further clarify the operating point, $(V_{sq})$ is substituted for equations 5.18 and 5.19 respectively. The dynamic responses of $(p)$ and $(w)$ are indicated in equation 5.23 where their natural and forced transient components are equal to zero.

$$\vec{V_g} = \hat{V}_{g^{e^{j(w_0 t+\theta_0)}}} \tag{5.15}$$

$$\vec{V_s} = V_{sdq^{ejp}}, \ \vec{i_g} = i_{gdq^{ejp}}, \ \vec{V_g} = \hat{V}_{g^{e^{j(w_0 t+\theta_0)}}}$$

$$V_{sdq^{ejp}} = L_g \frac{d}{dt}\left(i_{gdq^{ejp}}\right) + \hat{V}_{g^{e^{j(w_0 t+\theta_0)}}} \tag{5.16}$$

$$\vec{i_g} = i_{gdq^{ejp}}, \vec{i} = i_{dq^{ejp}}, \vec{i_L} = i_{Ldq^{ejp}}$$

$$i_{gdq} = i_{dq} - i_{Ldq} \tag{5.17}$$

$$i_{gd} = i_d - i_{Ld} \tag{5.18}$$

$$i_{gq} = i_q - i_{Lq} \tag{5.19}$$

$$V_{sd} = L_g \frac{di_{gd}}{dt} - L_g w i_{gq} + \hat{V}_g \cos(w_0 t + \theta_0 - p) \tag{5.20}$$

$$V_{sq} = L_g \frac{di_{gq}}{dt} - L_g w i_{gd} + \hat{V}_g \sin(w_0 t + \theta_0 - p) \tag{5.21}$$

$$\frac{dp}{dt} = w(t) = H(p) V_{sq(t)} \tag{5.22}$$

$$\frac{dp}{dt} = L_g H(p)\left(\frac{di_{gq}}{dt} + w i_{gd}\right) + \hat{V}_g H(p) \sin(w_0 t + \theta_0 - p) \tag{5.23}$$

$(V_{sq})$ = Voltage output.

$(I_d)$ and $(I_q)$ = Control input.

$(I_{Id})$ and $(I_{Iq})$ = Disturbance inputs.

### 5.4.2 STATCOM Dynamic Voltage (Small Signal)

The dynamic voltage at PCC (small signal) can be obtained from equations 5.20 to 5.22 around a steady state operating point. Let perturbed variable be defined, if $\left(\frac{\tilde{p}}{p0} \ll 1\right)$, then equation 5.25 is obtained. From equation 5.25, perturbed variable is substituted in equations 5.20 and 5.21. Hence, substitute for $(\hat{V}_g cos\ p0)$ and $(\hat{V}_g sin\ p0)$ in equations 5.27 and 5.29 from equations 5.26 and 5.27. Similarly, perturbed variation of equation 5.24 is substituted for in equation 5.22 and 5.30 is deduced. The Laplace transform of equations 5.28 to 5.31 produced equations 5.29 to 5.32. The equations 5.28 to 5.30 and its Laplace transform of equations 5.31 to 5.33 described a linear system that is the small signal equivalent of the system as described by equations 5.20 to 5.22. The dynamics of $(\hat{V}_{sd^{(s)}})$ in terms of $(\hat{I}_{gd^{(s)}})$ and $(\hat{I}_{gq^{(s)}})$ can be obtained by elimination of $(\hat{V}_{sq})$ in equations 5.32 and 5.35, then $(\widehat{\boldsymbol{P}})$ can be substituted in equation 5.31 thus, equation 5.34 is obtained. Where $G_d(s)$ and $G_q(s)$ are transfer function, which have parameters of $I_{gd}0$ and $I_{gq}0$. $I_d=0$, $I_{d0} = \hat{\boldsymbol{I}}_d = 0$, then the STATCOM exchanges a small amount of real power with PCC, such that $P_s = 0$ and the DC side power of $P_{loss} = VDCI_{loss}$. Based on equations 5.19 and 5.20, equations 5.35 to 5.37 are obtained. When $\hat{\boldsymbol{I}}_{gd}$ and $\hat{\boldsymbol{I}}_{gq}$ from equations 5.37 and 5.38 are substituted for in 5.34, the load and control effects are obtained in equation 5.39.

$$V_{sd} = V_{sd0} + \tilde{V}_{sd}$$

$$V_{sq} = 0 + \tilde{V}_{sq}$$

$$i_{gd} = i_{gd0} + i_{gd}$$

$$w_0{}^t + \theta_0 - p = -(p_0 + \widetilde{p}) \Longrightarrow \underbrace{\frac{dp}{dt}}_{w} = w_0 + \underbrace{\frac{\widetilde{dp}}{dt}}_{w} \quad (5.24)$$

$$cos(p_0 + \tilde{p}) \approx cosp_0 - (sinp_0)\tilde{p}$$

$$sin(p_0 + \tilde{p}) \approx sin\ p_0 + (cos\ p_0)\tilde{p} \quad (5.25)$$

$$V_{sd0} = -L_g w_{0igd0} + \hat{V}_g cosp_0 \quad (5.26)$$

$$0 = L_g w_{0igd0} - \hat{V}_g sinp_0 \quad (5.27)$$

$$\tilde{V}_{sd} = L_g \frac{\widetilde{di_{gd}}}{dt} - L_g w o \tilde{i}_{gq} - L_g i_{gd0\tilde{w}} - (\tilde{V}_g sinp_0)\tilde{p} \quad (5.28)$$

$$\tilde{V}_{sq} = L_g \frac{\widetilde{di_{gq}}}{dt} - L_g w o \tilde{i}_{gd} - L_g i_{gd0\tilde{w}} - (\tilde{V}_g cosp_0)\tilde{p} \quad (5.29)$$

$$\frac{\widetilde{dp}}{dt} = \tilde{w} = H(p)\tilde{V}_{sq} \quad (5.30)$$

$$\tilde{V}_{sd(s)} = L_{gs\tilde{I}gd(s)} - L_{gwo\tilde{I}gd(s)} - L_g(i_{gq0s} + woi_{gd0})\tilde{p}(s) \quad (5.31)$$

$$\tilde{V}_{sq(s)} = L_{gs\tilde{I}gq(s)} + L_{gwo\tilde{I}gd(s)} + L_g(i_{gd0s} + woi_{gq0})\tilde{p}(s) \quad (5.32)$$

$$\tilde{p}(s) = \frac{H(s)}{s}\tilde{V}_{sq(s)} \quad (5.33)$$

$$\tilde{V}_{sd(s)} = G_{d(s)\tilde{I}_{gd(s)}} + G_{q(s)\tilde{I}_{gd(s)}} \quad (5.34)$$

$$i_{gd0} \approx -i_{Ld0} \quad (5.35)$$

$$i_{gq0} = i_{q0} - i_{Lq0} \quad (5.36)$$

$$\tilde{i}_{gd} \approx -\tilde{i}_{Ld} \quad (5.37)$$

$$\tilde{i}_{gq} = \tilde{i}_q - \tilde{i}_{Lq} \quad (5.38)$$

$$\tilde{V}_{sd(s)} = \underbrace{\frac{-G_{d(s)\tilde{I}_{Ld(s)} - G_{q(s)\tilde{I}_{Lq(s)}}}}{load\ effect}} + \underbrace{\frac{-G_{q(s)\tilde{I}_{q(s)}}}{control\ effect}} \quad (5.39)$$

## 5.5 Regulatory Capability of STATCOM

The STATCOM regulation operation and the control diagram are depicted in Figures 5.3 and 5.4, where ($V_2$) is the STATCOM voltage and ($V_1$) is the grid voltage. If the voltage ($V_2$) is lower than ($V_1$), the current in the inductor is slightly displaced from the voltage ($V_1$), it produces an inductive current, then (Qs) becomes positive and STATCOM absorbs

reactive. When the voltage of the STATCOM exceeds the network voltage, the current across the inductor is slightly offset from the voltage $V_1$ that provides a capacitive current, then (Qs) is negative and the STATCOM produces a reactive power. When the voltage of the STATCOM is equal to the voltage of the network, the current through the inductor is nil and consequently there is no power exchange [199].

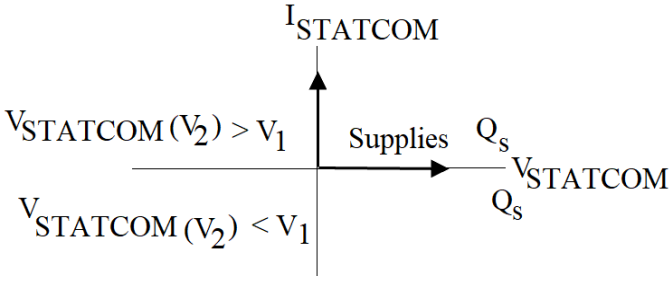


**Figure 5.3:** STATCOM Power Operation.

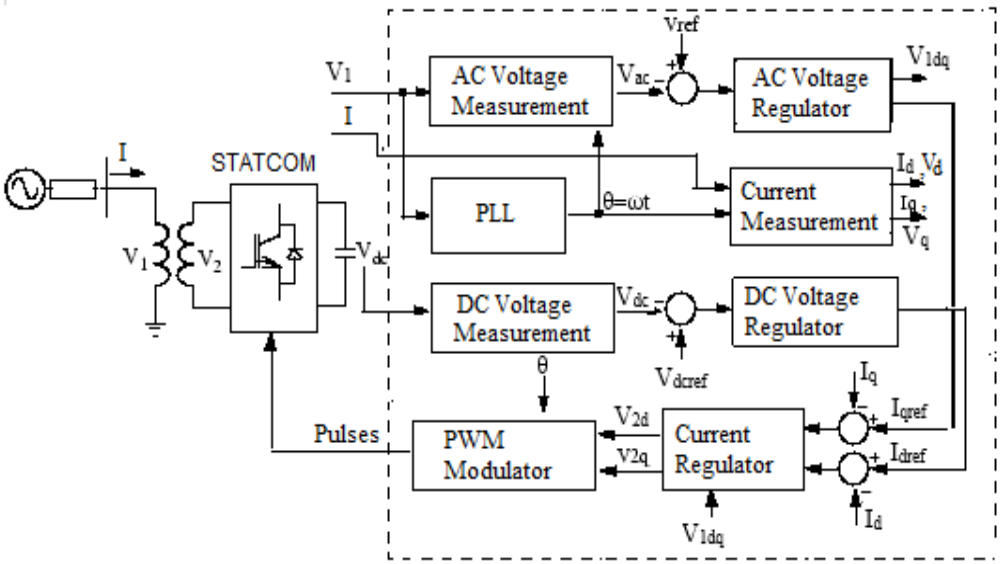


**Figure 5.4:** STATCOM and its Control System [202].

The 3-Ø voltage ($V_1$) is matched by Phase Locked Loop (PLL), and the direct axis and quadrature axis mechanisms of 3-Ø alternating current such as ($V_d$, $V_q$, $I_d$, and $I_q$) are configured by the output of the PLL (angle θ = ωt). The measured d and q mechanisms of (AC) positive sequence voltage/current, composed with (DC) voltage $V_{dc}$ are controlled. An outer regulation loop comprises an AC voltage regulator and a DC voltage regulator. The reference current $I_{qref}$ for the current regulator is from the output of AC voltage regulator ($I_q$

= current in quadrature with a voltage that controls reactive power flow). The reference current $I_{dref}$ for the current regulator is from the output of the DC voltage regulator ($I_d$ = current in phase with voltage that controls the active power flow). An inner current regulation loop consists of a current regulator. The magnitude and phase of the voltage generated by the STATCOM converter ($V_{2d}$ $V_{2q}$) from the $I_{dref}$ are controlled by current regulator, while DC voltage regulator and the AC voltage regulator (in voltage control mode) produces $I_{qref}$ reference currents. The direct power type regulator that predicts the voltage output, $V_2$ ($V_{2d}$ $V_{2q}$) from measurement $V_1$ ($V_{1d}$ $V_{1q}$) and the leakage reactivity of the transformer assist the current regulator. The change in reactive power is achieved by means of a voltage source converter (VSC) connected to the secondary side of a coupler transformer. The VSC utilizes forced-commutated power electronic devices (GTOs, IGBTs or IGCTs) to create a voltage $V_2$ from a DC voltage source.

### 5.5.1 Voltage and Current Feature of STATCOM

There are two ways in which STATCOM can be used, VAR control and voltage regulation mode. When STATCOM is in VAR control mode, its reactive power is maintained at a constant, whereas the voltage regulation mode of STATCOM can be described in Figure 5.5. If the reactive current remains within the minimum current values (-Imax, Imax) imposed by the nominal value of the converter, the voltage is controlled to the reference voltage Vref. However, a voltage droop is usually used between 1% and 4% at maximum reactive power output and the V-I characteristic has the slope indicated in the figure 5.5 [203]. In the voltage regulation mode, the V-I characteristic is stated in equation 5.40.

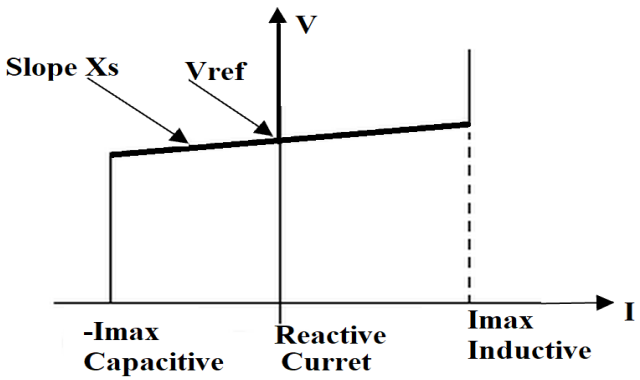


**Figure 5.5:** Voltage/Current feature.

V = Vref + Xs I (5.40)

V = Positive Voltage Sequence

Vref = Reference Voltage

Xs = Slope/Droop Resistance

I = Reactive Current, I>0 = Inductive Current.

By the adjustment of the phase angle and that of the reference point, the bus voltage can be varied with the STATCOM connected in parallel. When the grid voltage is on the high side or at the lower value over the boundary, STATCOM behaves in its constant current features. It can produce reactive capacity at the boundary such as capacitive and inductive compensation and independently control its output current over the rated maximum capacitive or inductive range of the amount of AC system voltage.

### 5.6 Simulation Analysis of Voltage Rise with STATCOM

The test system Figure 4.5 used for the investigation in this section is modelled in the MATLAB/SIMULINK environment as shown in Appendix A, Figure A1-A6. STATCOM is connected to the system to carry out the following investigations. The dynamic response of the STATCOM, voltage rise mitigation with the integration of a large RDGs penetration level at PCC and the mitigation comparison of STATCOM and SVC during grid disturbance conditions is carried out by connecting the SVC of the same rating as STATCOM to the system.

#### 5.6.1 Dynamic STATCOM Response

The STATCOM determines the grid voltage while producing reactive power in two different manners, viz; either by taking up or generating reactive power. This is due to voltage converter capability. To investigate STATCOM output control capability, from the dialog of the STATCOM's box, voltage control mode is selected, and droop variable slope adjusted to 0.00 and finally to 0.03 to provide a higher capacitive/inductive range. With the droop adjusted, the linear operation limit of the STATCOM is extended. The value of gains $(K_p)$ and $(K_i)$ chosen are 5 and 1000 to slow the STATCOM output response down

so that it does not cause overshoot to the reference voltage. The voltage at the PCC with RDG integration is programmed to be 1.0 per unit for the duration of 0.20 s, 0.97 per unit for 0.40 s, 1.030 per unit for 0.60 s, and back to 1.0 per unit. After the system is simulated, the effect of chosen large $(K_p)$ and $(K_i)$ can be observed in Figure 5.6 (a). An overshoot occurred at the STATCOM voltage, which is not acceptable as this can cause other damage to the system. Also the occurrence of an overshoot will cause the STATCOM voltage not to follow the PCC voltage. To avoid further occurrence of an overshoot in the system, the value of $(K_p)$ and $(K_i)$ are chosen not to be too large. The quicker the STATCOM response varies upon the parameter of the gain such that, the higher the regulatory gain, the better the STATCOM output. The effect of droop on the STATCOM characteristic is shown in Figure 5.6 (b-c), where the STATCOM positive sequencing voltage $(V_m)$ does not follow the PCC voltage when the droop is set to 0.03 as shown in Figure 5.6 (b). Whereas when the droop value is lower such as 0.00, the $(V_m)$ immediately followed the PCC voltage as depicted in Figure 5.6 (c). The bigger the droop, the smaller the slope and the more deviation of $(V_m)$ to PCC voltage and vice versa. For a given maximum capacitive/inductive range this droop is used to extend the linear operating range of the STATCOM and to ensure automatic load sharing with other voltage compensators that might be installed on the grid. The selection of Kp, Ki (gain) and the droop is done in such a way that the slope is not too high to avoid STATCOM output response being slow. The positive sequence output voltage of the STATCOM $(V_m)$ reactive power $(Q_m)$ absorbed (the value is positive) or generated (the value is negative) by the STATCOM and the PCC voltage are depicted in Figure 5.7.

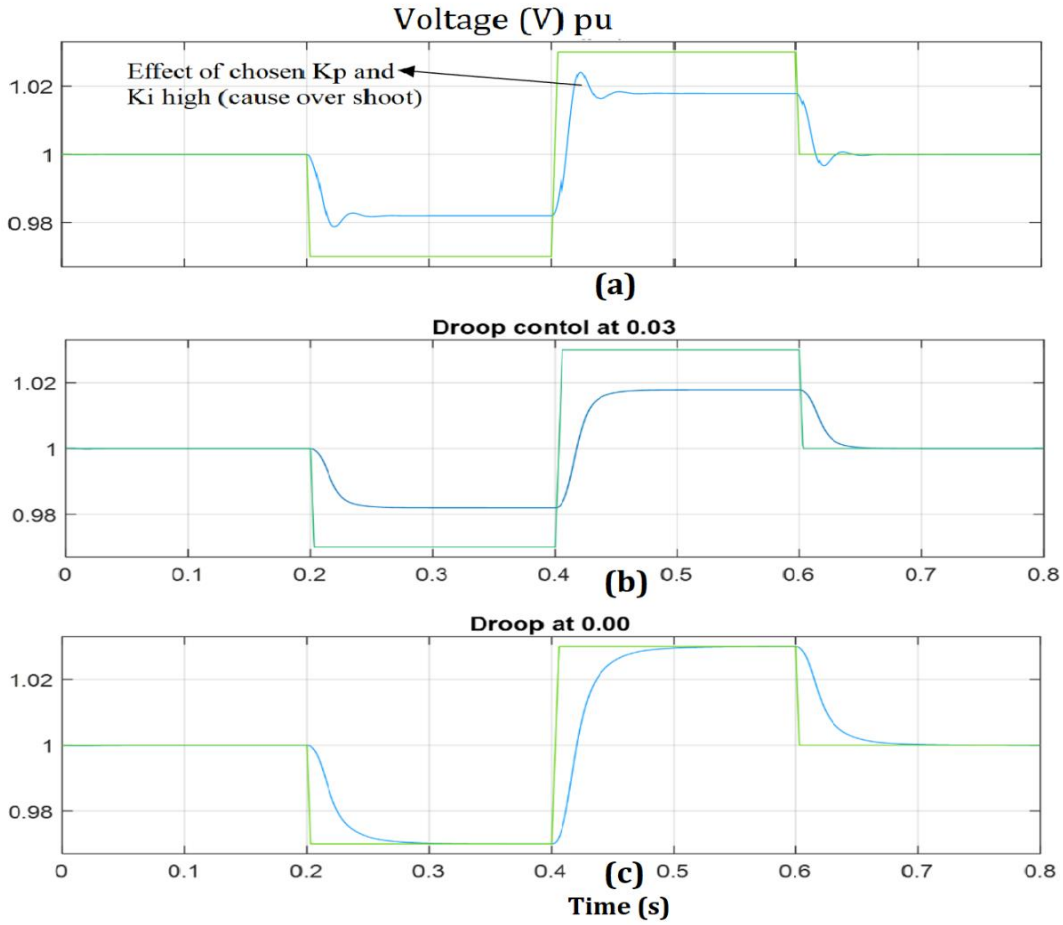


**Figure 5.6:** (a) Effect of regulating gain, (b) Effect of 0.03 droop and (c) Effect of zero droop.

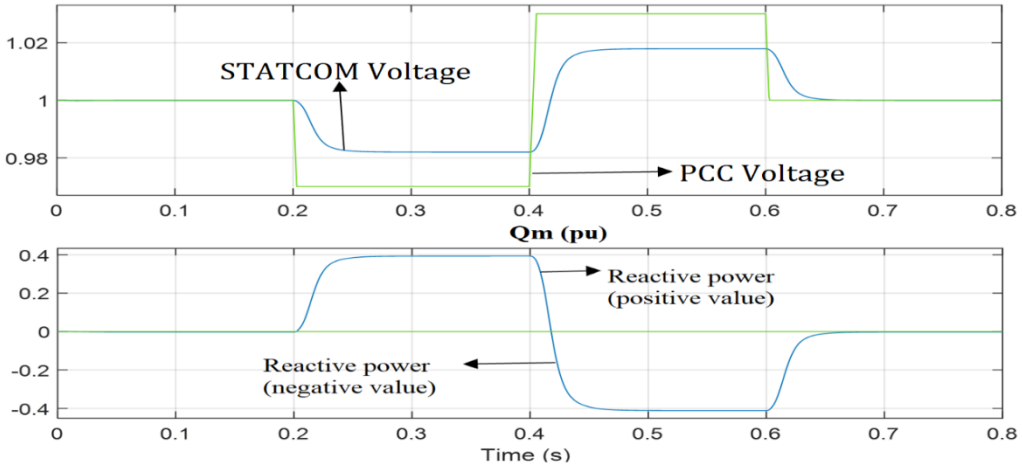


**Figure 5.7:** STATCOM and PCC voltage.

### .6.2 Voltage Rise Mitigation at PCC with STATCOM

The network simulation is repeated with RDG integration at PCC. The impacts of RDG improves the system voltage profile as discussed in Chapter 4, Table 4.2 to 4.4 and Figures 4.2 to 4.8. When the penetration levels of RDG is more than 80%, there is an occurrence of voltage rise at PPC which must be regulated for the continuous operation of RDG as specified by IEEE 1457-2018 and South Africa Grid Code Act or it must be disconnected as specified by IEEE 1457-2014. When 90% RDG penetration levels are injected at Bus 684, the results are shown in Figure 5.8 (a-c). Voltage rise occurs up to 1.13 pu without STATCOM installation which is not acceptable. The maximum permissible voltage at PCC is 1.1 pu as specified by the South Africa PCC voltage with RDGs integration.

The operation of the STATCOM is shown in Figure 5.8 (b and c). During the voltage rise condition, the operating mode of the STATCOM changes from the unity power factor to a voltage regulation mode to mitigate the voltage rise at the PCC to an acceptable range. It is observed during the voltage regulation mode that the STATCOM generates reactive power from -0.3 kVAR to -0.02 for the duration of 0.4 s to keep the PCC voltage to 1.1 pu and from -0.02 kVAR to 0.2 kVAR at the duration of 0.4 s to 0.8 s. More reactive power is generated to the PCC by the STATCOM to limit the voltage rise and finally sustain the PCC voltage to 1.09 pu while the system accepts more RDG penetration levels up to 120% without violation. Hence, the PCC voltage is within an acceptable range in agreement with IEEE 1547 and Southern Africa grid code requirement.

Figure 5.8 (d-f) shows the simulation results when PCC is changed from bus 5 to bus 6 to observe the impact of RDG. Voltage rise occurs between 0.2 s to 0.4 s up to 1.15 pu with 90 % RDG penetration levels, but reactive power is generated by the STATCOM to the PCC to keep the voltage within an acceptable level. The STATCOM maintains the PCC voltage at 1.1 pu while the voltage that flows across the grid is 1.021 pu as shown in Figure 5.9 which is within an acceptable range and the system takes up to 125 % penetration without PCC voltage violation. It is also shown in Figure 5.9 that the voltage measured in the other buses of the network is lower as compared to the voltage at PCC

in Figure 5.8, which means that PCC's voltage would always higher than any other bus of the netwotk.

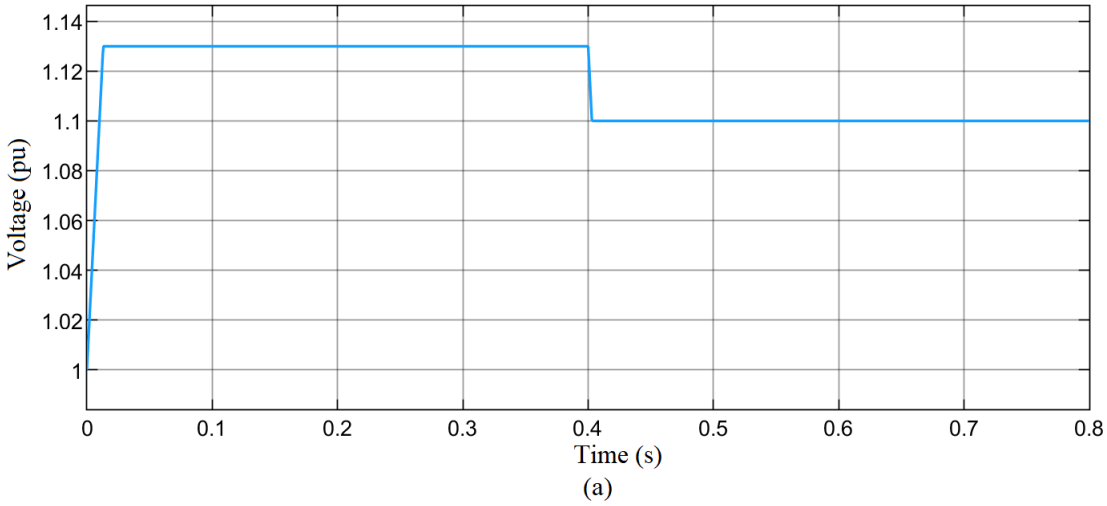


(a)

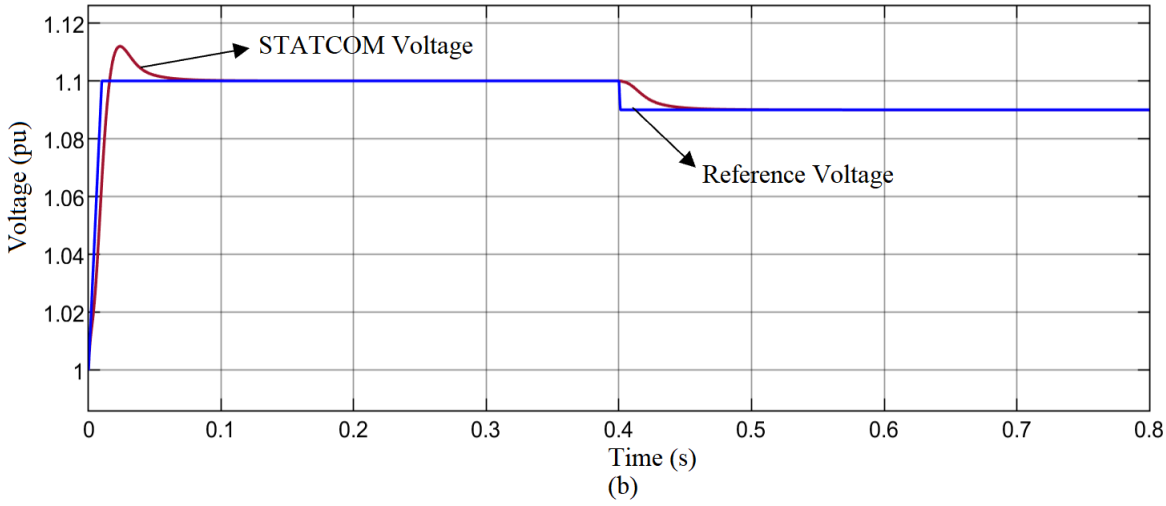


(b)

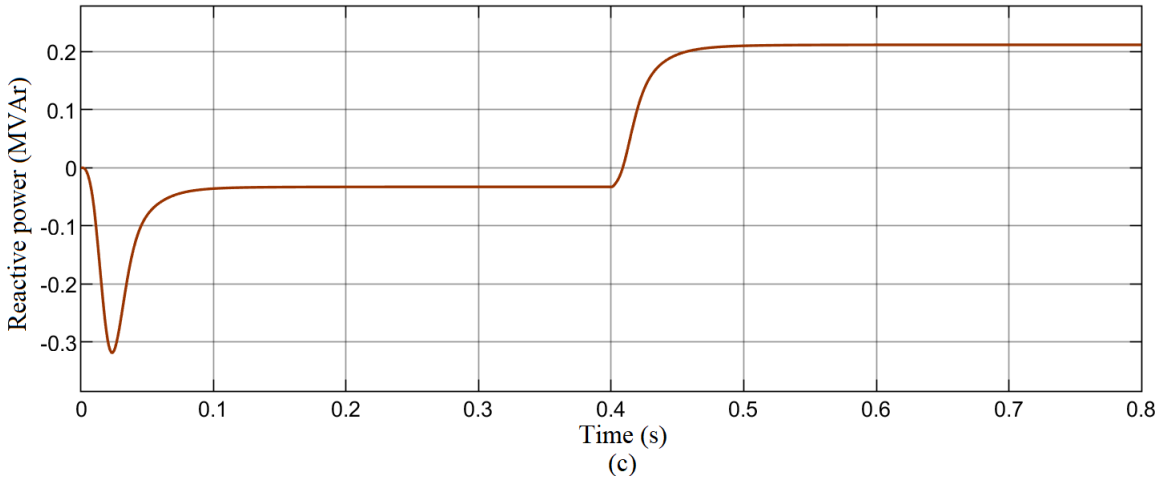


(c)

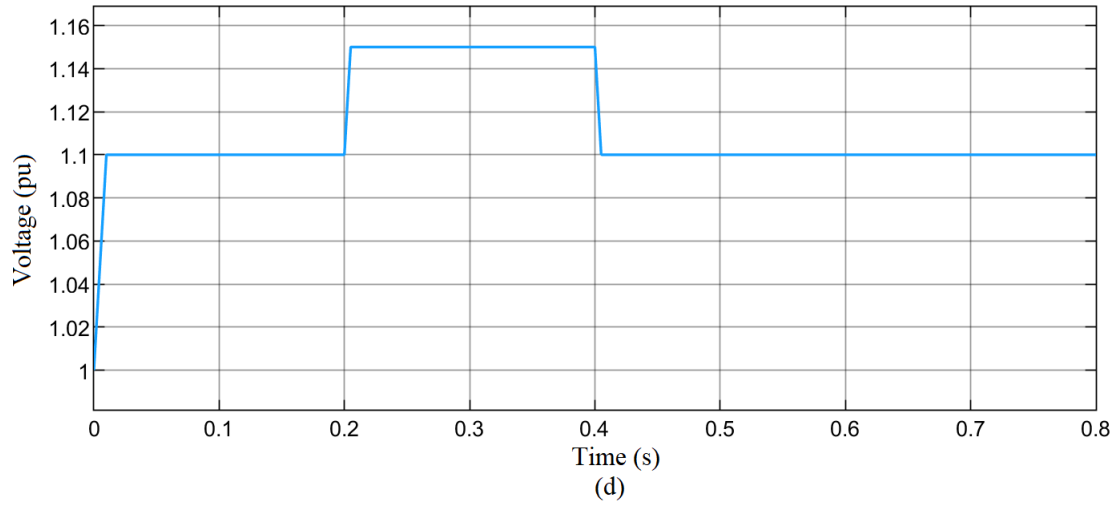


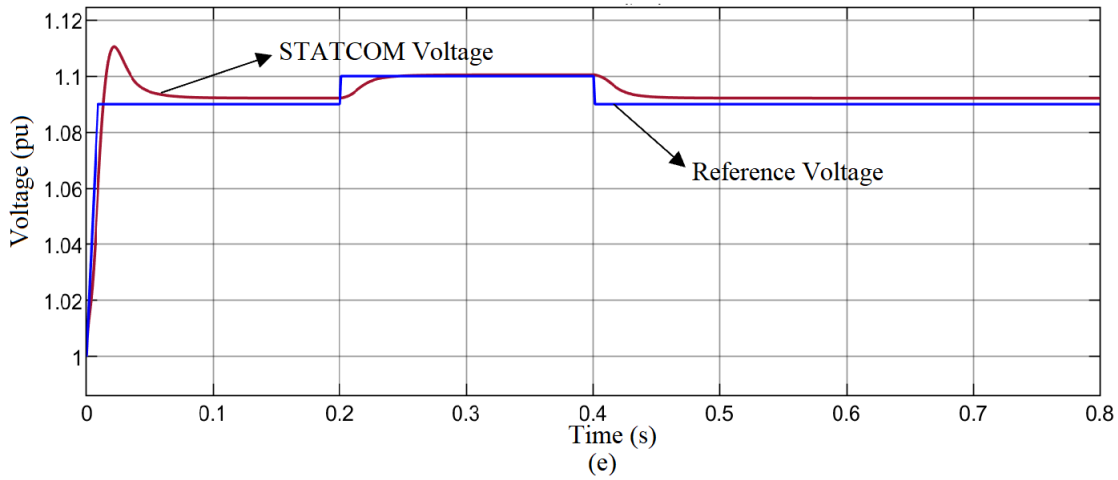


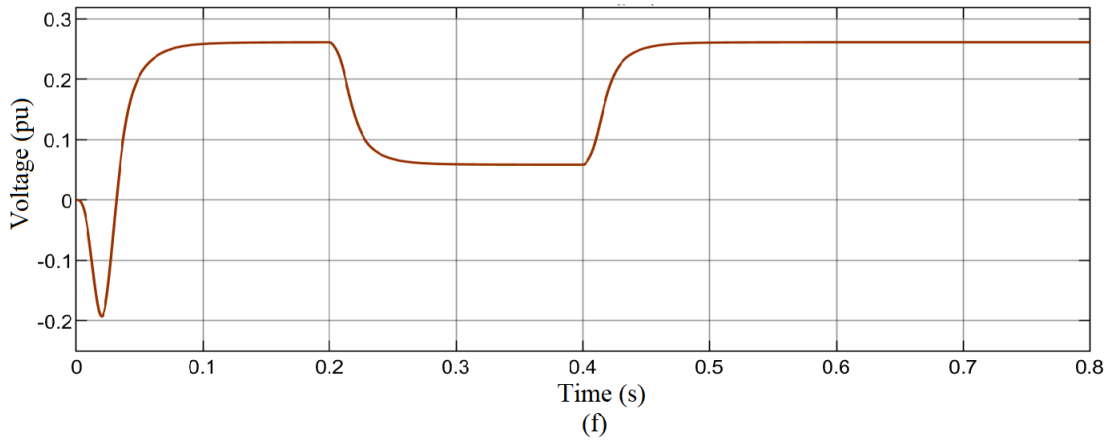


**Figure 5.8:** Voltage rise mitigation simulation results (a) Voltage rise at bus 5 with 90% RDG penetration, (b) Voltage mitigation at PCC with STATCOM, (c) Reactive power generated by STATCOM to minimize the voltage rise at PCC, (d) Voltage rise at bus 6

with 90% RDG penetration, (e) Voltage mitigation at PCC with STATCOM and (f) Reactive power generated by STATCOM to minimize the voltage rise at PCC.

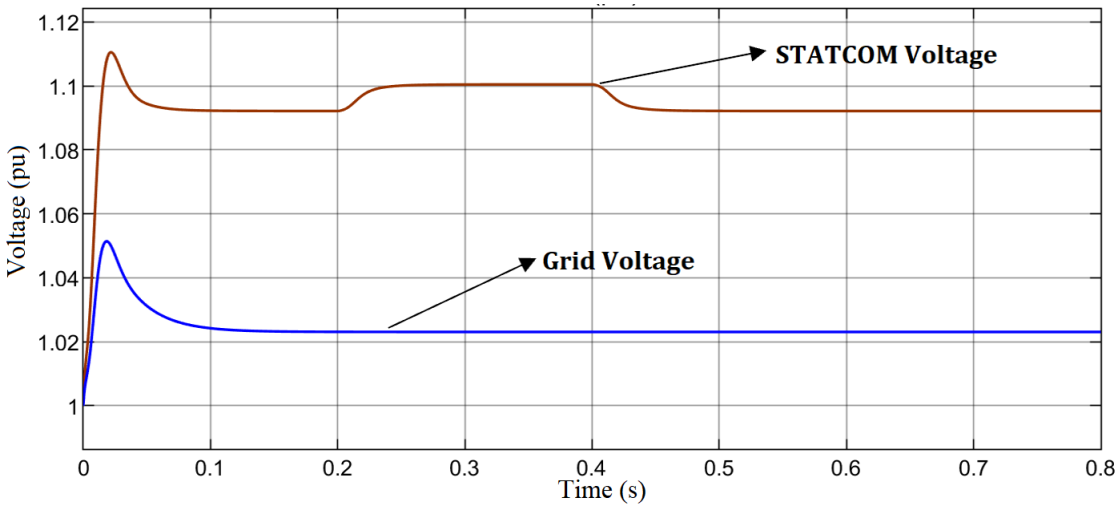


**Figure 5.9:** STATCOM and Grid Voltage.

### 5.6.3 Compensators Responses During Disturbances

This section presents RDG integration with various network disruption scenarios at PCC, such as single phase to ground fault, double phase to ground fault (2-Ø) and three-phase to ground fault (2-Ø)). The STATCOM and Static Volt/Amp Reactive Compensators (SVC) mitigation capacity are compared, where both STATCOM and SVC have a higher reactive control ability compared to other FACT devices as stated in the literature review [201], [202], [204], [203], [205], [206]. Various FACT devices are used for power quality mitigation in [201], [202], [204]. STATCOM and SVC are extensively used for reactive power compensation in [203], [205], [206], but their response capability during disturbances and voltage rise at PCC with large RDG integration are not covered. Hence, these two devices dynamic responses are compared during grid disturbances in this section.

Both STATCOM and SVC installed have a similar nominal rating and phasor model. The fault impedance is programmed to 31% at the PCC, the circuit breaker programming is selected to t = 0.20 s and the simulation lasts for 0.10 s. It is observed during the severe fault condition (three phase fault) that voltage dip occurs due to the disturbance at the PCC as shown in Figure 5.10. The capacitive reactive power produced by the SVC is -

0.49 (pu) while STATCOM produced -0.72 (pu) to keep the PCC voltage to 0.72 (pu) while Figure 5.11 depicts the dynamic response of the STATCOM and SVC during single-phase fault to ground, 2-Ø fault and 3-Ø fault to ground.

The STATCOM produces capacitive reactive power of -0.81 (pu) while SVC produces -0.64 (pu) during a single fault to ground in Figure 5.11 (a), -0.98 (pu) and -0.85 (pu) during 2-Ø to ground fault as shown in Figure 5.11 (b) and finally, -2.45 (pu) and -2.3 (pu) in Figure 5.11 (c) to keep the grid to 1 (pu) in Figure 5.11 (d). One of the deductions in this simulation is that the highest capacitive power produced with STATCOM declines linearly as the voltage reduces, while the highest capacitive power produced by SVC is proportionate to the square of the grid voltage. The STATCOM's inductive/capacitive output current is controlled independently of alternating current as compared to the thyristor-based variable static compensation (SVC). The STATCOM demonstrates a significant improvement in the dynamic fast voltage response than SVC as depicted in Figure 5.11. It is capable of delivering more capacitive power in the event of failure, which is a major advantage of STATCOM compared to SVC. Moreover, the STATCOM displays a quicker output response due to its voltage source converter characteristics as compared to the SVC that is slow. The STATCOM does not have a delay associated with the starting delay time due to valve firing of the Thyristor about 0.004 s in SVC. The simulation results indicate that to keep the nodal voltage magnitude at 1pu at the bus where the SVC or the STATCOM are connected, both devices inject -2.45 pu and -2.30 pu of reactive power respectively. In general, an improvement can be seen in the network's voltage profile in Figure 5.11 (d).

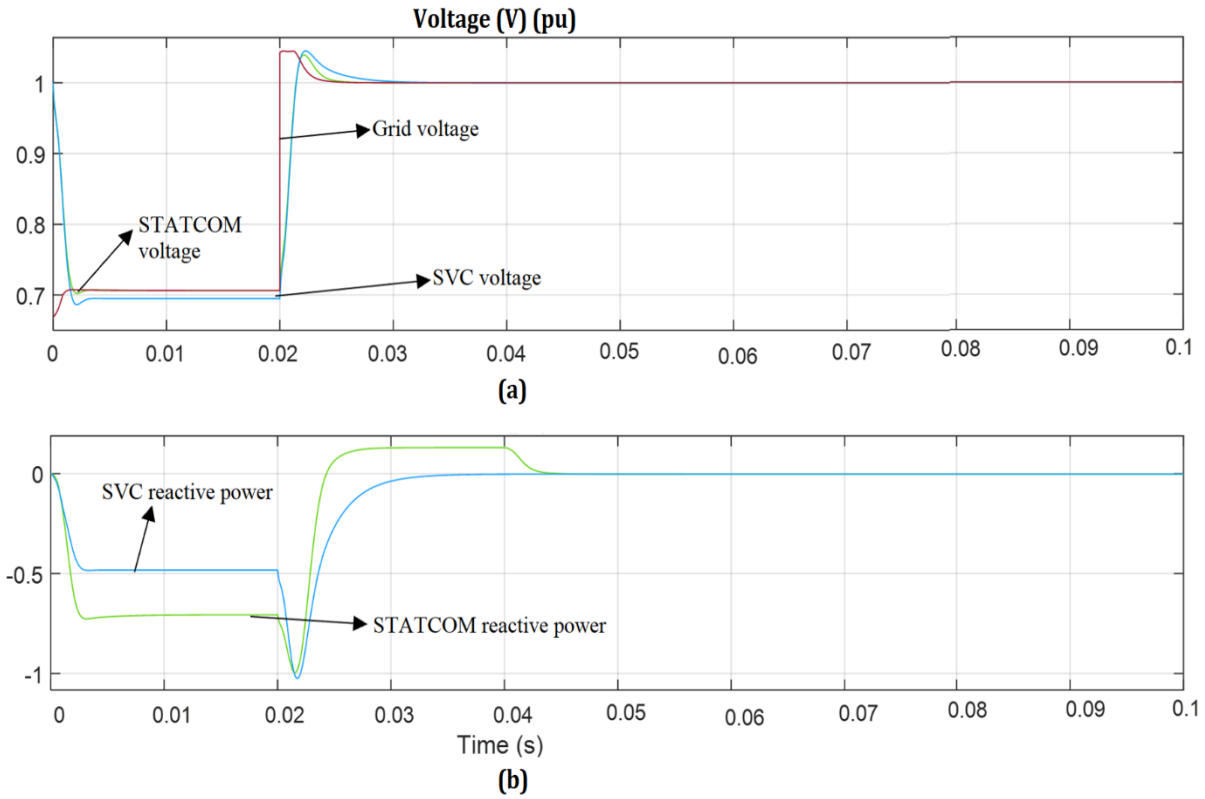


**Figure 5.10:** (a) Voltage dip at PCC and Reactive generated by STATCOM and SVC during the voltage dip.

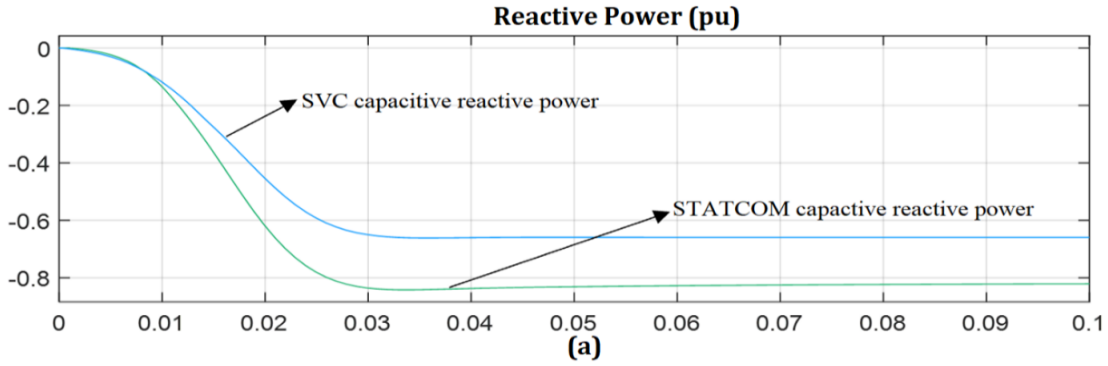

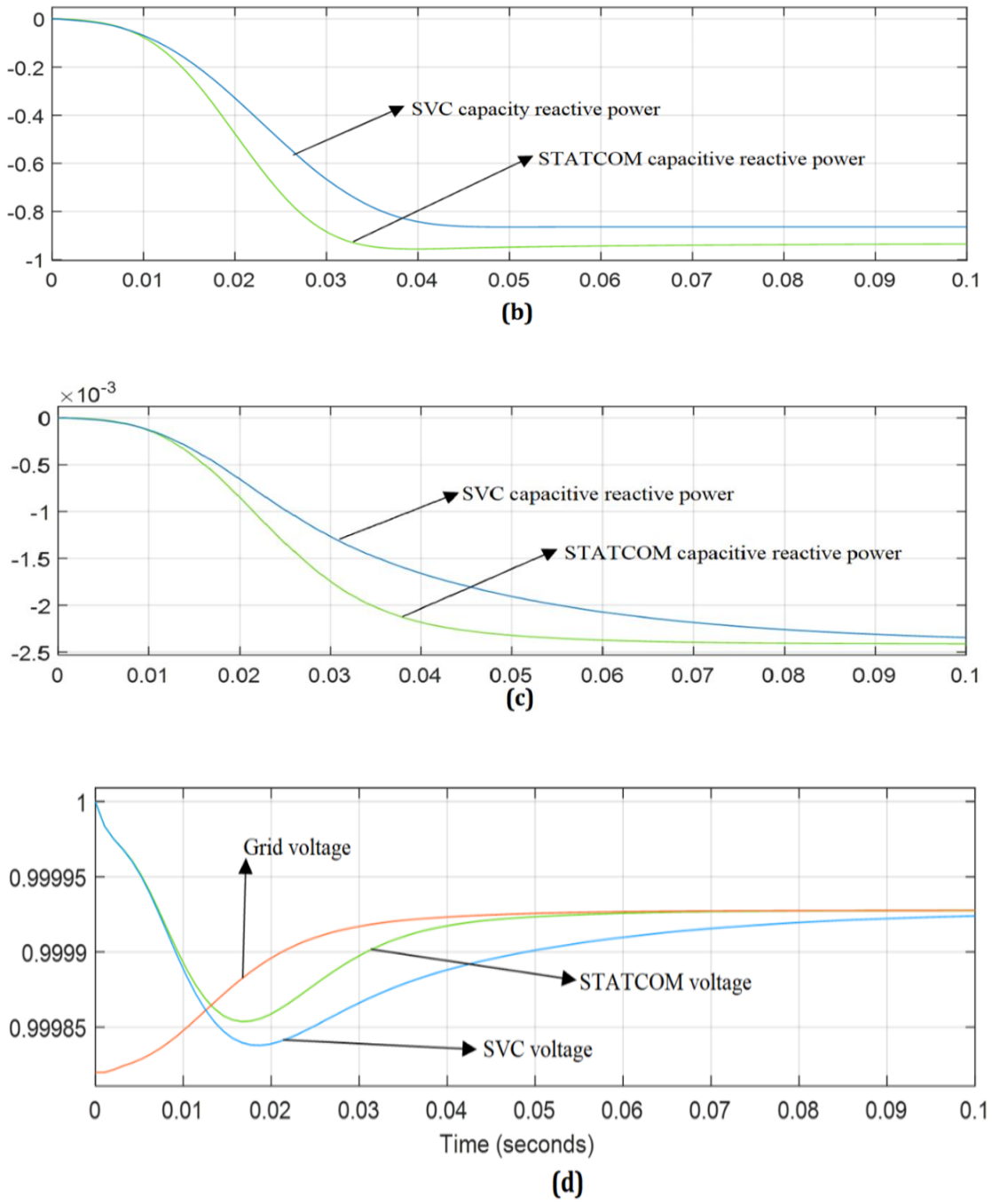


**Figure 5.11:** (a) Single phase fault to ground, (b) 2-Ø fault to ground and (c) 3-Ø fault to ground and (d) Grid voltage, STATCOM voltage and SVC voltage.

### 5.6.4 Simulation Comparison Between STATCOM and SVC

- The SVC generates less reactive power of 0.49 pu while STATCOM generates more reactive power of 0.72 pu during a fault condition with the same parameters and power rating which is similar to the research work done in [207].

- Grid voltage improves to 0.72 pu with STATCOM and 0.69 pu with SVC during fault conditions in Figure 5.10, with difference fault conditions such as single-phase fault. STATCOM reactive power generated 0.81 pu is higher than SVC reactive power generated 0.64 pu in Figure 5.11 (a). The double phase fault, the STATCOM reactive power generated 0.98 pu is still higher than SVC reactive power generated 0.85 pu in Figure 5.11 (b) and when the 3-Ø fault occurred on the network, STATCOM reactive power generated 2.45 pu is higher than SVC reactive power generated 2.30 pu in Figure 5.11 (c). Although, the value of the reactive capacitive power generated by both devices during the most severe network fault is very close, STATCOM produces more reactive power than SVC.

- At the occurrence of voltage dip due to disturbances, STATCOM has the capacity to generate more capacitive reactive power than SVC because the reactive capacitive power generated is proportionate to the square of the grid voltage or constant susceptance while the STATCOM maximum capacitive power generated decreases linearly with voltage decrease or constant current.

- STATCOM produces more capacitive power than SVC during a fault condition.

- STATCOM works the same way SVC does. However, at voltages below the normal voltage regulation range, the STATCOM can generate more reactive power compared to the SVC. The STATCOM shows a quicker response than SVC. This may be due to the fact that STATCOM uses pulse with modulation voltage source converter while SVC uses Thyristor and the starting delay time of Thyristor due to valve firing is about 0.004 s.

- The magnitude of the grid voltage remained within an acceptable limit during steady state with both devices and both devices can provide a voltage support [208] and keep the grid voltage to an acceptable level as shown in Figure 5.11 (d).

- STATCOM voltage always follows the reference voltage closely to keep the reference voltage at 1(pu) while SVC voltage does not follow the reference voltage closely as shown in Figure 5.11 (d).

- Both devices can have the capacity to absorb/generate reactive power and

therefore both can mitigate power quality problems during grid disturbances.

- STATCOM may be more expensive than the SVC depending on voltage, land requirements, construction time, operation and maintenance, repair, workers, substation equipment, access, roads, service, permits, licenses and financing, the transformer, the DC source, the semiconductors and the respective snubber to protect them, while for SVC cost depends on passive elements such as inductors and capacitors comprising TCR and TSC.

- The simulation results indicate that to keep the nodal voltage magnitude at 1pu at the bus where the SVC or the STATCOM is connected, both devices inject -2.45 pu and -2.30 pu of reactive power respectively. In general, an improvement can be seen in the network's voltage profile in Figure 5.11(d).

## 5.7 Summary

Chapter Five investigates the compensation strategy and its mathematical analysis, voltage rise regulation at PCC, compensator connection model, FACTS devices descriptions, dynamic response and modelling of STATCOM, regulatory capability of STATCOM, voltage rise mitigation at PCC with STATCOM, response of STATCOM during fault conditions, and simulation comparison between STATCOM and SVC. The overall deduction from this chapter’s investigation is that compensator devices can: generate and absorb reactive power, mitigate power quality challenges such as voltage rise and dips, improve network stability and increase power flow when installed in a distribution system. The outcome of the simulation results in this chapter show that the voltage rise at the PCC can be regulated by generating or absorbing reactive power to/from the system. With a compensator device installation and voltage rise control at PCC, a large RDG integration can continue operation without disconnected from the system.

# CHAPTER 6

# VOLTAGE RISE REGULATION WITH A GRID CONNECTED SOLAR PHOTO-VOLTAIC SYSTEM

## 6.1 Introduction

Most of the remote communities in Africa countries require sustainable electrical energy for everyday life. The extension of the central energy production system, transmission and distribution cannot reach these areas because of massive energy losses and huge energy costs. Isolated electrical power generation such as microgrids would be a possible solution to this problem. Microgrid system located in a remote area could have a lesser prerequisite due to the nature of the loads, such as streetlights and domestic needs as compared to the massive electrical network or macro network. The latest trend of power generation is by using renewable energy sources since they are clean, friendly, and naturally replenish on a human time scale [209], [210].

Countries across the globe are exploring their ecological approachable power sharing to reduce total dependence on the conventional method of power generation. Another option by which electrical power can be supplied to remote areas where there is no opportunity for grid connection is by making use of generating sets. This alternative is not encouraged however because of the risk of releasing harmful and poisonous gases into the atmosphere and causing global warming [211]. Scientists, researchers, and industrialists have shown a great interest in microgrids with Renewable Distributed Generation (RDG) development due to the advantages it can offer in terms of sustainability, reliability, modularity, and lower cost as compared to the conventional power generator and simple design implementation [212]. Renewable energy sources with battery storage integration have received attention in recent years because of their easy design, simple installation, and energy management strategy [213], [214]. Among these renewable energy resources, solar power is outstanding and popular because of its easy deployment to the power system and cheap maintenance costs as compared to the conventional method of electricity generation [215].

In South Africa, about 8.3 GW nominal capacity from different kinds of renewable energy were attained in 2020, where solar carried 2.5 GW out of this capacity [216]. Nevertheless, this is not enough, and more will soon be deployed across the country. The benefits of accessing energy from solar are numerous. There is no direct radiation, it is appropriate for low energy consumption and suitable for remote areas where there is no access to the electricity grid. There is a need for energy generation and power quality management strategies in a distribution network with renewable energy resources integration because of their integration issues at PCC, such as voltage rise, current distortion, and their intermittent nature in generating output. Winds do not blow for 24 hours every day. The same problem applies to the sun, in that its output is dependent on climatic conditions. The intermittent nature of the system, distortion occurrence at PCC, power quality issues, protection challenges because of voltage rise at PCC, and the network load variations would definitely have an impact on their voltage output and network stability. Therefore, these issues could make the microgrid/Distribution Network less reliable, resulting in a reduction in the renewable distributed generation penetration levels [217], [218], [219], [220], [221]. Hence, these constraints with RDG integration can be strategically managed and regulated at PCC if they are to stay connected at PCC as specified in by the Southern Africa grid code requirements, IEEE-1547 and IEEE-519 respectively.

This chapter investigates the voltage rise regulation with a grid connected Solar Photo-voltaic system. The chapter also discusses solar systems, solar and battery modelling, factors affecting solar array performance, energy management and solar power tracking. Design and simulation of a proposed microgrid for DUT, control strategy, load variation under PV system, effect of PV variation on the system, and the grid behaviours during STATCOM UPF and VR mode are analysed. The contributions of this chapter are summarized as follows:

- Strategic regulation of PCC voltage rise issue through the generation of positive reactive power without disconnecting renewable distributed generation integration with higher penetration levels.
- An in-loop second order integral filtering algorithm is designed to filter grid current distortions generated from the non-linear loads.
- Peak power point tracking error is minimized from the solar power tracking system

by the addition of an integral regulation algorithm.

- The output voltage and power of the PVAs is made reinforced and stable with fluctuation in loads and the sun's irradiation.

The research questions that guide this chapter are as follows:

- How can oscillation and error be regulated with peak power point tracking system?
- What is the impact of load and solar PVA variations at the PCC?

## 6.2 Solar System

Electrical energy can be generated from solar cells by transforming sun irradiance (incident light) to electricity by the method known as Photovoltaic effect. A typical solar cell is made of semiconductor materials, usually p-n semiconductor diodes, having a negative side facing the sun and a positive back side. The solar output voltage increases when its cells are connected in series with each other, and they form solar arrays. The amount of energy produced by the solar array is dependent on voltage/current at the peak power point, fill factor, open and short circuit voltage/current, while the temperature and the sum irradiance determine its performance. Solar array open circuit voltage reduces with increase in sun irradiance, short circuit current and operational temperature. Hence, there would be intermittent energy produced by the solar cells on a daily basis. Sometimes, peak power may not be accessed because of the variability of the sun's irradiance and temperature change. Solar cell representation in MATLAB/Simulink, and solar array equivalent circuit are shown in Figure 6.1, having shunt and series resistors, with a current source and a diode connected. In the diagram, $(I_{ph})$ is the photo current represented as a current source, $(I_d)$ and $(I_p)$ are the leakage currents flowing through the diode and the shunt resistor, respectively; $\text{while}\,(I_{pv})$ is the load current passing through the series resistor. The solar photovoltaic system involves the conversion of photonic energy to electrical energy, but with the change in temperature and climatic factors, the solar output voltage may vary [222]. Irrespective of the electrical analysis, the solar panels are modelled as a constant current source. Two or more solar cells connected in series/parallel and arranged in a frame form a solar panel or module while groups of solar panels make solar arrays.

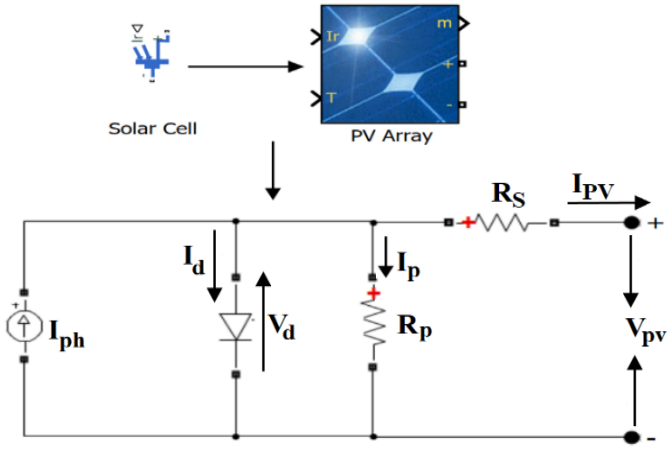


**Figure 6.1:** Solar cell, Array and Equivalent Circuit.

Considering the equivalent solar cell diagram in Figure 6.1, the solar cell current is represented by $(I_{PV})$, solar cell voltage $(V_{PV})$, the photo current $(I_{ph})$, a series resistor $(R_s)$, shunt resistor $(R_p)$, current across the diode $(I_d)$, $(I_p)$ is the current across the shunt resistor and $(V_d)$ for diode voltage. The solar current expression can be obtained in equation 6.1. From equation 6.2, (q) is the quantity of electron charge $(1.6 \times 10^{-19}\text{C})$, *(A)* is the ideality factor of the diode, *(K)* is the Boltzmann's constant $(1.38 \times 10^{-23}\frac{\text{J}}{\text{K}})$, (T) is the operating temperature and $(I_S)$ is the diode saturation current or dark current. The increase in the irradiation of the solar will result in the increase of solar voltage and power. Consequently, the temperature increase can have a negative impact on the output voltage and power [223].

$$(I_{PV}) = I_{ph} - I_d - I_p \tag{6.1}$$

$$I_{pv} = \left\{ I_{ph} - I_S \left( e^{\frac{q[V_{PV}+R_S I_{PV}]}{AKTN_{SE}}} \right) - 1 \right\} - \frac{(R_S I_{PV}+V_{PV})}{R_P N_{SE}} \tag{6.2}$$

### 6.3 Factors Affecting Solar System Performance

The life span of solar arrays, its generated output power and outdoor operation can be influenced by the type of PV material, irradiation intensity received, cell temperature, parasitic resistances, climate and other shading effects, fill-factor, inverter efficiency, dust, module orientation, weather conditions, geographical location, cable thickness etc. Some of these factors are discussed below.

### 6.3.1 Effect of Climate on Solar System

Climate change will lead to a change in solar power system output while *I-V/P-V* characteristics will vary as the irradiance of the solar system consists in the angle of incidence of the sun's rays. Consider the sun ray in the sky dome, the solar panel collector in Figure 6.2 to analyse the solar performance losses and cosine effect. Collector tilt *(β),* Azimuth *(γ)* and the Angle of incidence *(θ)* can be used to clarify the positioning of the solar collector surface with respect to the collector surface of the Sun. The Tilt, which is the angle between the plane of the collector or the aperture, the horizontal and Azimuth is the planar rotation East or West which an aperture will possess while the angle of incidence is the angle between the vector perpendicular to the collector plane. It is usually called the normal of the plane and the projection of the Sun's central beam to the collector surface. *(β)* and *(γ)* are positioned for reflection in the Northern Hemisphere, while the Sun's position is described using solar altitude angle ($\alpha_{solar}$) and the solar azimuth angle ($\gamma_{solar}$). *(β)* and *(γ)* are mostly fixed surfaces while *(θ)* can be varied and can be defined in equation 6.3. Arccosine is applied to equation 6.3 to obtain 6.4. The output voltage and current are affected by the change in the climatic condition. Thus, the highest access of power can be achieved at any point of solar system operation with the efficient peak power point technique capability to harness the irradiation, control the temperature and improve a steady output voltage.

$$Cos\ \theta = Sin\ \phi\ Sin\ \delta\ Cos\ \beta - Cos\ \phi\ Sin\ \delta\ Sin\ \beta\ Cos\ \gamma + Cos\ \phi\ Cos\ \delta\ Cos\ \beta\ Cos\ \omega + Sin\ \phi\ Cos\ \delta\ Sin\ \beta\ Cos\ \gamma\ Cos\ \omega + Cos\ \delta\ Sin\ \beta\ Sin\ \gamma\ Sin\ \omega \quad (6.3)$$

$$Cos\ \theta = Sin\delta\ (Sin\ \phi\ Cos\ \beta - Cos\ \phi\ Sin\ \beta\ Cos\ \gamma) + Cos\ \delta(Cos\ \phi\ Cos\ \beta\ Cos\ \omega + Sin\ \phi\ Sin\ \beta\ Cos\ \gamma\ Cos\ \omega + Sin\ \beta\ Sin\ \gamma\ Sin\ \omega) \quad (6.4)$$

Where *(ϕ, δ, β)* are Latitude, declination and tilt, *(ϕ, δ, β, γ)* are latitude, declination, tilt, and collector azimuth and *(ϕ, δ, β, γ, ω)* are latitude, declination, tilt, collector azimuth, and then the hour angle.

### 6.3.2 Shading effect

Solar cells are usually connected in series and parallel. They are connected in series to obtain desired output voltage and in parallel to have the same current flow across the

solar cells. Solar system shading occurs because of obstructions, fogs, structure, shadow, tree shadow, mists, etc. According to equation 6.2, the insolation minimizes the $(I_{ph})$. The current that flows in solar cells is constant if the solar panels are connected in series. If the shadow is cast to one of the cells, instead of the cell providing energy, it will break down and act as a load because of weakening of photocurrent [224]. However, when a cell is shaded from the cells connected in series due to cloud or shadow etc., the shaded cell will produce output current lower than that from other unshaded cells, resulting in the total current generated by the cells being dictated by the shaded cell causing loss of output power in the solar system. When the unshaded cells produce current that is higher which tries to pass across the shaded cell, the shaded cell will behave like a load where the shaded cell would be reverse-biased when connected in series with active cells. It will act like a load instead of a solar generator. Therefore, it will produce heat which will increase the system temperature and cause hot spots. The hot spot effect can cause damage within the module such as melted cells, and solar glass cracks. To minimise the shading effect in the solar system, diodes known as bypass diodes can be installed across the shaded solar cell. The installed diode will allow current to pass through, while no current will pass through the shaded cell. In a simple analysis, when a diode is connected across a solar cell or group of solar cells, the forward biased voltage will be equal to the solar cell voltage. When there is no shaded solar cell in the system, the system generates a voltage that will pass across the bypass diode in reverse bias, leading to the diode blocking the current passing through it. However, when there is any shaded cell in the system, there are voltage drops across the diode leading to forward bias of the diode causing current to pass through the diode instead of the shaded cell. The bypass diodes will clear the shading effect by bypassing the shaded module.

### 6.3.3 Effect of bypass diode

It has been argued above that bypass diodes can mitigate the solar system shading effect. However, installation of bypass diodes will cause voltage drop influence on the total string voltage that may interfere with the other parallel strings within the system, since equivalent array voltage is dictated by the string with the lowest voltage. A diode known as a blocking diode can be added to the system. A blocking diode prevents the current from flowing back to the weak string, and it will protect the shaded string from

draining current out of the unshaded strings. Blocking diodes also assist the solar system when the sun is not shining, in that current may flow back to the module, acting like a load. A blocking diode will stop the current from flowing back into the modules and damaging it. The microgrid solar system can be maximized by avoiding the shading effects from the solar collector. The effect of shading is the slowest reaction of the thermal response of the solar cell. When a solar collector is covered by cloud or shadow, the covered area will not be active as compared to the other part. Also, it will minimise the angle of incidence by directing the collector normal to the Sun and by decreasing the cosine projection effect.

### 6.3.4 Cosine effect

Figure 6.3 is a fragment of Figure 6.2 which can give a better explanation of solar panel sun ray tracking analysis. Figure 6.3 (a) shows the solar panels perpendicular to the angle of incidence ($\theta$) of the sun ray such that the incidence angle is equal to zero (at angle $90^0$) where the sun is direct above the fixed solar panel. Otherwise in Figure 6.3 (b) when the sun moves across the sky, if the equation 6.6 is not zero, the implication is that the amount of energy received by the solar fixed surface has reduced. Therefore, cosine effect will occur resulting in loss of incident energy. For solar efficiency to be maximized, cosine effect should be reduced to the minimum. The perpendicular vector $(G_p)$ in Figure 6.3 (c) is the absorption of suitable components from the sun and can be obtained in equation 6.7 while the parallel $(G_{pa})$ denotes the reflected or loss components which can be obtained in equation 6.8 without considering inefficiencies. The effect of performance losses $(G_{pa})$ can therefore be minimized to a minimum by the application of collector tilt (β) in Figure 6.3 (d). With the application of automatic tracking strategy by (β) adjustment, the solar panel can be set perpendicular to the sun, thereby reducing solar performance losses and the cosine effect will be minimal.

$$\theta = 0 \tag{6.5}$$

$$\theta \neq 0 \tag{6.6}$$

$$(G_p) = GCos\theta \tag{6.7}$$

$$(G_{pa}) = 1 - \frac{G_p}{Incident\ irradiance}\% \quad (6.8)$$

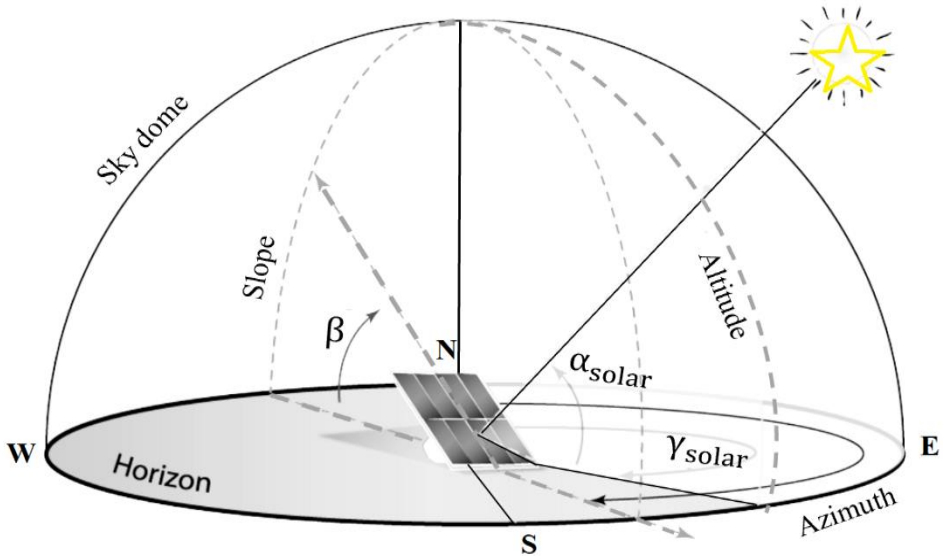


**Figure 6.2:** Solar and Sun collector surfaces.

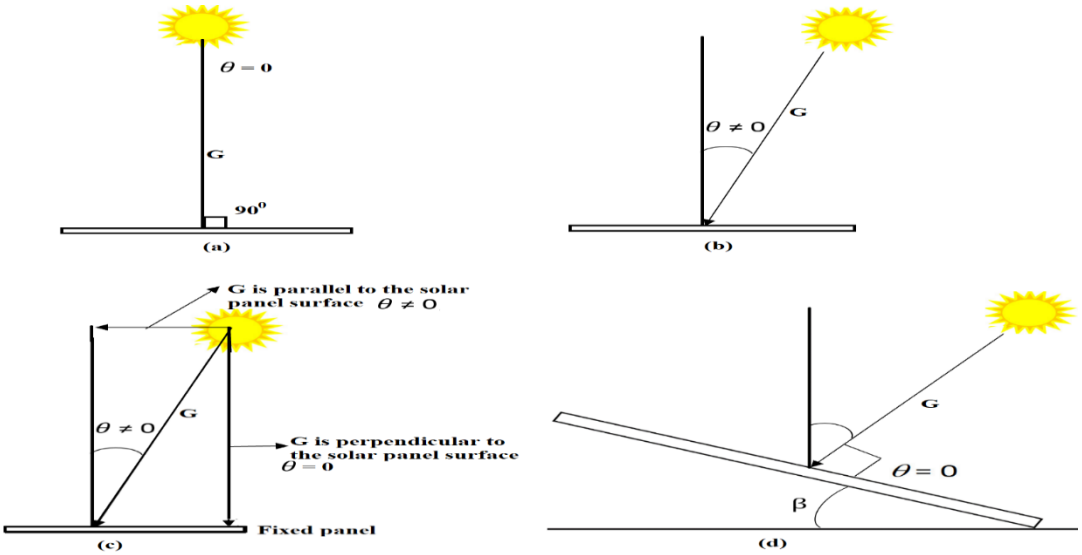


**Figure 6.3:** Solar collector and cosine effect.

### 6.3.5 Temperature effect

The current output varies with changes in the impact of the solar rays resulting in the constant output voltage of the solar system. Also, the magnitude of the solar system output can be shifted, giving a steady output current [225], [226]. An increase in the intensity of the sun, heat dissipated on the solar panel and the infrared wavelength which

cause wear on the solar cell can influence the solar panel temperature. An increase in the temperature causes decrease in voltage provided that all parameters remain constant. The resultant effect is power loss. But when temperature decreases, there would be an increase in voltage and power output generated. Therefore, the relationship between short circuit current, open circuit voltage and the solar panel temperature can be expressed in the equation below. The output voltage and the short circuit current can be obtained from equations 6.9 and 6.10 while $(a_1)$ and $(a_2)$ are the temperature coefficient, $(I'_{sc})$ and $(V'_{oc})$ are the reference parameters at solar intensity $(G')$ and temperature $(T')$.

$$V_{ov} = V'_{oc} + a_2(T - T') - (I_{sc} - I'_{sc})R_{se} \quad (6.9)$$

$$I_{sc} = I'_{sc}\left(\frac{G}{G'}\right) + a_1(T - T') \quad (6.10)$$

### 6.3.6 Parasitic Resistances, Fill-Factor and Solar Efficiency

The resistance of the solar system (series/parallel) can be referred to as **Parasitic Resistances (PR)**. The resultant effect of this resistance is amounted to the system losses $(I^2R)$. The occurrence of the losses in the system will reduce the solar array's efficiency. The system resistors connected in series form the solar array internal resistance (which is the resistance of the semiconductor itself), the metal contacts resistance, and impurities; while the parallel resistors form the leakage resistance which usually causes the leakage current. **Fill Factor (FF)** is the ratio of the maximum power from the solar cell to the product of open circuit voltage and short circuit current as defined in equation 6.14. (FF) measures the squareness of the solar voltage/current curve. The higher the solar voltage, the bigger the filler factor. The solar cell performance can be measured by their efficiency. The ratio of the power out of the solar cells to the input power from the sun can be described as the solar **efficiency,** which is dependent on the spectrum and intensity of the incident sunlight and the temperature of the solar cell. Equation 6.11 shows solar peak power from where the efficiency can be obtained. $(V_{oc})$ is the open circuit voltage, $(I_{sc})$ is short circuit current, $(\mathcal{E})$ is the solar efficiency, $(P_{in})$ is the input power from the sun, $(V_{pp}I_{pp})$ is the peak power point and (FF) is the fill factor. (FF) can also be obtained when solar power is differentiated with respect to the voltage

as shown in equation 6.15. The maximum theoretical FF from a solar cell can be determined by differentiating the power from a solar cell with respect to voltage and finding where this is equal to zero.

$$P_p = V_{oc} I_{sc} FF \tag{6.11}$$

$$\mathcal{E} = \frac{V_{oc} I_{sc} FF}{P_{in}} \tag{6.12}$$

$$FF = \frac{P_p}{V_{oc} \times I_{sc}} \tag{6.13}$$

$$FF = \frac{V_{pp} I_{pp}}{V_{oc} I_{sc}} \tag{6.14}$$

$$\frac{d(IV)}{dV} = 0 \tag{6.15}$$

$$V_{pp} = V_{oc} - \frac{nkT}{q} in \left( \frac{qV_{pp}}{nkT} + 1 \right) \tag{6.16}$$

## 6.4 Battery Modelling, Solar Power Tracking and Energy Management

Energy storage provides the power system with flexibility and is very useful in increasing the volume of renewable power that can be safely and securely connected to the grid. Solar battery modelling and solar power tracking strategy are discussed below.

### 6.4.1 Battery Modelling

Solar system irradiations are not stable due to climate factors [227], [228], thus, battery banks are vital in maintaining a continuous power delivery to the consumers. It is pertinent to note that the state of charge of any battery storage in a microgrid system will determine the limit of such battery storage. To determine how massive the microgrid system battery storage will be, the depth of discharge, ambient temperature, battery storage life and the capacity would be a critical determining factor [229]. When the microgrid battery storage is in the charging mode, the equation 6.17 can be obtained. Therefore, the Rate of Charge [RC(t)] can be defined in equation 7.18 while equation 6.19 describes microgrid battery storage when discharging. Rate of Discharge $(RD_{(t)})$ can be obtained in equation 7.20.

$$C_{energy}(t) = \left(\frac{P(t)-P_{load}(t)}{\mathcal{E}_{converter}} + PV_{power}(t)\right) \times \Delta t \times \mathcal{E}_{charging} \quad (6.17)$$

$$RC(t) = RC(t-1)(1-\mathfrak{Z}) + C_{energy}(t) \quad (6.18)$$

$$D_{energy} = \left(\frac{P_{load}(t)-P(t)}{\mathcal{E}_{converter}} - PV_{power}(t)\right) \times \Delta t \times \mathcal{E}_{discharging} \quad (6.19)$$

$$RD(t) = RD(t-1)(1-\mathfrak{Z}) - D_{energy} \quad (6.20)$$

Where $RD\ (t), RD\ (t-1)$ = State of charge at time (t) and (t-1).

$\mathfrak{Z}$ = Self discharge rate.

$\mathcal{E}_{\text{charging}}$ = Charging efficiency of the battery storage.

$PV_{power}(t)$ = Power generated by the PV.

*P(t)* = Actual power generated.

$P_{load}(t)$ = Load power of time (t).

$\mathcal{E}_{converter}$ = Converter efficiency.

$\Delta t$ = Change in time (t).

$\mathcal{E}_{discharging}$ = Discharging efficiency of the battery storage.

$C_{energy}$ = Charging energy.

$D_{energy}$ = Charging energy.

### 6.4.2 Solar Power Tracking

When the efficiency of solar cells is low and the power output must be at a maximum possible level regardless of any factors, there is a need for a high solar power tracking. Peak Power Point Tracking (PPPT) of a solar system is the method by which devices connected to the microgrid such as microgrid inverter systems, solar charger controllers etc., track peak power at the point where solar cells deliver the highest electrical energy

[230]. A PPPT system analyses the solar cell output power and determines when load should be connected to achieve maximum power in respective of environmental factors such as a change in load impedance and weather conditions. PPPT quickly and accurately tracks power and reduces oscillations. The control strategy depends on the voltage, current, and the duty cycle [231]. Each solar panel possesses an operating point that is constant at some point from which a peak power is delivered. Three methods are concentrated here by which PPPT of the solar system can be achieved viz: perturb and observe strategy, incremental conductance and fuzzy logic method. The relationship between output current *($I_0$),* input power $(P_{in})$ with duty circle *(D)* is depicted in Figure 6.4. Let the efficiency of the proposed microgrid in Figure 6.6 be ($\mathcal{E}$) and the derivative of power to the voltage of the solar system is $\left(\frac{dP}{dV}\right)$ which is used as tracking consideration. The power input is $(P_{in})$, voltage input is $(V_{in})$, $(I_0)$ and $(V_L)$ are the load current and load voltage while *(D)* is the duty cycle. PPP will be at the highest point in the equation 6.21. When the proposed circuit efficiency is considered, the power from the solar panel can be obtained in equation 6.22 while the input voltage can be obtained in equation 6.22. By substituting equation 6.22 into equation 6.21 to obtain equation 6.25. Therefore, at PPP in equation 6.26, when PPP is obtained in equation 6.20, then the equation 6.21 is valid. By considering equation 6.27, when $\left(\frac{dI_0}{dD}\right)$ is tracked, the solar system PPP can also be tracked. When the loads connected to the network are resistive in nature, input power can be obtained in equation 6.29. At PPP, equation 6.32 will be zero, which will also produce equation 6.33 at $\mathrm{D} = \mathrm{D}_{\mathrm{PPP}}$. For the resistive load connected to the system, tracking of zero slope at PPP is also valid.

$$\left(\frac{\mathrm{dP_{in}}}{\mathrm{dV_{in}}}\right) = \sin 0^0 = 0 \tag{6.21}$$

$$P_{in} = I_0 \frac{V_L}{\mathcal{E}} \tag{6.22}$$

$$V_{in} = \frac{V_L}{D} \tag{6.23}$$

$$\frac{dP_{in}}{dV_{in}} = \frac{V_L}{\mathcal{E}} \frac{dI_0}{dV_{in}} \tag{6.24}$$

$$= \frac{V_L}{\mathcal{E}} \frac{dI_0}{dD} . \frac{dD}{dV_{in}} = \frac{V_L}{\mathcal{E}} \frac{dI_0}{dD} . \left(\frac{-V_L}{V_{in}^2}\right) \quad (6.25)$$

$$= \frac{V_L^2}{V_{in}^2 . \mathcal{E}} . \frac{dI_0}{dD} \quad (6.26)$$

$$V = V_{PPP} \quad (6.27)$$

$$\frac{dI_0}{dV_{in}} = 0 \; at \; D = D_{PPP} = \frac{V_L}{V_{PPP}} \quad (6.28)$$

$$P_{in} = I_0^2 . \frac{R}{\mathcal{E}} \quad (6.29)$$

$$\frac{dP_{in}}{dV_{in}} = 2I_0 \frac{R}{\mathcal{E}} . \frac{dI_0}{dV_{in}} \quad (6.30)$$

$$= -\frac{2I_0 . R}{\mathcal{E} . V_{in}^2} \frac{dI_0}{dD} \quad (6.31)$$

$$\frac{dI_{out}}{dV_{in}} = 0 \quad (6.32)$$

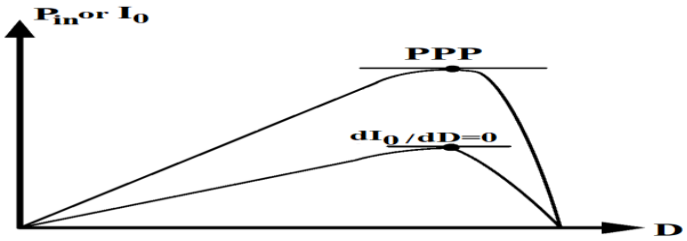


**Figure 6.4:** Input power and output current.

PPP is highest when $\left(\frac{dP_{in}}{dV_{in}}\right) = sin\, 0^0 = 0$ (6.33)

### 6.4.3 Power Management Approach

Microgrid management with battery storage and solar system integration involves a sound control strategy to enhance best power quality operation in agreement with IEEE-519, especially when no linear loads are connected to the network [186], [232]. In a microgrid system, when the system is in stand-alone mode when the consumption charges require more energy than the energy produced by the solar system, the storage of the microgrid would be in its discharge mode. Equation 6.34 can be used to access the

energy flow into the system. If the combination of the microgrid storage and the solar system cannot meet up with the power demanded, the shortfall in power may be compensated by the small generating set connected to the system. The generating set connection to the microgrid can be obtained from equation 6.35. By charging the battery storage to the highest level, the solar power generated would be dumped and the dummy load power consumed can be obtained in equation 6.36 while the flow chart of the microgrid system is presented in Figure 6.5.

$$P_{load}(t) \times \Delta t = P(t) \times \Delta t + \left(PV_{power}(t) \times \Delta t + D_{energy}(t)\right) \times \mathcal{E}_{converter} \quad (6.34)$$

$$P_{generating\ set} \times \Delta t = P(t) \times \Delta t + \left(PV_{power}(t) \times \Delta t - C_{energy}(t) \times \mathcal{E}_{converter}\right) \quad (6.35)$$

$$P_{dummy\ load}(t) \times \Delta t = \left(P(t) - P_{load}(t)\right) \times \Delta t +$$

$$\left(PV_{power}(t) \times \Delta t - C_{energy}(t)\right) \times \mathcal{E}_{converter} \quad (6.36)$$

Where:

$P_{load}(t)$ = Load power of time (t).

$\Delta t$ = Change in time (t).

P(t) = Actual power generated.

$PV_{power}(t)$ = Power generated by the PV.

$D_{energy}$ = Discharging energy.

$\mathcal{E}_{converter}$ = Converter efficiency.

$P_{generating\ set}$ = Power of the generator.

$P_{dummy\ load}(t)$ = Power of the dummy load.

$\mathcal{E}_{discharging}$ = Discharging efficiency of the battery storage.

$C_{energy}$ = Charging energy.

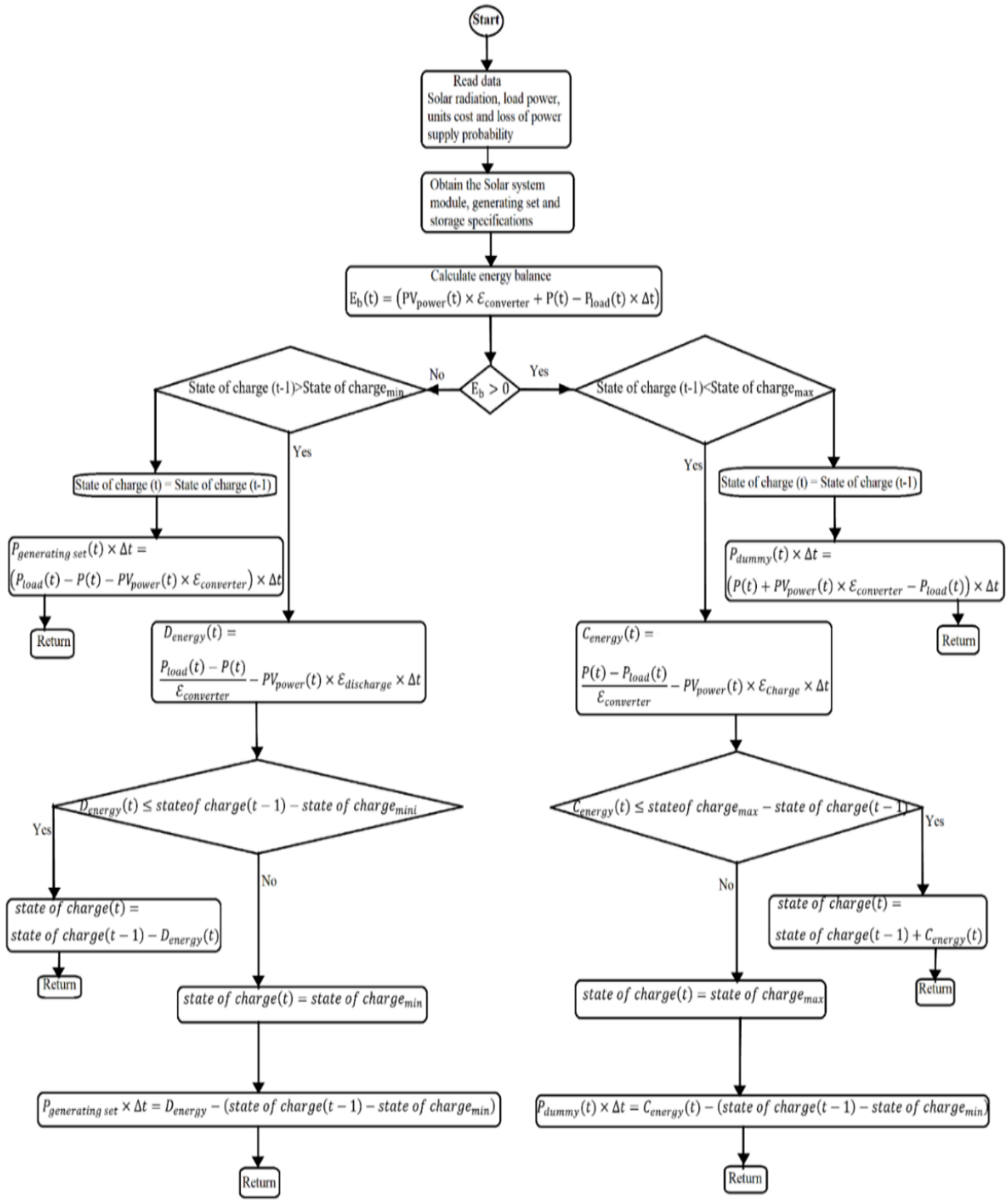


**Figure 6.5:** Microgrid Flow Chart Energy Management.

## 6.5 Grid Code Management

Grid code is the technical requirements for RDG integrated to DN to ensure monitoring and control of power quality challenge at PCC. Since the power flows are bidirectional

with integration of RDG, the code specifies the RDG parameters connecting to national grid that must meet. It usually differs significantly from country to country because of the unique nature of each country's power generation characteristics and network. It usually concerns voltage levels, normal/critical frequency variation with intervals and requirements to generating units and sometimes, the national regulatory frameworks are subject to continuous changes and revisions. The Southern Africa grid code requirement for RDG connection at PCC is in the range of -15% to +10% around the nominal voltage [187]. IEEE-1547-2013 gives compulsory obligations for the interconnection of RDG with electric power systems, i.e., that RDG should be disconnected with higher/lower variation of voltage at PCC while IEEE-2018 provides an option of voltage regulation capacity at PCC ± 5 % [186].

## 6.6 Proposed Microgrid System for Durban University of Technology Steve Biko Campus

Durban University Technology (DUT) comprises approximately 33 000 students located in the beautiful cities of Durban and Pietermaritzburg (PMB) of KwaZulu-Natal (KZN). The DUT is divided into 7 campuses spread across Durban. The 7 campuses are ML Sultan, Steve Biko, Brickfield, Ritson, City campus, Riverside, and Indumiso Campus. This proposed microgrid system is limited to the Steve Biko campus and it is the part of research and development (R&D) project for the institution. The Steve Biko campus shall be grouped into 7 blocks where they act as consumers or loads. Block A will comprise A1, A2,….,A6, block B shall be S2, S3,…….,S11, block C shall be Alan Pittendrigh Library and lecture venue, block D is D1,..,D4, block E is residence (D5, E, J, K, L, N, O, and Q), Block F is (F1, G1, G2, H, M, P) and block G shall be a health clinic. The alphabets A, B, …., G mentioned here are assumed to be loads. The proposed project consists of solar systems integrated together with the aid of a converter such as a Voltage Source Converter (VSC) in a distribution network as depicted in Figure 6.6. The solar is counted as non-controllable element while the battery storage system shall be regulated with respect to the algorithm optimization across the remote-control switch and power electronic converter. The proposed microgrid will integrate solar (PVAs) and a smart meter is connected to the loads. Real time monitoring of electrical signal remotely shall be part of the control strategy with a telecommunication facility. Forecasting will be carried

out by weather stations for proper control and monitoring. The purpose of the project is to provide an uninterrupted power supply to the Steve Biko campus, creating: an improvement in the power quality supply to the campus, power factor improvement, reactive power control and voltage rise regulation at PCC.

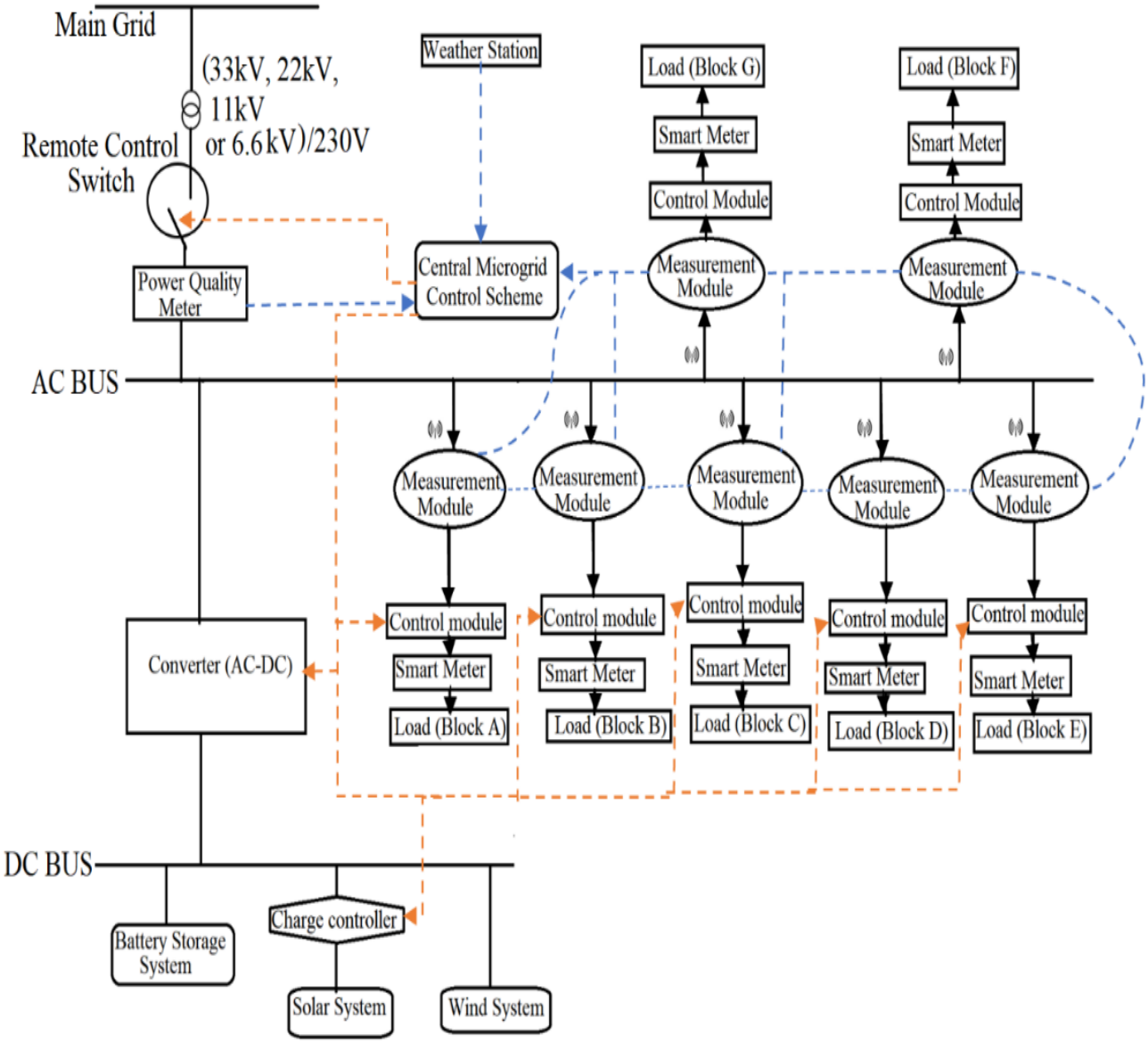


**Figure 6.6: Proposed Microgrid System for DUT.**

### 6.6.1 Description of the Proposed System

The circuit in Figure 6.7 depicts the proposed schematic microgrid for the DUT. The power conversion of the circuit is divided into two stages conversion such that the first stage is

Direct Current to Direct Current (DC-to-DC), while the other stage is Direct Current to Alternating Current (DC-to-AC). The orange arrows represent the microgrid controller signals, as well as the signal from the substation to the microgrid and vice versa in case there is no power supply from the substation, while the green arrows represent the power quality measurement signal that compares microgrid measured parameters to that of the substation for improvement and reading. The small antenna shape represents wireless signal communication between the measuring devices. In the DC–DC stage of the system, a boost converter is employed to boost the PVA's voltage output, while the incremental conductance plus integral regulator controller extracts the highest power from the solar array. In DC-to-DC stage of the system, a boost converter is employed to boost the PVAs voltage output, while the incremental conductance plus integral regulator controller extracts the highest power from the solar array. Hence, the general power and voltage are strengthened and regulated at the PCC as specified by IEEE-1547 and by the Southern Africa grid code requirement. This ensures continuous operation PVAs which is the second stage of the conversion (DC-to-AC). The harmonics produced by the Pulse Width Modulation (PWM) of the (VSC) are attenuated by the inductor $(L_f)$. The installed in-loop filtering circuit eliminates high frequency distortions at the PCC before power flows to the grid. The solar system is connected to the Direct Current (DC) bus through the power electronic converter. The equivalent circuit of the proposed microgrid is depicted in Appendix B, Figure 3, where:

$V_{pv}$ = Solar system output voltage.

$V_{c1}$ = Capacitor voltage.

$I_{l1}$ = Inductor current.

$C_1$ = The capacitor.

$d_1$ = Converter duty cycle.

$V_{bat}$ = Battery Voltage.

$I_{l2}$ = Inductor current of the battery.

$V_{c2}$ = Capacitor voltage of the battery.

$d_2$ = Converter duty cycle of the battery.

The mathematical representation of the solar system and the battery storage system are given by equations 6.37 to 6.40, while equation 6.41 through equation 6.42 express the integration of solar and storage system using a power electronic converter device. The equation parameters are defined thus:

$I_d$ = Direct axis current such as active power injected into the system.

$I_q$ = Quadrature current such reactive power injected into the system with respect to the reference $(\mathrm{dq})$.

$V_{dc}$ = Direct Current coupling voltage.

$m_d$ and $m_q$ = Converter modulation indices.

$\omega$ = Fundamental frequency.

$V_d$ and $V_q$ = Synchronous AC voltage.

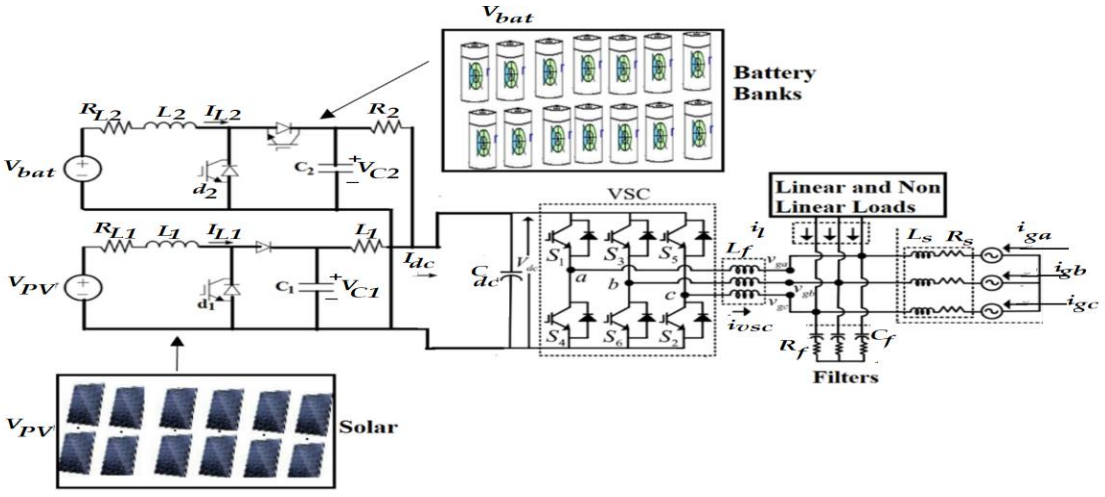


**Figure 6.7:** Proposed Equivalent Circuit for DUT Microgrid.

$$\frac{dI_{L1}}{dt} = \frac{V_{pv}}{L_1} - \frac{R_{L1}}{L_1} I_{L1} - \frac{V_{c1}}{L_1}(1 - d_1) \quad (6.37)$$

$$\frac{dV_{C1}}{dt} = \frac{V_{dc}}{R_1 C_1} - \frac{V_{C1}}{R_1 C_1} I_{L1} - \frac{I_{L1}}{C_1}(1 - d_1) \quad (6.38)$$

$$\frac{dI_{L2}}{dt} = \frac{V_{bat}}{L_2} - \frac{R_{L2}}{L_2} I_{L2} - \frac{V_{c2}}{L_2}(1 - d_2) \quad (6.39)$$

$$\frac{dV_{C2}}{dt} = \frac{V_{dc}}{R_2 C_2} - \frac{V_{C2}}{R_2 C_2} I_{L2} - \frac{I_{L2}}{C_2}(1 - d_2) \quad (6.40)$$

$$\frac{dI_d}{dt} - \frac{R_L}{L_L} I_d + \omega I_q + \frac{V_{C17}}{2L_L} m_d - \frac{V_d}{L_L} \quad (6.41)$$

$$\frac{dI_q}{dt} = -\frac{R_L}{L_L} I_q - \omega I_d + \frac{V_{C17}}{2L_L} m_q - \frac{V_q}{L_L}$$

$$\frac{dV_{dc}}{dt} = \frac{2}{C_{dc}}\left[\frac{1}{R_1}(V_{c1} - V_{dc}) + \frac{1}{R_2}(V_{c2} - V_{dc}) - \frac{3(V_d I_d + V_q I_q}{2V_{dc}}\right] \quad (6.42)$$

Therefore, $(I_{L1})$, $(V_{c1})$, $(I_{L2})$, $(V_{c2})$, $(I_d)$, $(I_q)$, and $(V_{dc})$ are the state variables of the system, where $(d_1)$, $(d_2)$, $(m_q)$ and $(m_d)$ are the control input while $(V_q)$, $(V_d)$, $(V_{bat})$, $(V_{pv})$ are the disturbances. In microgrid hierarchical control, the secondary control scheme provides the highest limit power reference $(I_{L1}^*)$ for the solar system to perform. The highest power point is obtained by the maximum power point tracking (DC-to-DC converter) which is the point where the solar array and the battery storage or grid are optimized, while the amount of power absorbed or injected to the network from the battery is controlled by current reference $(I_{L2}^*)$. It can work in different modes such as reactive power supply mode, shaving mode or voltage regulation mode. The references $(I_d^*)$ and $(I_{L2}^*)$ generated from secondary control side feed the consumer loads properly and control the active and the reactive power of the system. The direct current coupling voltage $(\mathrm{V_{dc}})$ control the voltage at DC coupling to keep the microgrid power in equilibrium. When the control variable is defined by (y), the (x) as states and $(x^e)$ as the equilibrium point. Thus, the system error can be obtained from the equations 6.43 to 6.47, where (d) is the disturbance of the system. The equation 6.48 shows the similarity of the solar system and the battery control with a control output and input. A control strategy can be therefore derived which can stabilize the dynamic of the proposed microgrid subsystem. To linearize the dynamic $(I_{L1})$ in equation 6.36 above, the control input $(d_1)$ can be obtained

in equation 6.49. The Proportional integral controller (PI) and $(v_1)$ can be expressed properly in equations 6.50 and 6.51. Zero steady state and convergence of the system can be guaranteed to meet the required performance if the integral and proportionate $(K_{i1})\ and\ (K_{pi})$ are obtained. As $(d_1)$ is calculated in equation 6.49, $(d_2)$ can also be obtained for the battery system in equation 6.52 while PI is added in equations 6.53 and 6.54. To enhance the solar system performance, $(K_{i2})$ is the integral gain while $(K_{p2})$ is the proportional gain.

The integration of the solar system and the battery bank into the network are achieved by a converter. The converter's active and reactive power can be controlled by the direct current $(I_d)$ and the quadrature current $(I_q)$. To linearize the converter dynamic behaviours, the modulation indices of the direct and quadrature axis $(m_d)$ and $(m_q)$ can be obtained in equations 6.55 and 6.56 respectively. The (PI) inserts $(v_{d,q})$ into the system thus, by similarity to equations 6.53 and 6.54, 6.55 and 6.56 can be obtained where $(K_{id,q})$ is the integra gain and $(K_{Pd,q})$ is the proportionate gain. To determine the dynamic mathematical derivation of the DC coupling voltage in equation 6.57, considering the hierarchical control strategy from the proposed model, secondary control injects reference current $(I_{L2}^*)$ to the battery storage system, therefore, all available power can be injected into the DC coupling by the converter. To obtain the reasonable quantity of power into the system, the reference current $(I_d^*)$ must be known such that direct current coupling voltage transforms to its reference $(V_{DC}^*)$. The perturbation analysis can be obtained by adding an external control loop that is connected in series to the $(V_{dc})$ voltage and making the current dynamic $(I_{d,q})$ much faster than the voltage dynamics. Therefore, $(I_d)$ can be made to attain an equilibrium position $(I_d^*)$ in the direct current bus voltage dynamic evaluation due to the separation of the time scale. To secure the difference in the time scale of voltage and current, the controller gains should therefore be allotted. From the equation 6.59, $(I_d)$ can be obtained for linearization of $(\mathrm{V_{DC}})$ in equation 6.60 and by applying a controller *(PI)* to $(v_{dc})$ in equations 6.61 and 6.62, a direct current link can be balanced through the reference current. Thereby $(V_{DC})$ is controlled with respect to $(V_{DC}^*)$. The active and the reactive power can be autonomously controlled while reference current $\left(I_q^*\right)$ controls current $(\mathrm{I_q})$ to inject a quantity of reactive power into the network. Thus, the reference $\left(I_q^*\right)$ is obtained in 6.63 and the $(Q^*)$ is the network reactive

power. When a control strategy is planned and provided, there is a need to make the rest of the dynamic of the network stable. With the uncontrolled variable $(V_{C1})$ and $(V_{C2})$, the equilibrium point of the dynamic can be derived in equations 6.64 and 6.65. By linearizing the variable $(V_{C1})$ and $(V_{C2})$ toward the equilibrium position, the variable stability can be further established by the Jacobian sign in the equations 6.66 and 6.67. The assumption in equation 6.66 is that if current $(I_{L1})$ is positive the Jacobian $(J_1)$ is negative, for the reason that the voltage losses in the inductor $(R_{L1}I_{L1})$ are less than the solar system voltage. This is the physical limitation of the system. Similarly, by assumption in equation 6.67, if $(I_{L2})$ is positive, the negative values vary depending on the battery charge and discharge value. Therefore, a derivation can be found for $(V_{C2})$ stability zone in equation 6.68 due to the negativity of the Jacobian $(J_2)$. Conclusively, the non-controlled dynamics have a stable point of balance within the limitations mentioned.

$$\tilde{x} = x - x^e \tag{6.43}$$

$$x = [V_{c1}, V_{c2}, V_{c3}]^T \tag{6.44}$$

$$x^e = [I_{L1}^*, V_{C1}^e, I_{L2}^*, V_{c2}^e, I_d^*, I_q^*, V_{dc}^*]^T \tag{6.45}$$

$$y = [I_{L1}, I_{L2}, I_d, I_q]^T \tag{6.46}$$

$$d = [V_{PV}, V_{bat}, V_d, V_d]^T \tag{6.47}$$

$$\begin{cases} \dot{x} = f(x,d) = g(x)u \\ y = I_{L1,2} \end{cases} \tag{6.48}$$

$$d_1 = \frac{1}{V_{c1}}\left(L_1 v_1 - P_{pv} + R_{L1}I_{L1} + V_{C1}\right) \tag{6.49}$$

$$v_1 = K_{P1}(I_{L1} - I_{L1}^*) - \alpha_1 \tag{6.50}$$

$$\dot{\alpha}_1 = K_{i1}(I_{L1} - I_{L1}^*) \tag{6.51}$$

$$d_2 = \frac{1}{V_{c2}}(L_2 v_2 - V_{bat} + R_{L2}I_{L2} + C_{V2}) \tag{6.52}$$

$$v_2 = -K_{p2}(I_{L1} - I_{L2}^*) - \alpha_2 \tag{6.53}$$

$$\dot{\alpha}_2 = K_{i2}(I_{L2} - I_{L2}^*) \tag{6.54}$$

$$m_d = \frac{2}{V_{DC}}\left(L_l v_d + R_l I_d - \omega L_1 I_q + V_d\right) \tag{6.55}$$

$$m_q = \frac{2}{V_{DC}}\left(L_l v_q + R_l I_q - \omega L_1 I_d + V_q\right) \tag{6.56}$$

$$v_{d,q} = -K_{Pd,q}\left(I_{d,q} - I_{d,q}^*\right) - \alpha_{d,q} \tag{6.57}$$

$$\dot{\alpha}_{d,q} = -K_{id,q}\left(I_{d,q} - I_{d,q}^*\right) \tag{6.58}$$

$$\dot{V}_{DC} = \left\{\frac{1}{R_1}(V_{C1} - V_{DC}) + \frac{1}{R_2}(V_{C2} - V_{DC}) - \frac{3(V_d I_d^* - V_q I_q^*)}{2V_{DC}}\right\} \tag{6.59}$$

$$I_d^* = \frac{2V_{DC}}{3V_d}\left\{-\frac{C_{dc}}{2}v_{dc} + \frac{1}{R_1}(V_{C1} - V_{DC}) + \frac{1}{R_2}(V_{C2} - V_{DC}) + \frac{V_q I_q^*}{2V_{DC}}\right\} \tag{6.60}$$

$$v_{dc} = -K_{Pdc}(V_{DC} - V_{DC}^*) - \alpha_{dc} \tag{6.61}$$

$$\dot{\alpha}_{dc} = -K_{idc}(V_{DC} - V_{DC}^*) \tag{6.62}$$

$$I_q^* = \frac{2Q^*}{3} \tag{6.63}$$

$$V_{C1}^e = \frac{V_{DC}}{2} \pm \sqrt{V_{DC}^2 + 4R_1 I_{L1}(-V_{PV} + R_{L1} I_{L1})} \tag{6.64}$$

$$V_{C2}^e = \frac{V_{DC}}{2} \pm \sqrt{V_{DC}^2 + 4R_2 I_{L2}(-V_{bat} + R_{L2} I_{L2})} \tag{6.65}$$

$$J_1 = -\frac{1}{R_1 C_1} - \frac{1}{C_1}\frac{I_{L1}^*}{V_{C1}^{e2}}\left(V_{V_{PV}} - R_{L1} I_{L1}\right) \tag{6.66}$$

$$J_2 = -\frac{1}{R_2 C_2} - \frac{1}{C_2}\frac{I_{L1}^*}{V_{C2}^{e2}}(V_{bat} - R_{L2} I_{L2}) \tag{6.67}$$

$$\frac{V_{bal}}{2R_{L2}} - \frac{1}{R_{L2}}\sqrt{\left(V_{bal}^2 + 4\frac{R_{L2}}{R_2}\right)} < I_{L2} < \frac{V_{bal}}{2R_{L2}} + \frac{1}{R_{L2}}\sqrt{\left(V_{bal}^2 + 4\frac{R_{L2}}{R_2}\right)} \tag{6.68}$$

### 6.6.2 Control Strategy of the Circuit

Consider the pulse generator control circuit in Figure 6.8, where when strategically controlling the pulse (S) of the PWM-VSC output using the *(IC+PI)* strategy, energy is

extracted from the solar system through the first stage of the power conversion phases. The solar reference voltage ($V_pV_{ref}$) and pulse *(S)* are estimated by the *(IC+PI)* algorithm. The generated solar voltage ($V_{pv}$) is compared with the solar reference voltage ($V_pV_{ref}$) to produce solar reference current ($I_pV_{ref}$) through the outer loop integral regulator (PI). The generated solar current ($I_{pv}$) and the solar reference current ($I_pV_{ref}$) are compared to produce the duty ratio (D) through the inner loop integral regulator (PI). Therefore, the duty ratio (D) produces a high frequency pulse *(S)* through the (PWM) for DC-to-DC conversion stage. The second power conversion stage, which is the (PWM-VSC) stage, maintains the active and reactive, and transferred the extracted power output from the solar system at the PCC. The (PWM-VSC) operates in unity power factor and voltage regulation mode, which also controls the voltage rise at the PCC to the minimum. When solar system output power generation is at the maximum and the load demanded is low, (PWM-VSC) will be in voltage regulation mode where it will generate reactive power to the grid to control the voltage rise at PCC and minimize the voltage to an acceptable level.

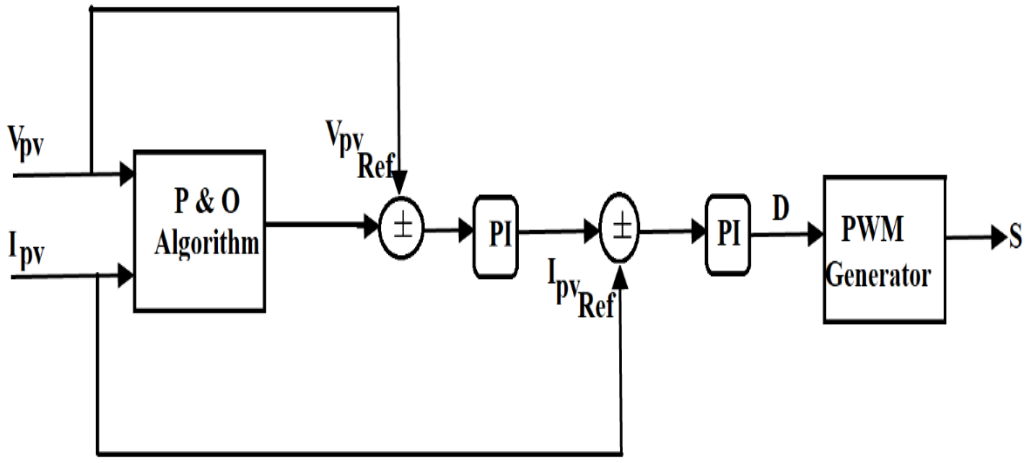


**Figure 6.8: Pulse generator.**

Figure 6.9 depicts the gating pulse generated from $(S_1, S_2, S_3, \dots, S_6)$ to control PWM-VSC where the device current is controlled. $(I^*_{Gr})$ can be approximated by detecting $(I_{LA}, I_{LB})$, $(V_{pccAB}, V_{pccBC})$, and $(V_{dc})$ while $(V_{pccA}, V_{pccB}, V_{pccC})$ can be approximated from the point of common coupling line voltage, where:

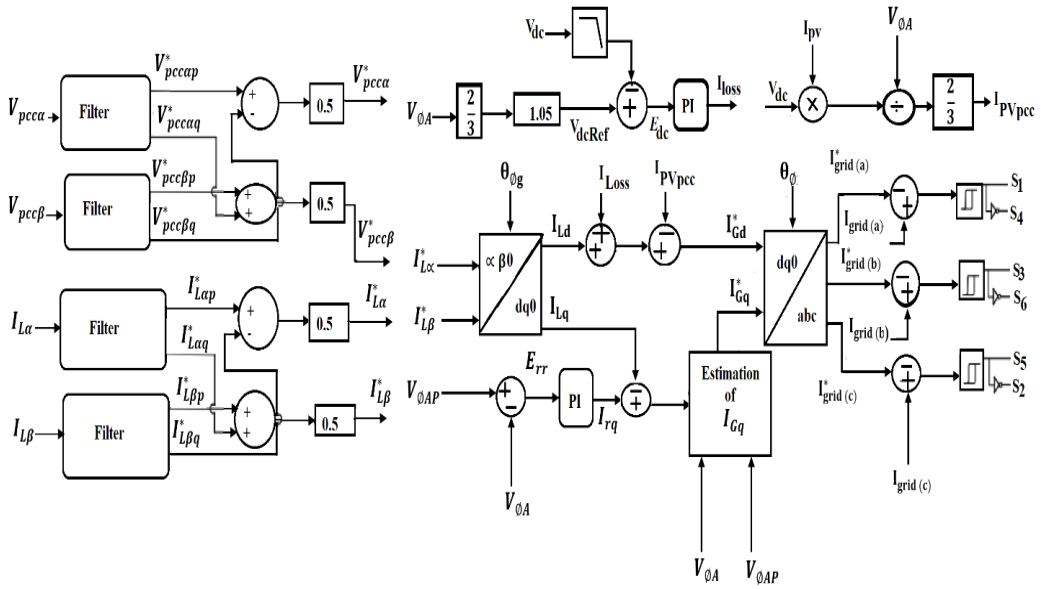


**Figure 6.9:** Generated Pulse for VSC.

$(I_{Gr}^{*})$ = Grid Reference Current.

$(I_{LA}, I_{LB})$ = Load Current.

$(V_{pccAB}, V_{pccBC})$ = PCC Line Voltage.

$(V_{dc})$ = DC Link Voltage.

$(V_{pccA}, V_{pccB}, V_{pccC})$ = PCC Phase Voltage.

The filtering circuits in Figure 6.10 filter the unwanted disturbance/distortion or unbalance signals from the load current and phase voltage at the point of common coupling where their components are approximated before the reference grid current. The filtering stages of the control is of an in-loop type which has a super harmonic rejection capability. The current that flows across the loads and the phase voltage at the point of common coupling are transformed to stationary reference frame control known as αβ-control. It regulates control signals in stationary two-phase frame $(I_{L\alpha})$, $(I_{L\beta})$ and $(V_{pcc\alpha})$, $(V_{pcc\beta})$. Any unwanted signals generated from the point of common coupling are suppressed by the filtering circuit while the approximated quadrature components and undistorted in-phase signal are$(I_{L\alpha p}^{*})$, $(I_{L\beta p}^{*})$, $(V_{pcc\alpha p}^{*})$ and $(V_{pcc\beta p}^{*})$ of $(I_{L\alpha})$, $(I_{L\beta})$ and $(V_{pcc\alpha}^{*})$, $(V_{pcc\beta}^{*})$. In the

same way, $(I^*_{L\alpha q})$, $(I^*_{L\beta q})$ and $(V^*_{pcc\alpha q})$, $(V^*_{pcc\beta q})$ are undistorted quadrature of $(I_{L\alpha})$, $(I_{L\beta})$ and $(V_{pcc\alpha})$, $(V_{pcc\beta})$. The undistorted components generated can be distorted provided that if the detected current that flows across the loads and approximated in-phase/quadrature signals is used to approximate the positive sequence of the fundamental components and the phase voltage at the point of common coupling $(I^*_{L\alpha})$, $(I^*_{L\beta})$ and $(V^*_{pcc\alpha})$, $(V^*_{pcc\beta})$ such that they can be expressed in equations 6.69, 6.70, 6.71 and 6.72. The PWM-VSC has a voltage regulation mode and unified power factor mode of operation. The amplitude of the phase angle at the point of common coupling and the grid phase angle are vital to synchronize and control the device mode of operation as expressed in equations 6.73 and 6.74.

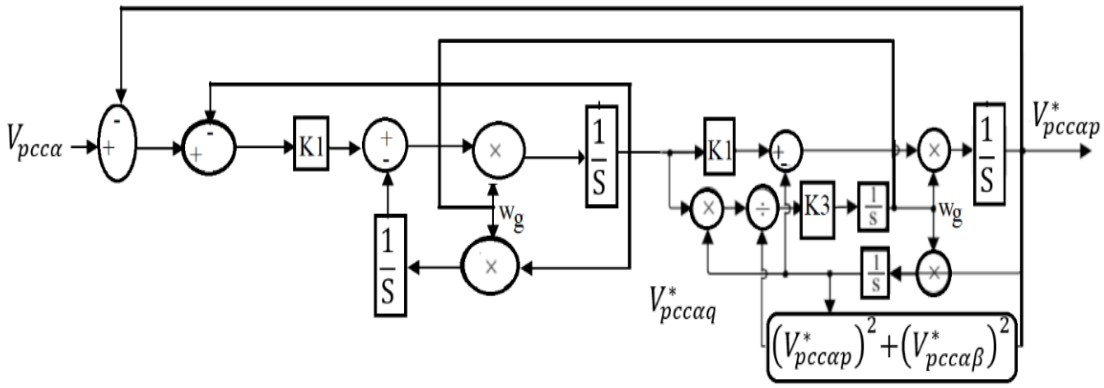


**Figure 6.10:** In-Loop Filtering Algorithm.

$$V^*_{pcc\alpha} = 0.5\left(V^*_{pcc\alpha p} - V^*_{pcc\beta q}\right) \quad (6.69)$$

$$V^*_{pcc\beta} = 0.5\left(V^*_{pcc\alpha q} - V^*_{pcc\beta p}\right) \quad (6.70)$$

$$I^*_{L\alpha} = 0.5\left(I^*_{L\alpha p} - I^*_{Lq}\right) \quad (6.71)$$

$$I^*_{L\beta} = 0.5\left(I^*_{L\alpha p} - I^*_{L\beta q}\right) \quad (6.72)$$

$$V_{\emptyset A} = \sqrt{\left(V^*_{pcc\alpha}\right)^2 + \left(V^*_{pcc\beta}\right)^2} \quad (6.73)$$

$$\theta_{\emptyset g} = tan^{-1}\left(\frac{V^*_{pcc\beta}}{V^*_{pcc\alpha}}\right) \quad (6.74)$$

($I_{Gd}^{*}$) denotes the active power across the grid and is the d-axis component of the grid current. The value of ($I_{Gd}^{*}$) can be negative or positive. The negative value of the component means that the grid is drawing active power while the positive value shows that the load is drawing active power from the grid, which depends on the solar power generation, load demanded and VSC losses in that particular period as expressed in equation 6.75. ($I_{Ld}^{*}$) can be obtained through the transformation of ($I_{L\alpha}^{*}$) and ($I_{L\beta}^{*}$) to dq-axis reference frame. ($V_{dc}$) is the sustained and established reference value of the voltage ($V_{dcRef}$) when ($I_{loss}$) absorbs active power from the grid and its VSC losses. The component is obtained through the processed error between the ($V_{dc}$) and ($V_{dcRef}$) by the approximation of the (PI) controller. To avoid overmodulation in the system, the approximated amplitude voltage at the point of common coupling adjusts the direct current link voltage. The expression for ($V_{dcRef}$), DC link error and the solar power output at the PCC can be obtained in equations 6.76 to 6.79. DC link integral controller's stress minimizes when ($I_{PVpcc}$) is off. It provides the feed forward capability for VSC control and gives an idea of generating power ahead of VSC synchronism. It also provides such capability that when there is a quick change of solar power output, best dynamic performance is enhanced. ($I_{Gq}^{*}$) denotes reactive power across the grid and is the q-axis component of the grid current. The operation depends on the device mode. When the device is in a unified power factor mode and ($I_{Gq}^{*}$) is maintained at zero position, VSC generates reactive power to the load while there is less or no reactive power across the grid. When there is a maximum power output generated from the solar power, and the load demanded is low, the voltage at the PCC will rise above the maximum allowable limit. In such a scenario, the device will switch to its voltage regulation mode whereby the load and the grid absorb reactive power from the VSC. Hence, the power factor of the grid is less than the unity. ($I_{Gq}^{*}$) is defined in equation 6.80. ($I_{Lq}^{*}$) is the approximated current that controls the voltage amplitude at the point of common coupling to avoid a voltage rise. It can also be obtained by error differential between the peak voltage amplitude at the point of common coupling and the phase voltage amplitude through the integral controller. By the transformation of the d-q axis ($I_{Gd}^{*}$), ($I_{Gq}^{*}$) to a-b-c reference frame with inverse park transformation analysis, the approximated ($I_{GRef}^{*}$) can be

obtained. The differential between the detected grid current and approximated grid current will result in the gating pulses $S_1, S_2, S_3 \ldots, S_6$.

$$I_{Gd}^{*} = I_{Ld}^{*} + I_{loss} - I_{PVpcc} \quad (6.75)$$

$$V_{dcRef} = 1.05 \times 2 \times V_{\emptyset A} \quad (6.76)$$

$$I_{loss\,k+1} = I_{loss\,k} + K_{pdc} \times (e_{dc\,k+1} - e_{dc\,k}) + K_{i\,dc} \times e_{dc\,k+1} \quad (6.77)$$

$$e_{dc} = V_{dcRef} - V_{dc} \quad (6.78)$$

$$I_{PVpcc} = \frac{2 \times P_{pv}}{3 \times V_{\emptyset A}} \quad (6.79)$$

$$(I_{Gq}^{*}) = \begin{pmatrix} 0\ if\ V_{\emptyset A} V_{\emptyset Amax} \\ -I_{Lq}^{*} + I_{VRq}\ otherwise \end{pmatrix} \quad (6.80)$$

$$I_{VRq\,k+1} = I_{VRqk} + K_{pVR} \times (e_{VR\,k+1} - e_{VR\,k}) + K_{i\,VR} \times e_{VR\,k+1} \quad (6.81)$$

$$e_{VR} = V_{\emptyset Amax} - V_{\emptyset A} \quad (6.82)$$

$I_{Gd}^{*}$ = d-axis Grid Current.

$I_{Ld}^{*}$ = d-axis Load Current.

$I_{loss}$ = VSC Losses.

$I_{PVpcc}$ = Solar Power Output at PCC.

$I_{VRq}$ = Approximated current component that control PCC voltage.

$I_{Lq}^{*}$ = q-axis Load current.

$V_{\emptyset A}$ = Amplitude of the Phase Voltage.

$e_{VR}$ = Error.

## 6.7 Result and Discussion

A Simulink model of the peak power point tracking (as shown in Appendix A, Figure A3-A8) is designed comprising 1.008 MW at $1000\ W/m^2$ Photo Voltaic Arrays (PVAs). The system consists of 64 parallel strings and each of the strings consist of 5 modules SPR-315E connected in series $(10 \times 64 \times 315 \times 5 = 1.008\ \mathrm{MW})$. The Temperature is measured in degree centigrade and the Irradiance of the sun in $(\mathrm{W/m^2})$. The PV array block has two inputs that allow for the variation of the sun's irradiance and the temperature across the two inputs of the solar array block. Direct Current to Direct Current (DC-to-DC) boost converters of 5-kHz inputs are connected to the PVAs output while the outputs are connected to the DC bus of 3-Ø-3-levels Pulse Width Modulation Voltage Source Converter (PWM-VSC). The desired voltage is produced by the tracking system by varying the duty cycle while Peak power is being accessed from the PVAs terminals by means of (IC + IR), otherwise known as Peak Power Point Tracking (PPPT) strategy. The voltage source converter possesses internal and external control capabilities. The quadrature current components $(I_d)$, $(I_q)$ that represent the active and reactive current are controlled by the internal part of the PWM-VSC, while the external aspect of the PWM-VSC controls the DC link voltage. PWM-VSC is kept at 20% more than the rating of the Solar farm. The boost converter improves the PVAs voltage output from 295 VDC to 500 VDC. The PWM-VSC makes use of converted modulating reference voltage signals $(V_{abc\ Ref})$ from outputs voltage $(V_d)$ and $(V_q)$ of the current controller, usually from 500 VDC to 260 VAC at the Point of Common Coupling (PCC). A filtering circuitry is connected to the network to eliminate any distortion generated by the PWM-VSC. The designed network in MATLAB/Simulink is simulated, the grid voltage and that of current are in phase between 0 to 0.05 s which means that the system undergoes unity power factor mode operation as shown in Figure 6.11 (a) such that the angle between the grid voltage and the current is zero. The unity power factor exists because there is no phase difference (during the period of 0 and 0.05 s) in the grid voltage and the current. Thus, the whole part of the main power supply does the useful work. Hence, there is no voltage fluctuation, no power wasting, no transient voltage problem, and very low loss occurring at unity power factor. The PVA's output power generated is 840 kW between 0.15 s to 0.4 s which is not its full rated power, and the duty cycle is fixed at 0.6 s as shown in Figure 6.11 (b-

c). During this period, the PPPT controller is not yet enabled. It has not started regulating PV voltage by varying the duty cycle in order to extract peak power, the voltage at that point is therefore calculated using equation 6.83 and obtained 200 V. However, the rated power of the PVAs is 1.008 MW at $1000\ W/m^2$. Moreover, at 0.4 s, the peak power point tracking (PPPT) algorithm control is turned on as shown in Figure 6.11 (d). The PVAs voltage output regulation (IC + IR) starts operation by varying the duty cycle in Figure 6.11 (e) to extract the peak power. The peak power tracked by the PPPT is about 1.005 MW at the duty cycle of 0.45, while the rated value is 1.008 MW. By estimation, about 0.003 kW is lost in the boost converter. By calculation using equation 6.84, the simulated result in Figure 6.11 (f) which is 295 V, is slightly higher than the calculated result (273.5 V). It shows that the boost converter efficiency is about 83%. The solar voltage output is about 1005 V between 0 to 0.61 s, it reaches 295 V at 0.55 s and maintains its stability. The boost converter boosts the PVAs's voltage at 0.61 s from 295 V to 500 V and the system reaches its steady state at 0.62 s, while the duty cycle of the boost converter is maintained at 0.41 as shown in Figure 6.11 (g). The 3-ø-3-level PWM-VSC converts the 500 V DC link voltage to 260 V AC as shown in Figure 6.11 (h). The PVAs and the grid (PCC) parameters are 5000-kVA 260V/22kV in a three-phase coupling transformer. Further simulation investigations are carried out to evaluate the network performance during load variation with constant PVAs generation to PCC network impact when undergoing Unity Power Factor (UPF), Voltage Regulation (VR) mode. The network behaves like STATCOM and the grid impact when there is no generation from PVAs at PCC.

$$VPV = (1 - D) \times Vdc \tag{6.83}$$

$$= (1 - 0.6) \times 500 = 200\ V$$

$$\text{PV Module Specification} = \text{Nser} \times \text{Vmp} \tag{6.84}$$

$$= 5 \times 54.7 = 273.5\ \text{V}$$

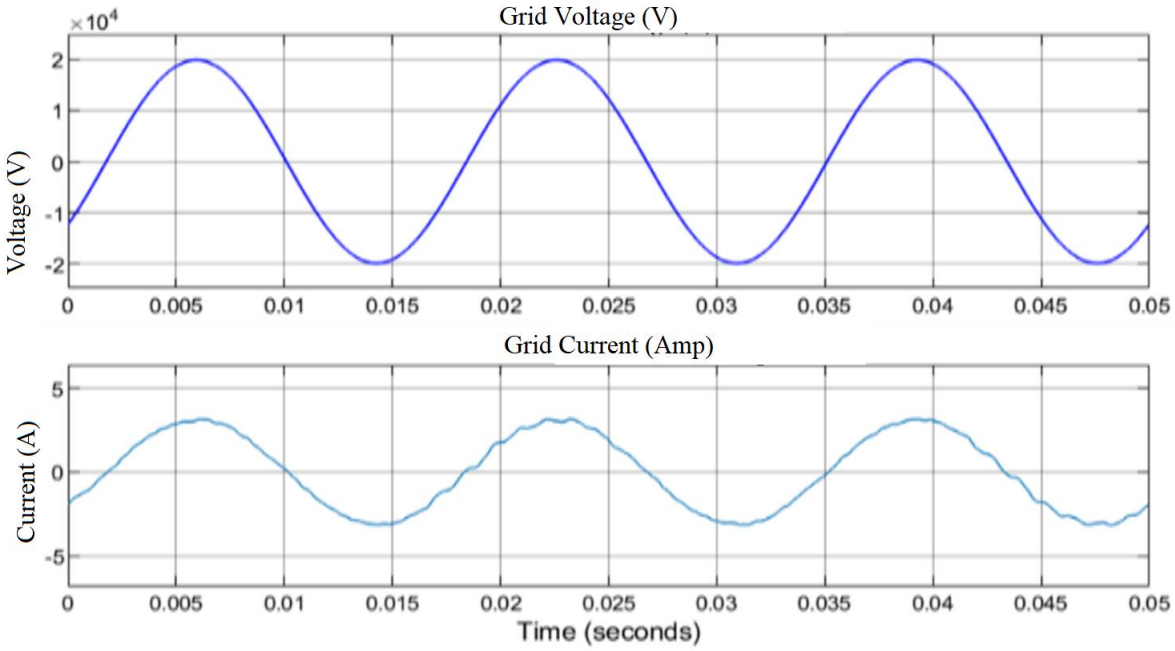
Grid Voltage (V)
×10^4
Voltage (V)
2
1
0
-1
-2
0
0.005
0.01
0.015
0.02
0.025
0.03
0.035
0.04
0.045
0.05
Grid Current (Amp)
Current (A)
5
0
-5
Time (seconds)

(a)

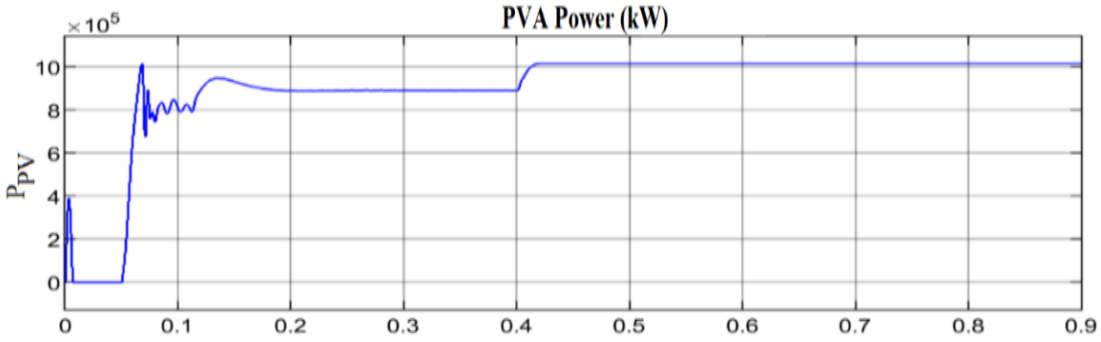
PVA Power (kW)
×10^5
P_PV
10
8
6
4
2
0
0
0.1
0.2
0.3
0.4
0.5
0.6
0.7
0.8
0.9

(b)

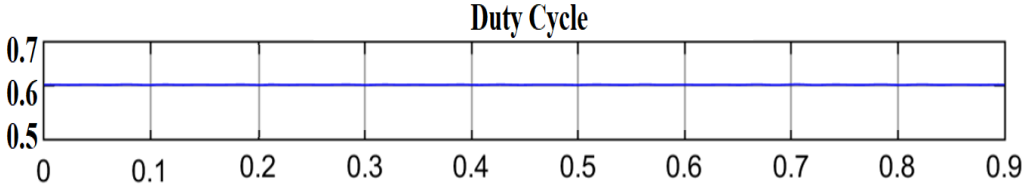
Duty Cycle
0.7
0.6
0.5
0
0.1
0.2
0.3
0.4
0.5
0.6
0.7
0.8
0.9

(c)

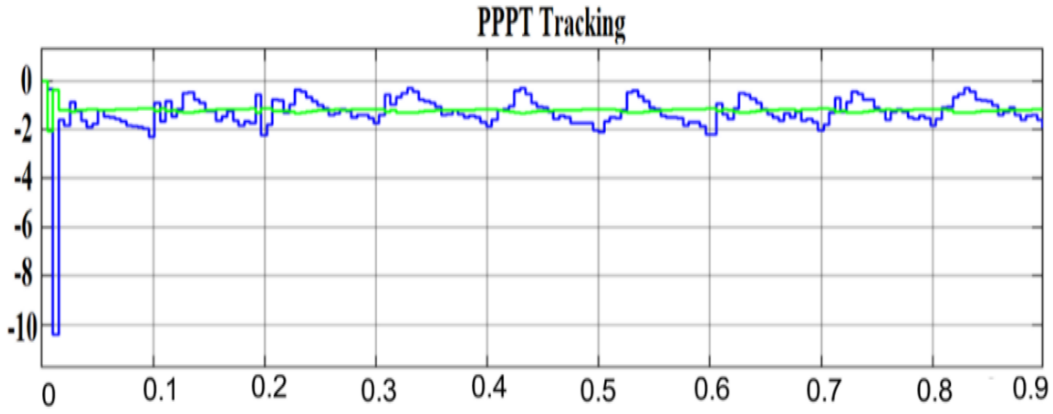
PPPT Tracking
0
-2
-4
-6
-8
-10
0
0.1
0.2
0.3
0.4
0.5
0.6
0.7
0.8
0.9

(d)

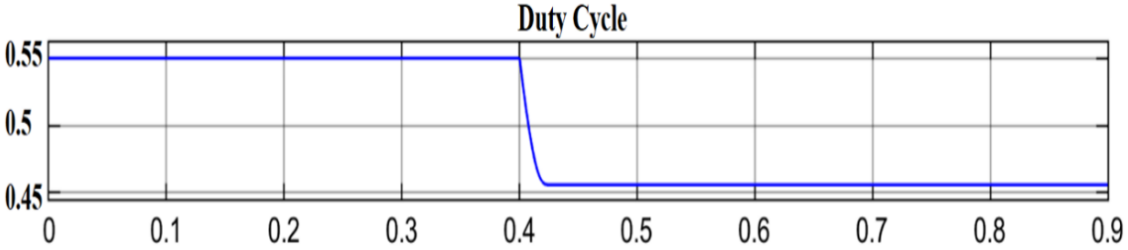
Duty Cycle
0.55
0.5
0.45
0
0.1
0.2
0.3
0.4
0.5
0.6
0.7
0.8
0.9

(e)

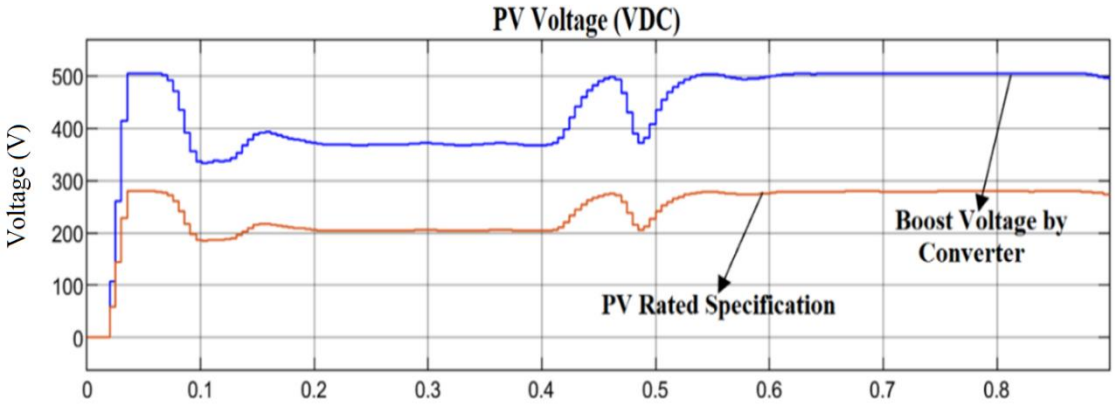
PV Voltage (VDC)
Voltage (V)
500
400
300
200
100
0
0
0.1
0.2
0.3
0.4
0.5
0.6
0.7
0.8
Boost Voltage by Converter
PV Rated Specification

(f)

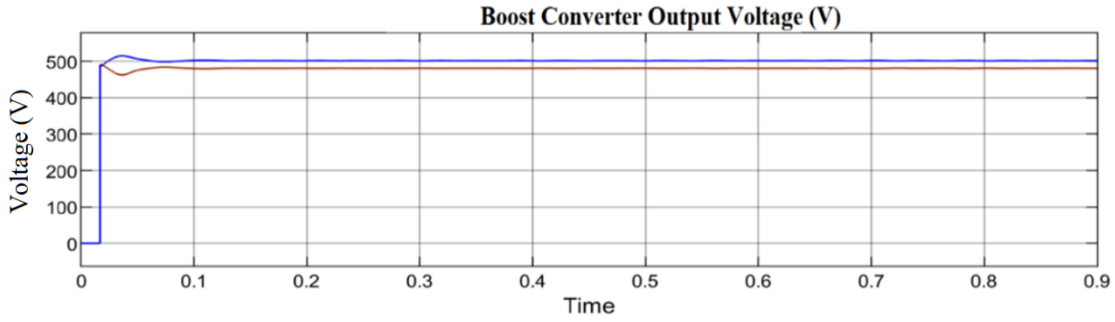


(g)

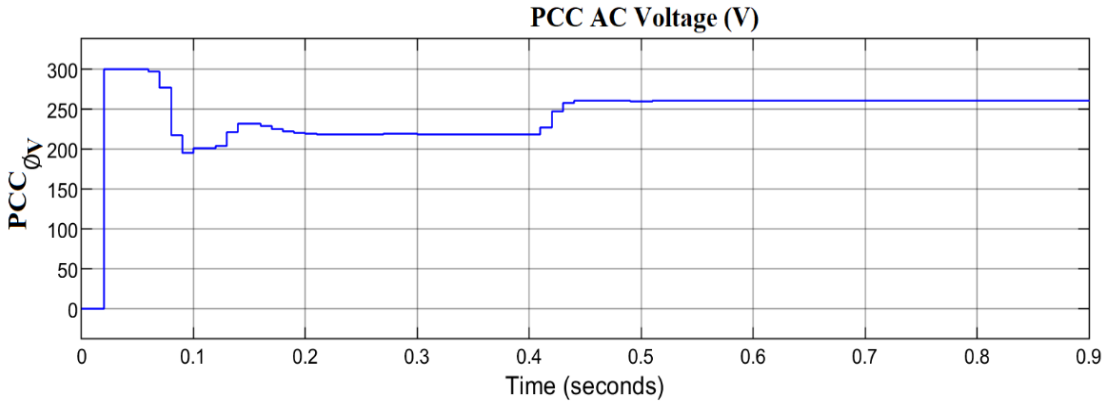


(h)

**Figure 6.11:** (a) UPF Mode Operation, (b) PV Output Power, (c) Boost Converter Duty cycle, (d) PPPT Tracking, the blue is the tracking sequence while the green line is the error regulator (e) Boost Converter Duty Cycle, (f) PV Output Voltage, (g) Boosted Voltage, (h) PWM-VSC Converting 500 V to 260 VAC.

### 6.7.1 Loads variation with constant PVAs generation

This section discusses the investigation carried out to determine the effect of load fluctuation on the rated solar farm performance while the power of the PVAs is kept constant at a rated capacity. The system performance is also evaluated when the network operation is in voltage regulation or unity power factor mode and when undergoing unity power factor operation alone, depending on the amount of voltage rise at the point of common coupling. Figure 6.12 (a) shows when loads demanded are varied by switching off the loads on the phase two at 0.4 s and phase three loads at 0.6 s. The power generated to the AC grid increases $(P_{Grid})$ as shown in Figure 6.12 (b) when there is a

reduction in the loads demanded ($P_{Load}$) across the network, while the PVA's output remains within its rated capacity, whereas the grid current amplitude ($I_{Grid}$) also increases, resulting in a further drop in voltage in the feeder impedance of the AC grid. Similarly, the decrease in the loads demanded also causes the amplitude of the phase voltage ($V_{\emptyset A}$) at the PCC to increase. Figures 6.12 (d-e) show the network simulation outcomes when the network is undergoing UPF operation from the STATCOM, such that the grid's reactive power is zero, i.e., $Q_{Grid} = 0$. The point of common coupling phase voltage amplitude rises above the acceptable range, even with the load demanded from the system, which is not in agreement with the IEEE-1547-2018 and Southern Africa grid code regulation at point of common coupling publication in [135], [187] that established uniform criteria and requirements for interconnection of distributed energy resources (DER) with electric power systems (EPS) and associated interfaces. It is observed that during no-load conditions between 0.6 s and 0.9 s, the point of common coupling phase voltage amplitude ($V_{\emptyset A}$) rises above 330 V as shown in Figure 6.12 (e) and is unacceptable because it is more than 10% of the rated value of the PCC. The South Africa Grid Code Act accepts ± 15% to +10% RDG voltage variation connection at the point of common coupling for large renewable distributed generation above 100 kW, while IEEE-1547 stipulated ±6% variation for PVA connection at the point of common coupling of alternating current/voltage.

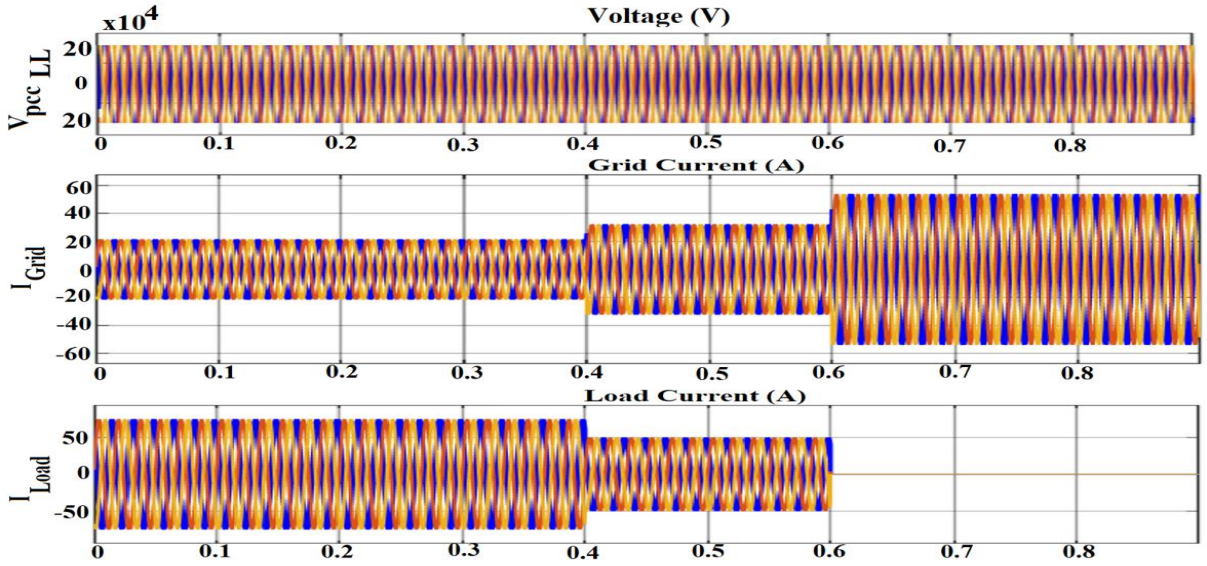


(a)

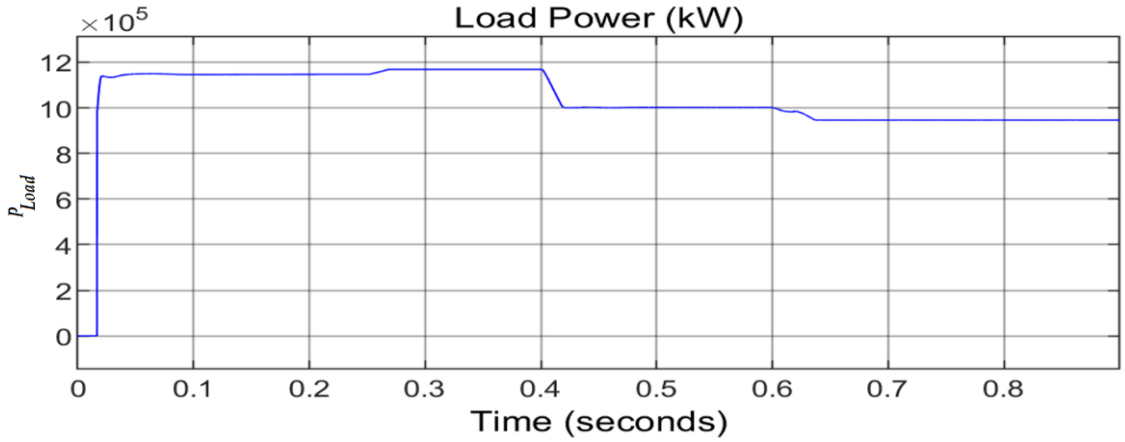
Load Power (kW)
×10^5
P_Load
Time (seconds)

(b)

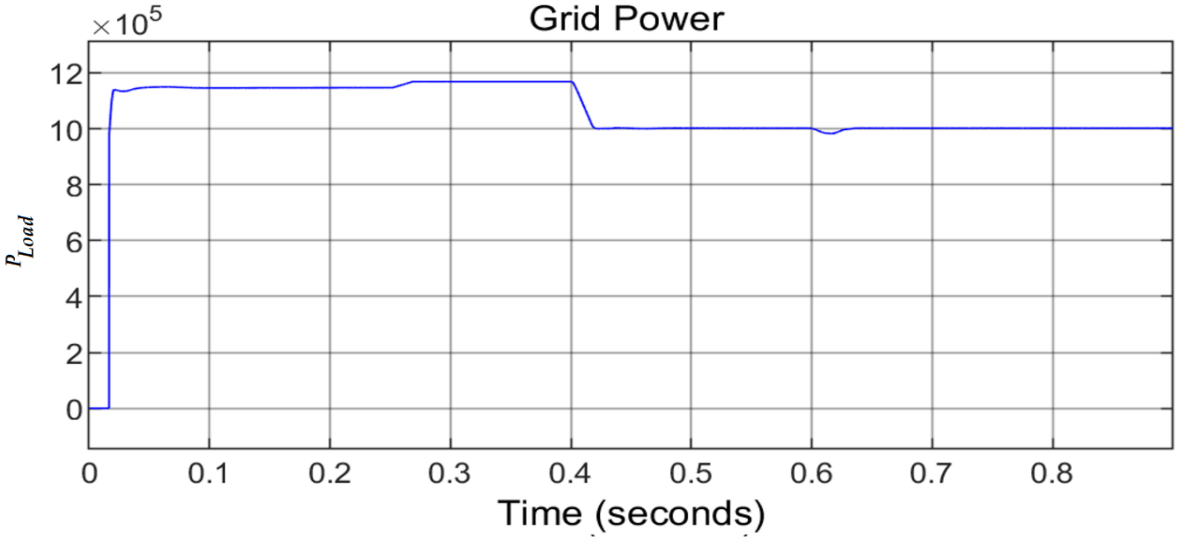
Grid Power
×10^5
P_Load
Time (seconds)

(c)

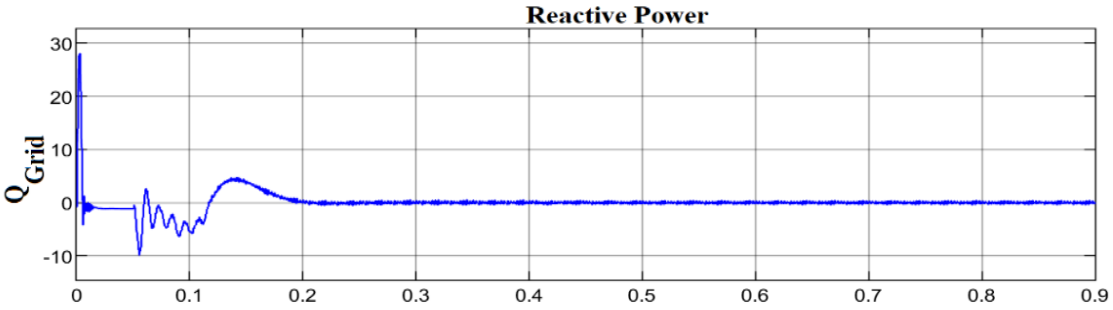
Reactive Power
Q_Grid

(d)

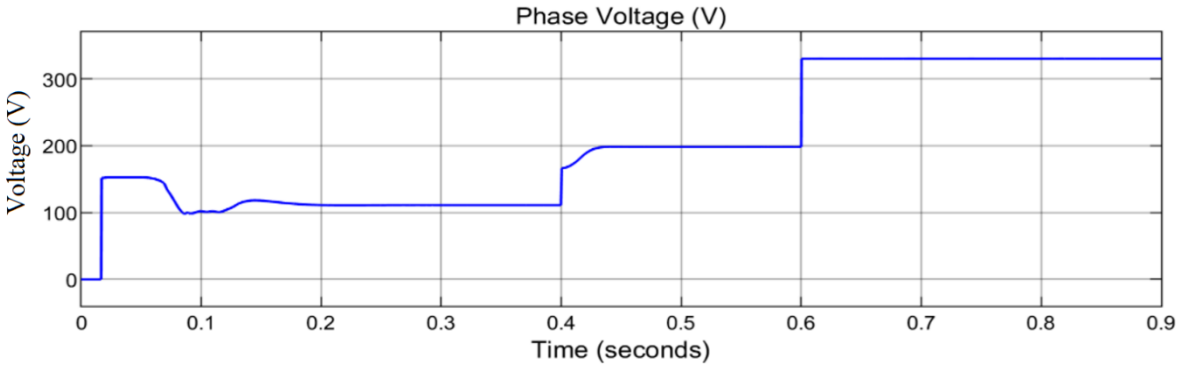


(e)

**Figure 6.12:** Voltage rise with Zero Grid Reactive Power (a) load varies at 0.4 s to 0.6 s, and switched off at 0.6 s to 0.9 s, grid current increases. (b) Reduction in the load power between 04 s to 0.9 s (c) Increase in power to the grid due to reduction in the load between 0.6 s to 0.9 s. (d) Reactive power during unity power factor mode of the STATCOM. (e) Increase in the phase voltage.

### 6.7.2 Proposed method with UPF and VR Mode

The results of the proposed method are depicted in Figure 6.13 (a-j) where the network is operating normally such that the system is in its unity power factor mode at rated loads demand and PVA. However, at 0.4 s, the phase voltage amplitude $(V_{\emptyset A})$ at the PCC rises because of the reduction in the loads demanded within the system. Consequently, the operating mode of the network changes from the unity power factor to a voltage regulation mode to minimize the voltage rise at the PCC to an acceptable range, in relation to IEEE 1547 and Southern Africa grid code requirement. It is observed during the voltage regulation mode that the network's reactive power increases from zero $(Q_{Grid} = 0)$ to 1.15 kVAR. Also at 0.4 s, when the loads demanded reduces to zero, $(Q_{Grid})$ increases from 1.15 kVAR to 5 kVAR. This causes more power to be transported to the AC grid, resulting in a greater drop in the impedance of the feeder and, therefore, more reactive power being generated to the grid to limit the voltage rise at the point of common coupling. The phase voltage amplitude $(V_{\emptyset A})$ is within an acceptable range, in agreement with IEEE 1547 and Southern Africa grid code requirement. It can be observed that phase voltage increases up to 250 V, which is less than the maximum allowable range. However, there is no reflection of power quality challenges noticed due to an unbalanced or non-linear

load in the system, because the network currents are balanced during the operation. The network measured parameters such grid RMS Value of Voltage/Current, grid current $(I_g)$ harmonics, during the experiment are depicted in Table 1, which are withing an acceptable range during grid compensation.

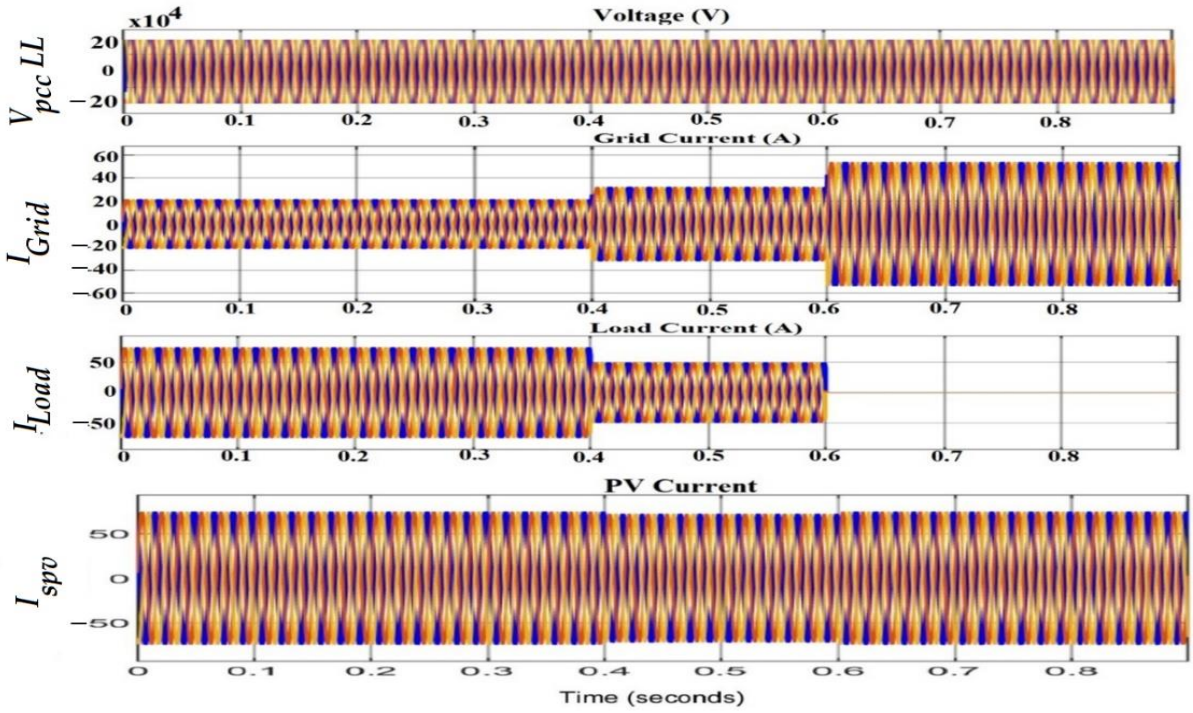


(a)

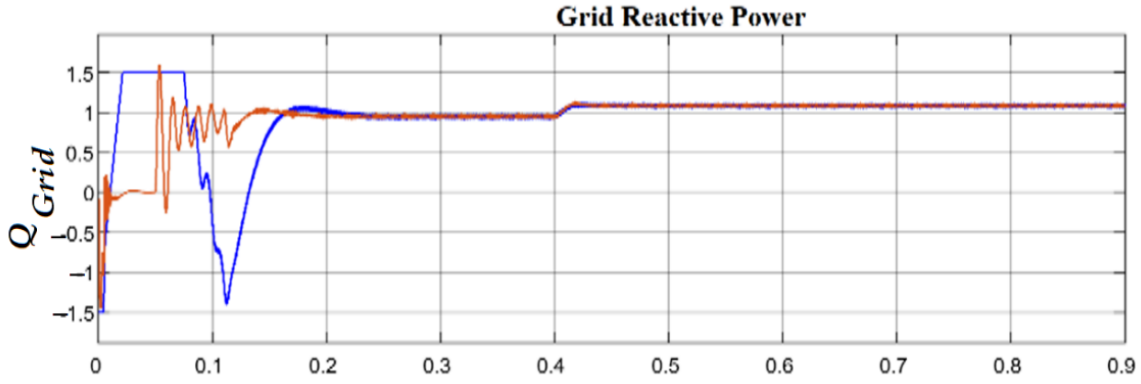


(b)

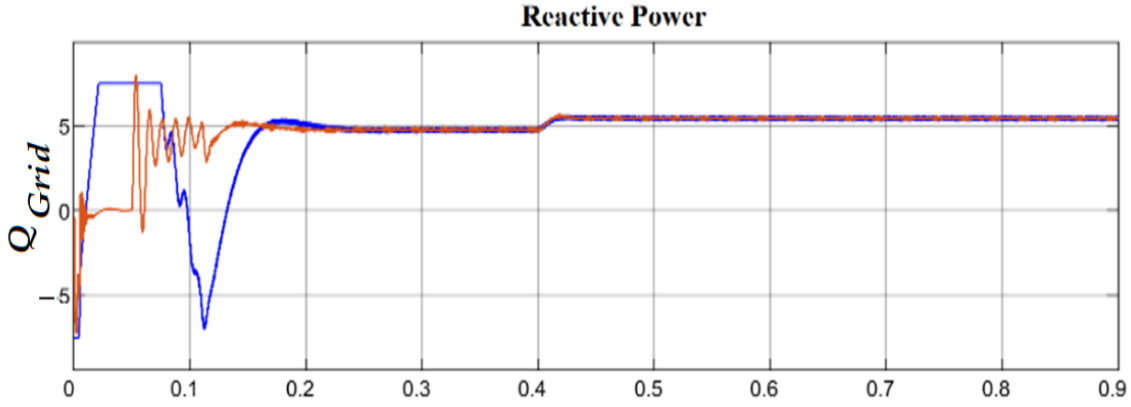
Reactive Power
$Q_{Grid}$
5
0
−5
0
0.1
0.2
0.3
0.4
0.5
0.6
0.7
0.8
0.9

(c)

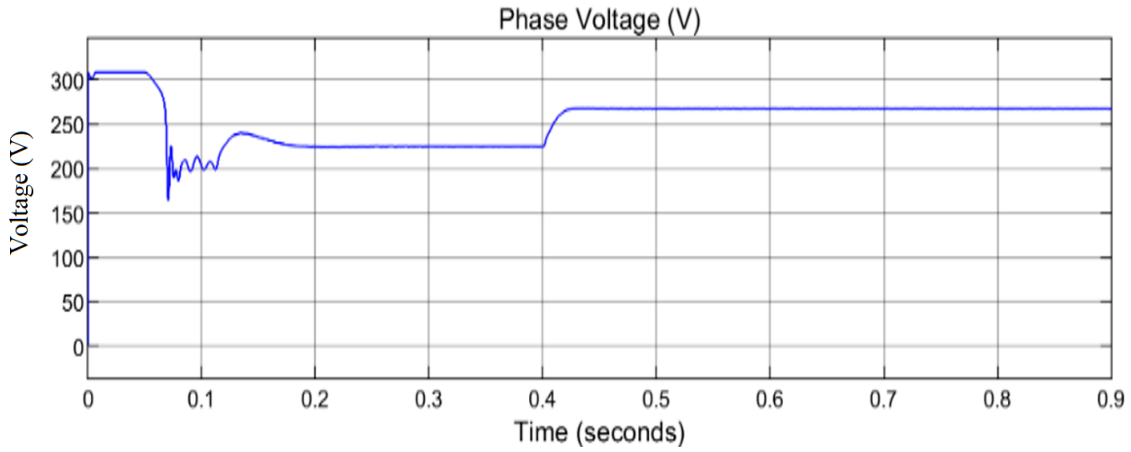
Phase Voltage (V)
Voltage (V)
300
250
200
150
100
50
0
0
0.1
0.2
0.3
0.4
0.5
0.6
0.7
0.8
0.9
Time (seconds)

(d)

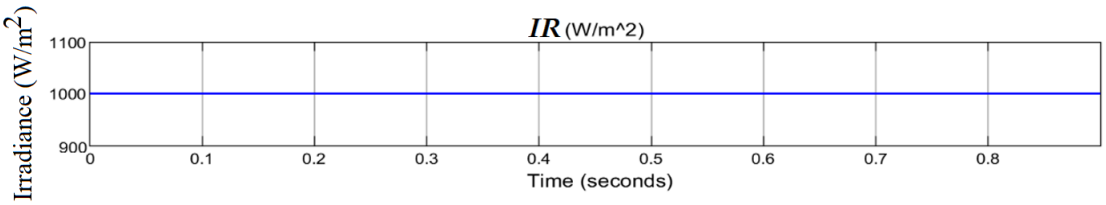
IR (W/m^2)
Irradiance (W/m$^2$)
1100
1000
900
0
0.1
0.2
0.3
0.4
0.5
0.6
0.7
0.8
Time (seconds)

(e)

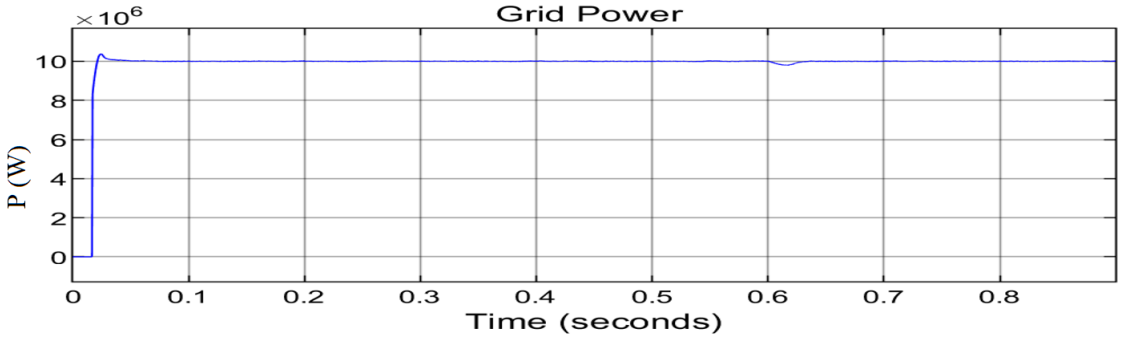
Grid Power
×10^6
P (W)
Time (seconds)

(f)

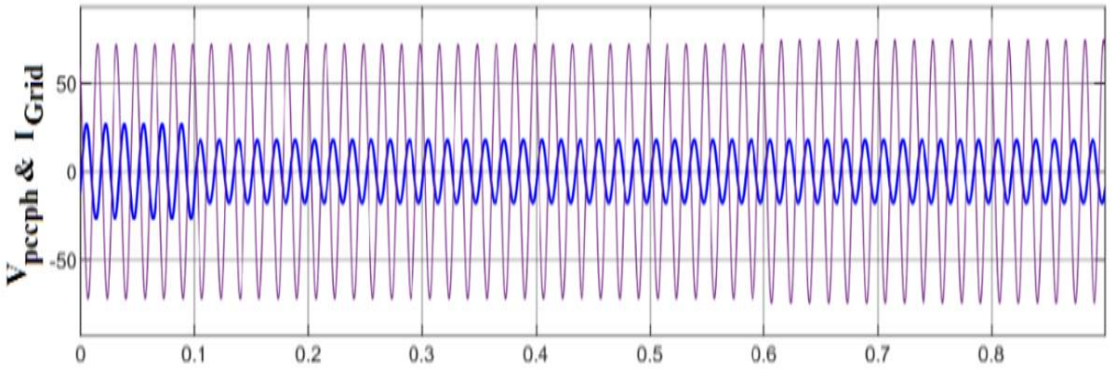
V_pccph & I_Grid

(g)

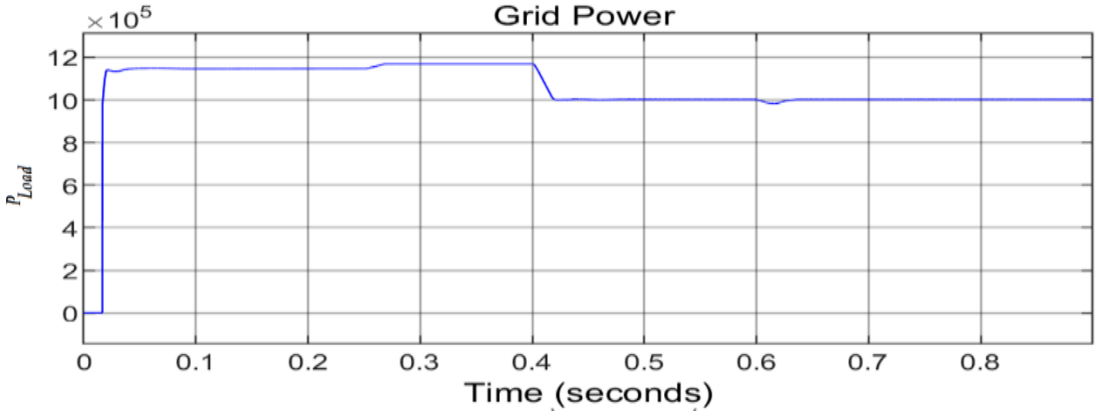
Grid Power
×10^5
P_Load
Time (seconds)

(h)

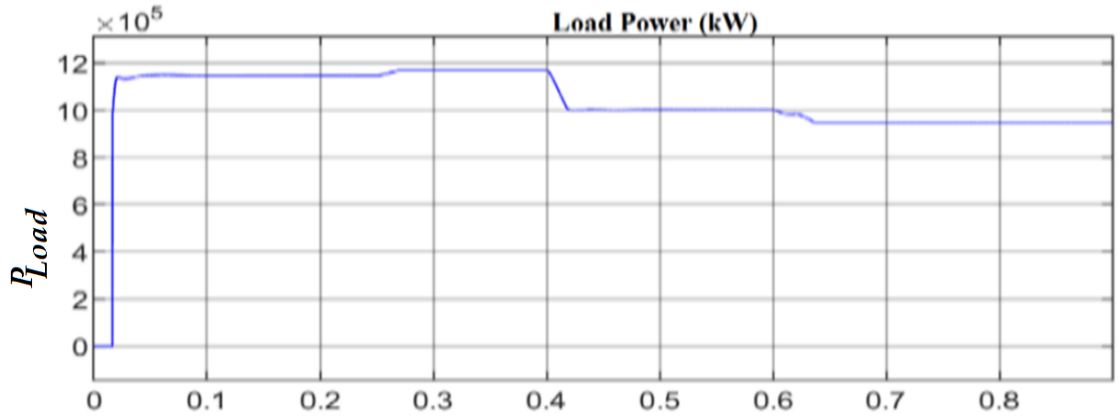


(i)

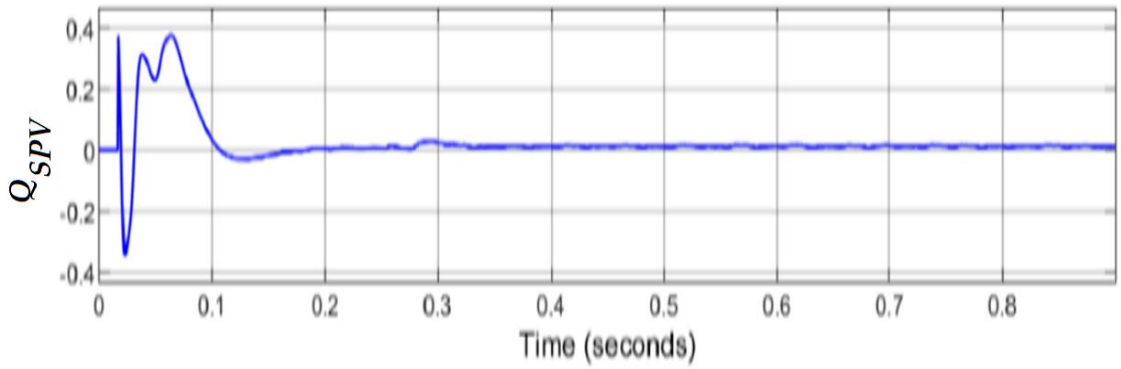


(j)

**Figure 6.13.** (a) PCC Voltage, Grid Current, Load Current, and PV Current, (b) Grid Reactive Power (0 – 1.15 kVAR), (c) Grid Reactive Power (1.15 – 5 kVAR), (d) Phase Voltage, (e) Solar Irradiance, (f) Normal Rated Power, (g) Flow of PCC Voltage and Grid Current, (h) Grid Power, (i) Load Power and (j) Reactive Power.

**Table 6.1:** Gid RMS Value of Various Voltage/Current.

| | **Voltage/Current/Power Factor** | **Grid RMS** | **% THD Value** |
|---|---|---|---|
| | $V_{Grid}$ | $ab$ = 14.14 kV, $bc$ = 14.14 kV, $ca$ =14.15 kV | 2.01 %, 2.01 %, 2.0 % |
| **Rated Load** | $I_{Grid}$ | Ig =55.10 A, 0.99 pf, Ig = 55.10 A, 0.99 pf, Ig = 55.12 A, 0.99 pf | 3.3 %, 3.3 %, 3.4 % |
| | $I_{Load}$ | $I_a$ = 59.10 A, 0.99 pf, $I_b$ = 59.22 A, 0.99 pf, $I_c$ = 59.59 A, 0.99 pf. | 26.6 %, 26.8 %, 26.9% |
| | $PV_{Current}$ | $I_{spva}$ = 55.5 A, 0.99 pf, $I_{spvb}$ = 55.5 A, 0.99 pf, $I_{spvc}$ = 55.56 A, 0.99 pf | 16.01 %, 16.01 %, 16.21 % |
| | $V_{Grid}$ | $ab$ = 14.34 kV, $bc$ = 14.34 kV, $ca$ =14.34 kV | 5.3 %, 6.3 %, 5.4 % |
| **Unbalance** | $I_{Grid}$ | $I_{ga}$ = 60.10 A, 0.99 pf, $I_{gb}$ = 60.10 A, 0.99 pf, $I_{gc}$ = 60.12 A, 0.99 pf | 4.3 %, 4.3 %, 5.4 % |
| | $I_{Load}$ | $I_a$= 0 A, 0.99 pf, $I_b$ = 15.1 A, 0.99 pf, $I_c$ = 15.4 A, 0.99 pf | 0 %, 4.3 %, 5.4 % |

| | | | |
|---|---|---|---|
| | $PV_{Current}$ | $I_{spva}$= 55.5 A, 0.99 pf, $I_{spvb}$ = 70.5 A, 0.99 pf, $I_{spvc}$ = 69.56 A, 0.99 pf | 18.3 %, 25.3 %, 22.4 % |
| | $V_{Grid}$ | $ab$ = 14.50 kV, $bc$ = 14.50 kV, $ca$ =14.54 kV | 0.6 %, 0.6 %, 0.45% |
| **No-loads and** | $I_{Grid}$ | $I_{ga}$ = 69.20 A, 0.99 pf, $I_{gb}$ = 69.6 A, 0.99 pf, $I_{gc}$ = 69.9 A, 0.99 pf | 0.3 %, 0.7 %, 0.4 % |
| | $I_{Load}$ | $I_a$ = 0 A, $I_b$ = 0 A, $I_c$ = 0 A | 0.0 %, 0.0 %, 0.0 % |
| | PV currents | $I_{spva}$ = 69.20 A, 0.99 pf, $I_{spvb}$ = 69.6 A, 0.99 pf, $I_{spvc}$ = 69.9 A, 0.99 pf | 0.9 %, 0.8 %, 0.85 % |

### 6.7.3 PVAs Variation

The Figure 6.14 (a–i) shows the impact of the network when the $(P_{PV})$ varies from rated to zero. The solar power $(P_{PV})$ varies rapidly when solar irradiance fluctuates from $1000\ \mathrm{W/m^2}$ to $0\ \mathrm{W/m^2}$. There is nothing to be tracked by PPPT after 0.4 s, as the power generated by the solar farm is zero and $(V_{dc})$ reduces to less than 400 V. The grid power and the grid current $(I_{Grid})$ and $(P_{Grid})$ vary with load power, while the rated value of the load power $(P_L)$ remains unchanged. Originally, the voltage rise at the point of common coupling is because of the drop at the feeder impedance (negative, which means it produces energy) when power is fed to the AC grid. However, the drop in the feeder impedance reduces due to the decrease in the power transported to the AC grid with $(P_{PV})$, hence, the phase voltage amplitude $(V_{\emptyset A})$ reduces. Moreover, when solar power generated is equal to zero, power is absorbed from the AC grid and the drop in the feeder impedance is positive (the energy is being consumed); therefore, the phase voltage amplitude is less than the rated voltage (249 V) and the regulating operation is carried

out in the system, such that the system behaves like STATCOM by active filtering characteristics. The grid reactive power maintains a zero position when $(V_A)$ at the PCC is less than the maximum voltage amplitude while the network operation is in unity power factor mode, such that $(I_q = 0)$.

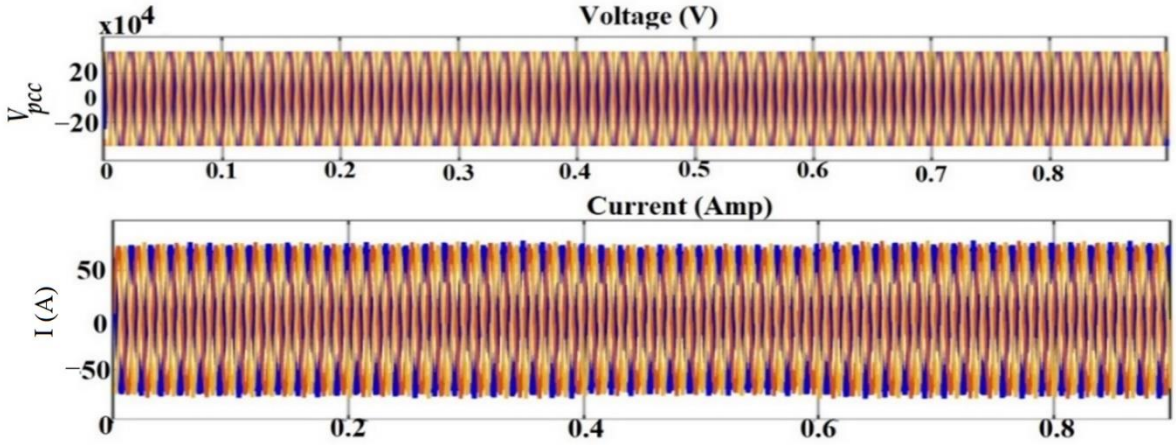


(**a**)

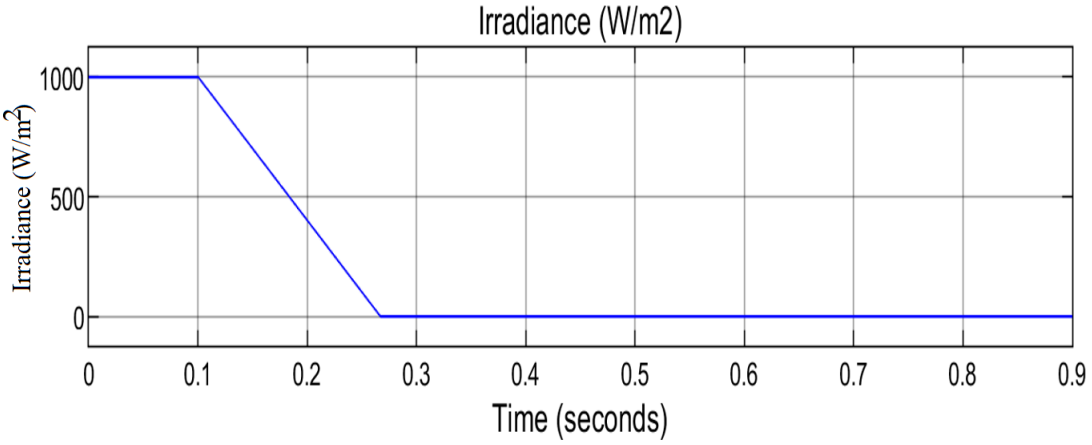


(**b**)

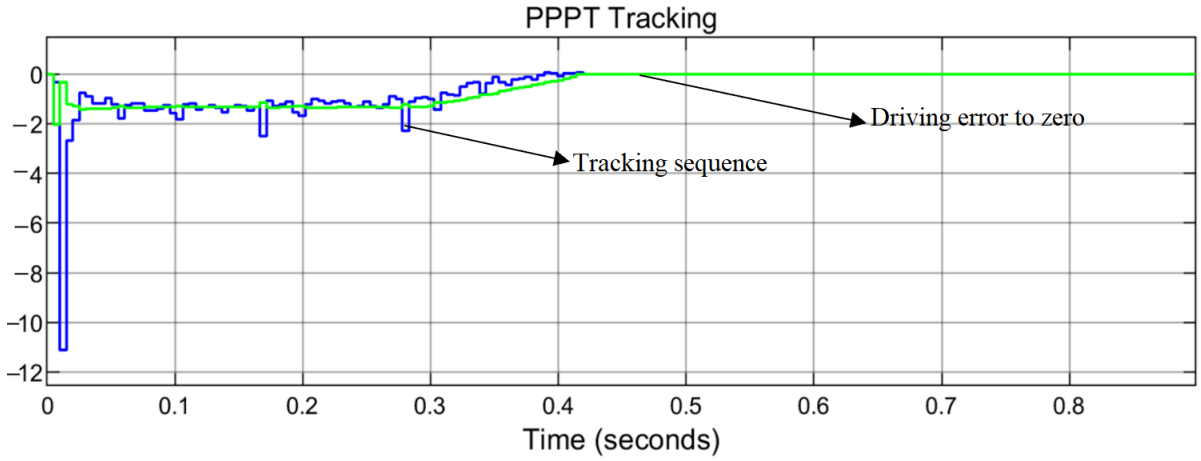
PPPT Tracking
Driving error to zero
Tracking sequence
Time (seconds)

(**c**)

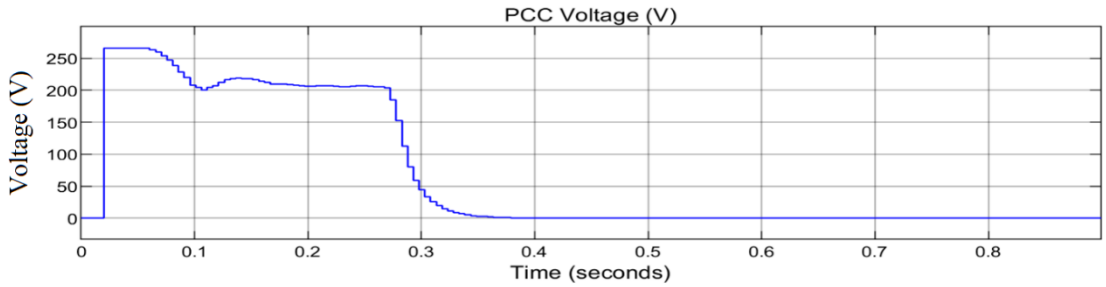
PCC Voltage (V)
Voltage (V)
Time (seconds)

(**d**)

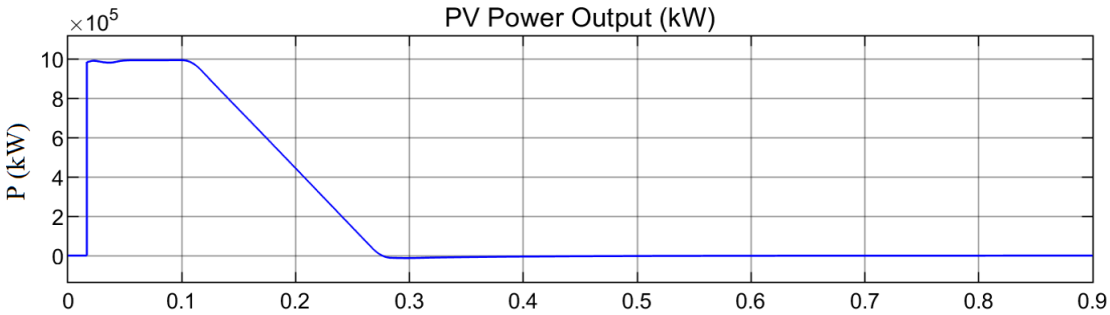
PV Power Output (kW)
×10^5
P (kW)

(**e**)

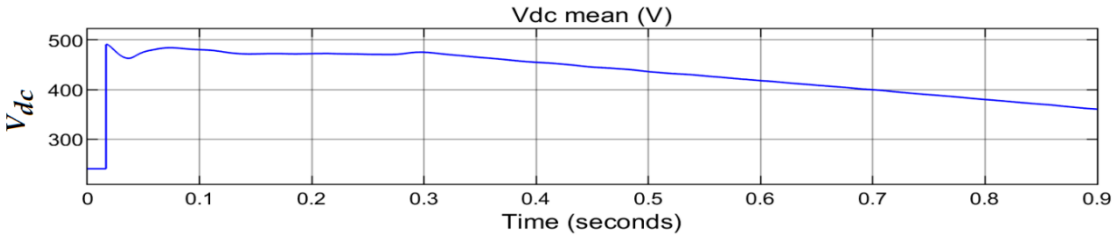
Vdc mean (V)
Vdc
Time (seconds)

(**f**)

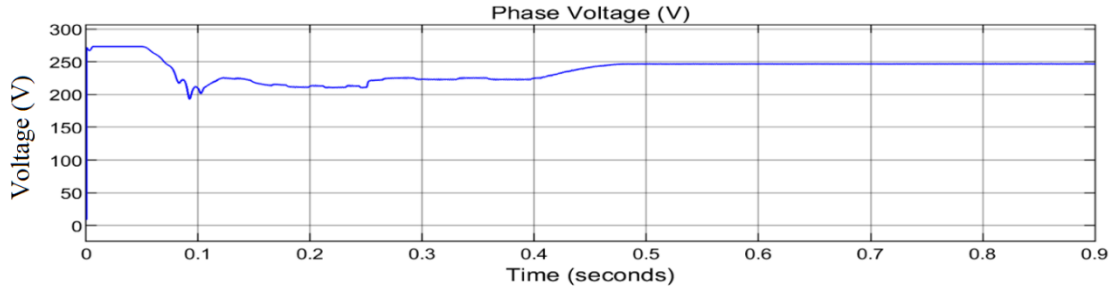


(**g**)

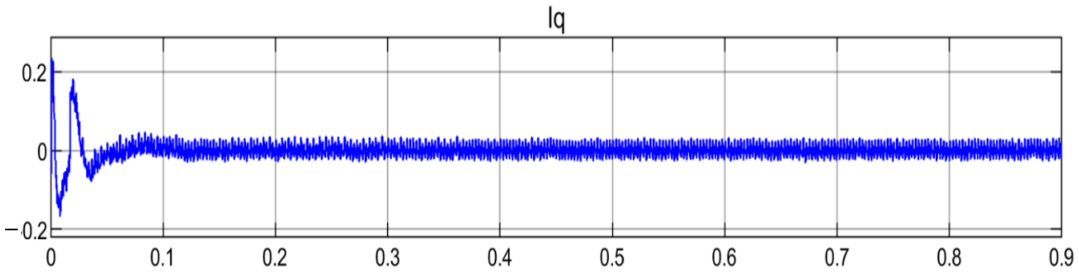


(**h**)

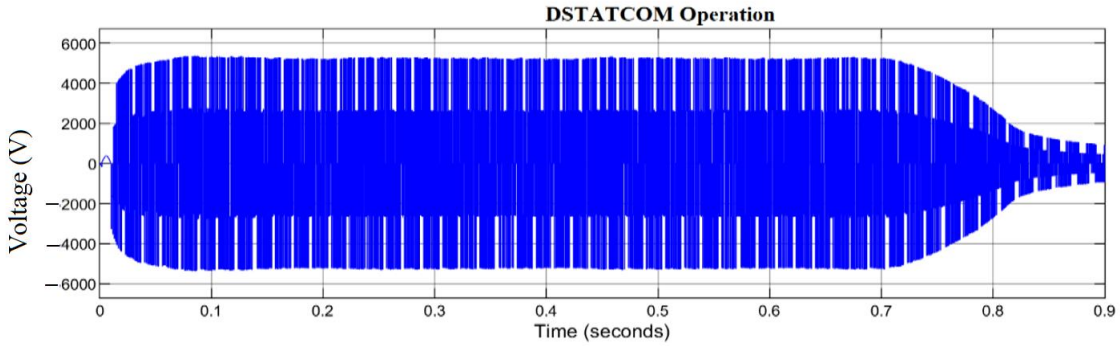


(**i**)

**Figure 6.14:** (a) PCC Line Voltage and Current, (b) Solar Irradiance, (c) Peak Power Point Tracking, the blue is the tracking sequence while the green line is the error regulator (d) PCC Phase Voltage, (e) PV Power Output, (f) DC Voltage, (g) Solar Voltage, (h) Grid Reactive Power and (i) STATCOM Voltage.

## 6.8. Conclusion

The research investigation in this paper shows that variation in the consumer's loads (reduction) can cause an increase in the power generated from PVAs to the grid, as well as an increase in current amplitude, reduction in voltage of the feeder impedance and an increase in phase voltage amplitude at the PCC. When the system is undergoing unity power factor mode, PCC voltage amplitude tends to rise with loads, and PCC phase voltage amplitude rises above an acceptable range with no-load. Similarly, load reduction causes voltage rise at PCC during UPF mode, which can be regulated by changing to voltage regulation mode. Generation of positive reactive power to the grid by the STATCOM reduces voltage rise at PCC, which also regulates the phase voltage while solar PVAs are in continuous operation, which justified the first research question mentioned in the introduction. Furthermore, fluctuation in the sun's irradiation causes a decrease in PVA power generation, resulting in variation of the grid current and power. The impact of zero PVA generation causes power to be absorbed from the grid, which causes a positive in the feeder impedance, leading to the reduction in the voltage amplitude. This satisfies the second research question but is corrected when the system operates in its voltage regulation mode. If the active power generated by the PVAs is higher than that of the local consumers, excess power is delivered to the grid. The operation of PVAs has been presented in this paper to solve power quality issues, such as a voltage rise at the point of common coupling. It is therefore recommended that the PCC of PVAs should be strategically monitored and regulated to avoid power quality challenges whenever there is load variation and no generation from PVAs.

## 6.9 Summary

This chapter investigates the voltage rise regulation with a grid connected Solar Photo-voltaic system. Solar system, solar and battery modelling, factors affecting solar array performance, energy management and solar power tracking are adequately discussed. Design and simulation of a propose microgrid for DUT, control strategy, load variation under PV system, effect of PV variation on the system, and the grid behaviours during STATCOM UPF and VR mode are analysed. The overall contributions of this chapter are as follows: strategic regulation of PCC voltage rise through the generation of positive re-active power without disconnecting renewable distributed generation integration with higher penetration levels can be achieved in a distribution network, in-loop second order integral filtering algorithm can get rid of or filter any form of grid current distortions generated from the non-linear loads in a distribution network. Peak power point tracking error can be minimized from the solar power tracking system by the addition of integral regulation algorithm. The output voltage and power of the PVAs can be reinforced and stable when a compensator is installed in the network, even with fluctuation in the sun’s irradiation and the loads.

# CHAPTER 7

# GRID VOLTAGE REGULATION UNDER VARYING SOLAR IRRADIATION

## 7.1 Introduction

The concept of introducing solar systems would provide electricity accessibility to remote rural areas that have no access to the grid system. Countries of the world are planning to reduce fossil fuel emissions due to its negative effect to human health and the environment by substituting traditional fossil fuel-based means of energy generation with renewable energy resources as solar power. Solar power is more popular because it is cheap to maintain, clean, renewable on a human time scale and produces no noise disturbance. Grid integration of the solar system is expected to grow more in the future due to the decrease in the cost of solar components, power electronic interface development and the government support tariff. However, the power output of PV solar system is intermittent in nature depending on sun irradiance and the temperature operation of the solar cell. Hence, it is vital to extract maximum power from solar panels in all conditions. This section of the thesis presents the tracking method of peak output power of a photovoltaic solar system connected with a DC-DC boost converter using an improved Incremental Conductance with Integral Regulator Strategy (IC+IR). The simulation results show that peak power can be harnessed from the solar panel with stable output voltage under varying operating conditions. This chapter investigates grid voltage regulation under varying solar irradiation. It explores the solar tracking algorithms, perturb and observe strategy, incremental conductance, improved incremental conductance with integral regulator to track peak power point of the solar system, modelling of a boost converter, proposed converter restoration scheme, and converter block/de-block scheme. The contribution of this chapter is as follows:

- Improved Incremental Conductance with Integral Regulator Strategy (IC+IR) is used to track peak power point of the solar.
- Automatic block and de-blocking restoration control scheme are designed in controlling the converter switching mechanism to prevent the device from

fault current/grid fault and voltage rise.

- Oscillation occurrence at the output power due to the error signal generated between the instantaneous conductance and the incremental conductance are attenuated by the integral regulator.

- Grid voltage stability during variable load, solar irradiance, and temperature.

### 7.2 Solar Tracking Algorithms

Several tracking algorithms have been developed recently to access peak power at any certain sun irradiance and temperature [233]. Perturb and Observation method is quite a popular algorithm due to its simple and quick application, but the production of oscillation at its output level is a setback. Also, it can track Peak Power Point Tracking (PPPT) at a wrong direction if there is a quick change in the direction of the sun's irradiance [234]. Incremental Conductance is another algorithm that possesses the advantage of improved capability as compared to the perturb and observation method. However, the method has the disadvantage of reduction in efficiency because it can swing the PPT round [231], [235], hence, there is a need for a modified incremental conductance algorithm that is robust, stable and devoid of swing. To carry out the investigation of grid voltage regulation with varying solar irradiance, a solar system is integrated into the grid at the (PCC) with the aid of power electronic devices such as a DC-to-DC converter  otherwise, a stand alone is considered. This section of the thesis presents an improved Incremental Conductance with Integral Regulator Strategy (IC+IR) to access the solar array peak power point for perfect efficiency, time reduction, and error minimization. The error signal is generated at PPP during instantaneous conductance and the incremental conductance is reduced to zero by a proportional integral (PI) controller in the closed-control loop diagram. The overall result provides stability of the output signals (i.e., voltage, current) of the PV and to supply constant power output to the load at a variable solar irradiance and temperature.

#### 7.2.1 Overview of Perturb and Observe Strategy

The perturb and observe method of PPPT of the solar system is the simplest method of power tracking strategy. This is a process by which an operating voltage is adjusted and

forces the power of a solar system to the hill level and sustains it. It is otherwise known as hill-climbing. In this method, an increment in an operating voltage is sustained to the maximum when there is an improvement in the power generated, but it will stop when the power is about to drop. The very point at which the power generated is highest just prior starting to fall is known as Peak Power Point (PPP). The power output of the solar system has the tendency to vary due to its non-linear characteristics, change in temperature and irradiation [236]. The power generated is being compared to the previous power produced by computing the system voltage. The current, negative or positive signs in the variation in power and voltage obtained influences the decision in the direction of the algorithm. Also, the two successive values are taken and measure the variation in power and voltage by controlling the duty circle and the step size of the PPPT to establish the power loss and the speed of the system. If there is no voltage produced, Perturb and Observe Algorithm (P & OA) will oscillate around the PPPT. When there is an increase in voltage produced, a change in the power level will be verified by the (P & OA). An increase in voltage means that the power generated will be improved by P & OA. The drawback is that the voltage level never remains at the same level when PPP is reached similar to the power level. The PPPT strategy makes use of an iteration approach in attaining voltage $(V_{PPPT})$ and the current $(I_{PPPT})$ through which the solar system generates its highest power with the influence of temperature and irradiation. The flow chart of P & O is depicted in Figure 8.1, and it is summarised as follows:

- $(I_k)$ and $(V_k)$ data are collected from solar panels where $(I_k)$ and $(V_k)$ are solar panel current and voltage.
- $(P_k)$ is calculated from $(I_k)$ and $(V_k)$.
- Power and voltage data are saved.
- The data are verified for the next successive $(\mathrm{k}+1)^{\mathrm{th}}$ immediate and repeat the first step.
- The data processed at $(k+1)^{th}$ immediately are subtracted from the data processed at $K^{th}$.

- If $\left(\frac{dp}{dv} < 0\right)$ on the solar curve on the right side, the slope of the graph will be negative. Similarly, if $\left(\frac{dp}{dv} > 0\right)$ on the solar curve on the left side the slope will be positive. Consequently, the reduced duty cycle appears at the right side of the curve, and excessive duty appears on the left side of the curve.

- Depending on the polarity of the slope after subtraction, the algorithm decides the change in the duty cycle.

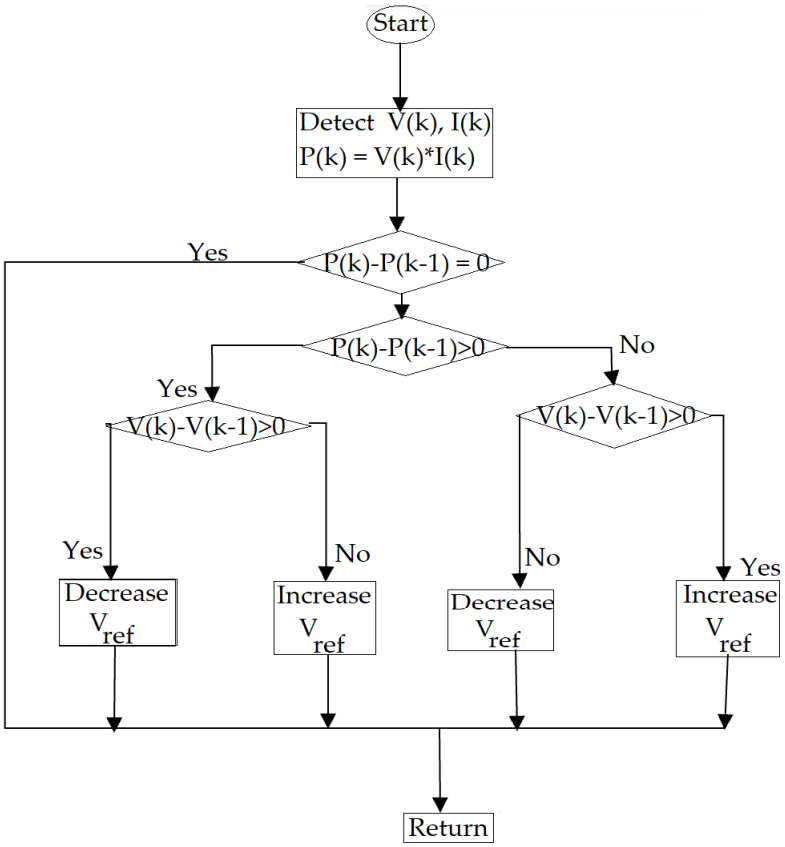


**Figure 7.1:** Perturb and Observation flow chart.

### 7.2.2 Incremental Conductance

Incremental conductance works on the principle that the slope of the solar power graph is negative at right hand side and positive at left hand side but equal to zero. This is otherwise known incremental conductance $\left(\frac{dI}{dV}\right)$, which can obtain the solar power derivative with respect to voltage $\left(\frac{dp}{dV}\right)$. The strategy of an incremental conductance is

based on the derivative of solar system power and voltage equal to zero at PPP. It locates PPP due to equality of instantaneous conductance $\left(G = \frac{1}{V}\right)$ and conductance increment $\left(G = \frac{\Delta I}{\Delta V}\right)$. Since solar systems current depends on voltage, the solar power can be obtained. When equation 7.1 is equal to zero consequently, the highest power point can be obtained when the incremental conductance is equal to the negative of the instantaneous conductance as depicted in equation 8.6 and the voltage at that point is known as PPP voltage in equation 7.7. This PPP voltage is sustained by the controller until there is a change in the solar irradiation $(\Delta I)$ due to atmospheric condition variation. Figure 7.2 shows the incremental conductance algorithm, and the algorithm process decreases or increases $(V_{ref})$ to trace the new PPP.

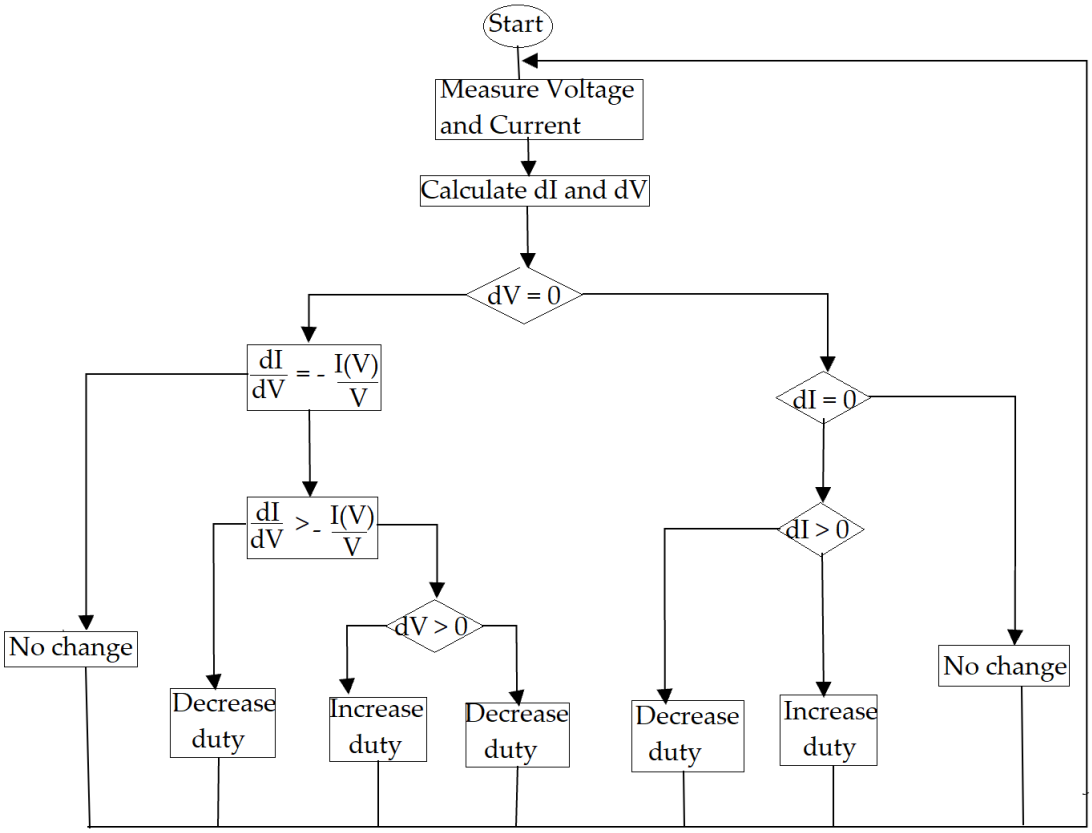


**Figure 7.2:** Flowchart of Incremental Conductance.

The speed of PPP tracking is dependent on the increment step. The higher the step increases the faster the PPP tracking, hence, it may not exactly operate at PPP but oscillate around it. Therefore, with the strategic control of the converter device installed,

load resistance can be matched to the $\left(\frac{V_{oc}}{I_{sc}}\right)$. This occurs where $(V_{ov})$ is the open circuit voltage and $(I_{sc})$ is short circuit current of the solar system. The Incremental Conductance method involves further calculation in the regulator which can track varying conditions more quickly than the perturb and observe method, nevertheless, oscillations can be generated at the output power due to the error signal generated between the instantaneous conductance and the incremental conductance.

$$at\ PPP, \frac{dP}{dV} = 0 \quad (7.1)$$

$$P = I \times V \quad (7.2)$$

$$P = I(V) \times V \quad (7.3)$$

$$\frac{dP}{dV} = V \times \frac{dI}{dV} + I(V) \quad (7.4)$$

$$V \times \frac{dI}{dV} + I(V) = 0 \quad (7.5)$$

$$\frac{dI}{dV} = -\frac{I(V)}{V} \quad (7.6)$$

$$at\ PPP, V_{ref} = V_{PPP} \quad (7.7)$$

### 7.3 Improve Incremental Conductance with Integral Regulator Strategy.

The principle of PPPT is to move the operating point by increasing $V_{PV}$ (decreasing the duty cycle D) when $\frac{\partial p_{pv}}{\partial v_{pv}}$ is positive or decreasing $V_{PV}$ (increasing the duty cycle D) when $\frac{\partial p_{pv}}{\partial v_{pv}}$ is negative. The integral regulator scheme is added to the incremental conductance to minimize oscillation, obtain a perfect efficiency, reduce error, and reduce time taken in tracking PPP as depicted in Figure 7.3. Figure 7.3a depicts the block diagram of the IC+IR. The PPP can be tracked by comparing the instantaneous conductance $\frac{I}{V}$ to the incremental conductance $\frac{dI}{dV}$. The condition $\frac{I}{V} + \frac{dI}{dV}$ = 0, to obtain PPP in equation 7.8 is rarely assured. The system operating point will be on the right of PPP in equation 7.9, and on the left of PPP in equation 7.10. Hence, a new parameter $e$ is introduced as $\frac{I}{V} +$

$\frac{dI}{dV} \leq e$. This error signal is regulated by an integral regulator to adjust PV output voltage. From the flow chart of an improved IC in Figure 7.3b, when $\Delta v$ is small, the controller feedback will be slow resulting in losses of power, when $\Delta v$ is big, inaccuracy of $V_{opt}$ arises, and the undesirable oscillations appear in the controller results. The amplitude of the oscillations around the PPP is controlled by the value $e$. It decreases with the increase of $e$ and for a moderately great value of $e$, the operating point moves away from the true PPP. Thus, the value of $e$ should be precisely determined for improved performance of the PPPT system. When $e$ = 0 has been reached because of the adjustment carried out, the PV module power will be maintained at the PPP. The error signal generated at PPP during instantaneous conductance and the incremental conductance is reduced to zero by the application of the integral regulator strategy which is used to derive the error signal (*e*) to zero in equation 7.12. When the integral regulator is added to the incremental conductance, there will be a reduction in the output oscillation, resulting in a better digital resolution of the output, perfect control, and adaptation of the solar PV system to the ever-changing climatic condition. Thus, the system efficiency is improved. The integral controller improves the precision of both the system's large step sizes when the operational level is far from the PPP and when the small step sizes of PPP is reached to extract the maximum possible level of power. The integral regulator does the manipulation by accumulating the instantaneous error, then multiplies it by the integral gain and adds it to the controller output. To reach the maximum power, the source impedance is equal to output impedance such that by varying the duty cycle of the converter, source and output impedance is matched, hence, the maximum power can be attained. When error $\left(\frac{dI}{dV} + \frac{I}{V}\right)$ is minimized, the regulator output will be equal to the Duty cycle correction. The error signal (*e)* obtained in IC is processed through a IR controller to eliminate error *e* in equation 7.13 where $K_{pb} and\ K_{ib}$ are the gain of the *IR* controller. The output signal $U_{IR}$ of *IR* controller is further fed to PWM, which generates the corresponding pulses for the IGBT of the boost converter. The updated duty cycle *D(new)* is modified in equation 7.16.

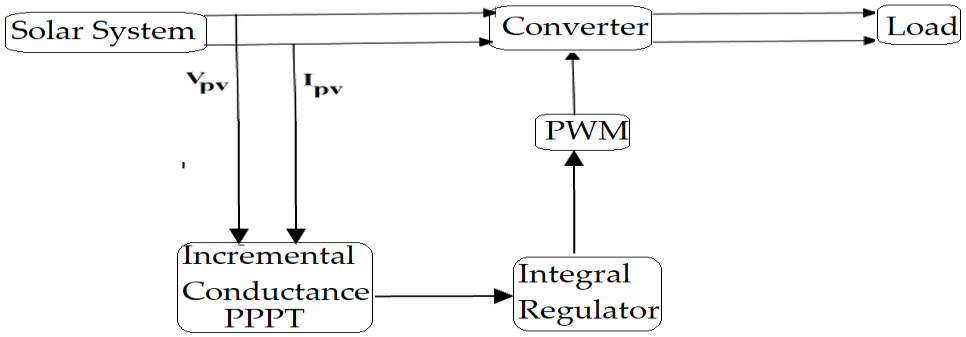


(a)

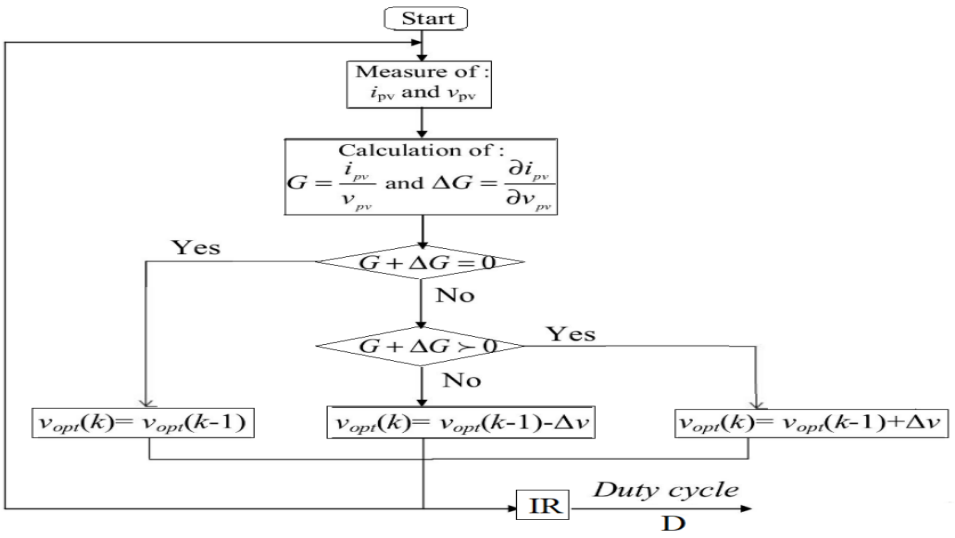


(b)

**Figure 7.3:** (a) Block Diagram of Incremental conductance with integral regulator, (b) IC MPPT technique flowchart.

$$\frac{I}{V} + \frac{dI}{dV} = 0 \; at \; PPP \tag{7.8}$$

$$\frac{I}{V} + \frac{dI}{dV} < 0 \tag{7.9}$$

$$\frac{I}{V} + \frac{dI}{dV} > 0 \tag{7.10}$$

$$e = \frac{I}{V} + \frac{dI}{dV} \tag{7.11}$$

$$e = 0 \tag{7.12}$$

$$U_{IR} = eK_{pb} + \frac{K_{ib}}{s}e \quad (7.13)$$

$$D_{new} = D_{previous} + U_{IR} \quad when\ e > 0 \quad (7.14)$$

$$D_{new} = D_{previous} \quad \text{when e = 0} \quad (7.15)$$

$$D_{new} = D_{previous} - U_{IR} \quad whem\ e < 0 \quad (7.16)$$

### 7.4 Boost Converter Modelling

The effective implementation of the PPP tracking method involves a converter, (usually DC-to-DC converter). To guarantee the optimization output power allocation of the solar PV system, a boost converter is vital for the variant weather condition. Figure 7.4 depicts the proposed boost converter and IC+IR for PPPT Technique. As the input decoupling capacitance (C) is connected in shunt with the PV array, the input inductance of the converter (L) is vital for PPPT dynamics. Thus, it guides the PPPT process and regulates the PV voltage to exactly match the voltage at the PPPT.

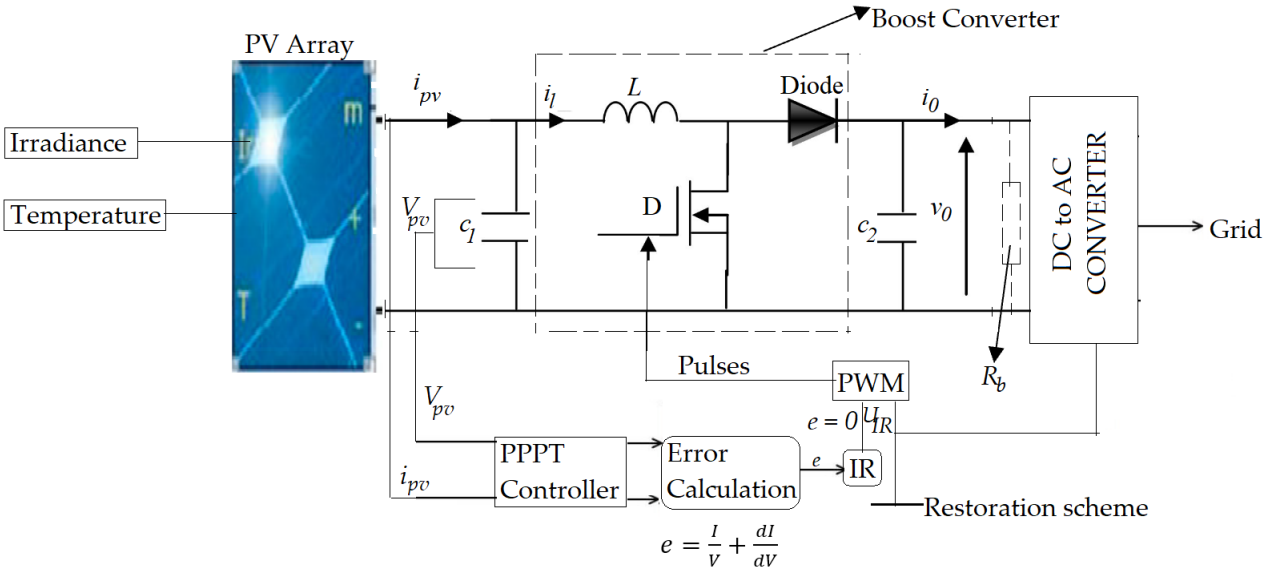


**Figure 7.4:** Proposed Boost Converter and IC+IR PPPT Technique.

The challenges of low power output occurrence are common to the conventional *IC* technique, where PPP accomplishment is limited resulting in the reduction of the tracking efficacy. The proposed method in this paper overcomes this shortcoming. The error signal *e* obtained in IC is processed through IR controller to eliminate error. The proposed IC+IR algorithm to access PPP is demonstrated using a DC-to-DC boost converter in Figure 7.4 and its mathematical model of the converter can be expressed in equations 7.17 to 7.19.

$$\frac{\partial v_{pv}}{\partial t} = \frac{i_{pv} - i_l}{C_1} \tag{7.17}$$

$$\frac{\partial i_l}{\partial t} = \frac{v_{pv} - (1-D)v_0)}{l} \tag{7.18}$$

$$\frac{\partial v_0}{\partial t} = \frac{(1-D)i_l - \left(\frac{v_0}{R}\right)}{C_2} \tag{7.19}$$

When $R_b$ is put into consideration in Figure 7.4, after applying Laplace transform, the overall transfer function of the boost converter can be expressed in equation 7.20.

$$G_i(s) = \frac{(V_0 C_2)s + 2.\frac{V_0}{R_b}}{(LC_2)S^2 + \frac{L}{R_b}.S + (1-D)^2} \tag{7.20}$$

The parameters of a discrete RI controller can be achieved by a continuous RI regulator. The transfer function of the continuous RI regulator can be expressed in equation 7.21

$$G_s(s) = K_{pb} + \frac{K_{ib}}{s} \tag{7.21}$$

## 7.5 Propose Converter Restoration Scheme

The block and de-block control scheme of the converter is considered as an event activated module to simplify the interfaces between different modules. Logic B is the block signal at the input of the converter, normally low or zero as depicted in Figure 7.5. When the converter receives the signal, it automatically blocks the converter. With the advent of fault on the grid, the circuit breaker and the disconnector are properly coordinated to carry out the fault isolation process. The fault is sensed by the converter and receives a blocking signal while the circuit breaker receives the opening signal and isolates the fault. During this period, the converter behaves like a rectifier diode. The proposed converter

control scheme consists of block/de-block module, the monitor module and auto de-block module. The voltage, current, disconnector and converter information are collected, analysed and re-arranged into different kind of signal such as event signal, logic signal etc., by the control monitor and transmitted the signal to the next module as operation signal.

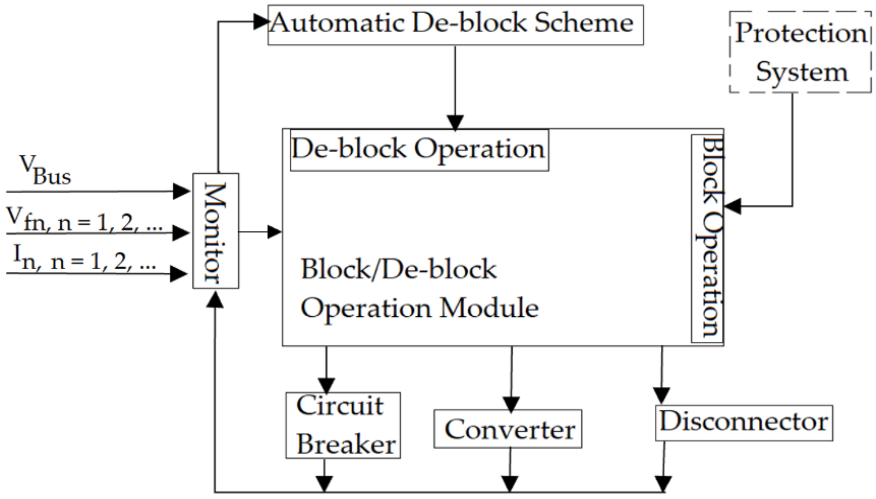


**Figure 7.5:** Proposed diagram of converter restoration scheme.

### 7.6 Converter Block/De-Block Scheme

The block and de-block operation orders to the converter are generated by the block/de-block module as depicted in Figure 7.6. The block/de-block module comprises 4 input and 2 output, where the input (a) is the state of opening the grid circuit breaker when the state is low or zero, the input (b) is the event to de-block the converter after the closing of the circuit breaker by the AND gate, the input (c) is the event to block the converter when it receives an unwanted signal such as over-voltage or a fault current which will reset the [Set-Reset (SR)] trigger and the (Q) will go to zero or low state thereby opening the circuit breaker. The reset input resets the device to its original state with an output Q which will be either at high level 1 or low level 0 depending on the set/reset condition. The SR logic is one-bit bistate device which has 2 inputs known as set and reset. The device is Set (S) when the output is 1and Reset (R) when the output is zero (0). The blocking of the converter is vital to the grid switching devices protected from fault current, voltage rise and under-voltage. At the clearing of the grid fault event, the converter is de-block to

restore power. When de-block signal is received by the converter, the circuit breaker will turn off before the converter de-block. The input (d) is any fault occurrence that may occur from the DC side.

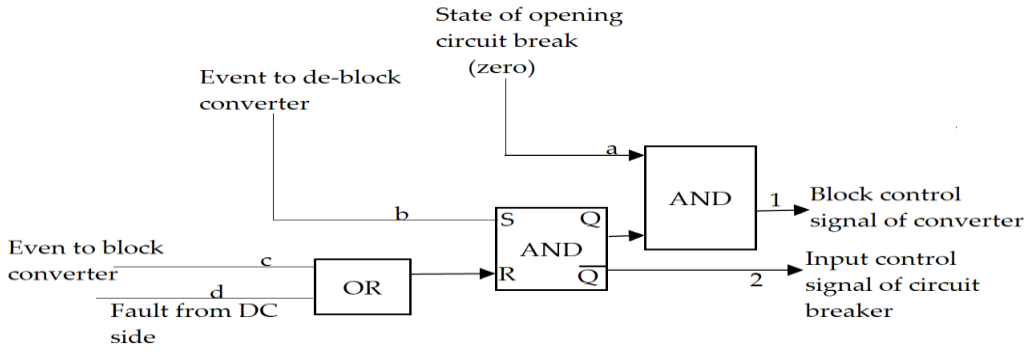


**Figure 7.6:** Converter Block/De-block module strategy.

**Table 7.1:** OR Gate Truth Table

| OR Gate | | | AND Gate | | | | | | | |
|---|---|---|---|---|---|---|---|---|---|---|
| Input | | Output | Input | | Output | S | R | Q | $\bar{Q}$ | Description |
| A | B | Y = A+B | A | B | Y = A. B | 1 | 0 | 0 | 1 | Set $\bar{Q}$ = 1 |
| 0 | 0 | 0 | 0 | 0 | 0 | 1 | 1 | 0 | 1 | No change |
| 0 | 1 | 1 | 0 | 1 | 0 | 0 | 1 | 1 | 0 | Set $\bar{Q}$ = 0 |
| 1 | 0 | 1 | 1 | 0 | 0 | 1 | 1 | 1 | 0 | No change |
| 1 | 1 | 1 | 1 | 1 | 1 | 0 | 0 | 1 | 1 | invalid |

## 7.7 Test System Description

The A 100.7 kW, 330 SunPower arrays (SPR-305E-WHT-D) solar PV system is utilized for three-phase grid integration under varying solar irradiation. IC+IR technique is proposed to extract peak power from the solar PV array. The solar PV array feeds 100.7 kW power to the grid through DC-to-DC boost converter followed by DC-AC conversion through voltage source inverter (VSI). The output voltage of the solar PV array that corresponds to maximum power serves as the input of the DC-DC boost converter whose gating pulse is generated from the IC+IR PPPT algorithm. The output of the DC-to-DC converter is connected to VSI through a dc-link capacitor whose value is maintained constant at 500V to balance power flow within the designed system. The Three-phase VSI is fed on solar PV injects active power into grid operating under UPF. A dc voltage of 500V is converted to 260VAC by VSI. A 100kVA, 260V/20kV three-phase transformer is employed to interface VSI with the grid. The block and deblock operation modules are incorporated into the converter to generate the block and de-block signal sequences for the converter as shown in Appendix A, Figure A5-A9 and is designed with MATLAB/Simulink environment. The solar module consists of two inputs, the temperature in degree and the irradiance in W/m$^2$). The converter used is a 3-phase, 3-levels Voltage Source Converter and it has internal and external control strategies. The internal control strategy adjusts the direct and quadrature currents $(I_d)$ and $(I_q)$ of the active and reactive current components while the external control strategy adjusts the voltage of the DC link. The system temperature and the solar irradiation characteristics are obtained at 25$^0$C and 1000W/m$^2$ respectively. On the system peak power, the network improves from 273 to 500 V DC. The tracking controller varies and optimizes the duty cycle of the converter to access the peak power. The power factor is kept at unity by the *(VSC)* by setting $(I_q)$ to zero and converts Direct Current (DC) voltage link from 500 V DC to 260 V AV. The converted output voltages of the current regulator $(V_d)$ and $(V_q)$ are modulated and utilized by the pulse width modulation generator. A 10 kVAR filtering unit is connected to the *(VSC)* output to minimize harmonics generated by the converter. The phase lock loop, voltage and current regulators of the control system uses 100 µs sample time while it takes 1 µs to obtain an appropriate pulse width modulation waveform.

### 7.7.1 Simulation, Result and Discussion

The network is simulated for 3 s. At t = 0.05 s, a time delay block has been introduced in the signal path of both boost converter and VSI to delay the insertion indices before a converters switch occurs in the continuous model as shown in Figure 7.7a. It is applied to prevent the effect of higher phase current and total capacitor voltage deviation and unwanted signals such as switch-on instantaneous input current surge drawn by an electrical device connected to the grid when first turned on. The converter behaves as rectifier between 0.01 to 0.05 and the direct current link capacitor is charged to about 578.6851 V in Figure 7.7b, while the solar voltage obtained is 320.986 V in Figure 7.7c. The value obtained is equal to the open circuit voltage in equation 23. At t = 0.05 s, boost converter and VSI are de-blocked in Figure 7.7a, and the duty cycle of the boost converter is fixed at D = 0.5 in Figure 7.7d. The direct current link voltage is controlled and maintained at a state of 500.8393 V at t = 0.205 s in Figure 7.7e. Hence, the solar PV steady state voltage is obtained in equations 7.22 to 7.27. The calculated steady state voltage of 250.32 V in equation 41 is approximately agreed with the simulated value of 249.5447 V in Figure 7.7f. The grid current and voltage are kept at unity power factor such that they are in phase. The solar and the grid output power obtained are 95.3199 kW and 93. 5221 kW respectively in Figure 7.7g which are not equal to the rating of the solar PV (100.7 kW).

$$PV_{voltage} = N_{series} \times V_{oc} \tag{7.22}$$

$$PV_{voltage} = 5 \times 64.2 \tag{7.23}$$

$$PV_{voltage} = 321\ V \tag{7.24}$$

$$PV_{steady\ voltage} = (1 - D) \times Vdc \tag{7.25}$$

$$PV_{steady\ voltage} = (1 - 0.5) \times 500.64 \tag{7.26}$$

$$\mathrm{PV_{steady\ voltage}} = 250.32\ \mathrm{V} \tag{7.27}$$

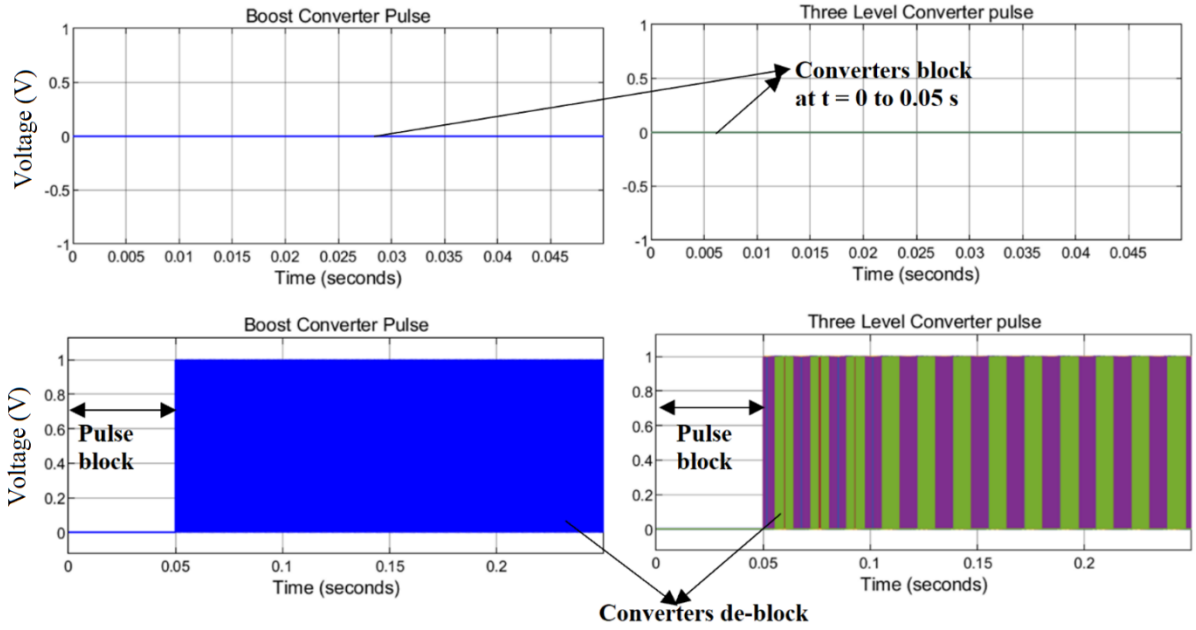
Boost Converter Pulse
Three Level Converter pulse
Converters block
at t = 0 to 0.05 s
Voltage (V)
Time (seconds)
Pulse
block
Converters de-block

(a)

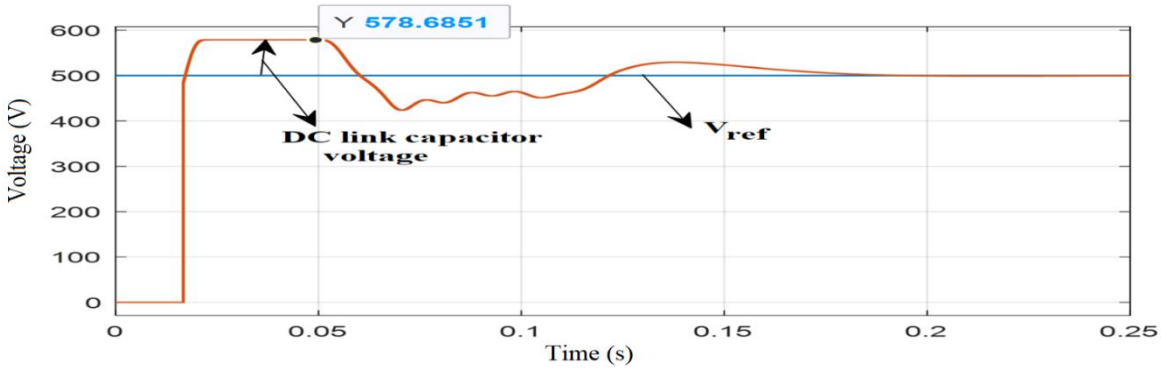
Y 578.6851
DC link capacitor
voltage
Vref
Voltage (V)
Time (s)

(b)

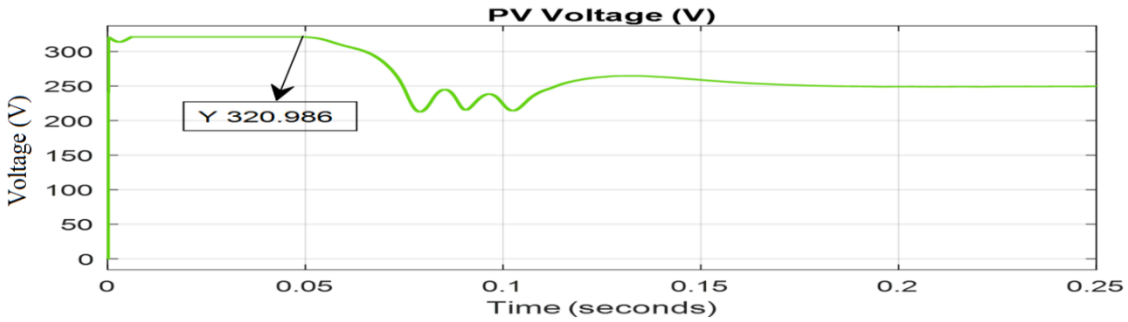
PV Voltage (V)
Y 320.986
Voltage (V)
Time (seconds)

(c)

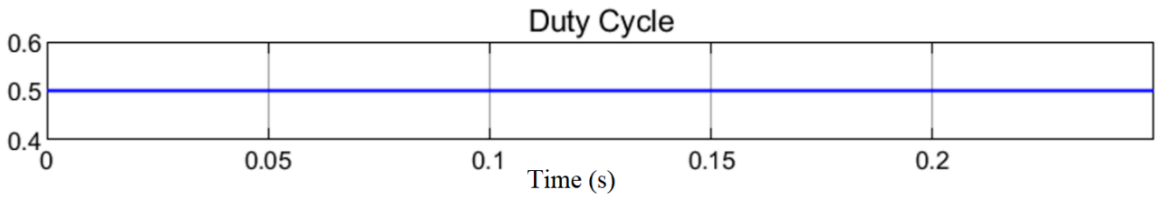
Duty Cycle
0.6
0.5
0.4
0
0.05
0.1
0.15
0.2
Time (s)

(d)

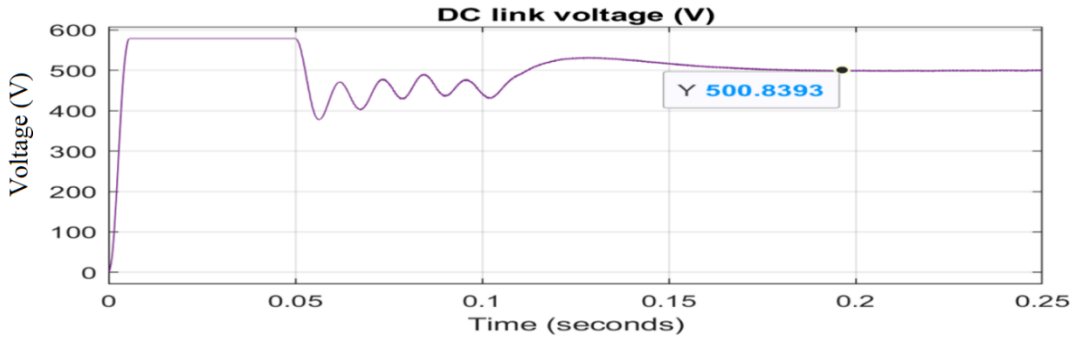
DC link voltage (V)
Voltage (V)
600
500
400
300
200
100
0
Y 500.8393
0
0.05
0.1
0.15
0.2
0.25
Time (seconds)

(e)

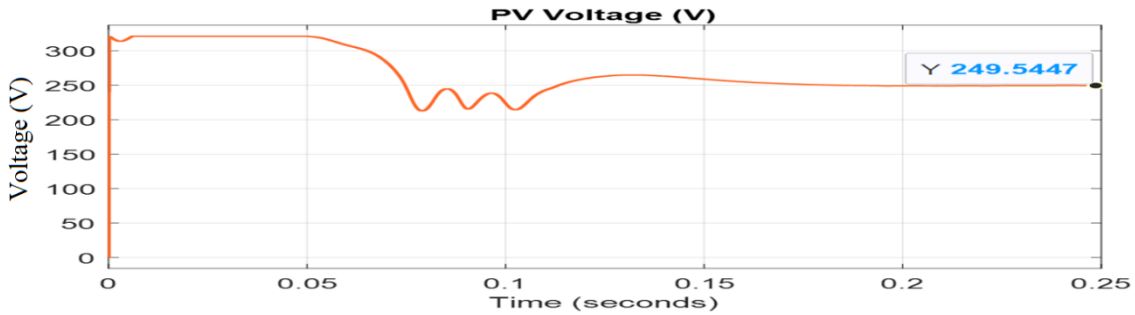
PV Voltage (V)
Voltage (V)
300
250
200
150
100
50
0
Y 249.5447
0
0.05
0.1
0.15
0.2
0.25
Time (seconds)

(f)

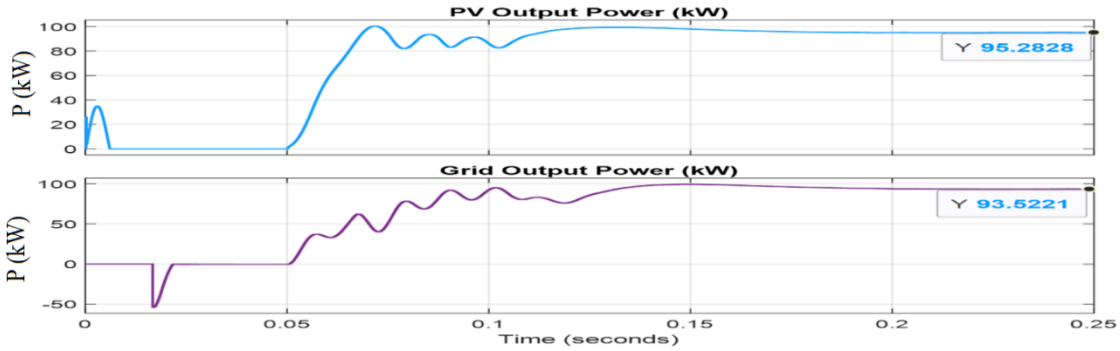
PV Output Power (kW)
P (kW)
100
80
60
40
20
0
Y 95.2828
Grid Output Power (kW)
P (kW)
100
50
0
-50
Y 93.5221
0
0.05
0.1
0.15
0.2
0.25
Time (seconds)

(g)

**Figure 7.7:** (a) Converters Block and De-block graph, (b) DC link and reference voltage, (c) Solar Voltage corresponding to open circuit voltage, (d) Boost converter duty cycle, (e) Regulated DC link voltage, (f) Solar output voltage and power, (g) Solar and Grid Output power.

At t = 0.4 s to 0.6 s, PPP tracking is enabled while the PPP regulator initiates the regulation processing by controlling and varying the duty cycle to extract the peak power. Figure 7.8a depicts the simulation results for solar PV output power and voltage, grid output power and the duty cycle. The solar PV peak power attained is 100.361 kW, the grid power output is 98.7236 kW, the solar PV voltage improves from 251.6923 V to 273.5001 V at t = 0.42 s and sustained the value till t = 0.6 s while the duty cycle goes to 0.44807 and maintained stability at 0.45433 in Figure 8a. The simulation result obtained from the solar PV output voltage in Figure 8a is compared with the solar array specification in equation 7.28. Both results are the same in equation 7.30. The error generated is minimized and reduced to zero at t = 0.42 s by the regulator controller in Figure 7.8b.

$$Solar\ output\ specification = N_{ser} \times Voltage \tag{7.28}$$

$$solar\ output\ specification = 5 \times 54.7 \tag{7.29}$$

$$273.5\ \mathrm{V} \tag{7.30}$$

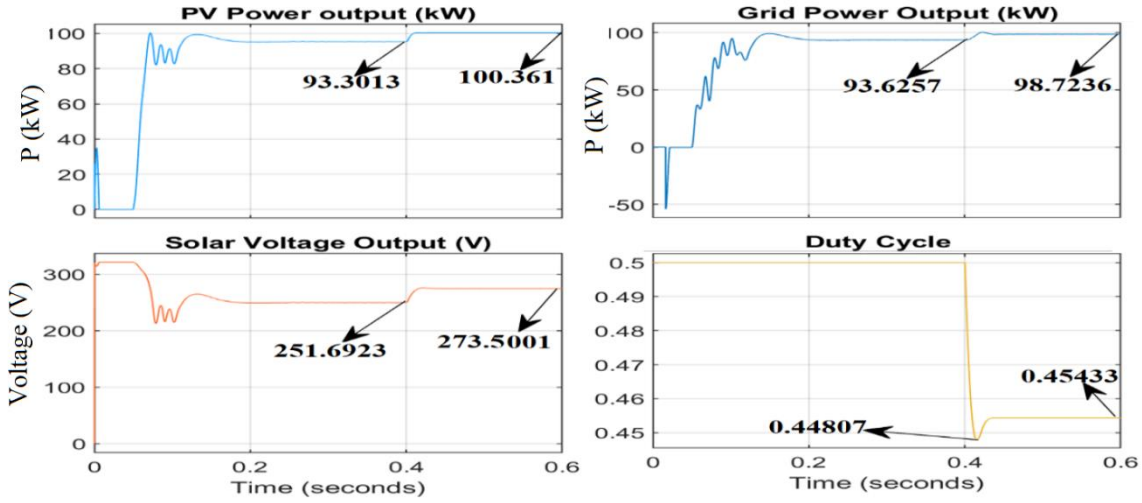


(a)

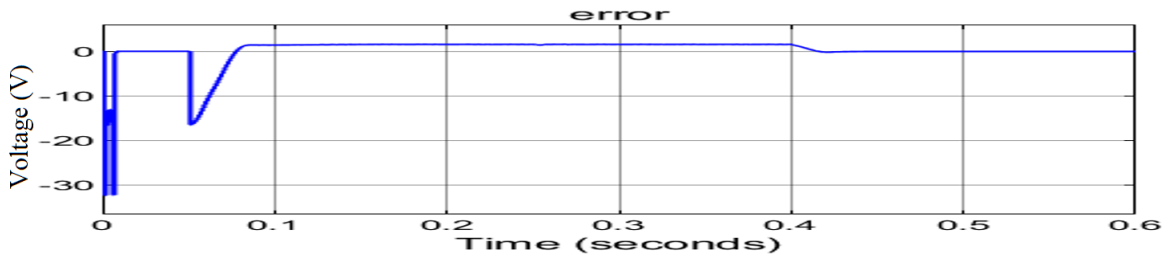


(b)

**Figure 7.8:** (a) PPP Tracking (b) Regulator Reduces Error to Zero at t = 0.4 s.

The simulation response between t = 0.62 s and 1.5 s show that there is a variation in the solar PV irradiance in Figure 7.9, where the irradiance of the sun changes suddenly from $1000\ \mathrm{W/m^2}$ to $251.116\ \mathrm{W/m^2}$ within 0.5 s and maintained stability for 0.1 s. It changes from 251.116 W/m$^2$ to 686.7565 W/m$^2$ within 0.5 s in Figure 7.9a. The temperature remains constant at 25 degrees at t = 1.5 s in Figure 7.9b. The duty cycle keeps changing at t = 1.5 s in Figure 7.9 c but remains stable at t = 2.1 s while D = 0.46007. The variation in the irradiation of the sun results in the reduction of the solar PV and the grid output power. Also, the solar PV output power changes within 0.5 s from 100.361 kW to 25 kW and stable at 69.9254 kW. The grid output power changes from 98.7236 kW to 28.2 kW and remains stable at 65.4836 kW within 0.6 in Figure 7.9d while the temperature remains unchanged at 25 degrees. When *t* is between 1.2 s to 1.54 s, the irradiation of the sun restores back from 251.116 W/m$^2$ to 1000 W/m$^2$ within 0.5 s while the temperature changes within 0.1 s from 25 to 50 degrees in Figure 7.9b. The total duration of the change in the sun irradiation is 1.1 s, during this period, the output power is low, but the IC+IR (the green colour in Figure 7.9e) locates PPP due to equality of conductance *(G=1/V)* and conductance increment *(G=*$\Delta I/\Delta V$*)* while PPP tracking algorithm keeps tracking the peak power. The solar voltage output attains 295 V but remains stable at 290 V at 2.1 s in Figure 7.9f. The application of the *IR* minimizes the error signal, ripples and the oscillation generated at the sliding surface between the instantaneous and incremental conductance in Figure 7.9g. The variation in the irradiation causes the voltage at the boost converter to fluctuate between 0.6 s to 1.6 s in Figure 7.9h but VSI keeps the grid voltage stable throughout the sun irradiation variation in Figure 7.9i. The VSI prevents the occurrence of voltage dip in the grid during the variation in irradiation,

temperature and load. Grid voltage remains within the acceptable range and the current drawn by the loads are very low during the change in the sun irradiation in Figure 7.9j. However, the solar PV output power may change suddenly due to a sudden change in solar irradiation due to the deflection of the incoming beam, clouds, airborne aerosols, snow, ice and reflectivity of the ground surface impacts. However, with the application of the proposed IC+IR algorithm in this research paper to track the solar PV PPP, an acceptable grid voltage and stable solar PV array's voltage output can be achieved. This satisfied the research question stated at the beginning of this thesis. The integral controller improves the precision of both the system's large step sizes when the operational level is far from the PPP and when the small step sizes of PPP is reached to extract the maximum possible level of power. It also minimizes the error (*dI/dV+I/V)* between the instantaneous conductance and the incremental conductance, reduce ripple and improves the accuracy.

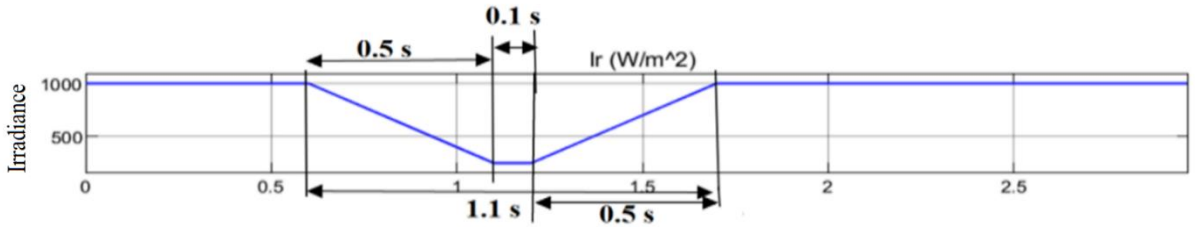


(a)

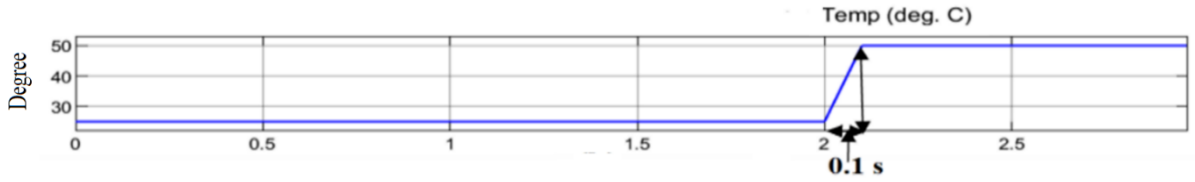


(b)


(c)

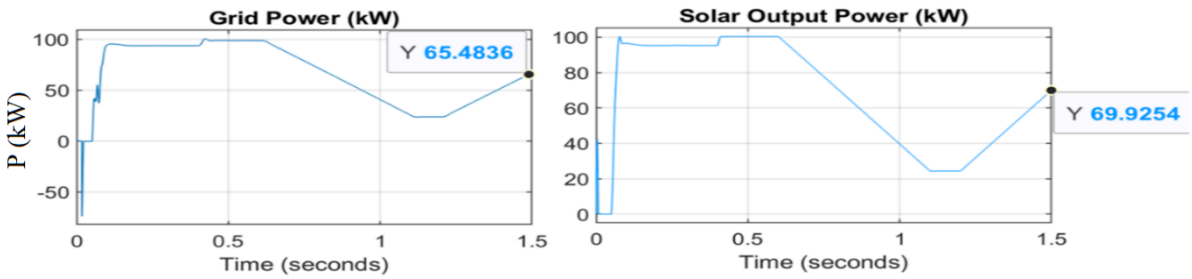
Grid Power (kW)
Y 65.4836
P (kW)
Time (seconds)
Solar Output Power (kW)
Y 69.9254
Time (seconds)

(d)

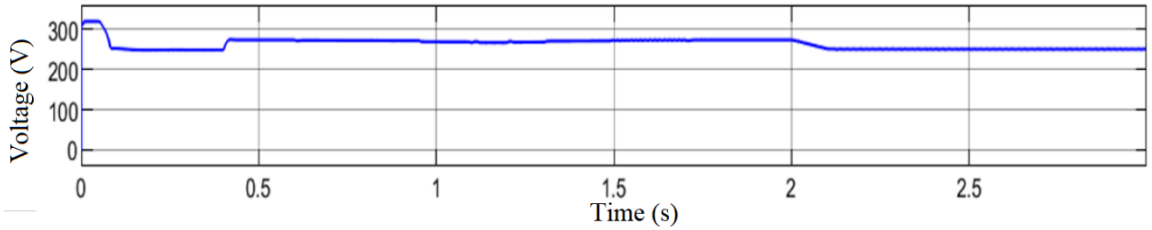
Voltage (V)
Time (s)

(e)

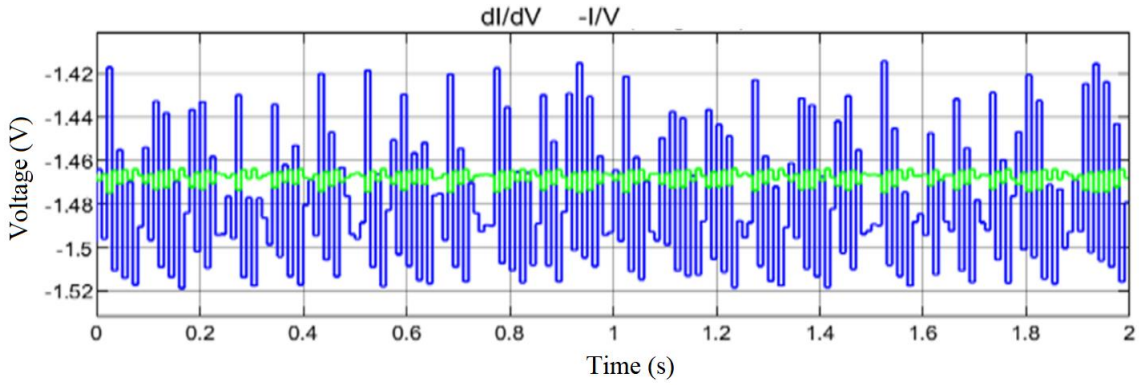
dI/dV -I/V
Voltage (V)
Time (s)

(f)

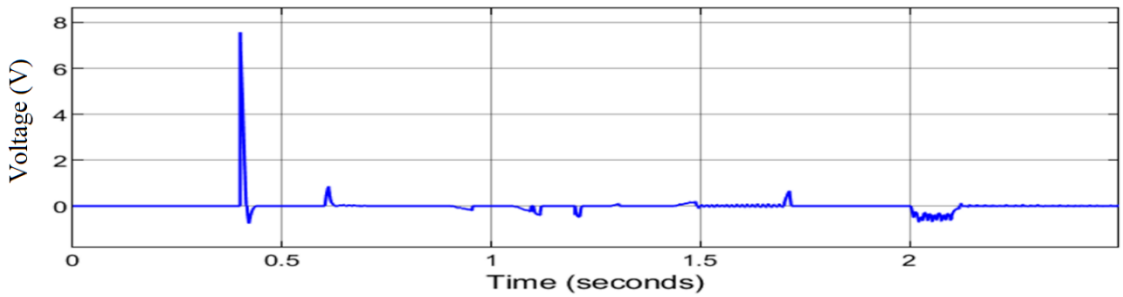
Voltage (V)
Time (seconds)

(g)

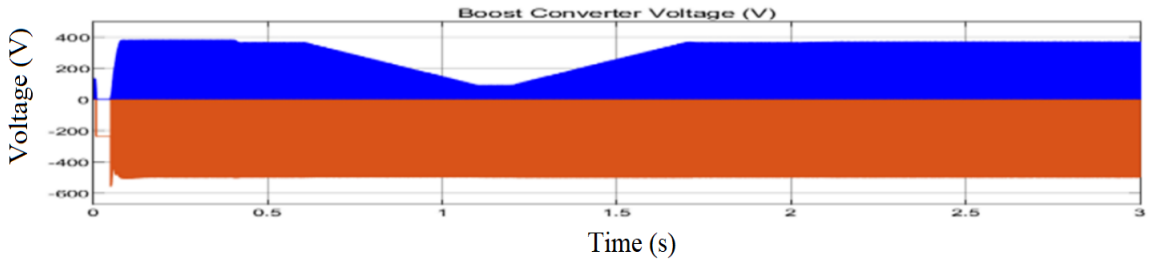


(h)

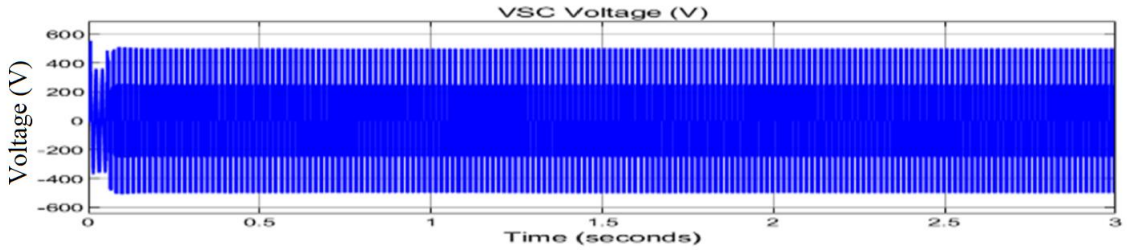


(i)

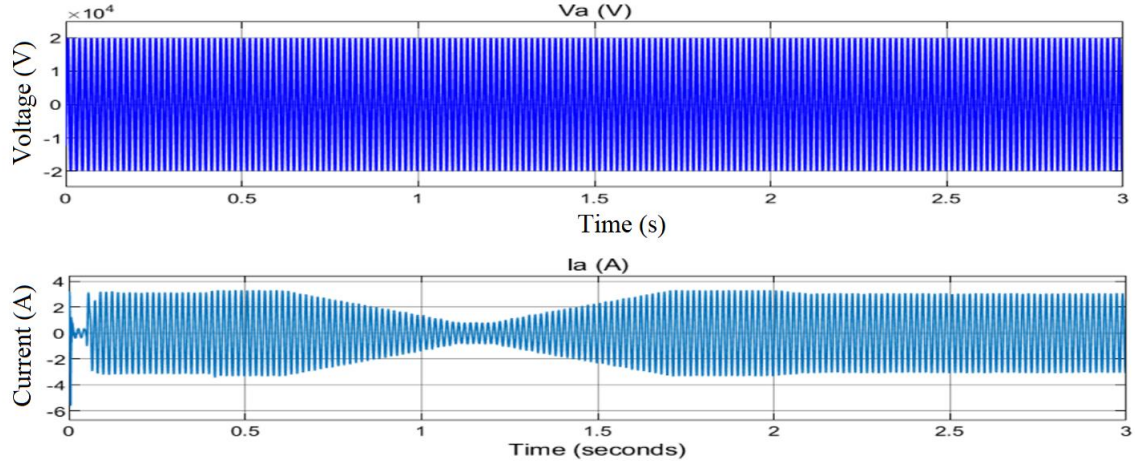


(j)

**Figure 7.9:** (a) Change in the sun Irradiance, (b) Change in the temperature, (c) Duty cycle, (d) Grid and solar output power (e) Solar output Voltage, (f) Incremental conductance algorithm tracking PPP, (g) Error minimizes by the application of Integral regulator scheme, (h) Boost converter and (i) VSC voltage, (j) Grid voltage and current.

## 7.8 Summary

This chapter presents an improved incremental conductance with an integral regulator to extract peak power output from solar photovoltaic array. The proposed method provides an excellent and accurate results in tracking peak power output, an acceptable grid voltage is maintained during weather variations. Hence, ripples and errors (dI/dV+I/V) from PPP tracking of the sliding surface between the instantaneous and incremental conductance are regulated by the integral control application. The proposed converter restoration scheme which incorporates block/de-block control is aimed at protecting the VSC from the grid disturbance and fault current. There is a reduction in the solar output voltage oscillations resulting in a better digital resolution of the output power, perfect control and adaptation of the solar system to the ever-changing climatic condition, thus, the system efficiency is improved. This chapter would recommend two important aspects to plant owners who want to ensure their plant's safety. One is the plant monitoring through the application of an inverter restoration scheme that incorporates block/de-block control and the other is to ensure the safety of the operator, protecting them from shocks and accidents due to the grid faults in solar panels.

# CHAPTER 8

# CONCLUSIONS AND RECOMMENDATIONS FOR FUTURE WORKS

## 8.1 Conclusion

The research investigations carried out in this thesis are divided into two parts. The first part presents in detail the prospect of renewable energy resources. The second part investigates the voltage rise mitigation at PCC with a large RDGs integration into a distribution network.

### 8.1.1 Assessment on the Prospect of Renewable Energy Resource in Africa

***Findings:***

- Most of the renewable energies are still in a developmental stage. The existing capacity still has vast untapped potential while some has not been accessed at all. Very few are in a production phase. RDGs deployment can result in additional economic benefits, such as job creation and socioeconomic growth in rural areas and be a core factor of any low-carbon strategy.

### 8.1.2 Voltage Mitigation at PCC with Large RDG Integration

***Findings:***

- With RDG integration into the power system, power flow is not only unidirectional but bidirectional.
- The is no concern for under voltage in a distribution network with RDG integration because it can improve voltage profiles.
- RDG integration can make a weak network become an active system by the injection of active/reactive power at the PCC.
- There is a potential voltage rise threat at PCC with a large RDG penetration level at the PCC.

- A large integration of RDG to a distribution network can cause reverse power flows to substations due to the node voltage at which RDG is connected to a distribution network that is higher than any other node in the system. The weak node will become an active node, while a further increase in the number of RDGs and penetration levels would result in the power flowing in both directions, that is, to the substation and to the farthest bus in the system.

- Integration of a large RDG can cause voltage rise at PCC.

- Compensator devices with reactive power generation/absorption capabilities can minimize voltage rise at PCC.

- Peak power point tracking error and oscillation can be attenuated with incremental conductance and integral regulator schemes.

- Solar system output voltage and power can be kept stable during load fluctuation, sun irradiance variation and temperature with incremental conductance and integral regulator scheme.

### 8.1.3 Deductions

- RDG integration improves voltage profiles of a distribution network.

- Large RDG integration causes a voltage rise at PCC.

- Voltage rise can be suppressed at PCC with a compensator that can generate/absorb reactive power.

- Grid voltage fluctuation, voltage dips, variation can be minimized with the installation of grid compensators.

- It is therefore important to note that before considering RDG integration to the power system, the power system operator should consider the possibility of power being exported back to the substation in case there is an over generation of power from RDG as this will give them the choice of installing a transformer that can tolerate the operation of reverse power flow.

## 8.2 Recommendation for Future Work

- To further improve power quality of RDG integration at PCC, these future research directions are recommended, online monitoring of power quality parameters can be achieved by considering continuous measurement of voltages, currents, and phase shifts using power quality analyzers to set alarms to warn when these parameters are out of limit.

- An automation system can be developed such that it depends on the unbalance of electrical consumers of different phase and introduces or removes larger units of electrical consumers from one phase to another.

- The impact of the battery banks installation with PPPT optimization of the system is not put into consideration in this study but shall be investigated upon in the near future work.

- Comparison of the impacts of pulse width modulation and PPPT for Solar PVAs charge control for efficient power quality management at PCC shall be investigated and their economic consideration shall be considered.

# REFERENCES

[1] U. Mirza, N. Ahmad, T. Majeed and K. Harijan, “Wind Energy Development in Pakistan,” *Renew. Sustain. Energy Rev,* vol. 11, no. 9, p. 2179–2190, 2007.

[2] M. A. Chaudhry, R. Raza and S. A. Hayat, “Renewable Energy Technologies in Pakistan: Prospects and Challenges,” *Renew. Sustain. Energy Rev,* vol. 13, no. 7, p. 1657–1662, 2009.

[3] H. Abunima and J. Teh, “Reliability Modeling of PV Systems Based on Time Varying Failure Rates,” *IEEE Access,* vol. 8, p. 14367–14376, 2020.

[4] S. Bhattacharya, T. Ramachandran, A. Somani and J. H. Donald, “Impacts of Energy Flexibility in Transactive Energy Systems With Large-Scale Renewable Generation,” *IEEE Access,* vol. 10, pp. 14870-14879, 2022.

[5] P. Mikail and E. T. Belgin, “Optimal Allocation of Renewable Distributed Generations Using Heuristic Methods to Minimize Annual Energy Losses and Voltage Deviation Index,” *IEEE Access,* vol. 10, pp. 21455-21474, 2022.

[6] R. Alejandro, B. Santiago and B. Mostafa, “Integration of Distributed Energy Resources to Unbalanced Grids Under Voltage Sags With Grid Code Compliance,” *IEEE Transactions on Smart Grid,* vol. 13, no. 1, pp. 355 - 366, 2022.

[7] S. A. Ahmed, T. Dave and H. M. Tarek, “Impact Assessment and Mitigation Techniques for High Penetration Levels of Renewable Energy Sources in Distribution Networks: Voltage-control Perspective,” *Journal of Modern Power Systems and Clean Energy,* vol. 10, pp. 450 - 458 , 2022.

[8] S. Ayyadi and M. Maaroufi, “Optimal Framework to Maximize the Work-place Charging Station Owner Profit While Compensating Electric Vehicles Users,” *Math. Problems Eng.,* pp. 1-12, 2020.

[9] M. B. Shafik, G. I. Rashed and H. Chen, “Optimizing Energy Savings and Operation of Active Distribution Networks Utilizing Hybrid Energy Resources and Soft Open Points: Case Study in Sohag, egypt,” *IEEE Access,* vol. 8, p. 28704–28717, 2020.

[10] K. G. Khajeh, D. Solatialkaran, F. Zare and N. Mithulananthan, “Harmonic Analysis of Multi-parallel Grid Connected Inverters in Distributionnetworks: Emission and Immunity Issues in the Frequency Range of 0-150kHz,” *IEEE Access,* vol. 8, p. 56379–56402, 2020.

[11] H. Ren and X. Shi, “Study on Switching Overvoltage of 500kV Hydropower Station with GIL Outgoing Line,” in *International Conference on Power, Energy and Electrical Engineering (CPEEE)*, Shiga, Japan, 2022.

[12] S. A. Augusto, D. A. Luis, I. B. Danilo, T. Elisabetta and P. M. Fernando, “Integrated Local and Coordinated Overvoltage Control to Increase Energy Feed-In and Expand DER Participation in Low-Voltage Networks,” *IEEE Transactions on Sustainable Energy,* vol. 13, no. 2, pp. 1049 - 1061, 2022.

[13] S. K. Deepa and J. S. Savier, “Impact analysis of Distributed Generation Integration on Distribution Network Considering Smart Grid Scenario,” in *IEEE Region 10 Symposium (TENSYMP)*, Cochin, India, 2017.

[14] C. Bogdan-Ionut, S. Dezso, A. Elena, K. Tamas, A. M. Vlad and T. Remus, “Improved Voltage Regulation Strategies by PV Inverters in LV Rural Networks,” in *IEEE International Symposium on Power Electronics for Distributed Generation Systems (PEDG)*, Aalborg, Denmark, 2022.

[15] H.G. Ignacio, Z. Zhipeng, B. N. Mike and D. Sasa Z, “DG Locational Incremental Contribution to Grid Supply Level,” *IEEE Transactions on Industry Applications,* vol. 58, no. 1, pp. 5 - 14, 2022.

[16] R. Wesam, M. Morcos, S. B. Robert, A. P. Aaqib, M. B. Miroslav and Z. Dao, “Analysis of the Capacitor-Less D-STATCOM for Voltage Profile Improvement in Distribution Network With High PV Penetration,” *IEEE Open Journal of Power Electronics,* vol. 3, pp. 255 - 270, 2022.

[17] S. A. Augusto, D. O. A. Luis, I. B. Danilo, T. Elisabetta and P. M. Fernando , “Integrated Local and Coordinated Overvoltage Control to Increase Energy Feed-In and Expand DER Participation in Low-Voltage Networks,” *IEEE Transactions on Sustainable Energy,* vol. 13, no. 2, pp. 1049 - 1061, 2022.

[18] R. Alejandro, B. Santiago and B. Mostafa, “Integration of Distributed Energy Resources to Unbalanced Grids Under Voltage Sags With Grid Code

Compliance," *IEEE Transactions on Smart Grid,* vol. 13, no. 1, pp. 355 - 366, 2022.

[19] M. H. Bollen and F. Hassan, Integration of Distributed Generation in the Power System, USA: Hoboken, NJ: Wiley, 2011.

[20] R. M. Elavarasan, G. M. Shafiullah, S. Padmanaban, N. M. Kumar, A. Annam, A. M. Vetrichelvan, L. Mihet-Popa and J. B. Holm-Nielsen, "A comprehensive Review on Renewable Energy Development, Challenges,and Policies of Leading Indian States with an International Perspectiv," *IEEE Access,* vol. 8, p. 74432–74457, 2020.

[21] M. U. Afzaal, I. A. ISajjad, A. B. Awan, K. N. Paracha, M. F. Khan, A. R. Bhatti, M. Zubair, W. U. Rehman, S. Amin, S. S. Haroon, R. Liaqat, W. Hdidi and I. Tlili, "Probabilistic Generation Model of Solar Irradiancefor Grid Connected Photovoltaic Systems Using Weibull Distribution," *Sustainability,* vol. 12, no. 6, p. 2241, 2020.

[22] A. Welfle, P. Thornley and M. Röder, "A Review of the Role of Bioenergy Modelling in Renewable Energy Research & Policy Development,'', vol. 136, May 2020, Art. no. 105542," *Biomass Bioenergy,* vol. 136, no. 105542, pp. 1-17, 2020.

[23] J. Z. Thellufsen, H. Lund, P. Sorknæs, P. A. Østergaard, M. Chang, D. Drysdale, S. Nielsen, S. R. Djørup and K. Sperling, "Smart Energy Cities in a 100% Renewable Energy Context," *Renew. Sustain. Energy Rev,* vol. 129, no. 109922, pp. 1-11, 2020.

[24] D. Ali and A. U. Rehman, "Adoption of Autonomous Mining System in Pakistan Policy, Skill Set, Awareness and preparedness of Stakeholders," *Resour. Policy,* vol. 68, no. 101796, pp. 1-13, 2020.

[25] R. Pranoy, H. JiangBiao, Z. Tiefu and V. S. Yash, "Recent Advances of Wind-Solar Hybrid Renewable Energy Systems for Power Generation: A Review," *IEEE Open Journal of the Industrial Electronics Society,* vol. 3, pp. 81 - 104, 2022.

[26] A. Loiy, D. A. Adnan, M. A. Ahmad, A. Mohammad, A. Abdulaziz and A. M. Mohamed, "A Demand Supply Matching-Based Approach for Mapping Renewable Resources Towards 100% Renewable Grids in 2050," *IEEE Access,* vol. 9, pp. 58634-58651, 2021.

[27] H. Junjie, L. Xuetao, S. Mohammad and X. Shiwei, “Optimal Operation of Energy Hubs With Large-Scale Distributed Energy Resources for Distribution Network Congestion Management,” *IEEE Transactions on Sustainable Energy,* vol. 12, no. 3, pp. 1755-1765, 2021.

[28] L. A. Metz, O. R. Davidson, P. R. Bosch and R. Dave, “Contribution of Working Group III to the Fourth Assessment Report of the Intergovernmental Panel on Climate Change,” Ambridge Univ, Cambridge, U.K, 2007.

[29] D. Apostolopoulou and M. McCulloch, “Optimal Short-term Operation of a Cascaded Hydro-Solar Hybrid System: A Case Study in Kenya,” *IEEE Trans. Sustain. Energy,* vol. 10, no. 4, p. 1878–1889, 2018.

[30] I. Fairley, P. Evans, C. CWooldridge, M. Willis and I. Masters, “Evaluation of Tidal Stream Resource in a Potential Array Area via Direct Measurements,” *Renew. Energy,* vol. 57, p. 70–78, 2013.

[31] L. Grzegorz, S. Beata, C. Katarzyna, Z. Grzegorz and W. Magdalena, “Influence of Photovoltaic Development on Decarbonization of Power Generation—Example of Poland,” *Energies,* vol. 14, no. 22, p. 7819, 2021.

[32] D. Apostolopoulou, Z. DeGrève and M. McCulloch, “Robust Optimization for Hydroelectric System Operation Under Uncertainty,” *IEEE Trans. Power Syst,* vol. 33, no. 3, p. 3337–3348, 2018.

[33] G. P. Steven and J. C. William, “Model Validation of Hydrodynamic Loads and Performance of a Full-scale Tidal Turbine Using Tidal Bladed, International Journal of Marine Energy, 16, 279-297, 2016,” *Energies,* vol. 16, pp. 279-297, 2016.

[34] D. Borkowski and T. Wegiel, “Small Hydropower Plant with Integrated Turbine-Generators Working at Variable Speed,” *IEEE Trans. Energy Convers,* vol. 28, no. 2, p. 452–459, 2013.

[35] S. Jaber, “Environmental Impacts of Wind Energy,” *J. Clean Energy Technol.,* vol. 1, no. 3, p. 251–254, 2013.

[36] H. Kazari, H. Oraee and B. C. Pal, “Assessing the Effect of Wind Farm Layout on Energy Storage Requirement for Power Fluctuation Mitigation,” *IEEE Trans. Sustain. Energy,* vol. 10, no. 2, p. 558–568, 2019.

[37] S. Anita, K. Iwona, G. Miroslava and G. Radomir, “The Criteria for Suitable Location of Geothermal Power Plant,” in *International Scientific Conference on Electric Power Engineering (EPE),*, Kouty nad Desnou, Czech Republic, 2017.

[38] M. Malinowski, J. I. Leon and H. Abu-Rub, “Solar Photovoltaic and Thermal Energy Systems: Current Technology and Future Trends,” *Proc. IEEE,,* vol. 105, no. 11, p. 2132–2146, 2017.

[39] J. Holmes and L. Papay, “Prospects for Electricity from Renewable Resources in the United States,” *Journal of Renewable and Sustainable Energy,* vol. 3, no. 4, 2011.

[40] Y. Syaifuddin, N. Muhammad, Irhamni and M. Dewi, “Biomass waste as a renewable energy in developing bio-based economies in Indonesia: A review,” *Renewable and Sustainable Energy Reviews,* vol. 160, pp. 1-12, 2022.

[41] F. Zabihian and A. Fung, “Fuel and GHG Emission Reduction Potentials by Fuel Switching and Technology Improvement in the Iranian Electricity Generation Sector,” *Int. J. Eng,* vol. 3, no. 2, p. 159, 2009.

[42] S. R. Sharvini, Z. Z. Noor, C. S. Chong, L. C. Stringer and R. O. Yusuf, “Energy Consumption Trends and their Linkages with Renewable Energy Policies in East and Southeast Asian Countries: Challenges and Opportunities,” vol. 28, pp.,” *Sustain. Env,* vol. 28, p. 257–266, 2018.

[43] A. Sameer and C. S. Umesh, “Hydroelectric Power,” in *Energy Science & Technology: Opportunities and Challenges*, US, Studium Press LLC, 2016.

[44] A. Qazi, “Towards Sustainable Energy: A Systematic Review of Renewable Energy Sources, Technologies, and Public Opinions,” *IEEE Access,* vol. 7, p. 63837–63851, 2019.

[45] R. Sukanta, B. Shawli, K. Yogesh and K. D. Sudhir, K. D, “Recent technology and challenges of wind energy generation: A review,” *Sustainable Energy Technologies and Assessments,* vol. 52, pp. 1-17, 2022.

[46] Worldometers, “Worldometers Africa Population,” 2020. [Online]. Available: https://www.worldometers.info/worldpopulation/africa-population/. [Accessed 2021].

[47] F. Mazza, B. Buchner and V. Micale, “Understanding the Landscape Tracking Finance for Electricity and Clean Cooking Access in High-impact Countries,” in *Sustainable Energy for All*, Washington, USA, 2017.

[48] USAID, “Power Africa,” 2019. [Online]. Available: https://www.usaid.gov/powerafrica/nigeria. [Accessed 2021].

[49] A. K. Sonja, S. S. Wei, A. S. Arshad, B. Poovarasi, M. Saad and T. Nisha, “Energy Policies Shaping the Solar Photovoltaics Business Models in Malaysia,” *Energy Policy,* vol. 163, pp. 1-14, 2022.

[50] L. S. Vinay, H. J. Vernon and V. Anthony, “Opening Doors to the World,” World Bank Publications, Washington, 2017.

[51] M. Hulme, R. Doherty, T. Ngara, M. New and D. Lister, “African Climate Change: 1900-2100,” *Clim. Res,* vol. 17, no. 2, p. 145–168, 2001.

[52] P. D. Jones, D. H. Lister, T. J. Osborn, C. Harpham, M. Salmon and C. P. Morice, “Hemispheric and Large-scale Land-surface Air Temperature Variations: An Extensive Revision and an Update to 2010,” *Res.,* vol. 117, no. 5, p. 1–17, 2015.

[53] F. Mwasilu and J. W. Jung, “Potential for Power Generation from Ocean-wave Renewable Energy Source: A comprehensive Review on State-of-the-art Technology and Future Prospects,” *IET Renew. Power Gener,* vol. 13, no. 3, p. 2019, 363–375.

[54] M. Vikas, R. Subba and J. K. Seelam, “Tidal Energy: A Review,” in *Proc. Int. Conf. Hydraul. Water Resource Coast. Eng*, India, 2016.

[55] A. Roberts, “Current Tidal Power Technologies and their Suitability for Applications in Coastal and Marine Areas,” *J. Ocean Eng. Mar. Energy,* vol. 2, p. 227–245, 2016.

[56] R. Howell, N. Qin, J. Edwards and N. Durrani, “Wind Tunnel and Numerical Study of a Small Vertical Axis Wind Turbine,” *Renewable Energy,* vol. 35, no. 2, p. 412–422, 2010.

[57] T. Fujio, N. Shoji and Y. Ken-ichiro , “Experimental Studies on Dynamic Performances of Wind Power Plants Composed of Series-Connected Wind Generators and Synchronous-Compensator-Commutated Thyristor Inverter,” *IEEE Transactions on Industry Applications,* vol. 57, no. 4, pp. 4001-4008, 2021.

[58] T. Yacine, S. Chun-Lien, L. Abderezak, U. M. Muhammad, M. Mojtaba , M. G. Josep and C. V. Juan , “Design of Cost-Effective Compensators to Enhance Voltage Stability and Harmonics Contamination of High-Power More Electric Marine Vessels,” *IEEE Transactions on Industry Applications,* vol. 57, no. 4, pp. 4130-4142, 2021.

[59] H. Lingxi, Z. Shuqing, W. Yingdong, Z. Biao and J. Qirong, “A Dynamic Series Voltage Compensator for the Mitigation of LCC-HVDC Commutation Failure,” *IEEE Transactions on Power Delivery,* vol. 36, no. 6, pp. 3977-3987, 2021.

[60] E. E. Ahmed, A. V. Evgeniy, A. R. Pavel and I. P. Dmitry, “Power Flow Control Using Transformer-less Static Synchronous Series Compensators,” in *International Youth Conference on Radio Electronics, Electrical and Power Engineering (REEPE)*, Moscow, Russia, 2021.

[61] M. A. Camil, A. Gómez-Expósito, M. V. Guillermo and J. M. Maza-Ortega, “Optimal Coordinated Operation of Distributed Static Series Compensators for Wide-Area Network Congestion Relief,” *Journal of Modern Power Systems and Clean Energy,* pp. 1-1, 2021.

[62] W. Ping and C. Minjie, “Analysis and Design of Series Voltage Compensator for Differential Power Processing,” *IEEE Journal of Emerging and Selected Topics in Power Electronics,* pp. 1-1, 2021.

[63] S. Hojoon, S. Yeongrack and H. Jung-Ik, “Grid Current Shaping Method with DC-Link Shunt Compensator for Three-Phase Diode Rectifier-Fed Motor Drive

System," *IEEE Transactions on Power Electronics,* vol. 32, no. 2, pp. 1279-1288, 2017.

[64] Z. Wolanski and T. O. Boon, "Conceptual Study of a Shunt Power Quality Compensator," *IEEE Transactions on Power Delivery,* vol. 11, no. 2, pp. 1059-1065, 1996.

[65] A. P. Marcelo, C. Salvador, K. Georgios, P. Josep and P. A. Ricardo, "Modular Multilevel Converters: Recent Achievements and Challenges," *IEEE Open Journal of the Industrial Electronics Society,* vol. 1, pp. 224-239, 2021.

[66] A. K. Mehrdad, S. Hassan, C. Ilhami, S. B. Shahab and E. Kei, "Optimal Location of FACTS Devices in Order toSimultaneously Improving Transmission Lossesand Stability Margin Using Artificial BeeColony Algorithm," *IEEE Access,* vol. 9, pp. 125920-125929, 2021.

[67] A. D. Roux and H. D. Mouton, "A Series-shunt Compensator with Combined UPS Operation," in *IEEE International Symposium on Industrial Electronics Proceedings*, Pusan, Korea (South), 2001.

[68] A. P. Marcelo, C. Salvador, K. Georgios, P. Josep and P. A. Ricardo, "Modular Multilevel Converters: Recent Achievements and Challenges," *IEEE Open Journal of the Industrial Electronics Society,* vol. 2, pp. 224-239, 2021.

[69] H. Awad, H. Nelsen, F. Blaabjerg and M. J. Newman, "Operation of Static Series Compensator Under Distorted Utility Conditions," *IEEE Transactions on Power Systems,* vol. 20, no. 1, pp. 448-457, 2005.

[70] L. Haijun, M. Yihan, X. Xiong and W. Lucai , "A Method for Nonlinear Error Compensation of Load Cell Based on Neural Network With Second Derivative Constraints," *IEEE Sensors Journal,* vol. 21, no. 15, pp. 16997-17004, 2021.

[71] B. Ehsan, B. Massimo, R. S. Jan and M. Aravind, "A Novel Capacitor-Voltage Balancing Strategy for Double-Y STATCOM Under Unbalanced Operations," *IEEE Transactions on Industry Applications,* vol. 57, no. 3, pp. 2692-2701, 2021.

[72] L. Daorong, S. Chenxing, Y. Yu, L. Xiang, H. Haibing and X. Yan, "Flexible Nonsinusoidal Zero Sequence Voltage Injection Method to Extend Negative

Sequence Current Compensation Range for Star-Connected CHB STATCOM," *IEEE Transactions on Power Electronics,* vol. 36, no. 10, pp. 11357-11371, 2021.

[73] B. P. Sathish, C. K. Sundarabalan, N. S. Srinath;, T. S. Krishnan, G. S. Priya, C. Balasundar, J. Sharma, G. Soundarya, S. Pierluigi and H. A. Hassan , "Power Quality Enhancement in Sensitive Local Distribution Grid Using Interval Type-II Fuzzy Logic Controlled DSTATCOM," *IEEE Access,* vol. 9, pp. 59888-59899, 2021.

[74] T. Tomasz , G. J. Shantha, G. Mariusz, P. Andrzej, S. Viknash , L. Wenzhao and M. G. Josep , "Review of Power Quality Issues in Maritime Microgrids," *IEEE Access,* vol. 9, pp. 81798-81817, 2021.

[75] C. Soham, M. Susovan and K. B. Sujit, "Coordination of D-STATCOM & SVC for Dynamic VAR Compensation and Voltage Stabilization of an AC Grid Interconnected to a DC Microgrid," *IEEE Transactions on Industry Applications,* pp. 1-11, 2021.

[76] V. Lavr and M. Zdeněk, "Dynamic Stability Improvement of Power System by Means of STATCOM With Virtual Inertia," *IEEE Access,* vol. 9, pp. 116105-116114, 2021.

[77] B. Aliasghar, B. Rui, D. G. Misagh, V. Mehdi and U. R. Waqas, "Evolutionary Algorithm-Based Adaptive Robust Optimization for AC Security Constrained Unit Commitment Considering Renewable Energy Sources and Shunt FACTS Devices," *IEEE Access,* vol. 9, pp. 123575-123587, 2021.

[78] H. B. Nagesh and P. S. Puttaswamy, "Enhancement of Voltage Stability Margin Using FACTS Controllers," *International Journal of Computer and Electrical Engineering,* vol. 5, no. 2, pp. 1-5, 2013.

[79] M. Sohrab, D. Subash, T. Dimitrios, M. S. Dalila, L. Meng, W. Xiaojun, Z. Pei and H. Jinghan, "Optimization of FACTS Devices: Classification, Recent Trends, and Future Outlook," in *IEEE 4th International Electrical and Energy Conference (CIEEC)*, Wuhan, China, 2021.

[80] B. Miodrag and D. Dražen, "Hybrid Mmultilevel Converter for Variable DC Link Voltage Operation," *Transactions on Power Electronics and Applications,* vol. 6, no. 2, pp. 178-190, 2021.

[81] D. Li, L. Yuzhuo and W. L. Yun, “A New Current Source Converter Using AC-Type Flying-Capacitor Technique,” *IEEE Transactions on Power Electronics,* vol. 36, no. 6, pp. 10307-10316, 2021.

[82] S. Jayadeep, R. A. Sabha and M. Rakesh, “Distribution Static Compensator Using an Adaptive Observer Based Control Algorithm With Salp Swarm Optimization Algorithm,” *Transactions on Power Electronics and Applications,* vol. 6, no. 1, pp. 52-62, 2021.

[83] A. K. Mohamed, N. N. George and M. M. Christopher, “DSTATCOM Application for Distribution Network Power Quality Enhancement: A Review,” in *IEEE PES/IAS PowerAfrica*, Nairobi, Kenya, 2021.

[84] B. M. Rudresh, C. J. Sudhakar, V. D. Avinash and N. D. Sateesh , “Optimal Placement of Multiple STATCOM and It’s Impact on Voltage Stability,” in *International Conference on Advanced Computing and Communication Systems (ICACCS)*, Coimbatore, India, 2021.

[85] P. Vitor, C. Armando, F. Daniel and S. Fernando, “A Multilevel Converter Topology for a STATCOM System Based on Four-Leg Two-Level Inverters and Cascaded Scott Transformers,” *IEEE Transactions on Power Delivery,* pp. 1-12, 2021.

[86] P. Basanagouda and S. B. Karajgi, “A Review on Optimal Placement of FACTS Devices in Deregulated Environment- A Detailed Perspective,” in *International Conference on Electrical, Electronics, Communication, Computer, and Optimization Techniques (ICEECCOT)*, Mysuru, India, 2017.

[87] J. Tibin, E. U. Carlos, L. Jun and F. C. Paul, “Asset Management Strategies for PowerElectronic Converters in Transmission Networks:Application to Hvdc and FACTS Devices,” *IEEE Access,* vol. 6, pp. 21084-21102, 2021.

[88] S. C. Gajendra, G. S. Abdul Gafoor Shaik, P. M. Om , P. Sanjeevikumar and B. H. Jens, “Comprehensive Review of Distributed FACTSControl Algorithms for Power QualityEnhancement in Utility Grid With RenewableEnergy Penetration,” *IEEE Access,* vol. 8, pp. 107614-107634, 2021.

[89] B. Aliasghar, B. Rui, D. G. Misagh, V. Mehdi and U. R. Waqas, “Evolutionary Algorithm-Based Adaptive RobustOptimization for AC Security Constrained

UnitCommitment Considering Renewable EnergySources and Shunt FACTS Devices," *IEEE Access,* vol. 9, pp. 123575-123587, 2021.

[90] C. Wu, Y. Han, N. Yang and C. Xu, "Modeling and Fractional-order Adaptive Nonsingular Terminal Sliding Mode Control for Fractional-order Ferroresonance System," in *Chinese Control Conference (CCC)*, Dalian, China, 2017.

[91] A. Toqeer, W. Asad, M. E. Rajvikram, I. Junaid, P. Manoharan and S. Umashankar, "Analysis of Fractional Order Sliding Mode Control in a D-STATCOM Integrated Power Distribution System," *IEEE Access,* vol. 9, pp. 70337-70352, 2021.

[92] L. Jeremias, "Fast Fourier Transform for Extracting Frequencies Component of Power System Harmonics," *Jurnal Pengembangan Wilayah dan Masyaraka,* vol. 9, no. 2, pp. 26-37, 2010.

[93] H. Mageed, A. S. Nada, S. Abu-Zaid and R. S. Salah Eldeen, "Effects of Waveforms Distortion for Household Appliances on Power Quality," *Journal of Metrology Society of India,* vol. 34, no. 4, p. 559–572, 2019.

[94] W. Yibo, Y. Bo and W. Xianglin, "Study on Time-frequency Hybrid Noise Reduction Method of Low Voltage Power-line signal Based on Reactive Compensation," in *IEEE International Symposium on Next-Generation Electronics*, Changsha, China, 2021.

[95] M. Partha, B. Jaydeb and S. Angsuman, "Power Supply Noise Aware Physical Design with Decoupling Capacitance Allocation in System-on-Chip," in *Devices for Integrated Circuit (DevIC)*, Kalyani, India, 2021.

[96] R. B. Manisha, D. Rahul and S. R. Surendra, "Simultaneous Switching Noise Reduction in High Speed Circuits," in *IEEE International Conference on Communication Information and Computing Technology (ICCICT)*, Mumbai, India, 2021.

[97] S. N. Shravan, F. Yongping and R. K. Peter, "Auxiliary Feed-Forward Noise Cancellation Techniques for a Generic Type-II Ring Oscillator Phase Locked Loop," *IEEE Transaction on Circuits and Systems Express Briefs,* vol. 68, no. 5, pp. 1670-1674, 2021.

[98] A. Rash, “Harmonics-What are they, How to Measure Them and How to Solve the Problem (in Connection with Standards IEEE 1159-1995 and IEEE 519-1992),” in *Proceedings of 19th Convention of Electrical and Electronics Engineers in Israel*, Jerusalem, Israel, 1996.

[99] Halpin, “Revisions to IEEE Standard 519-1992,” in *IEEE/PES Transmission and Distribution Conference and Exhibition*, Dallas, TX, USA, 2006.

[100] M. M. Swamy, S. L. Rossiter, M. C. Spencer and M. Richardson, “Case Studies on Mitigating Harmonics in ASD Systems to Mmeet IEEE 519-1992 Standards,” *IEEE Industry Applications Society Annual Meeting,* vol. 1, pp. 685-692, 1994.

[101] E. W. Gunther, “Interharmonics Recommended Updates to IEEE 519,” in *IEEE Power Engineering Society Summer Meeting,*, Chicago, IL, USA, 2002.

[102] E. W. Gunther, “Interharmonics in Power Systems,” in *Power Engineering Society Summer Meeting. Conference Proceedings* , Vancouver, BC, Canada, 2001.

[103] K. Piotr and W. Grzegorz, “Dependence of Voltage Fluctuation Severity on Clipped Sinewave Distortion of Voltage,” *IEEE Transactions on Instrumentation and Measurement,* vol. 70, pp. 2006008-2006013, 2021.

[104] M. F. McGranaghan and D. R. Mueller, “Designing Harmonic Filters for Adjustable-Speed Drives to Comply with IEEE-519 Harmonic Limits,” *IEEE Transactions on Industry Applications,* vol. 35, no. 2, pp. 312-318, 1999.

[105] B. Julio, A. Matilde and I. D. Ramón, “Voltage Notch Detection and Analysis Using Wavelets,” in *IEEE International Conference on Virtual Environments, Human-Computer Interfaces, and Measurement Systems* , Istambul, Turkey, 2008.

[106] L. Shengyu, X. Youze, L. Chenglong, Z. Bin, Z. Yanlong, W. Xiaoli and G. Li, “A 0.025% DC Current Mismatch Charge Pump for PLL Applications,” in *IEEE International Midwest Symposium on Circuits and Systems (MWSCAS)*, Lansing, MI, USA, 2021.

[107] S. S. Kwang, P. Sung-Jun and K. Feel-Soon, “Internal Parameter Estimation of Lithium-Ion Battery Using AC Ripple With DC Offset Wave in Low and High Frequencies,” *IEEE Access,* vol. 9, pp. 76083-76096, 2021.

[108] M. Mohamed, H. Mahmoud, B. S. Jaleleddine and A. Kamal Al-Haddad, “A Third-Order MAF Based QT1-PLL That is Robust Against Harmonically Distorted Grid Voltage With Frequency Deviation,” *IEEE Transactions on Energy Conversion,* vol. 36, no. 3, pp. 1600-1613, 2021.

[109] W. Aimin, L. Sheng, Z. Qi, H. Yang, W. Jianzhou and H. Zhengyou, “Calculation of transformer DC-bias Current in AC Power Systems Considering Metro Stray Current,” in *Asia Conference on Power and Electrical Engineering (ACPEE)*, Chongqing, China, 2021.

[110] C. Alessio, C. Riccardo, R. Diego and V. Alessandro, “Digital Strategy to Compensate Offset Currents into DC-DC Dual Active Bridge Converter Simulations,” in *IEEE Fourth International Conference on DC Microgrids (ICDCM)*, Arlington, VA, USA, 2021.

[111] A. S. Akinyemi and K. Awodele, “Voltage Profiles Improvement with Wind Energy Converter Connected to a Distribution Network,” in *Southern African University Power Engineering Conference (SAUPEC)*, Johannesburg, South Africa, 20015.

[112] A. S. Akinyemi and I. E. Davidson, “Impact of Renewable Energy Generation on Voltage Flicker with Dynamic Load Connected to Distribution Network,” *International Journal of Applied Engineering Research,* vol. 14, no. 14, pp. 3137-3145, 2019.

[113] A. S. Akinyemi, “Optimum Impacts of Renewable Energy Generation on Voltage Dip and Voltage Profile in a Distribution Network,” *International Journal of Scientific & Engineering Research,* vol. 10, no. 8, pp. 280-291, 2019.

[114] N. D. Rudra, S. Sangeeta and K. P. Chinmoy, “Effect and Analysis of Unbalanced Voltage on Induction Motor Torque,” in *International Conference on Recent Innovations in Electrical, Electronics & Communication Engineering (ICRIEECE)*, Bhubaneswar, India, 2018.

[115] C. Shivam and B. S. Shashi, “Effects of Voltage Unbalance and Harmonics on 3-Phase Induction Motor During the Condition of Undervoltage and Overvoltage,” in *International Conference on Signal Processing and Integrated Networks (SPIN)*, Noida, India, 2019.

[116] H. Adel, S. Amir and V. Maria, “A Linear AC Power Flow Model for Unbalanced Multi-Phase Distribution Networks Based on Current Injection Equations,” *IEEE Transactions on Power Systems,* vol. 36, no. 4, pp. 3806-3809, 2021.

[117] I. A. Aderibigbe, “A New Definition of Voltage Unbalance Using Supply Phase Shift,” *Journal of Control, Automation and Electrical Systems,* pp. 1-8, 2019.

[118] O. O. Osaloni and A. S. Akinyemi, “Voltage Profile improvement and Loss Reduction in LV Distribution network using Genetic Algorithm,” *International Journal of Scientific & Engineering Research,* vol. 10, no. 7, pp. 1857-1863, 2019.

[119] W. Shengyi, D. Liang, F. Xiaoyuan and H. Qiuhua, “Deep Reinforcement Scheduling of Energy Storage Systems for Real-Time Voltage Regulation in Unbalanced LV Networks With High PV Penetration,” *IEEE Transactions on Sustainable Energy,* vol. 12, no. 4, pp. 2342-2352, 2021.

[120] S. G. Juan, P. V. Pedro, C. L. Juan , H. N. Phuong and G. P. Nikolaos, “A Linear AC-OPF Formulation for Unbalanced Distribution Networks,” *IEEE Transactions on Industry Applications,* vol. 57, no. 5, pp. 4462-4472, 2021.

[121] NEMA, “Motors and Generators, ANSI/NEMA Standard MG1-1993,” NEMA, 1993.

[122] IEEE, “IEEE Standard Test Procedure for Polyphase Induction Motors and Generators IEEE Standard 112,” IEEE, 1991.

[123] R. C. Dugan, M. F. McGranaghan and H. W. Beaty, “Electrical Power Systems Quality,” McGraw-Hill, New York, 1996.

[124] L. Wel, Q. Ziwei, W. Qi, W. Yu, L. Fusuo, Z. Ling and C. Shuo, “Transient Voltage Control of Sending-End Wind Farm Using a Synchronous Condenser Under Commutation Failure of HVDC Transmission System,” *IEEE ACCESS,* vol. 9, pp. 54900-54911, 2021.

[125] Y. Chunya and L. Fengting , “Analytical Expression on Transient Overvoltage Peak Valueof Converter Bus Caused by DC Faults,” *IEEE Transactions on Power Systems,* vol. 36, no. 3, pp. 2741-2744, 2021.

[126] IEEE, “IEEE Recommended Practice for Monitoring Electric Power Quality,” IEEE Std, 2019.

[127] IEEE, “IEEE Guide on the Surge Environment in Low-Voltage (1000 V and less) AC Power Circuits,” IEEE, 2002.

[128] C. Xiaoyuan, J. Shan, C. Yu, G. Huayu, X. Qi and S. Boyang, “Transient Modeling and Loss Analysis of SiCMOSFETs at Cryogenic and Room Temperatures,” *IEEE Tranactions on Applied Super Conductivity,* vol. 31, no. 8, pp. 140040-1400404, 2021.

[129] C. Shiyue, Y. Jun, L. Yuan, P. Jinxin, H. Sen and C. Zhaoyang, “Coupling Mechanism Analysis and TransientStability Assessment for MultiparalleledWind Farms During LVRT,” *IEEE Transaction on Sustainable Energy,* vol. 12, no. 4, pp. 2132-2145, 2021.

[130] IEEE, “IEEE Recommended Practice for Powering and Grounding Electronic Equipment,” IEEE, 2006.

[131] IEEE, “Power Quality Course and IEEE Standards Bundle,” IEEE, 2012.

[132] K. Kahle, “Proceedings of the CAS-CERN Accelerator School: Power Converters,,” CERN, Baden, Switzerland, 2014.

[133] H. Sumaiya, M. M. Kashem, S. Danny and M. A. Rahman, “A Novel Dual Slope Delta Modulation Technique fora Current Source Inverter Based Dynamic VoltageRestorer for Mitigation of Voltage Sags,” *IEEE Transactions on Industry Applications,* vol. 57, no. 5, pp. 5437-5447, 2021.

[134] IEEE, “Revision of IEEE Std 1453-2011: IEEE Recommended Practicefor the Analysis of Fluctuating Installations on Power Systems,Standard,” IEEE, 2015.

[135] IEEE, “IEEE Standards Coordinating Committee 21: IEEE Std 1547–2018(Revision of IEEE Std 1547-2003) IEEE Standard for Interconnectionand Interoperability of Distributed Energy Resources with AssociatedElectric Power Systems Interface, Standard 1547–2018,” IEEE, 2018.

[136] M. J. Alam, K. M. Muttaqi; and D. Sutanto, “Battery Energy Storage to Mitigate RapidVoltage/Power Fluctuations in Power Grids Dueto Fast Variations of Solar/Wind Outputs,” *IEEE Access,* vol. 9, pp. 12191-12202, 2021.

[137] P. Dhrupa and C. Anandita, “Mitigation of Voltage Fluctuation in Distribution System using Sen Transformer with Variable Loading Conditions,” in *International Conference on Advances in Electrical, Computing, Communication and Sustainable Technologies (ICAECT)*, Bhilai, India, 2021.

[138] X. Jingren and L. Yingming, “Voltage Flicker Mitigation Strategy Based on Individual Pitch Control of Wind Turbine,” in *International Conference on Measuring Technology and Mechatronics Automation (ICMTMA)*, Beihai, China, 2021.

[139] B. Badrinarayan, C. R. Kamalesh Chandra Rout and N. D. Rudra Narayan Dash, “Voltage Flicker Mitigation Using VSC-Based STATCOM to Improve Power Quality,” in *International Conference on Power Electronics and Energy (ICPEE)*, Bhubaneswar, India, 2021.

[140] A. J. Wilkins, J. Veitch and B. Lehman, “LED Lighting Flicker and Potential Health Concerns: IEEE Standard PAR1789 Update,” in *IEEE Energy Conversion Congress and Exposition*, Atlanta, GA, USA, 2010.

[141] IEEE, “IEEE Draft Standard for Measurement and Limits of Voltage Fluctuations and Associated Light Flicker on AC Power Systems,” IEEE, 2021.

[142] C. Kwun-Hok, G. Yuan and K. T. Philip, “A Customized AC Hybrid LED Driver With Flicker Reduction for High Nominal Range Applications,” *IEEE Transactions on Circuits and Systems II: Express Briefs,* vol. 68, no. 5, pp. 1635-1639, 2021.

[143] J. Dixon, L. Moran, J. Rodriguez and R. Domke,, “Reactive Power Compensation Technologies: State-of-the-Art Review,” *IEEE Proceedings,* vol. 93, no. 12, pp. 2144-2164, 2005.

[144] K. Chan-Ki, “Dynamic Coordination Strategies Between HVDC and STATCOM,” in *Transmission & Distribution Conference & Exposition: Asia and Pacific*, Seoul, Korea (South), 2009.

[145] O. B. Nayak, A. M. Gole, D. G. Chapman and J. B. Davies, “Dynamic Performance of Static and Synchronous Compensators at an HVDC Inverter Bus in a Very Weak AC System,” *IEEE Trans. Power Syst,* vol. 9, no. 3, p. 1350–1358, 1994.

[146] C. Guo, Y. Liu, C. Zhao, X. Wei and W. Xu, “Power Component Fault Detection Method and Improved Current Order Limiter Control for Commutation Failure Mitigation in HVDC,” *IEEE Trans. Power Del,* vol. 30, no. 3, p. 1585–1593, 2015.

[147] Z. Wei, Y. Yuan, X. Lei, H. Wang, G. Sun and Y. Sun, “Direct Current Predictive Control Strategy for Inhibiting Commutation Failure in HVDC Converter,” *IEEE Trans. Power Syst,* vol. 29, no. 5, p. 2409–2417, 2014.

[148] C. Soham, M. Susovan and K. B. Sujit, “Coordination of D-STATCOM & SVC for Dynamic VAR Compensation and Voltage Stabilization of an AC Grid Interconnected to a DC Microgrid,” *IEEE Transactions on Industry Applications,* pp. 1-1, 2021.

[149] C. R. Ibhan, K. P. Siba and S. Anshuman, “Parallel Hybrid Converter-Based STATCOM and Capacitor Voltage Control Technique,” *IEEE Journal of Emerging and Selected Topics in Power Electronics,* vol. 9, no. 5, pp. 5597 - 5612, 2021.

[150] H. Ehsan, A. Mohammadreza, A. Mehdi, Z. M. Javad and M. G. Josep, “Secondary Control for a D-STATCOM DC-Link Voltage Under Capacitance Degradation,” *IEEE Transactions on Power Electronics,* vol. 36, no. 11, pp. 13215-13224, 2021.

[151] R. Ezequiel, L. Ramon, D. T. Christopher D. Townsend, G. F. Glen, D. T. Hossein and P. Josep , “Constrained Control of Low-Capacitance Delta Cascaded H-Bridge StatComs: A Model Predictive Control Approach,” *IEEE Transactions on Power Electronics,* vol. 36, no. 12, pp. 14312-14328, 2021.

[152] B. Ehsan, B. Massimo, R. S. Jan and M. Aravind, “A Novel Capacitor-Voltage Balancing Strategy for Double-Y STATCOM Under Unbalanced Operations,” *IEEE Transactions on Industry Applications,* vol. 57, no. 3, pp. 2692-2701, 2021.

[153] L. Daorong Lu, S. Chenxing, Y. Yu, L. Xiang, H. Haibing and X. Yan, “Flexible Nonsinusoidal Zero Sequence Voltage Injection Method to Extend Negative Sequence Current Compensation Range for Star-Connected CHB STATCOM,” *IEEE Transactions on Power Electronics,* vol. 36, no. 10, pp. 11357-11371, 2021.

[154] R. Ezequiel, L. Ramon, Q. Liu, D. T. Christopher, G. F. Glen, C. Salvador and P. Josep, “Enhancing Inductive Operation of Low-CapacitanceCascaded H-Bridge StatComs Using OptimalThird-Harmonic Circulating Current,” *IEEE Transactions on Power Electronics,* vol. 36, no. 9, pp. 10788-10800, 2021.

[155] Z. Xuesong, Z. Weibao, M. Youjie, G. Kairui, Y. Jie and W. Congcong , “Control Strategy Research of D-STATCOM Using Active Disturbance Rejection Control Based on Total Disturbance Error Compensation,” *IEEE Access,* vol. 9, pp. 50138-50150, 2021.

[156] M. S. Naeem, D. V. Ananth, N. B. Muhamad, P. S. Chowdary, V. S. Chakravarthy, S. Kona and C. S. Suresh, “A Common Capacitor Based Three LevelSTATCOM and Design of DFIG Converter for aZero-Voltage Fault Ride-Through Capability,” *IEEE Access,* vol. 9, pp. 105153-105179, 2021.

[157] Z. Yang, W. Yuqing, Z. Donghui, C. Xin and G. Chunying, “Broadband Impedance Shaping Control Scheme ofMMC-Based STATCOM for Improving the Stabilityof the Wind Farm,” *IEEE Transactions on Power Electronics,* vol. 36, no. 9, pp. 10278-10292, 2021.

[158] I. M. Mohamed , S. M. Haitham, A. Mansour , F. E. Mohamed and S. M. Sherif , “Near-Optimal PI Controllers of STATCOM for Efficient Hybrid Renewable Power System,” *IEEE Access,* vol. 9, pp. 34119-34130, 2021.

[159] V. Lavr and M. Zdeněk, “Dynamic Stability Improvement of Power System by Means of STATCOM With Virtual Inertia,” *IEEE Access,* vol. 9, pp. 116105-116114, 2021.

[160] H. W. Jong, W. Lei, M. L. Sung , P. Jong-Bae and H. R. Jae , “D-STATCOM d-q Axis Current Reference ControlApplying DDPG Algorithm in the DistributionSystem,” *IEEE Access,* vol. 9, pp. 145840-145851, 2021.

[161] W. Xi, W. Mengting, S. Mohammad, F. Shuang and C. Xi, “Model-Free Adaptive Control of STATCOM for SSO Mitigation in DFIG-Based Wind Farm,” *IEEE Transactions on Power Systems,* vol. 36, no. 6, pp. 5282-5293, 2021.

[162] B. Badrinarayan, C. R. Kamalesh and N. D. Rudra , “Voltage Flicker Mitigation Using VSC-Based STATCOM to Improve Power Quality,” in *International*

*Conference on Power Electronics and Energy (ICPEE)*, Bhubaneswar, India, 2021.

[163] S. K. Rajashree and P. T. Mohan, “Assessment of an Improved Voltage Flicker Remediation Treatment Method Employing VSC-Based STATCOM,” in *International Conference on Trends in Electronics and Informatics (ICOEI)*, Tirunelveli, India, 2021.

[164] IRENA, “Market integration of distributed energy resources –innovation landscape brief, https://www.irena.org/-/media/Files/IRENA/Agency/Publication/2019/Feb/IRENA_Market_integration_distributed_system_2019.pdf?la,” IRENA, 2020.

[165] “Distributed Energy Resources, IESO. Available: http://www.ieso.ca/en/Learn/Ontario-Power-System/A-Smarter-Grid/Distributed-Energy-Resources,” IESO, 2020.

[166] S. Padarbinda, M. Swati, P. Ranjeeta, B. Subrat and M. Sanhita, “Optimal Allocation of Distributed Generation in Distribution system by Using Black Widow Optimization Algorithm,” in *International Conference for Emerging Technology (INCET)*, Belagavi, India, 2021.

[167] R. Viral and D. K. Khatod, “Optimal Planning of Distributed Generation Systems Indistribution System: A Review,” *Renew Sustain Energy Rev,* vol. 16, no. 4, p. 5146–65, 2012.

[168] P. P. Rajendra, K. S. Asheesh and S. Devender, “International Journal of Engineering, Science and Technology,” *Planning of Different Types of Distributed Generation with Seasonal Mixed,* vol. 4, no. 1, pp. 1-13, 2012.

[169] M. S. Hassan, A. Ahmed, S. Masahito, I. Jun and M. D. Gamal, “Parallel Operation of Split-Source Inverters for PV Systems: Analysis and Modulation for Circulating Current and EMI Noise Reduction,” *IEEE Transaction on Power Electronics,* vol. 36, no. 6, pp. 9547-9564, 2021.

[170] L. I. Wenguo, L. I. Yong, Z. Mingmin, D. Aqi, L. Jiaiasheng, Z. Qiuxiang, Z. Lincheng and Z. Saiwen, “A Fully Decentralized Multi-Agent Fault Locationand Isolation for Distribution Networks With DGs,” *IEEE Access,* vol. 9, pp. 27748-27757, 2021.

[171] X. Huang, K. Wang, B. Fan, Q. Yang, G. J. Li, G.J, D. Xie and L. M. Crow, “Robust Current Control of Grid-tiedInverters for Renewable Energy Integration under Non-Ideal Grid Conditions,” *IEEE Trans. Sustain. Energy,* vol. 11, no. 1, pp. 1-12, 2020.

[172] R. Ebrahimi, V. Eslampanah, H. M. Kojabadi, M. Azizian, N. N. Esfetanaj and D. Zhou, “A Robust Fuzzy-based Control Technique for Wind Farm Transient Voltage Stability Using SVC and STATCOM: Comparison Study,” in *Conference on Power Electronics and Applications*, Lyon, France, 2020.

[173] L. D. Mensah, O. Y. John and S. A. Muyiwa, “Performance Evaluation of a Utility-scale Grid-tied Solar Photovoltaic(PV) Installation in Ghana,” *Energy for Sustainable Development,* vol. 48, p. 82–87, 2019.

[174] E. Park, S. J. Kwon and A. P. Del Pobil, “Can Large Educational Institutes Become Free from Grid Systems? Determination of Hybrid Renewable Energy Systems in Thailand,” *Appl. Sci,* vol. 9, p. 2319, 2019.

[175] H. H. Hossam, Y. Abdel-Raheem Youssef, I. Hamdan, A. Maqusood and E. M. Essam, “Performance Assessment of Robust P&O Algorithm Using Optimal Hypothetical Position of Generator Speed,” *IEEE Access,* vol. 9, pp. 30469 - 30485, 2021.

[176] J. Driesen and F. Katiraei, “Design for Distributed Energy Resources,” *IEEE Power and Energy Mag,* vol. 6, no. 3, pp. 30-40, 2008.

[177] L. Wang and D. N. Truong, “Stability Enhancement of a Power System with a PMSG-based and a DFIG-based Offshore Wind Farm Using a SVC with an Adaptive-Network-based Fuzzy Inference System,” *EEE Transactions on Industrial Electronics,* vol. 60, no. 7, pp. 2799-2807, 2002.

[178] K. M. Bhargavi, N. S. Jayalakshmi, D. N. Gaonkar, A. Shrivastava and V. K. Jadoun, “A Comprehensive Review on Control Techniquesfor Power Management of IsolatedDC Microgrid System Operation,” *IEEE Access,* vol. 9, pp. 32196-32228, 2021.

[179] L. Meng, M. Savaghebi, F. Andrade, J. C. Vasquez, J. M. Guerrero and M. Graells, “Microgrid Central Controller Development and Hierarchical Control

Implementation in the Intelligent Microgrid," in *IEEE Applied Power Electronics Conference and Exposition (APEC)*, Charlotte, NC, USA, 2015.

[180] R. F. Bastos, T. Dragi˘cevi´c, J. M. Guerrero and R. Q. Machado, "Decentralized Control for Renewable DC Microgrid with Composite Energy Storage System and UC Voltage Restoration Connected to the Grid," in *Annual Conference of the IEEE Industrial Electronics Society*, Florence, Italy, 2016.

[181] H. Wen, K. Zheng and Y. Du, "Hierarchical Coordinated Control for DC Microgrid with Crowbar and Load Shedding Control," in *International Future Energy Electronics Conference and ECCE*, Kaohsiung, Taiwan, 2017.

[182] R. E. Brown, J. Pan, X. Feng and K. Koutlev, "Siting Distributed Generation to Defer T & D Expansion," in *Transmission and Distribution Conference and Exposition*, Atlanta, GA, USA, 2001.

[183] A. S. Akinyemi, M. Kabeya and I. E. Davidson , "Analysis of Voltage Rise Phenomena in Electrical Power Network with High Concentration of Renewable Distributed Generations," *Scientific Reports,* vol. 12, pp. 1-22, 2022.

[184] K. W.H, "Radial distribution test feeders," in *Power Engineering Society Winter Meeting*, Columbus, 2001.

[185] K. W.H, "Radial distribution test feeders," *IEEE Transactions on Power Systems,* vol. 6, no. 3, p. 975 – 985, August 1991.

[186] IEEE Standard , "EEE Recommended Practice and Requirements for Harmonic Control in Electric Power Systems, IEEE Standard," IEEE Standard, 2014.

[187] NERSA, "Grid Connection Code for Renewable Power Plants (RPPs) Connected to the Electricity Transmission System (TS) or the Distribution System (DS) in South Africa," RSA Grid Code Secretariat, South Africa, 2014.

[188] R. C. Dugan, M. F. McGranaghan, S. Santosa and H. W. Beaty, "Electric Power Systems Quality," New York, McGraw-Hill, 2002, p. ch. 9.

[189] B. Blazic and I. Papic, “Voltage Profile Support in Distribution Networks — Influence of the Network R/X Ratio,” in *International Power Electronics and Motion Control Conference*, Poznan, Poland, 2008.

[190] L. K. Sree and K. M. Vijaya, “Dynamic Voltage Stability Enhancement of A Wind Farm Connected To Grid Using Facts- A Comparison,” in *International Conference on Circuits and Systems in Digital Enterprise Technology (ICCSDET)*, Kottayam, India, 2020.

[191] C. Tian, L. Chenghao, Z. Gao, Y. Rao, W. Cui and P. Xueqing, “Study on Different Modes of Reactive Power Compensation and Reactive Power CoordinatedControl for Wind Farm,” in *IEEE Industrial and Commacial Power System*, Weihai, China, 2020.

[192] K. Arrik and S. Sirdeep, “Integration of wind farm in power system using STATCOM,” *International Journal of Scientific & Engineering Research,* vol. 4, no. 4, pp. 1293-1299, 2013.

[193] Z. Xinsong, X. Yangyang, L. Shengnan, L. Cheng and G. Yunxiang, “Joint Planning of Distributed PV Stations and EV. Charging Stations in the Distribution Systems Based on Chance-Constrained Programming,” *IEEE Access,* vol. 9, pp. 6756-6768, 2021.

[194] S. A. Fahad, “DC Microgrid Planning, Operation, and Control: A Comprehensive Review,” *IEEE Access,* vol. 9, pp. 36154-36172, 2021.

[195] N. A. Lahaçani, D. Aouzellag and B. Mendil, “Contribution to the improvement of voltage profile in electrical network with wind generator using SVC device,” *Renewable Energy,* vol. 35, no. 1, pp. 243-248, 2010.

[196] C. Canizares, “Power flow and transient stability models of FACTS controllers for voltage and angle stability studies,” *IEEE Power Engineering Society Winter Meeting,* vol. 2, pp. 1447-1454, 2000.

[197] M. A. Alinezhad and M. Kamarposhti, “Comparison of SVC and STATCOM in Static Voltage Stability Margin Enhancement,” *International Science Index,* vol. 3, no. 2, pp. 722-727, 2009.

[198] I. Faegheh, V. Behrooz, A. Mehrdad and R. Mohammad, “Comparison of using SVC and STATCOM to provide Reactive Power for a Grid-connected Wind Power Plant to Stabilize the output Voltage during start up and Fault conditions,” *Science International (Lahore),* vol. 25, no. 4, pp. 703-706, 2013.

[199] A. Yazdani and R. Iravani, Voltage Converters in Power System, USA: John Willy and Sons, Inc.,Publication, 2010.

[200] C. Gokhan and R. Ghadir, “Placement and Performance Analysis of STATCOM and SVC for Damping Oscillation,” in *Electric Power and Energy Conversion Systems (EPECS)*, Istanbul, 2013.

[201] D. Patel, A. Nagera and K. Roy, “Application of static compensator to improve the power quality of grid connected induction generator based wind farm,” in *Advances in Engineering, Science and Management (ICAESM)*, Nagapattinam, 2012.

[202] N. G. Hingorani and L. Gyugyi, Understanding FACTS; Concepts and Technology of Flexible AC Transmission Systems, IEEE Press Book, 2000.

[203] N. G. Hingorani and L. Gyugyi, Understanding FACTS, New York: IEEE Press, 1999.

[204] M. A. Kamarposhti and H. Soltani, “The study of Maximum Loading Point in Investigation of Capacitor Performance with Power Electronic Shunt Devices,” in *International Conference on Electrical and Electronics Engineering,* Bursa, Turkey, 2009.

[205] R. M. Mathur and R. K. Varma, Thyristor-Based FACTS Controllers for Electrical Transmission Systems, New York: IEEE Press/Wiley, 2002.

[206] R. K. Varma and S. Mohan, “Mitigation of Fault Induced Delayed Voltage Recovery (FIDVR) by PV-STATCOM,” *IEEE Transaction on Power Systems,* vol. 35, no. 6, pp. 4251-4262, 2020.

[207] Q. I. Jun, W. Zhao and X. Bian, “Comparative Study of SVC and STATCOM Reactive Power Compensation for Prosumer Microgrids with DFIG-based Wind Farm Integration,” *IEEE Access,* vol. 20, pp. 1-9, 2020.

[208] S. F. Tarannum and S. S. Kamble, “A Study on Application of Static Synchronous Compensator (STATCOM) in Power Quality Improvement,” in *Proceedings of the International Conference on Smart Electronics and Communication*, Baltimore, MD, USA, 2020.

[209] K. Tazi, M. F. Abbou and F. Abdi, “Performance Analysis of Micro-Grid Designs with Local PMSG Wind Turbines,” in *Springer*, Berlin, Germany, 2019.

[210] S. M. Bhagavathy and G. Pillai, “PV Microgrid Design for Rural Electrification,” *Designs,* vol. 2, no. 3, p. 33, 2018.

[211] R. M. Elavarasan, G. M. Shafiullah, S. Padmanaban, N. M. Kumar, A. Annam, A. M. Vetrichelvan, L. Mihet-Popa and J. B. Holm-Nielsen, “A comprehensive Review on Renewable Energy Development, Challenges and Policies of Leading Indian States with an International Perspective,” *EEE Access,* vol. 8, p. 74432–74457, 2020.

[212] M. F. Zia, M. Benbouzid, E. Elbouchikhi, S. M. Muyeen, K. Techato and J. M. Guerrero, “Microgrid Transactive Energy: Review, Architectures, Distributed Ledger Technologies and Market Analysis,” *IEEE Access,* vol. 8, p. 19410–19432, 2020.

[213] Y. S. Kim, E. S. Kim and S. I. Moon, “Frequency and Voltage Controlstrategy of Standalone Microgrids with High Penetration of Intermittent Renewable Generation Systems,” *IEEE Trans. Power Syst,* vol. 31, no. 1, p. 718–728, 2016.

[214] S. B. Naderi, M. Negnevitsky, A. Jalilian, M. T. Hagh and K. M. Muttaqi, “Optimum resistive type fault current limiter: An efficient solution to achieve maximum fault ride-through capability of fixed-speed wind turbines during symmetrical and asymmetrical grid faults,” *IEEE Transactions on Industry Applications, vol. 53, no. 1, pp. 538-548, 2016,* vol. 53, no. 1, pp. 538-548, 2016.

[215] P. Ramanuja, K. M. Santanu, C. S. Suresh, K. S. Anurag and N. S. Noel, “Grid Integration of Small Scale Photovoltaic Systems in Secondary Distribution Network-A Review,” *IEEE Transaction on Industry Applications,* vol. 46, no. 3, pp. 3178-3195, 2020.

[216] C. Joanne and W. Jarrad, “Statistics of Utility Scale Power Generation in South Africa,” Council for Scientific and Industrial Research (CSIR), 2021.

[217] K. A. Khan and M. Khalid, “A Reactive Power Compensation Strategy in Radial Distribution Network with High PV Penetration,” in *Int.Conf. Renew. Energy Res. Appl. (ICRERA)*, Brasov, Romania, 2019.

[218] M. Dreidy, H. Mokhlis and S. Mekhilef, “Inertia Response and Frequency Control Techniques for Renewable Energy Sources: A review,” *Renew. Sustain. Energy Rev,* vol. 69, p. 144–155, 2017.

[219] G. Petrone, G. Spagnuolo, R. Teodorescu, M. Veerachary and M. Vitelli, “Reliability Issues in Photovoltaic Power Processing Systems,” *IEEETrans. Ind. Electron,* vol. 55, no. 7, p. 2569–2580, 2008.

[220] K. A. Khan, S. Shafiq and M. Khalid, “A strategy for Utilization of Reactive Power Capability of PV Inverters,” in *Proc. 9th Int. Conf. Power EnergySyst. (ICPES)*, 2019.

[221] A. Zerrahn and W. P. Schill, “Long-run Power Storage Requirements for High Shares of Renewables: Review and a New Model,” *Renew. Sustain.Energy Rev,* vol. 79, p. 1518–1534, 2017.

[222] A. K. Podder, N. K. Roy and H. R. Pota, “IET Review Power Gener,” *MPPT Methods for Solar PV system; A Critical Review Based on Tracking Nature,* vol. 13, no. 10, pp. 1615-1632, 2019.

[223] D. Anjan, P. Imtiaz, M. G. Dastgir, N. Asim, O. O. Temitayo, R. Hugo and S. Arif , “Voltage Regulation of Photovoltaic System with varying Loads,” in *Southeast Con*, Raleigh, NC, USA, 2020.

[224] A. R. Jordehi, “Maximum Power Point Tracking in Photovoltaic (PV) Systems: A Review of Different Approaches,” *Renew. Sustain. Energy Rev,* vol. 65, p. 1127–1138, 2016.

[225] B. Bendib, H. Belmili and F. Krim, “A survey of the Most Used MPPT Methods: Conventional and Advanced Algorithms Applied for Photovoltaic Systems,” *Renew. Sustain. Energy Rev,* vol. 45, p. 637–648, 2015.

[226] R. K. Shaik, C. Dhanamjayulu, P. Sanjeevikumar, B. H. Jens and M. Massimo, “A Novel Asymmetrical 21-Level Inverter for Solar PV Energy System With Reduced Switch Count,” *IEEE ACCESS,* vol. 9, pp. 11761-11775, 2021.

[227] H. U. Prabhu and M. R. Babu, “Performance Study of MPPT Algorithms of DC-DC Boost Converters For PV Cell Applications,” in *International Conference on Electrical Energy Systems (ICEES)*, Chennai, India, 2021.

[228] U. K. Muhammad , W. Khan , K. S. Karimov and A. S. Muhammad , “A New Proposed Hierarchy for Renewable Energy Generation to Distribution Grid Integration,” in *International Conference on Emerging Technologies (ICET)*, Peshawar, Pakistan, 2015.

[229] O. Ekren and B. Y. Ekren, “Size Optimization of a PV/Wind Hybrid Energy Conversion System with Battery Storage using Response Surface Methodology,” *Appl. Energy,* vol. 85, no. 11, pp. 1086-1101, 2008.

[230] M. H. Anowar and P. Roy, “A Modified Incremental Conductance Based Photovoltaic MPPT Charge Controller,” in *International Conference on Electrical, Computer and Communication Engineering (ECCE)*, 2019.

[231] M. Saibal and K. A. Ashok, “Comparative Analysis of Various P & O MPPT Algorithm for PV System Under Varying Radiation Condition,” in *International Conference on Power Electronics and Energy (ICPEE)*, Bhubaneswar, India, 2021.

[232] R. Abhishek, K. Seema and S. Bhim, “DSOGI-PLL With In-Loop Filter Based Solar Grid Interfaced System for Alleviating Power Quality Problems,” *IEEE Transactions on Industry Applications,* vol. 57, no. 1, pp. 730-740, 2021.

[233] B. Panda, B. Panda, A. Khillo, A. Pradhan and C. Jena, “PV Based DC-DC Converter Design Using MPPT for Stand Alone System,” *Int. J. Sci. Technol. Res.,* vol. 9, no. 2, pp. 5075-5079, 2020.

[234] J. L. Santos, L. Antunes, A. Chehap and C. Cruz, “A Maximum Power Point Tracker for PV System Using a High Performance Boost Converter,” *Elsevier Solar Energy,* vol. 80, no. 7, pp. 772-778, 2006.

[235] S. Khadidja, M. Mountassar and B. M'hamed, “Comparative Study of Incremental Conductance and Perturb Observe (P & O) MPPT Methods for Photovoltaic Application,” in *Internation Conferece on Green Energy Conversion System*, Tunisia, 2017.

[236] S. Krishnendu, M. Arkatanu, K. K. Mandal and T. Bhimsen, “Control Strategy for Active and Reactive Power Regulation of Grid Tied Photovoltaic System,” in *Innovations in Energy Management and Renewable Resources*, Kolkata, India, 2021.

[237] S. E. Abdelaziz, M. K. Abdelrazik and T. M. Hatem, “Solar Energy Potential in Africa: Is Covid-19 a Challenge or an Opportunity,” in *IEEE 48th Photovoltaic Specialists Conference (PVSC)*, Fort Lauderdale, FL, USA, 2021.

[238] I. Elzemeity, E. Ibrahim and A. Elzemeity, “Feasibility study of an Offshore Wind Farm with the Egyptian-Saudi Arabia HVDC Link,” in *International Conference on Renewable Energy: Generation and Applications (ICREGA)*, Al Ain, United Arab Emirates, 2021.

[239] M. Elsadek, A. Hatem, B. Eliwa, A. E. Shimy, A. Ashraf and T. Hatem, “Industrial Estate Powered by Photovoltacs in Egypt : A Study of Potential, Challenges and Environmental Impact,” in *IEEE 48th Photovoltaic Specialists Conference (PVSC)*, Fort Lauderdale, FL, USA, 2021.

[240] D. Kuznetsov and H. Mennen, “Analyse der Schlüsselfaktoren zur Entwicklung Erneuerbarer Energien in Deutschland,” *Agro-Industrial Complex of Russia,* vol. 23, no. 2, pp. 342-348, 2016.

[241] S. K. Sheryazov, M. V. Shelubaev and S. G. Obukhov, “Renewable Sources in System Distributed Generation,” in *International Conference on Industrial Engineering, Applications and Manufacturing (ICIEAM)*, Petersburg, Russia, 2017.

[242] R. Sharma, M. Singh and K. Jain, “Power System Stability Analysis with Large Penetration of Distributed Generation,” in *IEEE Power India International Conference (PIICON)*, Delhi, India, 2014.

[243] M. Z. Wanik, I. Erlich, A. Mohamed and A. A. Salam, “Influence of Distributed Generations and Renewable Energy Resources Power Plant on Power System

Transient Stability," in *IEEE International Conference on Power and Energy*, Kuala Lumpur, Malaysia, 2010.

[244] A. Mohamed, "Climate Change Risks in Sahelian Africa," *Reg. Environ. Chang.,* p. 109–117, 2011.

[245] A. Nicholson, D. J. Nash, B. M. Chase, T. M. Shanahan, S. W. Grab, D. Verschuren, M. U. Asrat and A. M. Lézine, "Temperature Variability Over Africa During the Last 2000 Years," *Holocene,* vol. 23, no. 8, p. 1085–1094, 2013.

[246] J. M. Collins, "Temperature Variability over Africa," *J. Clim,* vol. 24, no. 14, p. 3649–3666, 2011.

[247] B. G. New, M. B. Hewitson, D. B. Stephenson, A. Tsiga, A. Kruger, A. Manhique, J. C. Coelho, D. N. Masisi, E. Kululanga, E. Mbambalala, F. Adesina, H. Saleh, R. L. Kanyanga, J. Adosi, L. Bulane, L. Fortunata and M. L. Mdoka, "Evidence of Trends in Daily Climate Extremes over Southern and West Africa," *American Geophysical Union (AGU),* vol. 111, no. 14, pp. 1-11, 2006.

[248] H. Von, S. Barkhordarian and A. J. Bhend, "Consistency Obs. Near Surf. Temp. Trends with Clim. Chang. Proj. over Mediterr. Reg," *Climate Dynamics,* vol. 39, no. 10, p. 1695–1702, 2012.

[249] O. Richard and W. Q. Anyah, "Characteristic 20th and 21st Century Precipitation and Temperature Patterns and Changes Over the Greater Horn of Africa," *Int. J. Climatol,* vol. 32, no. 3, p. 347–363, 2012.

[250] C. Funk,, G. Eilerts, J. Verdin, J. Rowland and M. Marshall, "A Climate Trend Analysis of Sudan. USGS Fact Sheet," U.S. Department of the Interior, Sudan, 2011.

[251] T. S. Huang, A. G. Barnett, X. Wang, P. Vaneckova and G. Fitzgerald, "Projecting Future Heat-related Mortality Under Climate Change Scenarios: A Systematic Review," *Env. Heal. Perspect,* vol. 119, p. 90–1681, 2011.

[252] C. B. Field, M. Barros, T. F. Stocker, D. Qin, D. J. Dokken, K. L. Ebi, M. D. Mastrandrea, K. J. Mach, G. K. Plattner, S. K. Allen, P. M. Midgley and M. Tignor, "IPCC, in Managing the Risks of Extreme Events and Disasters to Advance Climate Change Adaptation. A Special Report of Working Groups I and II of the

Intergovernmental Panel on Climate," Cambridge University Press, New York, 2012.

[253] S. L. Simon and S. Kovats, "Quantitative Risk Assessment of the Effects of Climate Change on Selected Causes of Death, 2030s and 2050s," WHO Library Cataloguing, Switzerland, 2019.

[254] K. Kusakana, "A Review of Energy in the Democratic Republic of Congo," *Int. J. Energy Power Eng,* vol. 10, no. 6, pp. 1-10, 2016.

[255] K. Mensah, S. Boahen and K. O. Amoabeng, "Renewable Energy Situation in Ghana: Review and Recommendations for Ghana" Energy Crisis Gic. 2017-Eas001 Renewable Energy Situation in Ghana: Review and Recommendations for Ghana Energy Crises," Proc. 1st GHASKA," in *Proc. 1st GHASKA Innov. Conf*, Suwon, Korea, 2017.

[256] O. Bishoge, L. Zhang and W. Mushi, "The Potential Renewable Energy for Sustainable Development in Tanzania: A Review," *Clean Technol.,* vol. 1, no. 1, p. 70–88, 2018.

[257] D. Talla, F. Gaelle and A. Lucas, "Current Status of Renewable Energy in Cameroon," *North Am. Acad. Res,* vol. 1, no. 2, p. 71–80, 2018.

[258] O. Richard and W. Q. Anyah, "Characteristic 20th and 21st Century Precipitation and Temperature Patterns and Changes Over the Greater Horn of Africa," *Int. J. Climatol,* vol. 32, no. 3, p. 347–363, 2012.

[259] A. E. AbdelZahera, S. Elbarbarya, A. El-Shahatb and H. Mesbaha, "Geothermal resources in Egypt Integrated with GIS-based Analysis," *J. Volcanol. Geotherm Res.,* p. 1–13, 2019.

[260] A. Lashin, "Geothermal Resources of Egypt: Country Update," *Proceedings World Geothermal Congress,* p. 1–13, 2015.

[261] A. B. Stambouli, Z. Khiat, S. Flazi and Y. Kitamura, "Review and Use of the Algerian Renewable Energy for Sustainable Development," *Renew. Sustain. Energy Rev.,* vol. 13, no. 6, pp. 1584-1591, 2009.

[262] B. M. Khenfri and G. Mohammed, “Renewable Energy in Algeria Reality and Perspective,” *J. Inf. Syst. Technol. Manag,* vol. 3, no. 10, p. 1–19, 2018.

[263] K. J. Pushpendra, “Energy Resources and Demand in Botswana with Special Reference to Solar Energy,” *Renew. Energy,* vol. 5, no. 3, p. 535 544, 1993.

[264] B. M. Taele,, K. K. Gopinathan and L. Mokhuts’oane, “The Potential of Renewable Energy Technologies for Rural Development in Lesotho,” *Renew. Energy,* vol. 32, p. 609–622, 2006.

[265] G. Nhamo and S. Y. Ho, “Renewable Energy Policy Landscape in South Africa: Moving Towards a Low Carbon Economy,” *Trans. Ecol. Environ,* vol. 143, p. 266–276, 2011.

[266] H. Lucas and S. Pinnington, “Education and Training gaps in the Renewable Energy Sector,” *Sol. Energy,* vol. 173, p. 449–455, 2018.

[267] P. Trop and D. Goricanec, “Comparisons Between Energy Carriers Productions for Exploiting Renewable Energy Sources,” *Energy,* vol. 108, p. 155–161, 2016.

[268] F. Fornara, P. Pattitoni and M. Mura, “Predicting Intention to Improve Household Energy Efficiency: The Role of Value-belief-norm Theory, Normative and Informational Influence, and Specific Attitude,” *J. Environ. Psychol,* vol. 45, p. 1–10, 2016.

[269] K. Arunachalam, P. Venkateswaran and S. Goel, “Decentralized Distributed Generation in India: A review,” *J. Renew. Sustain. Energy,* vol. 8, no. 2, p. 1–20, 2016.

[270] R. Bansal, Handbook of Distributed Generation, Switzerland: Springer, 2017.

[271] S. Xu, Y. Xue and L. Chang, “Review of Power System Support Functions for Inverter-Based Distributed Energy Resources- Standards, Control Algorithms, and Trends,” *IEEE Open Journal of Power Electronics,* vol. 2, pp. 2644-1314, 2021.

[272] H. Qiu, W. Gu and F. You, “Bilayer Distributed Optimization for Robust Microgrid Dispatch With Coupled Individual-Collective Profits,” *IEEE Transactions on Sustainable Energy,* vol. 12, no. 3, pp. 1525-1538, 2021.

[273] E. Memmel, S. Schlüters, R. Völker, F. Schuldt, K. V. Maydell and C. Agert, “Forecast of Renewable Curtailment in Distribution Grids Considering Uncertainties,” *IEEE Access,* vol. 9, pp. 60828-60840, 2021.

[274] P. Jahangiri and D. C. Aliprantis, “Distributed Volt/Var Control by PV Inverters,” *IEEE Trans. Power Syst,* vol. 28, no. 3, p. 3429–3439, 2013.

[275] K. Turitsyn, P. Sulc, S. Backhaus and M. Chertkov, “Options for Control of Reactive Power by Distributed Photovoltaic Generators,” *Proc. IEEE,* vol. 99, no. 6, p. 1063–1073, 2011.

[276] Y. Kim, S. Ahn, P. Hwang, G. Pyo and S. Moon, “Coordinated Control of a DG and Voltage Control Devices Using a Dynamic Programming Algorithm,” *IEEE Trans. Power Syst,* vol. 28, no. 1, p. 42–51, 2013.

[277] J. Dowell and P. Pinson, “Very Short-term Probabilistic Wind Power Forecasts by Sparse Vector Auto-regression,” *IEEE Trans. Smart Grid,* vol. 7, no. 2, p. 763–770, 2016.

[278] M. H. Bollen and A. Sannino, “Voltage Control with Inverter-based Distributed Generation,” *IEEE Trans,* vol. 20, no. 1, p. 519–520, 2005.

[279] P. M. Carvalho, P. F. Correia and L. A. Ferreira, “Distributed Reactive Power Generation Control for Voltage Rise Mitigation in Distribution Networks,” *IEEE Trans. Power Syst,* vol. 23, no. 2, p. 766–772, 2008.

[280] S. Deshmukh, A. Pahwa and B. Natarajan, “Voltage/VAR Control Indistribution Networks via Reactive Power Injection Through Distributed Generators,” *IEEE Trans. Smart Grid,* vol. 3, no. 3, p. 1226–1234, 2012.

[281] T. Sansawatt, L. F. Ochoa and G. P. Har, “Smart Decentralized Control of DG for Voltage and Thermal Constraint Management,” *IEEE Trans. Power Syst,* vol. 27, no. 3, p. 1637–1645, 2012.

[282] M. Z. Degefa, M. Lehtonen, R. J. Millar, , A. Alahäivälä and E. Sa, “Optimal Voltage Control Strategies for Day-ahead Active Distribution Network Operation,” *Elect. Power Syst. Res,* vol. 127, p. 41–52, 2015.

[283] H. Gao, J. Chen, R. Diao and J. Zhang, “A HEM-Based Sensitivity Analysis Method for Fast Voltage Stability Assessment in Distribution Power Network,” *IEEE Access,* vol. 9, pp. 13344-13353, 2021.

[284] F. Engelbrecht, “Environmental Research Letters Projections of Rapidly Rising Surface Temperatures over Africa under Low Mitigation Related Content,” *Environ. Res. Lett.,* vol. 10, p. 85004, 2019.

[285] IEA, “Africa’s Energy Future Matters for the World,” Africa Energy Outlook, 2019. [Online]. Available: https://www.iea.org/africa2019/#. [Accessed 2021].

[286] T. Makonese, “Renewable Energy in Zimbabwe,” Renewable Energy in Zimbabwe,” in *International Conference on the Domestic Use of Energy (DUE)*, Cape Town, South Africa, 2016.

[287] D. H. Didane, N. Rosly, M. F. Zulkafli and S. S. Shamsudin, “Evaluation of Wind Energy Potential as a Power Generation Source in Chad,” *International Journal of Rotating Machinery,* vol. 1, pp. 1-10, 2017.

[288] M. Moner-Girona, k. Bódis, T. Huld, I. Kougias and S. Szabó, “Universal Access to Electricity in Burkina Faso: Scaling-up Renewable Energy Technologies,” *Environ. Research Lett.,* vol. 11, p. 1–15, 2016.

[289] D. Kukoyi, “The Renewable Energy Law Review - 2nd Edition Nigeria,” Tom Barnes, London, 2019.

# APPENDIX A

**Table A1:** Load data

| Bus A | Bus B | Active power (KW) | Reactive power (kVAr) | Line length /km | Resistance and Reactance/km |
|---|---|---|---|---|---|
| 632 | 645 | 0 | 0 | 0 | 0.625+j0.3125 |
| 632 | 633 | 35 | 6 | 2 | 0.625+j0.3125 |
| 633 | 634 | 35 | 6 | 2 | 0.625+j0.3125 |
| 645 | 646 | 35 | 6 | 2 | 0.625+j0.3125 |
| 650 | 632 | 35 | 6 | 2 | 0.625+j0.3125 |
| 684 | 652 | 35 | 6 | 2 | 0.625+j0.3125 |
| 632 | 671 | 35 | 6 | 2 | 0.625+j0.3125 |
| 671 | 684 | 35 | 6 | 2 | 0.625+j0.3125 |
| 671 | 680 | 35 | 6 | 2 | 0.625+j0.3125 |
| 671 | 692 | 35 | 6 | 2 | 0.625+j0.3125 |
| 684 | 611 | 35 | 6 | 2 | 0.625+j0.3125 |
| 692 | 675 | 50 | 20 | 5 | 0.625+j0.3125 |

**Table A2:** Load data

| Bus A | Bus B | Active power (KW) | Reactive power (KVAr) | Line length in KM |
|---|---|---|---|---|
| 632 | 645 | 200 | 116 | 0.1524 |
| 632 | 633 | 170 | 100 | 0.1524 |
| 633 | 634 | 480 | 270 | 0.1524 |
| 645 | 646 | 170 | 110 | 0.0914 |
| 650 | 632 | 230 | 132 | 0.610 |
| 684 | 652 | 300 | 200 | 0.244 |
| 632 | 671 | 170 | 151 | 0.610 |
| 671 | 684 | 375 | 202 | 0.091 |
| 671 | 680 | 118 | 93 | 0.305 |
| 671 | 692 | 270 | 80 | 0.091 |
| 684 | 611 | 950 | 770 | 0.091 |
| 692 | 675 | 128 | 86 | 0.152 |

**Table A3:** Transformer data

| Parameters | Value |
|---|---|
| Substation | 5 kVA |
| HV | 115 kV |
| LV | 4.16 kV |
| Frequency | 50 Hz |
| X | 8 |
| R | 1 Ω |
| Inline transformer | 0.5 MVA |
| HV | 4.16 kV |
| LV | 0.48 kV |
| X | 2 |
| R | 1.1 Ω |

**Table A4:** Converter parameter and DC load

| | |
|---|---|
| 12 pulse generators | 50 HZ, $30^0$ |
| Pulse width (degree) | 40 |
| Power electronic device | 2 Thyristors |
| | DC load |
| Resistive load | 4.6 MW |
| Inductor | 0.5e3 H |
| DFIG power | 2 MVA at 0.9 p.f |
| rectifier | 2 universal diodes |
| Snubber resistance | 2000 ohms |
| Snubber capacitance | 0.1e-6 F |
| Ron | 1 e-3ohms |

**Table A5:** Data for RDGs

| | |
|---|---|
| Rated power (Solar PV) | 10x100 kV |
| Power factor | Unity |
| Voltage | 1.008-MW 260V/4.16 kV |
| Parallel strings | 94 |
| SunPower SPR-315E (series) | 5 |
| Three-phase Voltage Source Converter (VSC) | 500 V DC to 260 V AC |
| Rated power (wind) | 300 kVA |
| Power factor | 0.98 |
| Voltage | 4.16 kV |
| Frequency | 50 HZ |
| Stator resistance | 0.00706 Ω |
| Stator inductance | 171 mH |
| Magnetizing inductance | 2.9 H |
| Rotor resistance | 5m Ω |
| Rotor inductance | 156 Mh |
| Pole pair | 0.013 |

| Converter parameter | |
|---|---|
| Converter maximum power | 0.5 |
| Grid side coupling inductor | 0.15 pu |
| Grid side coupling resistance | 0.0015 pu |
| Nominal DC bus capacity | 1000 μF |
| Nominal DC voltage | 1200 V |
| Coupling inductor current | [0 90] |
| Voltage regulator parameter | |
| Grid voltage ref | 1.0 pu |
| Grid side converter ref | 0 |
| Grid voltage regulator $k_p$ | 1.25 |
| Grid voltage regulator $k_i$ | 300 |
| Droop | 0.03 |

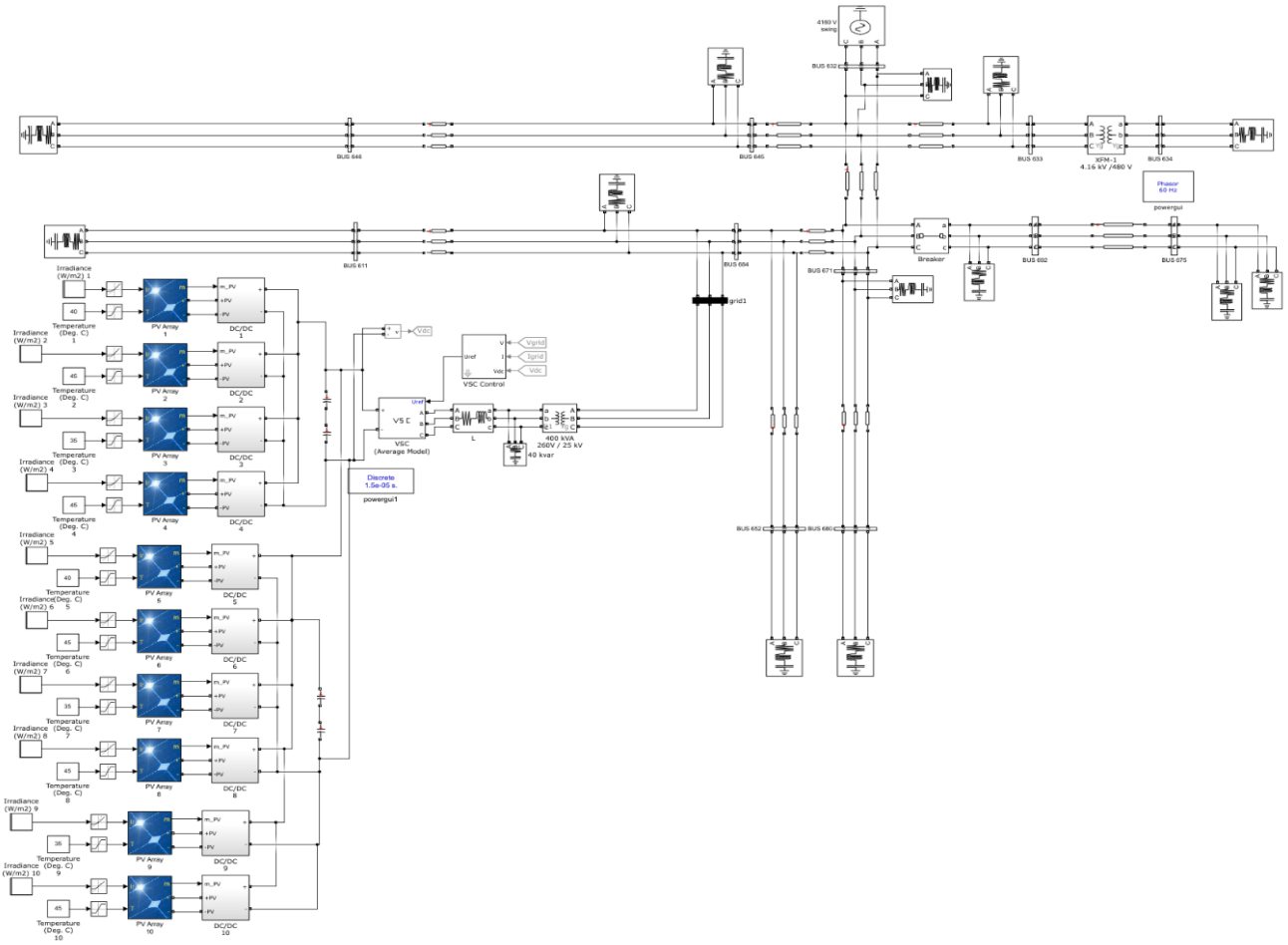

**Figure A1:** IEEE-13 Bus Test System without STATCOM connection

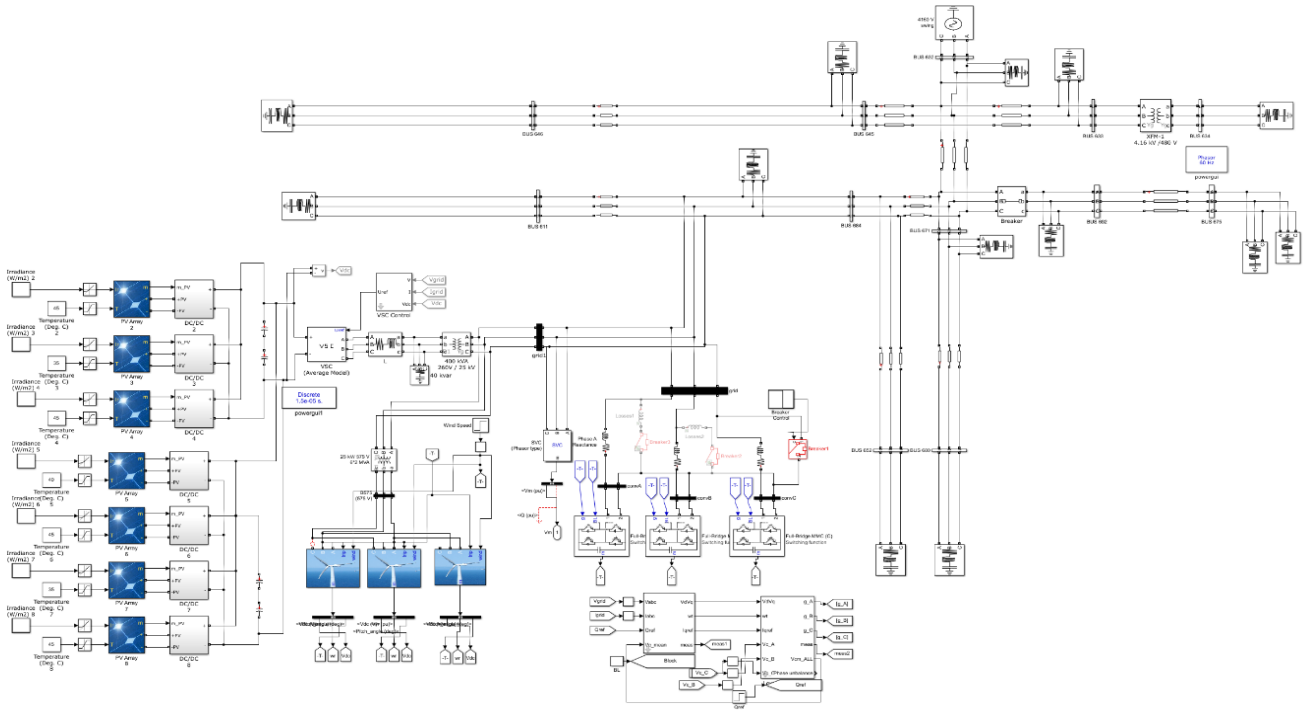

(a)

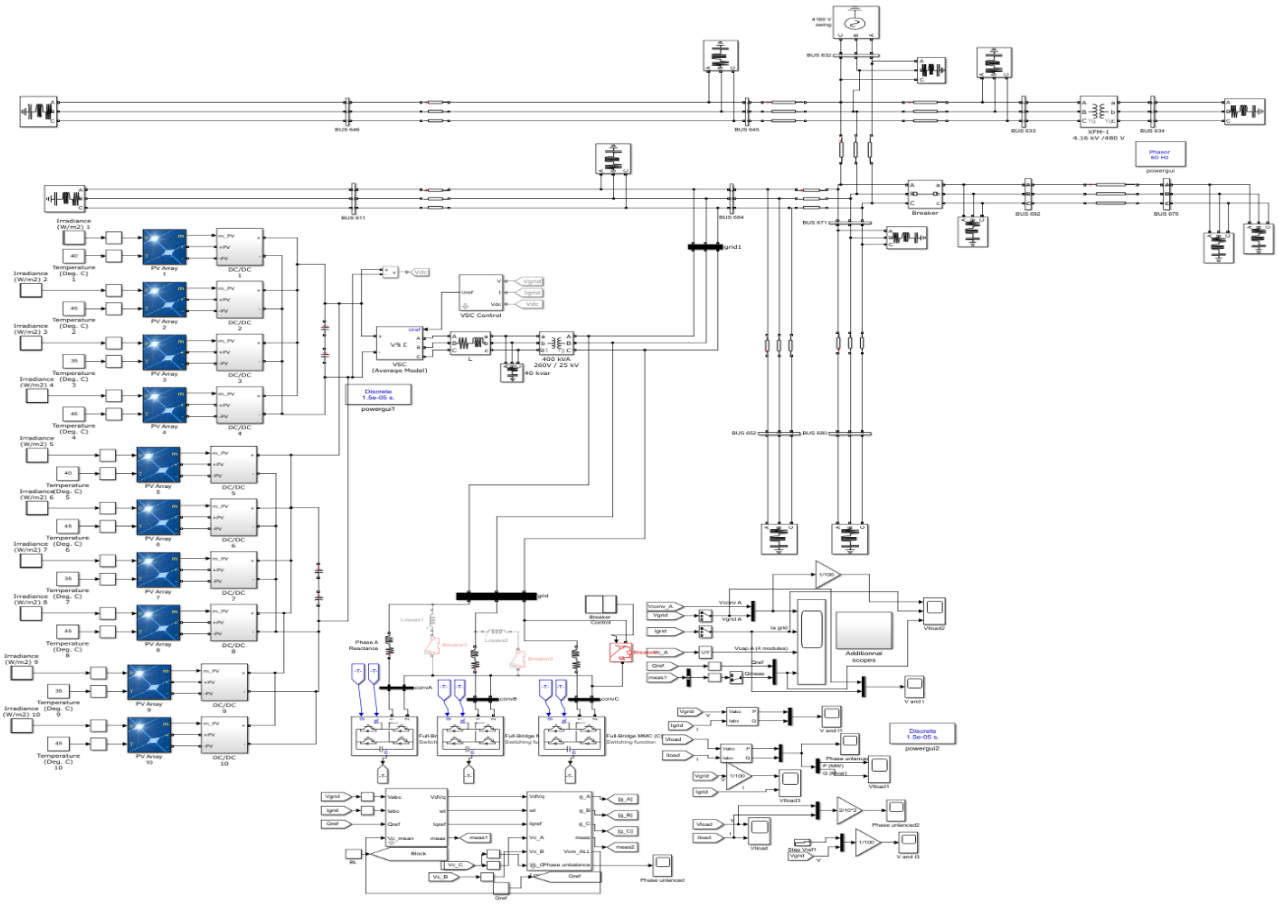

(b)

**Figure A2:** IEEE-13 Bus Test System with wind, Solar and STATCOM connection

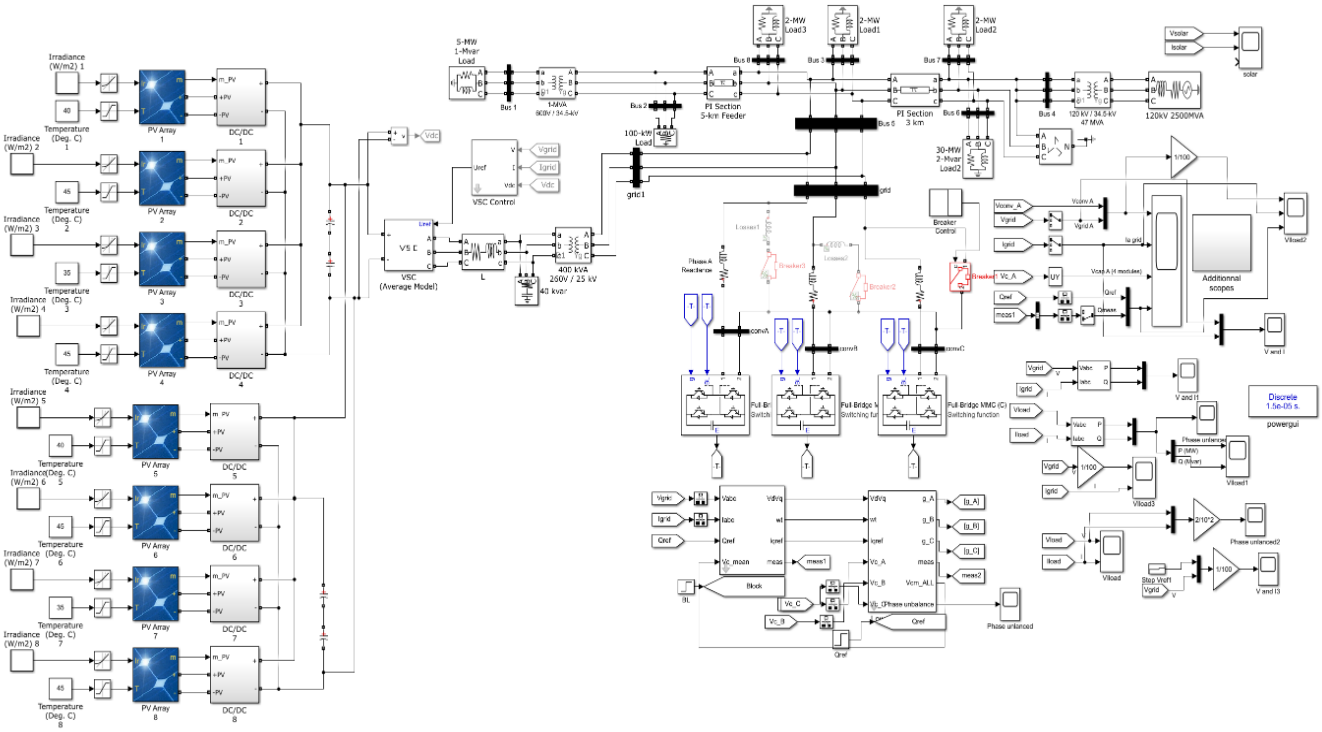

(a)

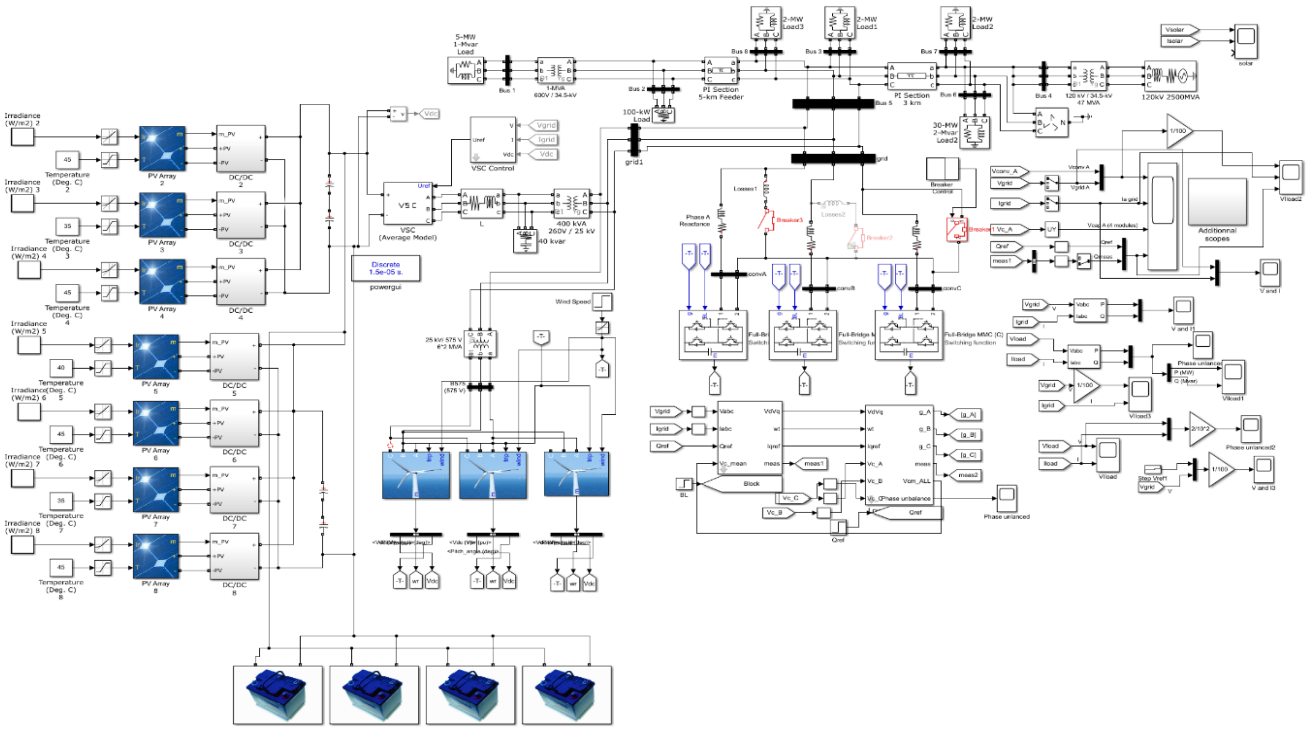

(b)

**Figure A3:** RDG (wind and solar PV) Integration with STATCOM connection

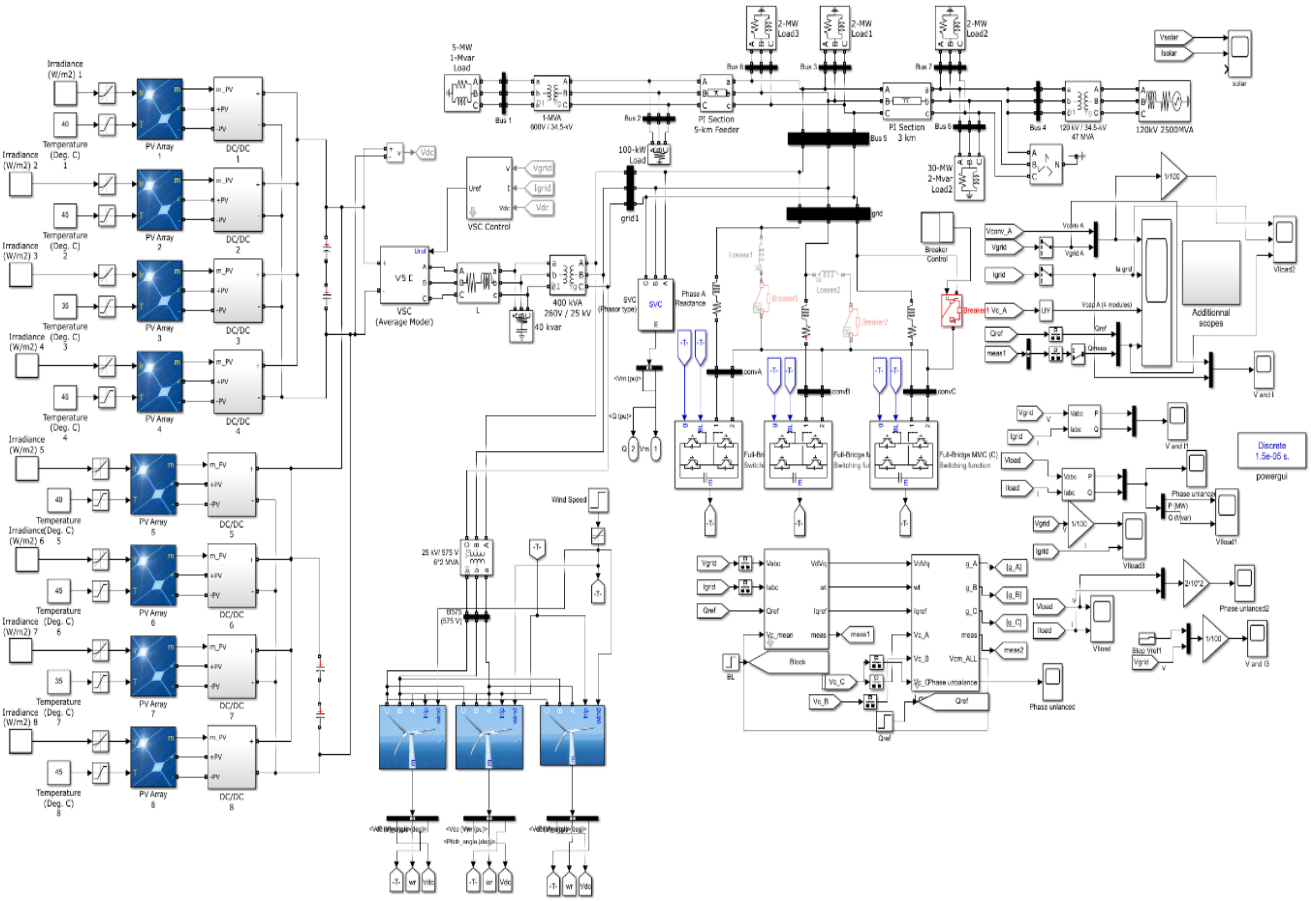

**Figure A4:** Test System without STATCOM connection

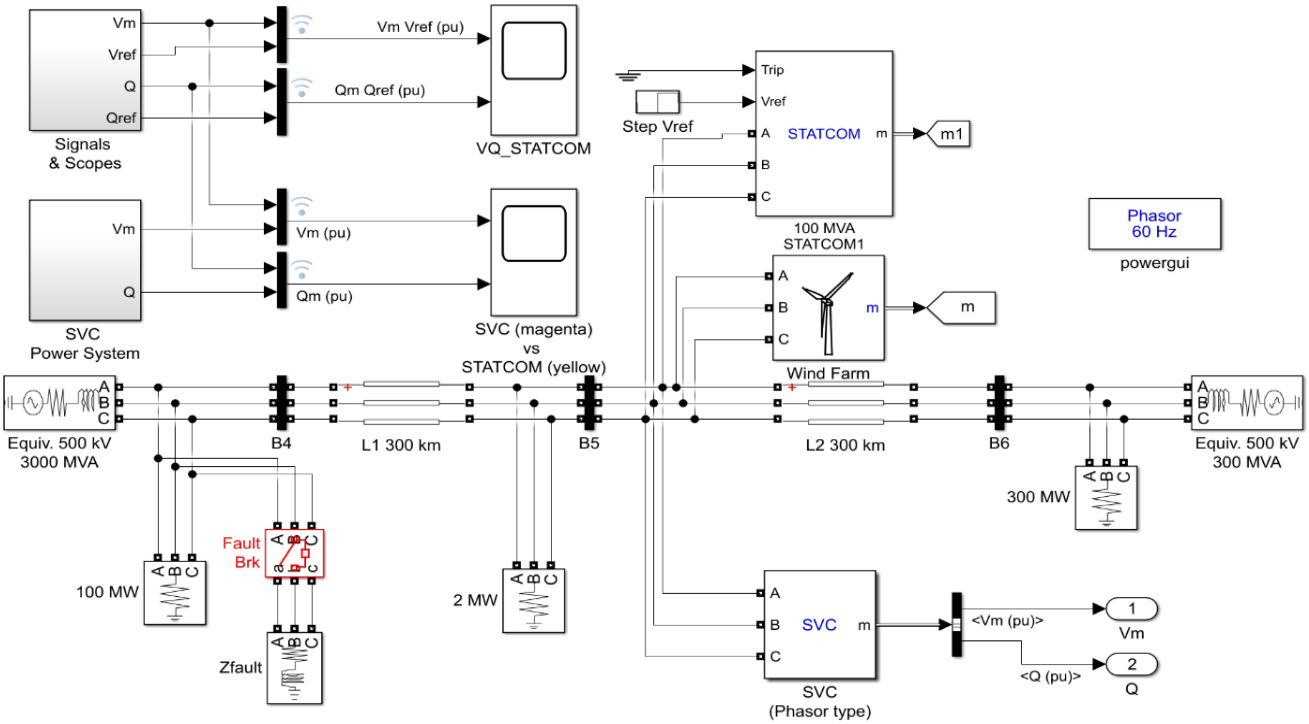


**Figure A5:** RDG (wind) Integration

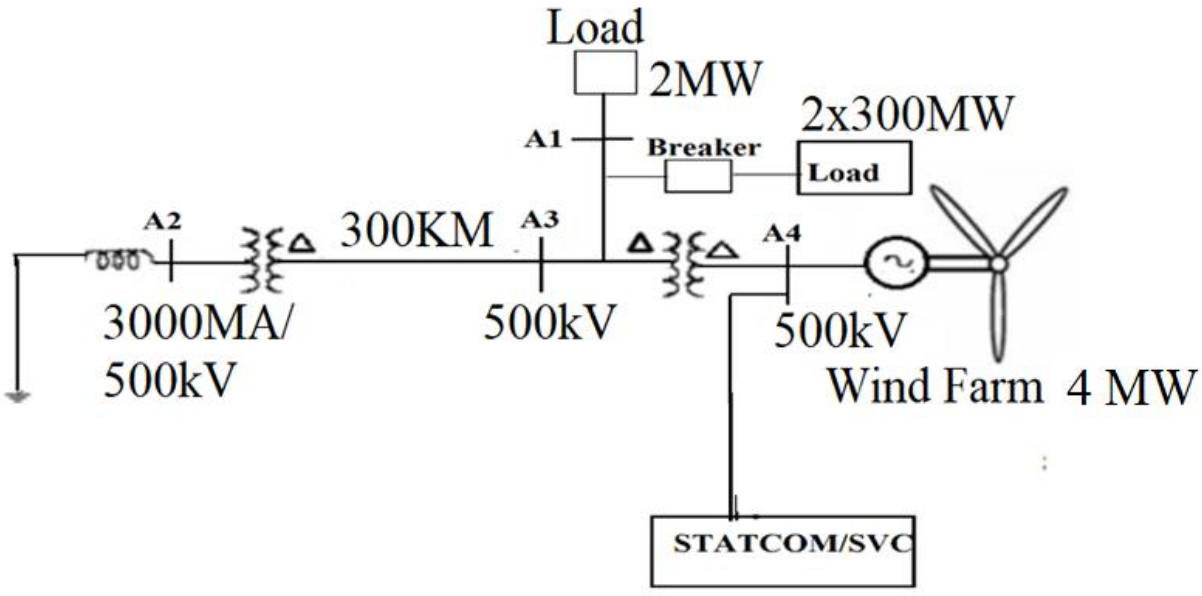


**Figure A6:** Circuit Equivalent modelled in MATLAB/SIMULINK

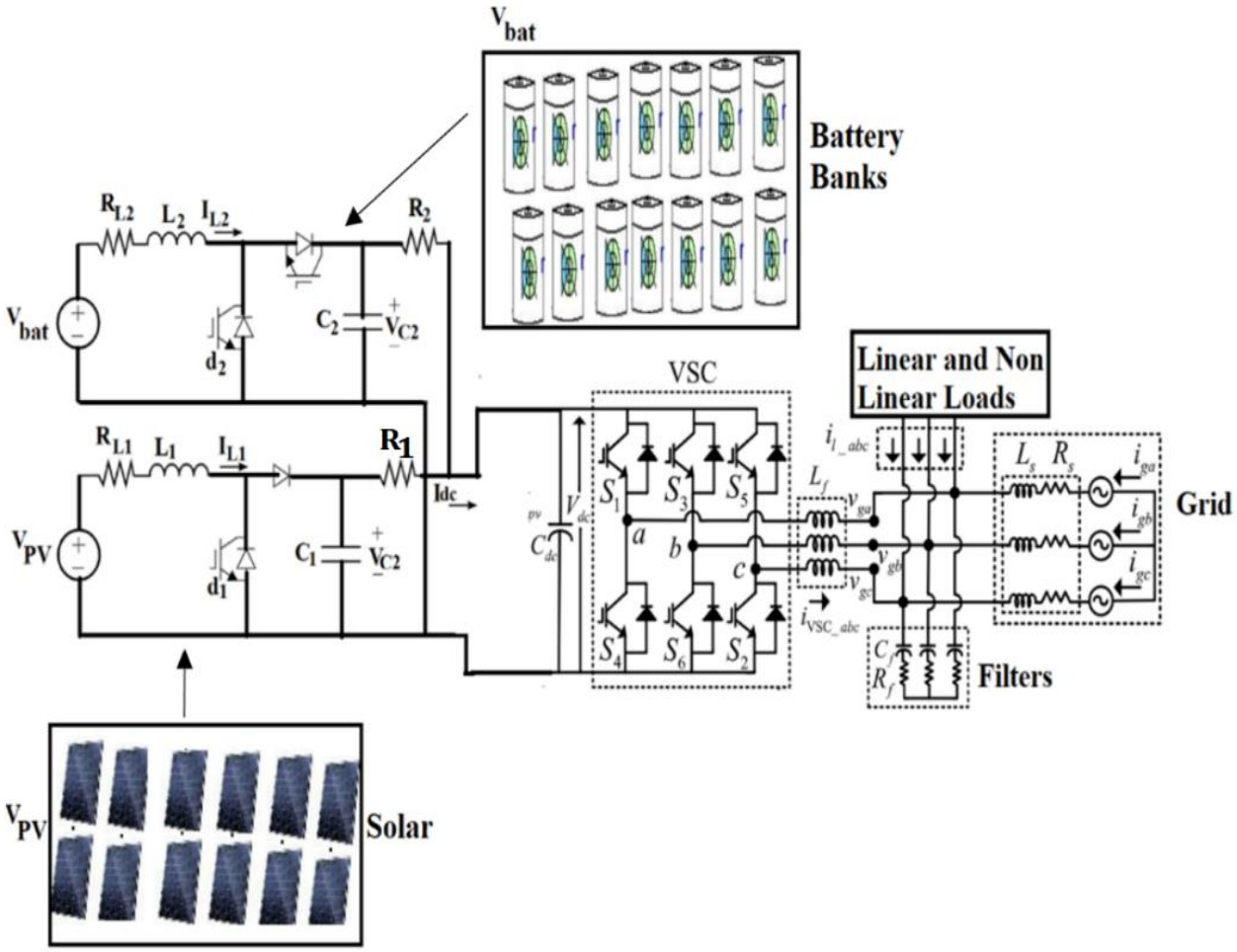


**Figure A7:** Proposed Equivalent Circuit for DUT Microgrid

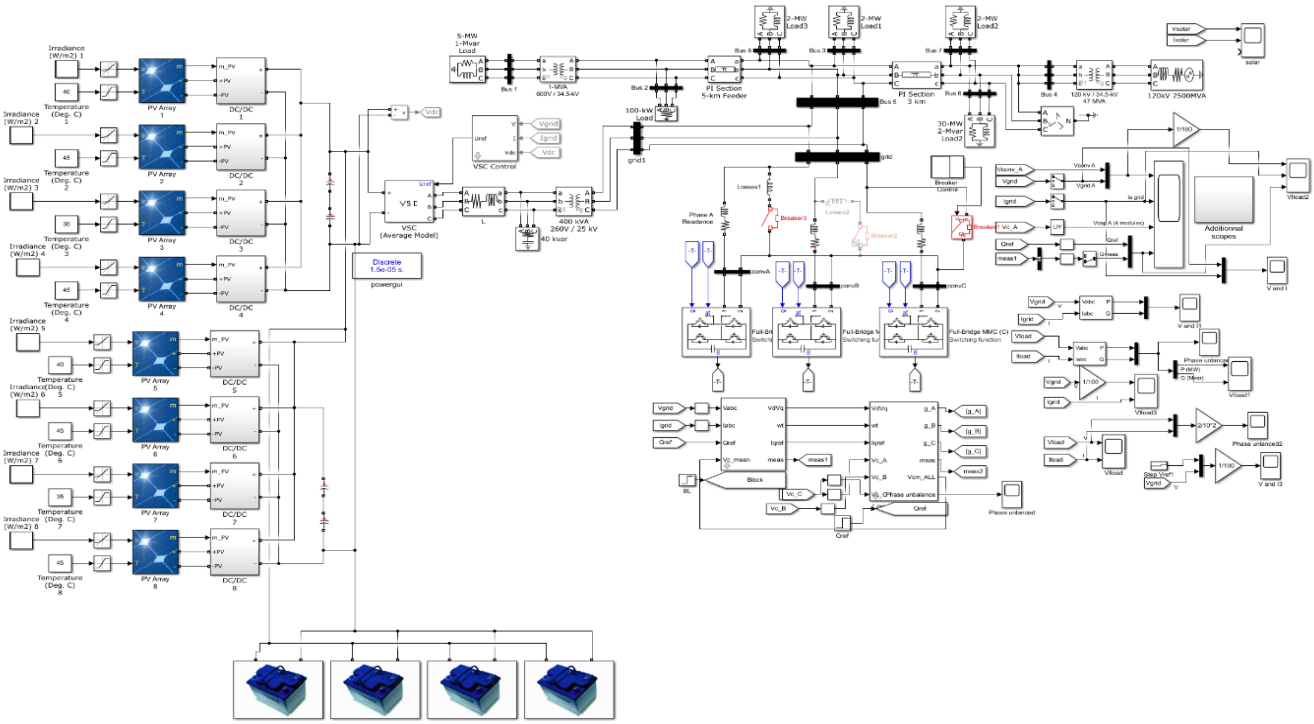

**Figure A8:** Proposed Equivalent Circuit for DUT Microgrid Designed in MATLAB/Simulink

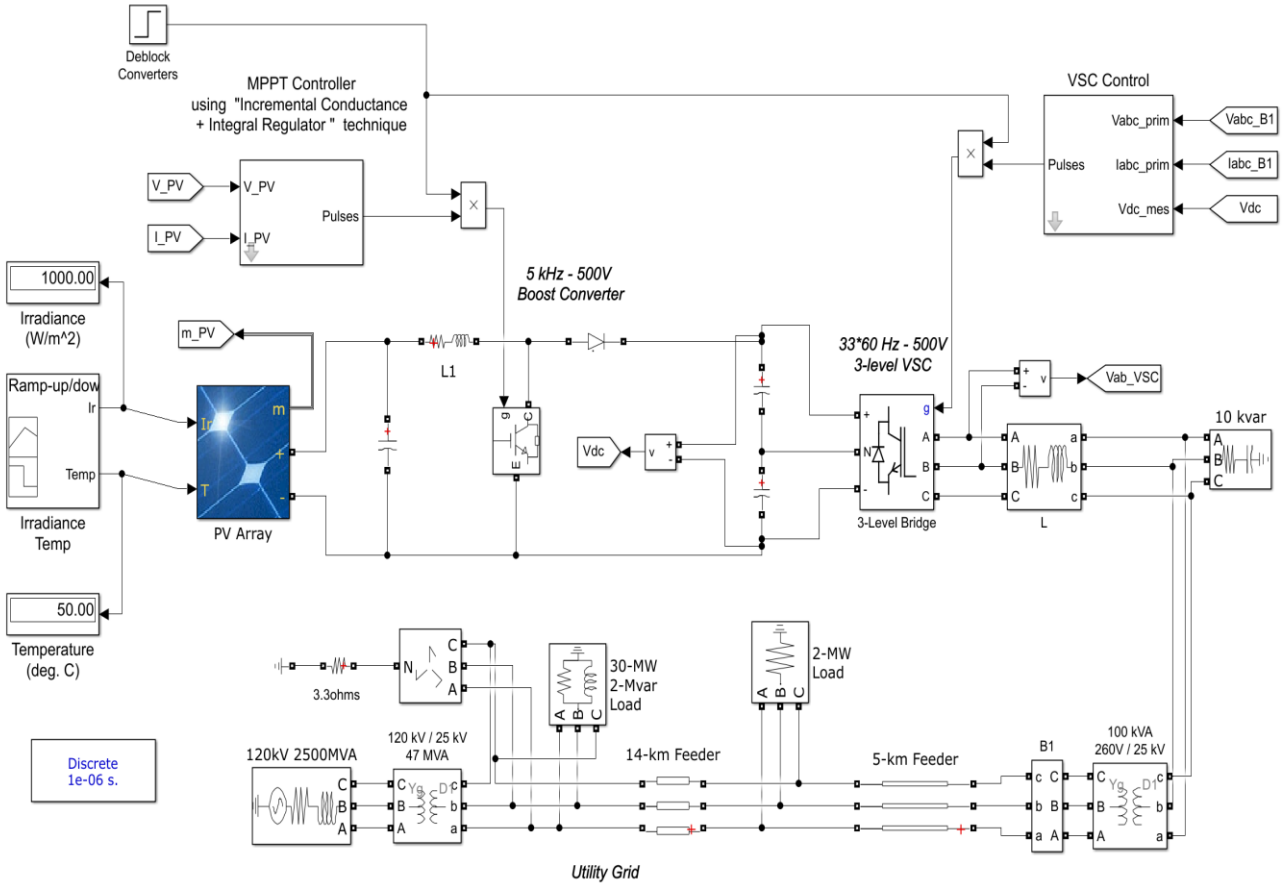


**Figure A9:** RDG Integration (solar) Test system

**Table A6:** Data for SVC and STATCOM

| | |
|---|---|
| Power rating | 5 MVA |
| Voltage (L-L) | 4.16 kV |
| Base power | 5 MVA |
| Reactive power limit | 2e6 – 1e6 |
| Average time delay | 4e-3 |
| Control parameter | |
| | |
| Voltage ref | 1.0 pu |
| Voltage regulator | [0 0.03] |
| Val control | 0.0 |

# APPENDIX B

## Static Synchronous Compensator (STATCOM)

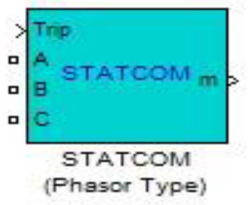


**Figure B1:** STATCOM block

**Inputs:**

- Trip - This input can be a logical signal (0 or 1). When the input is HIGH, the STATCOM is disconnected, and its control system is disabled.
- Vref - This input will only be visible if the option External control of reference voltage Vref is checked.

**Outputs:**

- m - Output vector containing many internal signals. Each of these signals can be accessed individually using a Bus Selector. The signals are:
- Va_prim (pu), Vb_prim (pu) and Vc_prim (pu) - The first three signals of the output vector contain the phasor voltages (phase to ground) Va, Vb and Vc at the STATCOM primary terminals.
- Ia_prim (pu), Ib_prim (pu), Ic_prim (pu) - These three signals contain the phase currents Ia, Ib and Ic flowing into the STATCOM.
- Vdc (V) - DC voltage.
- Vm (pu) - Positive-sequence value of the measured voltage (pu);
- Vref (pu) - Reference voltage.
- Qm (pu) - STATCOM reactive power. A positive value indicates inductive operation.
- Qref (pu) - Reference reactive power.
- Id (pu) - Direct-axis component of current (active current) flowing into STATCOM. A positive value indicates active power flowing into the STATCOM.
- Iq (pu) - Quadrature-axis component of current (reactive current) flowing into STATCOM. A positive value indicates capacitive operation.

- Idref (pu) - Reference value of direct-axis component of current flowing into the STATCOM.
- Iqref (pu) - Reference value of quadrature-axis component of current flowing into the STATCOM.
- modindex - The modulation index m of the PWM modulator. A positive number (m) between 0 and 1. When m equals to 1 it means that the VSC (Voltage-Sourced Converter) is generating the maximum voltage without over modulation.
- A, B and C - The three terminals of the STATCOM

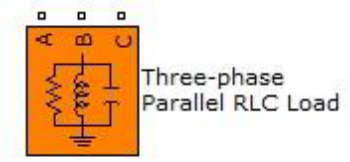


**Figure B2:** 3-phase load

The three-phase parallel RLC load block models a three-phase balanced load as a parallel combination of RLC elements. Its inputs and outputs are the three-phase terminals A, B and C.

This load absorbs active and reactive power proportionally to the square of the applied voltage to its terminals. The impedance value is constant for a specified frequency.

The user can define the nominal phase-to-phase voltage, the nominal frequency, the active power of the load and the inductive and capacitive reactive power, positive and negative Var, respectively.

The connection of the three phases of the load can also be defined with the following options:

- Y (grounded) - Neutral is grounded.
- Y (floating) - Neutral is not accessible.
- Y (neutral) - Neutral is made accessible through a fourth connector.
- Delta - Three phases connected in delta.

This block also gives the possibility to measure the three voltages across each phase of the Three-Phase Parallel RLC Load block terminals. The measurements can be accessed through a Multimeter block.

If the Branch voltages option is selected, the three voltages across each phase of the block are measured. For a Y connection, these voltages are the phase-to-ground or phase-to-neutral voltages and for a delta connection, these voltages are all phase-to-phase voltages.

If the Branch currents option is selected, the three total currents (sum of R, L and C currents) that flow through each phase of the load are measured. For a delta connection, these currents are the currents flowing in each branch of the delta.

Finally, if the Branch voltages and currents option is selected, the three voltages and three currents of the load are measured.

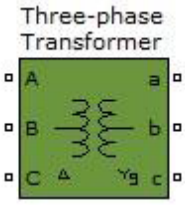


**Figure B3:** Three-phase transformer

The block implements a mode of a three-phase transformer using three single-phase transformers. It has as inputs and outputs the three-phase terminals (A, B, C, a, b and c).

The transformer is based on three single-phase transformers that can be either linear transformers or saturation transformers. This option can be made in the transformer's parameter menu. In this test platform, linear transformers were used for the simulations.

The two windings of the three-phase transformer can have one of the following connections:

- Y;
- Y with accessible neutral;
- Grounded Y;
- Delta (D1), delta lagging Y by 30 degrees;
- Delta (D11), delta leading Y by 30 degrees;

If the Y with accessible neutral option is selected, a new output will appear with the label N.

The parameters that can be defined are the nominal power, the frequency, the magnetization resistance and inductance and, for each winding, the phase-to-phase voltage, the winding resistance and the leakage inductance

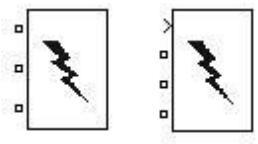

**Figure B4:** Three-phase fault blocks.

The block can simulate a three-phase fault in a network. It implements a three-phase circuit breaker where the opening and closing times can be controlled either from an external Simulink signal (if the external control mode is selected) or from an internal control timer (if the intern 86 control mode is selected). If the intern control mode is selected, the user can define the transition times in the parameter menu. As inputs and outputs, this block has the three-phase terminals that can be connected to the network and has as a possible input, the external control signal as mentioned before.

The Three-Phase Fault block uses three Breaker blocks that can be controlled individually, depending on the kind of fault that the user to simulate. The faults can be phase-to-phase, phase-to-ground or a combination of phase-to-phase and ground faults.

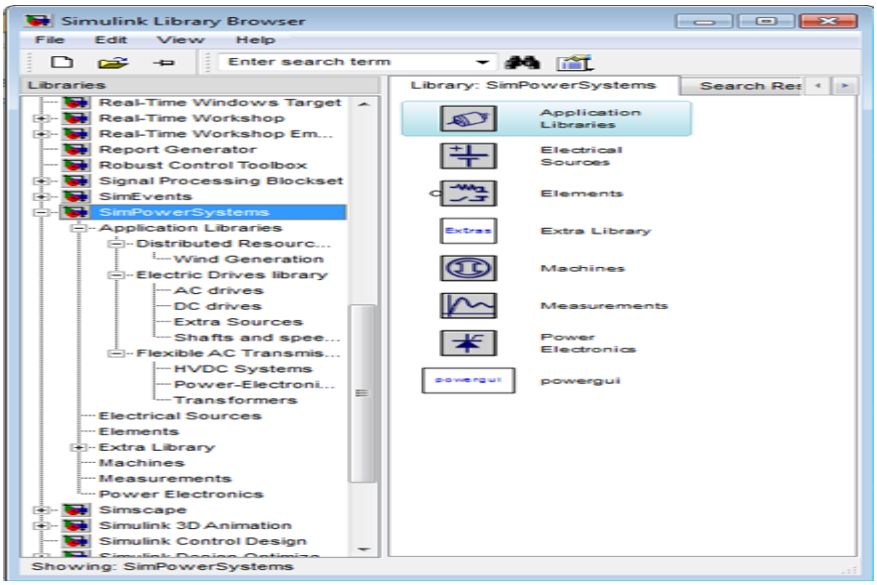


**Figure B5:** Modelling in MATLAB/SIMULINK

In building an electrical Circuit with powerlib Library, the grouped of an electrical components are contained in a library called powerlib, graphical user interface makes use of the Simulink functionality to interconnect various electrical components together. The following steps can be followed

- Open the SimPowerSystems main library by entering the command at the MATLAB prompt powerlib, the command displays a Simulink window showing icons of different block libraries. From the File menu of the powerlib window, open a new window containing your first circuit and save it. Open the Electrical Sources library and copy electrical source (e.g. Voltage source, current source, programmable source) block into the circuit window.
- Select any electrical component needed from the library element, machine and application library. Name and resize the block, interconnect the blocks by dragging lines from outputs to inputs of appropriate blocks.
- The voltage measurement block can be copied to measure the voltage; a display system (scope) is needed, which can be copied from the Simulink Sinks library.

**Powergui block**

For any simulation to be performed in the Simulink using elements from the SimPowerSystems library, Powergui block must be added to the model, it is necessary for the simulation of any Simulink model containing SimPowerSystems blocks. It is used to store the equivalent Simulink circuit that represents the state-space equations of the SimPowerSystems blocks

The presence of Powergui in the circuit designed allows different simulation solution. However, the simulations included in this thesis use the phasor solution method for the Wind Turbine Doubly-Fed Induction Generator

- Continuous method, which uses a variable step Simulink solver.
- Ideal Switching method.
- Discretization of the electrical system for a solution at fixed time steps.
- Phasor solution method.

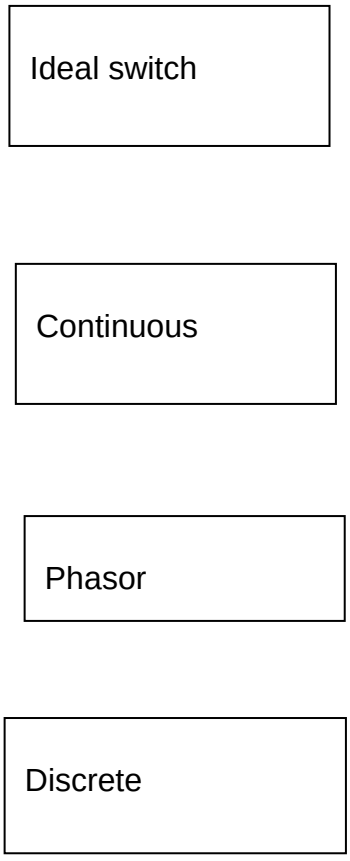


**Figure A6:** possible appearances of the Powergui block.

**Load model**

The Three-Phase Series RLC Load block implements a three-phase balanced load as a series combination of RLC elements. At the specified frequency, the load exhibits constant impedance. The active and reactive powers absorbed by the load are proportional to the square of the applied voltage

**Nominal phase-to-phase voltage**: The nominal phase-to-phase voltage of the load, in volts RMS (Vrms).

**Nominal frequency**: The nominal frequency, in hertz (Hz).

**Active power**: The three-phase active power of the load, in watts (W).

**Inductive reactive power**: The three-phase inductive reactive power QL, in vars. Specify a positive value, or 0.

**Capacitive reactive power**: The three-phase capacitive reactive power QC, in vars. Specify a positive value, or 0.

**Measurements**: Branch voltages can be selected to measure the three voltages across each phase of the Three-Phase Series RLC Load block terminals. For a Y connection, these voltages are the phase-to-ground or phase-to-neutral voltages. For a delta connection, these voltages are the phase-to-phase voltages. Branch currents can be selected to measure the three total currents (sum of R, L, C currents) flowing through each phase of the Three-Phase Series RLC Load block. For a delta connection, these currents are the currents flowing in each branch of the delta

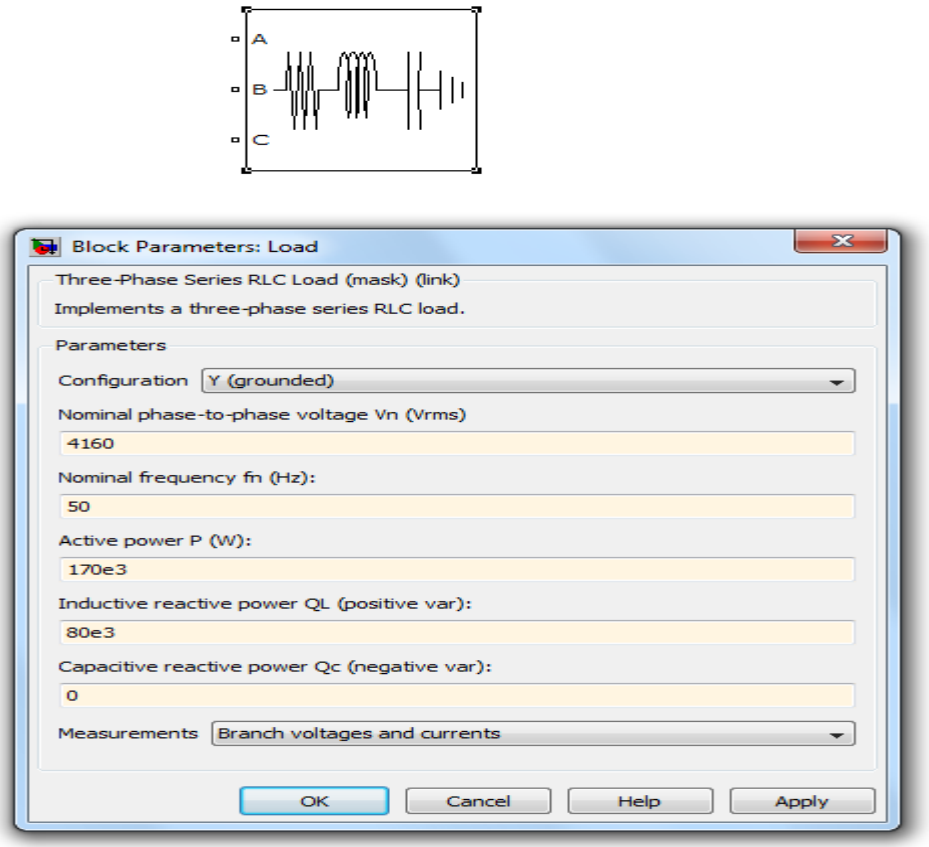


**Figure A7:** Three phase measurement and Bus bar

The Three-Phase V-I Measurement block is used to measure three-phase voltages and currents in a network. When connected in series with three-phase elements, it returns the three phase-to-ground or phase-to-phase voltages and the three-line currents. The block can output the voltages and currents in per unit (pu) values or in volts and amperes. If voltage and current are to be measured in pu, the Three-Phase V-I Measurement block does the following conversions:

$$V_{abc}(pu) = V_{abc}(pu) = \frac{V_{abc}(pu)}{\frac{V_{baseLL}}{\sqrt{3}} \times \sqrt{2}}$$

$$I_{abc}(pu) = \frac{I_{abc}(pu)}{\frac{P_{base}}{V_{base}.\sqrt{3}} \times \sqrt{2}}$$

Where VbaseLL is the base line-to-line voltage in volts RMS and Pbase is the three-phase base power in volts-amperes. The two base values VbaseLL and Pbase are specified in the Three-Phase Measurement block menu. Three phase measurement block can use to make bus bar model, this is done by clicking on “used a label” inside the three phase measurement block and try to reduce the block to a desired block.

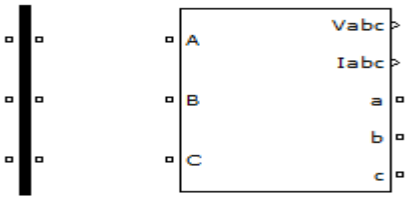


**Figure A8:** three phase measurements

## Representation of DFIG in Simulink (power toolbox)

The Figure below shows the representation of DFIG in the power system toolbox, the wind turbine and the generator has been built together as one unit. Parameters of the wind turbine and the generator can only be input into the system.

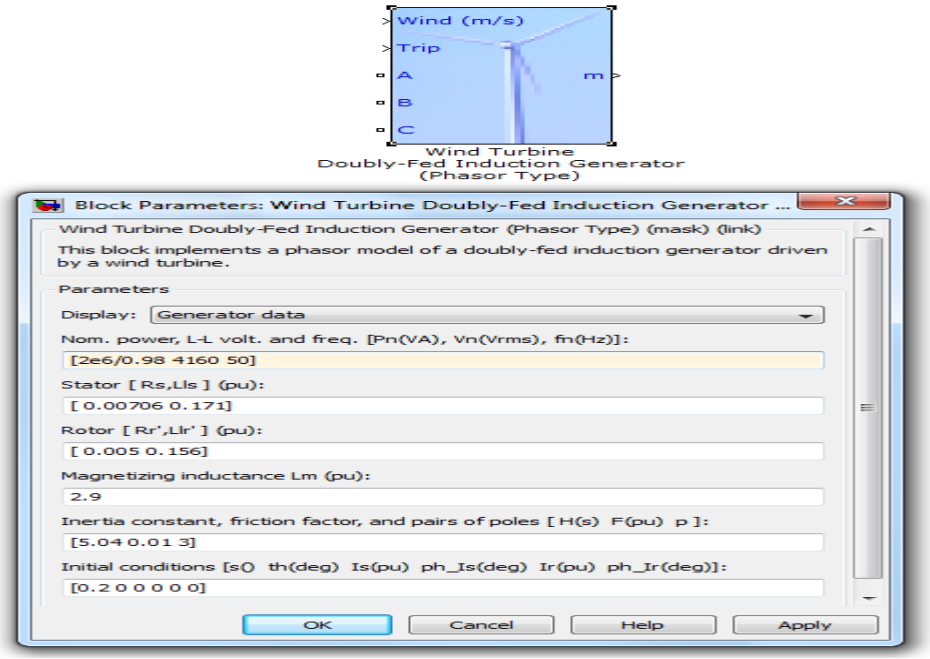


**Figure A9:** Simulink block for the DFIG

## Input

- **Wind (m/s) -** Input of the wind speed can be either a function or a constant. One can use an interpolation of several wind velocities to simulate the wind evolution over time. If the option External mechanical torque is selected, the wind velocity input will not be visible.

- **Trip** - Command signal of the wind turbine protection system. When the value of the trip is zero (LOW) the protection system isn't active. The protection system will be activated when the trip value is equal to one (HIGH), which will happen when any of the generator's measurements exceeds the reference values that were

established. When the system is activated, the wind turbine is turned off, which means that the generation of active and reactive power is equal to zero.

- **Tm** - This input will only be visible if the External mechanical torque option is selected. The mechanical torque must be negative for power generation. This input should be used with an external turbine model.

- **Vref** - This input is only visible when the Mode of operation parameter is set to Voltage regulation or when the External grid voltage reference is selected. We can define this reference value.

- **Qref** - This input is only visible when the Mode of operation parameter is set to Var regulation or when the External generated reactive power reference is selected. We can define this reference value.

- **Iq_ref** - This input is only visible when the parameter External reactive current Iq_ref for grid-side converter is selected. We can define this reference value.

**Outputs:**

1. **M** - Output vector which contains 8 signals from the Wind Turbine Doubly-Fed Induction Generator (WTDFIG). Each signal can be accessed individually using a Bus Selector. The signals are:

- Iabc (complex) (pu) - Phasor currents Ia, Ib e Ic, that flow in the WTDFIG terminals;

- Vabc (complex) (pu) - Phase to ground voltages Va, Vb e Vc at the WTDFIG terminals;

- Vdq_stator (pu) - **d** and **q** components of the stator voltage. Vd_stator and Vq_stator are respectively the real and imaginary components of the positive sequence voltage of the stator;

- Iabc_stator (complex) (pu) - Phasor currents Ia, Ib e Ic that flow in the stator;

- Idq_stator (pu) - **d** and **q** components of the stator current. Id_stator and Iq_stator are respectively the real and imaginary components of the positive sequence current in the stator;

- Vdq_rotor (pu) - **d** and **q** components of the rotor voltage. Vd_rotor and Vq_rotor are respectively the real and imaginary components of the positive sequence voltage of the rotor;

- Idq_rotor (pu) - **d** and **q** components of the rotor current. Id_rotor and Iq_rotor are respectively the real and imaginary components of the positive sequence current in the rotor;

- wr (pu) - Generator rotor speed in pu;

- Tm (pu) - Mechanical torque applied to the generator in pu;

- Te (pu) - Electromagnetic torque in pu
- Vdq_grid_conv (pu) - **d** and **q** components of the grid side converter voltage. Vd_grid_conv e Vq_grid_conv are respectively the real and imaginary components of the positive sequence voltage of the grid side converter
- Iabc_grid_conv (complex) (pu) - Phasor currents Ia, Ib e Ic that flow in the grid side converter
- P (pu) - Output active power of the WTDFIG in pu. If this value is greater than zero in means that there is generation of active power
- Q (pu) - Output reactive power of the WTDFIG in pu. If this value is greater than zero in means that there is a generation of reactive power
- Vdc (V) - DC voltage in the WTDFIG
- Pitch_angle (deg) - Pitch angle of the blades o the WTDFIG in degrees.
- A, B and C - The three terminals of the WTDFIG.